Study of the Cellular Role of GRP78/BiP mono-ADP-ribosylation in UPR and Cancer

Thesis

Study of the cellular role of GRP78/BiP mono-ADP-ribosylation in UPR and cancer

Gaia Fabrizio

Discipline: Life, Health and Chemical Sciences

Sponsoring establishments: Consorzio Mario Negri Sud / The Open University

Thesis submitted in accordance with the requirements of the Open University for the Degree of Doctor of Philosophy

September 2017

Abstract

Mono-ADP-ribosylation is a reversible post-translational protein modification that modulates the function of proteins involved in different cellular processes, including signal transduction, protein transport, transcription, cell cycle regulation, DNA (deoxyribonucleic acid) repair and apoptosis. In mammals, mono-ADP-ribosylation is catalyzed by three different classes of enzymes: ARTCs, ARTDs, and members of the sirtuin family.

In the present study, hARTC1-mediated mono-ADP-ribosylation was investigated in terms of the cellular compartments involved, target(s) and roles. The collected results demonstrated that hARTC1 protein and enzymatic activity is mainly localized to the endoplasmic reticulum (ER), in contrast to other ARTCs, which are either typically GPI-anchored enzymes in the plasma membrane, or secreted enzymes. Previous studies in my laboratory demonstrated that a protein macro domain was useful for the study of APD-ribosylation. The data reported here indicate, for the first time, that the macro domain can be used for immunofluorescence, allowing visualization of ADP-ribosylated proteins in intact cells, and in far-Western Blotting, allowing the detection of specific ADP-ribosylated targets. These methodologies were employed to demonstrate that the ER-localized chaperone, GRP78/BiP, was a prime target of hARTC1. A doubly mutated hARTC1 mutant was designed, and used as a specific control for hARTC1 expression. The mutant enzyme localized to the ER, but did not catalyze GRP78/BiP ADP-ribosylation.

The demonstration that GRP78/BiP was mono-ADP-ribosylated by hARTC1 suggested that hARTC1 could be a key regulator of GRP78/BiP-mediated functions. Consistent with the key role of GRP78/BiP in the ER stress response, it was found that hARTC1 was activated during short-term cell treatment with ER stressors, resulting in acute GRP78/BiP ADP-ribosylation. However, the mono-ADP-ribosylation of the chaperone did not trigger an unfolded protein response. Recently, hARTC1 has been associated with cancer, suggesting a possible role in cell proliferation. In line with these findings, the results presented here demonstrated that hARTC1 over-expression inhibited cell proliferation.

Table of contents

List of figures

List of tables

Chapter 1

Introduction

The function of proteins is frequently modulated by covalent modifications introduced after translation from RNA (ribonucleic acid). These covalent modifications are defined as post-translational modifications (PTMs), and they represent an essential mechanism used by cells to diversify protein functions and dynamically coordinate their signaling networks (Figure 1.1; Khoury, G.A. et al., 2011). Defects in PTMs have been linked to numerous developmental disorders and human diseases, highlighting the importance of PTMs in maintaining normal cellular states.

PTMs generally refers to the covalent addition of a functional group, or groups, to a protein, as in the most extensively studied case of phosphorylation, but proteins can also be modified by acetylation, glycosylation and nitrosylation. However, other frequently encountered PTMs consist of the conjugation of other proteins or peptides (e.g., ubiquitination, SUMOylation), changing of the chemical nature (e.g., deamidation, citrullination), or alterations in the structure (e.g., disulfide bond formation) of proteins (Figure 1.1; Khoury, G.A. et al., 2011).

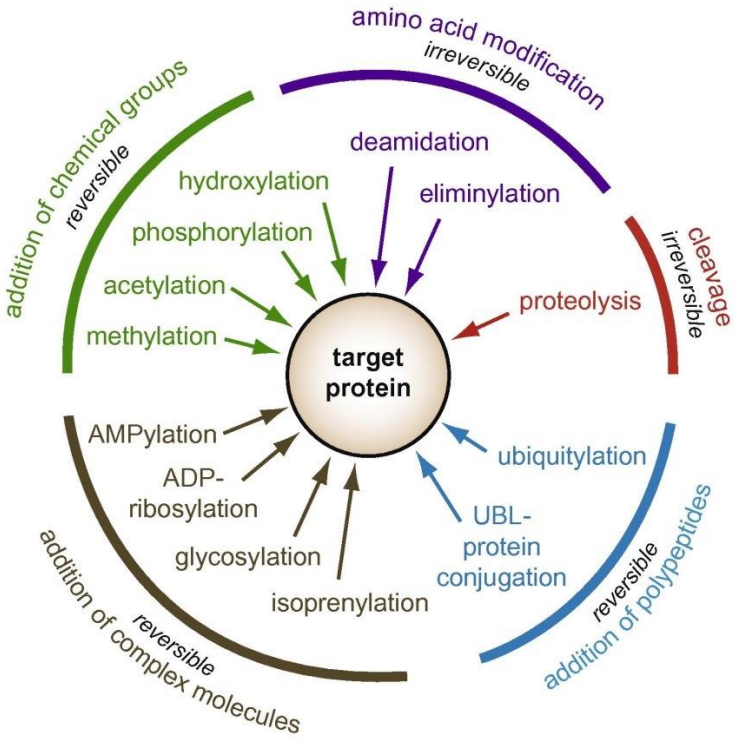

Taken from Ribet, D. and Cossart, P., 2010

Figure 1.1 The most common and important post-translational modifications (PTMs). PTMs can be distinguished based on the modification of the chemical structure of amino acid side chains, addition of chemical groups or complex molecules to specific amino acids, covalent linkage of polypeptides, and cleavage of the peptide bond between two amino acids.

Among the other PTMs, adenosine diphosphate (ADP)-ribosylation is receiving increasing attention due to its involvement in both physiological and pathophysiological processes, such as signal transduction, protein transport, transcription, DNA repair pathways, cell cycle regulation, apoptosis and necrosis. There are also increasing numbers of reports that link ADP-ribosylation to human diseases, including inflammation, neurodegeneration and cancer metastasis (Butepage, M. et al., 2015; Fabrizio, G. et al., 2015a; Gupte, R. et al., 2017).

ADP-ribosylation was discovered more than five decades ago and during the intervening years of research numerous enzymes, and some of their targets, have been isolated and characterized. The reaction, catalyzed by enzymes found in

organisms ranging from prokaryotes to mammals, consists of the enzymatic transfer of ADP-ribose from nicotinamide adenine dinucleotide (NAD^+) to acceptor proteins. In viruses and prokaryotes, ADP-ribosylation is mainly, but not exclusively, a mechanism used to take control of the host cell. In mammals, ADP-ribosylation serves to regulate protein functions, including cell-surface, nuclear and cytosolic proteins.

The effects of ADP-ribosylation are counteracted via enzymes that can reverse this PTM. By cleaving the covalent bond and releasing the ADP-ribose moiety the target protein is de-modified, but may also be subject to further modification. Three classes of proteins have been demonstrated to perform the reverse reaction: the ADP-ribosyl-hydrolases (ARHs), the poly-ADP-ribose-glycohydrolases (PARGs) and the macro-domain–containing proteins (Verheugd, P. et al., 2016). Some of the members of this last class have been only recently described as enzymes able to remove ADP-ribose modifications (Jankevicius, G. et al., 2013; Rosenthal, F. et al., 2013).

1.1 The ADP-ribosylation reactions

The transfer of ADP-ribose to a target protein can occur by non-enzymatic or enzymatic mechanism. In the first case, the reaction is known as glycation and it involves the covalent binding of ADP-ribose to reactive nucleophilic amino acid residues, primarily lysines and cysteines. Specifically, the ADP-ribose moiety can be non-enzymatically attached to a lysine residue through a keto-amine bond, or to a cysteine residue through either a thiazolidine or S-glycosidic bond

(Cervantes–Laurean, D. et al., 1996; McDonald, L.J. et al., 1992; McDonald, L.J. and Moss, J., 1993). The free ADP-ribose required for the reaction is produced as part of the turnover of either cyclic ADP-ribose or ADP-ribose polymers, or by hydrolysis of pre-existing ADP-ribosylated proteins. An example of physiologically relevant *in vivo* glycation is that of histone H1, which has been associated with various disease conditions (Cervantes–Laurean, D. et al., 1996; Rouf Mir, A. and Bashir, Y., 2015).

In the second case, the reaction is catalyzed by specific enzymes known as ADP-ribosyl-transferases (ARTs). ARTs cleave the N-glyosidic bond of β-NAD^+ producing a positively charged oxocarbenium intermediate which is subjected to a nucleophilic attack by either a single (mono-ADP-ribosylation) or multiple (poly-ADP-ribosylation) ADP-ribose moieties (Figure 1.2; Sung, V.M., 2015; Verheugd, P. et al., 2016). Besides the difference in the length of the ADP-ribose chain that they form, enzymatic ADP-ribosylation reactions differ also for the chemical nature of the ADP-ribosyl-protein bond. Ueda and Hayaishi were the first that distinguished between the nucleophilic attack by the guanidine group of arginine and that by the hydroxyl group of glutamic acid. The nucleophilic attack by the guanidine group of arginine leads to the formation of an N-glycosidic bond and is catalyzed by NAD-arginine ARTs. The nucleophilic attack by the hydroxyl group of glutamic acid, instead, leads to the formation of an O-glycosidic bond and is catalyzed by NAD-glutamate ARTs (Ueda, K. and Hayaishi, O., 1985). Moreover, the enzymatic ADP-ribosylation reactions differ also for the cell compartment in which they take

place, as initially reported by Shall (cytoplasm and cell membrane versus nucleus; Shall, S., 1995).

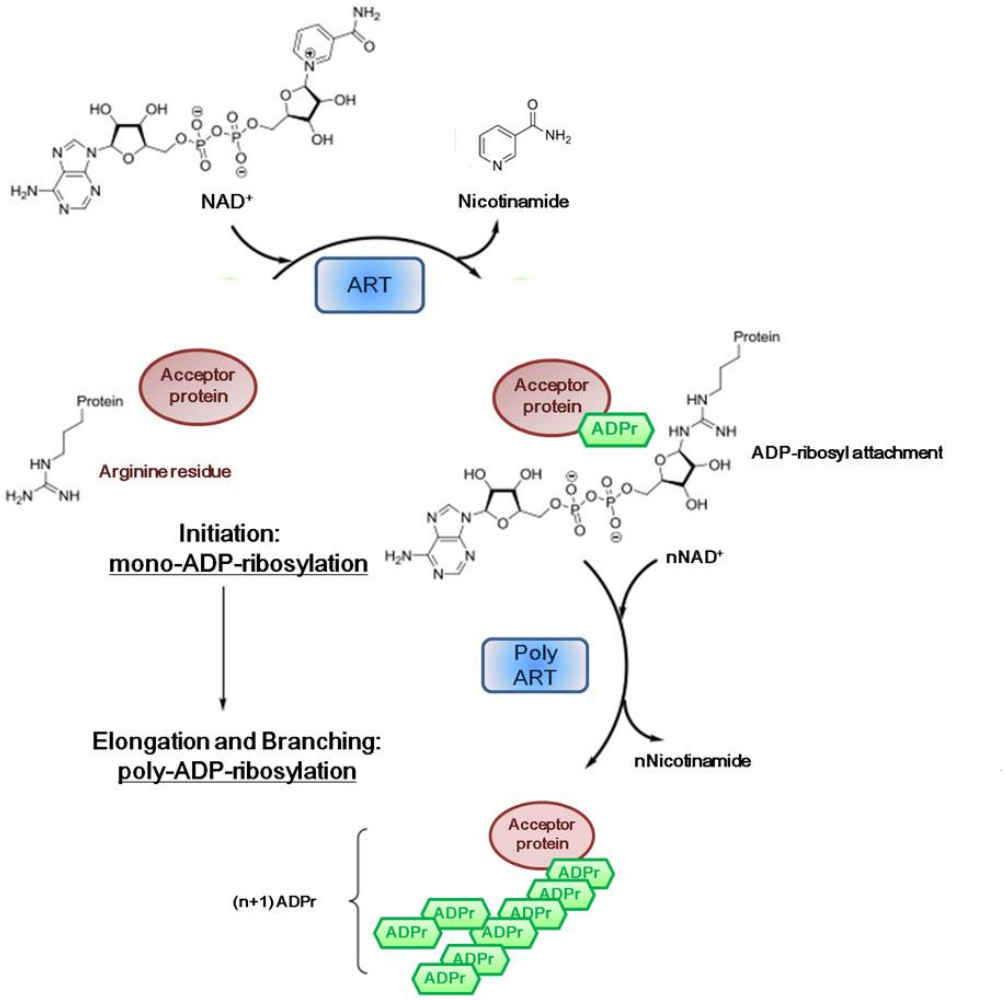

Figure 1.2 Cellular enzymatic ADP-ribosylation reactions. Cellular transferase enzymes can use NAD to catalyze either mono-ADP-ribosylation, attaching a single ADP-ribose molecule to target protein, or poly-ADP-ribosylation, catalyzing a multiple ADP-ribose chain elongation and branching.

Currently, 22 human genes encoding proteins with ADP-ribosyl-transferase activity have been discovered, but recent structural and enzymological evidences demonstrate that earlier proposed names and classifications of ARTs are no longer accurate. This earlier classification distinguished ADP-ribosylating enzymes as ADP-ribosyl-transferases (ARTs) or poly-ADP-ribose-polymerases (PARPs). For this

reason, a new nomenclature has been suggested for all ART enzymes. This new classification distinguishes clostridia-toxin-like ARTs (mono-ARTs; see Chapter 1.2) and diphtheria-toxin-like ARTs (mono- and poly-ARTs; see Chapter 1.3), with acronyms respectively ARTC and ARTD and numbers specifying the different proteins of the family (Table 1.1; Hottiger, M.O. et al., 2010).

New classification: Protein names	Old classifications: protein names	Aliases	Accession numbers
ARTD:			
ARTD1	PARP1, pART1	–	NP_001609.2
ARTD2	PARP2, pART2	–	NP_001036083.1, NP_005475.2
ARTD3	PARP3, pART3	–	NP_005476.3, NP_001003931.2
ARTD4	PARP4, pART4	vaultPARP	NP_006428.2
ARTD5	PARP5a, pART5, PARP5	Tankyrase-1	NP_003738.2
ARTD6	PARP5b, pART6, PARP6	Tankyrase-2	NP_079511.1
ARTD7	PARP15, pART7, PI-mART9	BAL3	NP_001106995.1, NP_689828.1
ARTD8	PARP14, pART8, PI-mART11	BAL2	NP_060024.2
ARTD9	PARP9, pART9, PI-mART10	BAL1	NP_001139574.1, NP_001139575.1
ARTD10	PARP10, pART10, PI-mART4	–	NP_116178.2
ARTD11	PARP11, pART11, PI-mART5	–	NP_065100.2
ARTD12	PARP12, pART12, PI-mART7	ZC3HDC1	NP_073587.1
ARTD13	PARP13, pART13, PI-mART8	ZC3HAV1, ZAP1	NP_078901.3, NP_064504.2
ARTD14	PARP7, pART14, PI-mART6	TiPARP, RM1	NP_056323.2
ARTD15	PARP16, pART15, PI-mART1	–	NP_060321.3
ARTD16	PARP8, pART16, PI-mART3	–	2NP_078891.2
ARTD17	PARP6, pART17, PI-mART2	–	NP_064599.
ARTC:			
ARTC1	ART1	CD296	NP_004305.2
ARTC2P[b]	ART2P	–	–
ARTC3	ART3	–	NP_001123488.1, NP_001123489.1, NP_001170.2
ARTC4	ART4	CD297	NP_066549.2
ARTC5	ART5	–	NP_001073004

Table 1.1 The new proposed classification of human ARTs.

Example of the new classification of human ARTD and ARTC enzymes, compared to the old protein classification. Family members are numbered on the basis of similarities in amino acid sequence, structure of the catalytic domain and postulated catalytic reaction. Several accession numbers denote individual isoforms. [b] Pseudogene in humans; *Art2* is duplicated in the mouse. Modified from Hottiger, M.O. et al., 2010.

The ARTC family is composed of a relatively small group of structurally related ecto-mono-ARTs, expressed at the cell surface or secreted into the extracellular compartment (Glowacki, G. et al., 2002; Koch-Nolte, F. et al., 2008). The ARTD is a large family of 17 proteins that comprises both poly-ARTs and mono-ARTs (Ame, J.C. et al., 2004; Hassa, P.O. et al., 2006; Hassa and Hottiger, 2008; Otto, H. et al., 2005; Schreiber, V. et al., 2006). Additionally, some members of the sirtuin family

have also been reported to catalyze ADP-ribosylation reactions under certain conditions, even though sirtuins are structurally distinct from ARTs and their predominant enzymatic activity is NAD^+-dependent protein deacetylation (Hawse, W.F. and Wolberger, C., 2009).

From a functional point of view, ADP-ribosylation reactions were originally identified as the mechanism of action of various bacterial toxins (Honjo, T. et al., 1968). Subsequently, they have also been discovered in bacteriophages and in eukaryotic cells. Viruses, like bacteriophage T4, use mono-ADP-ribosylation to regulate transcription and impose their genetic program over infected host cells (Alawneh, A.M. et al., 2016; Fabrizio, G. et al., 2015a; Goff, C.G., 1974; Laing, S. et al., 2011).

Diphtheria, cholera, pertussis, clostridia and many other bacterial toxins are mono-ARTs that can modify specific host proteins after their translocation into the mammalian host cell, resulting in pathological situations (Corda, D. and Di Girolamo, M., 2003; Di Girolamo, M. et al., 2005; Fabrizio, G. et al., 2015a; Holbourn, K.P. et al., 2006). However, bacteria use mono-ADP-ribosylation not only as a pathogenic mechanism, but also as a physiological mechanism to regulate certain own cellular functions. A well-known example is the mono-ADP-ribosylation of the enzyme dinitrogenase reductase involved in the nitrogen fixation of the photosynthetic bacterium *Rodospirillum rubrum* (Ludden, P.W. and Burris, R.H., 1976; Ludden, P.W., 1994; Nordlund, S. and Hogbom, M., 2013).

The finding that bacteria use mono-ADP-ribosylation to mimic eukaryotic cellular functions prompted investigators to looking for endogenous relatives of bacterial

toxins in animal cells. The first researchers who described mono-ADP-ribosylation in animals were Moss and colleagues, who were successful in purifying an ART from turkey erythrocytes (Moss, J. and Vaughan, M., 1978). Subsequently, other mono-ARTs were isolated from different vertebrate tissues. Particularly, proteins with ADP-ribosylation activity were purified from rabbit skeletal muscle and chicken bone marrow cells (Peterson, J.E. et al., 1990; Tsuchiya, M. et al., 1994; Zolkiewska, A. et al., 1992).

1.2 The ADP-ribosyl-transferases clostridia toxin-like (ARTCs)

The eukaryotic mono-ARTs family comprises seven members (ART1-7). In mammals only six mono-ARTs have been found (ART1, ART2.1 and ART2.2, ART3, ART4 and ART5), whereas three further forms have been described in birds (ART6A, ART6B and ART7; Okazaki, I.J. and Moss, J., 1999). According to the new nomenclature, the mammalian ecto-mono-ART family has been categorized as ARTCs (Hottiger, M.O. et al., 2010). The small group of proteins that composed the ARTC family has been numbered on the basis of similarities in amino acid sequence, structure of the catalytic domain and postulated catalytic reaction (Hottiger, M.O. et al., 2010). In humans, there are only four ARTCs, that are either active mono-ARTs (human [h]ARTC1, hARTC5) or inactive proteins (hARTC3, hARTC4). The gene encoding for ARTC2, which is duplicated in mouse and rat, is a pseudogene in humans that arises from three premature exonic stop codons (Koch-Nolte, F. et al., 1997; Prochazka, M., et al., 1991; Haag, F. et al., 1994).

The exon/intron structures of all human ARTCs, determined by comparative sequencing of full-length cDNA and genomic DNA clones, revealed that *artc* genes are composed of 3 to 11 exons. In each gene, a single long exon encodes most of the native protein, including the catalytic domain (Figure 1.3). Separate exons encode the N- and the C-terminal signal peptides. The gene for hARTC4 does not contain any additional coding exons, whereas the genes for hARTC1 and hARTC5 possess one additional small exon encoding the C-terminal end, and the gene for hARTC3 contains several small exons in this region. Moreover, the 5′ untranslated region of hARTC1, hARTC3 and hARTC5 is split into several distinct exons (Glowacki, G. et al., 2002). The last 3′ exons of hARTC1, hARTC3 and hARTC4 end in a stretch of hydrophobic amino acids that is a typical feature of GPI (glycosylphosphatidylinisotol)-anchored membrane proteins. These findings suggest that these enzymes are all ecto-enzymes anchored to the cell membrane. The only exception is that of hARTC5, which lacks this region and thus represents the only secreted enzyme (Glowacki, G. et al., 2002; Okazaki, I.J. and Moss, J., 1999; Stilla, A. et al., 2011).

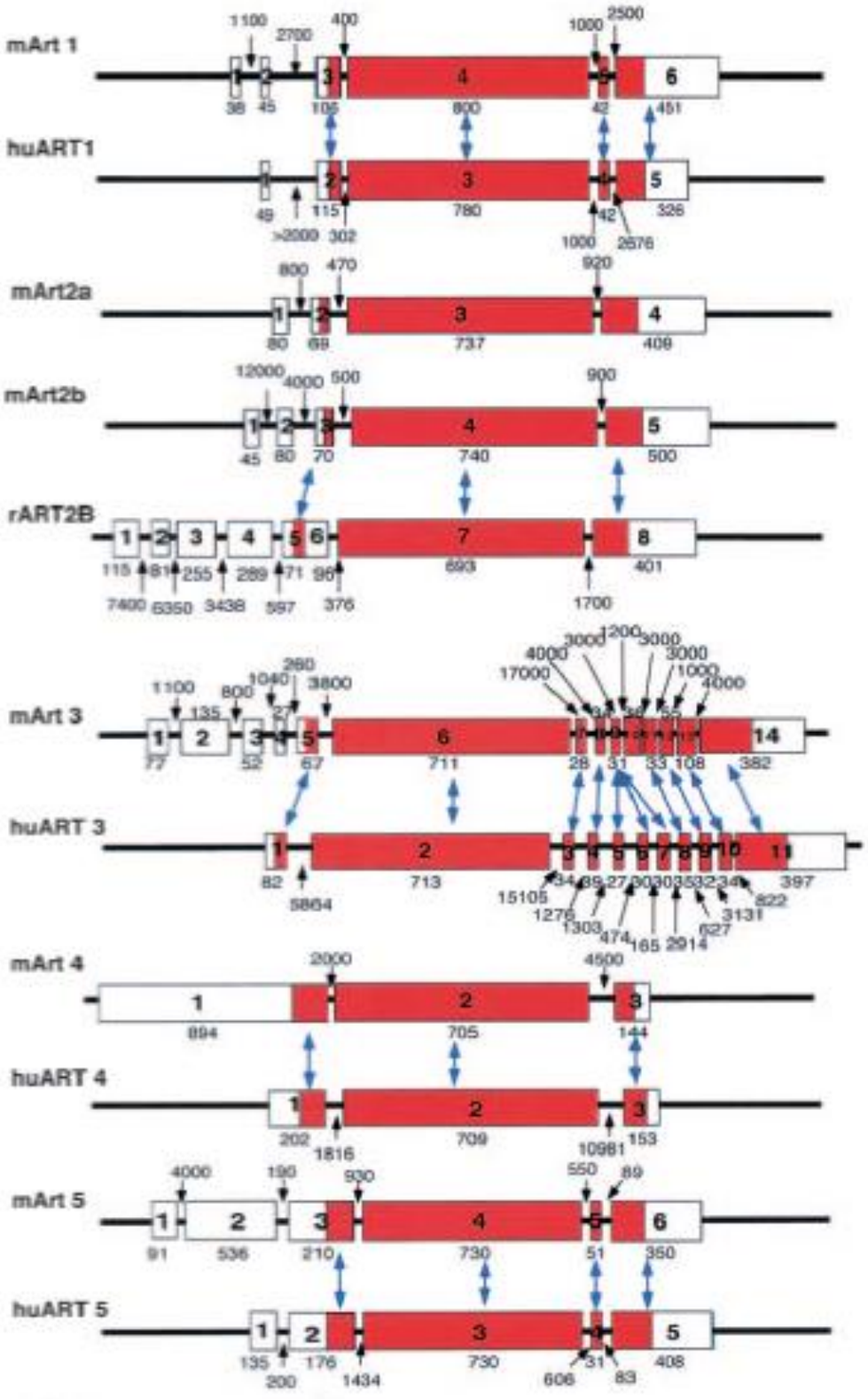

Modified from Glowacki, G. et al., 2002

Figure 1.3 Exon-intron structures of human and mouse ART genes. Introns are shown as lines and exons as boxes; the coding regions are depicted in red. The numbers indicate lengths of exons and introns in base pairs. Corresponding exons in ART orthologs are indicated by arrows.

From a topological point of view, the C-terminal region of ARTCs is folded into β-sheets, which is characteristic of GPI-anchored membrane proteins, whereas their N-terminus is an α-helix–rich region, a feature that represents a typical signal sequence for extracellular proteins. The catalytic domain of ARTCs can be divided into three different regions: an N-terminal region, which contains a conserved arginine residue; a central region, which is characterized by the serine-x-serine motif (where x can be threonine, serine or alanine) and is involved in the binding of NAD, and a C-terminal highly acidic region, which contains the catalytically crucial glutamate residue (Domenighini, M. et al., 1994; Domenighini, M., and Rappuoli, R., 1996). The crystal structure of rat ART2.2 has been determined and its comparison with several bacterial ARTs and chicken PARP crystal structures, revealed a common topology of the catalytic domain (Mueller-Dieckmann, C. et al., 2002). The catalytic domain is composed of a central six-stranded β-sheet and an α-helix that form the upper and the lower parts of the active sites (Choe, S. et al., 1992; Han, S. et al., 1999; Mueller-Dieckmann, C. et al., 2002). The strictly conserved glutamic acid is positioned in the fifth β-strand, whereas the other two residues that compose the conserved triad (arginine and serine) are positioned in the first and in the second β-strand, respectively (Bazan, J.F. and Koch-Nolte, F., 1997; Carrol, S.F. and Collier, R.J., 1984; Domenighini, M., and Rappuoli, R., 1996; Koch-Nolte, F. et al, 1996). Furthermore, a second important glutamic acid was found two residues upstream of the catalytic glutamate, in the loop connecting the fourth and fifth β-strands.

The loop preceding the glutamic acid is likely to be involved in the contact of the ARTs with target proteins and, therefore, in the control of target specificity (Han, S. et al., 2001). Mutational studies in ARTC1 from rabbit demonstrated that the conserved catalytic glutamate is necessary for the transfer of ADP-ribose on the arginine within the target protein, and that the neighbouring glutamate is equally important for the transfer (Hara, N. et al., 1996). Substitution of this second glutamic acid determines the abrogation of ADP-ribose transfer on arginine in several ARTCs. As shown by Stilla et al., the single mutation of the catalytic glutamate in ARTC2.1 of hamster (cARTC2.1) still resulted in a partial ADP-ribosyl-transferase activity (Stilla, A. et al., 2011). However, it was completely abolished with the additional mutation of the neighbouring glutamate, by which both the glutamate residues of the R-S-EXE motif were mutated (Stilla, A. et al., 2011). These findings support the hypothesis that this region is important for substrate recognition.

The sequence arginine-serine-glutamate (R-S-EXE) is typical of the arginine-specific ARTs. It was found in all the active ARTC enzymes: ARTC1, ARTC2 and ARTC5, whereas the motif is missing in ARTC3 and ARTC4 (Table 1.2; Friedrich, M. et al., 2006; Koch-Nolte, F. et al., 1997). Thus, they do not have measurable activities and their roles in cell biology are independent of ART activity, a situation that is also seen in the ARTD family and in the sirtuin family.

Table 1.2 Mammalian ARTC family.

Family	Enzymatic Status	Protein Name	Ribosylation Activity	Triad Motif
ARTC	Active	ARTC1/ART1	Mono	R-S-E
		ARTC2/ART2	Mono	R-S-E
		ARTC5/ART5 *	Mono	R-S-E
	Inactive	ARTC3/ART3	-	K-L-V
		ARTC4/ART4	-	G-S-E

* secreted enzyme

1.2.1 The active ARTCs

1.2.1.1 ARTC1

ARTC1 was the first mammalian arginine-specific ART to have been discovered. It is a 36 kDa (kilodalton) protein that was initially isolated and characterized from rabbit skeletal muscle microsomal membranes (Peterson, J.E. et al., 1990; Zolkiewska, A. et al., 1992). Subsequent studies revealed the protein was conserved among different species such as human, rabbit and mouse and that it was preferentially expressed at high level in cardiac and skeletal muscle (Okazaki, I.J. et al., 1996a).

The ARTC1 mono-ART activity has been fully described in myogenically differentiated cultured mouse skeletal muscle (C2C12) cells. As reported by Zolkiewska and Moss, the substrate of ARTC1 was the cell surface adhesion molecule integrin α7, whose ADP-ribosylation was suggested to have a role in myogenesis. Increased levels of ADP-ribosylation were observed during the differentiation of these cells into myotubes (Zolkiewska, A. and Moss, J., 1993). Integrins are integral membrane proteins with a role as receptors in mediating

cell-substratum and cell-cell adhesion. Signals from the extracellular matrix transduced by integrins control cell growth, shape, migration and differentiation. The selective expression of ARTC1 and integrin α7 in both cardiac and skeletal muscle, their similar developmental appearance, and the specific ADP-ribosylation, are consistent with the regulatory association between these two proteins. It has been suggested that mono-ADP-ribosylation of integrin α7 may modulate receptor signaling and could play a significant role in cell adhesion and in outside-insight cell signaling (Zolkiewska, A. and Moss, J., 1993).

Another identified substrate of ARTC1 is the human defensin human neutrophil peptide 1, (HNP-1), an arginine-rich peptide that is considered to be the major component of innate antimicrobial immunity (Paone, G. et al., 2002). It is also involved in adaptive immunity, since cytokine stimulation of human natural killer cells and T- and B-lymphocytes leads to the production of defensins. HNP-1 is mono-ADP-ribosylated by ARTC1 on arginine 14, as demonstrated by *in vitro* assays (Paone, G. et al., 2002). ADP-ribosylation alters its biological properties, decreasing cytotoxic and antimicrobial activity, whereas its ability to release interleukin 8 (IL-8) from epithelial cells is significantly increased. However, ADP-ribosylated HNP-1 retains its function as chemoattractant for recruiting leukocytes, similarly to the unmodified protein (Stevens, L.A. et al., 2009). It is possible that, once modified, HNP-1 acquires specific biological properties that can still result in the recruitment of neutrophils (after the release of IL-8 from epithelial cells), but also in the modulation of its own antimicrobial and cytotoxic activities (Paone, G. et al., 2002). This last aspect is extremely important considering the identification

of ADP-ribosylated HNP-1 also *in vivo*, in bronchoalveolar lavage fluids (BALF) of some smoker patients. This observation supports the idea that ADP-ribosylated HNP-1 is produced during the inflammatory response when it loses its antimicrobial activity (Paone, G. et al., 2002).

Additional substrates of ARTC1 have been identified in various different cell lines overexpressing this enzyme, and these include growth factors and membrane receptors. The basic fibroblast growth factor 2 (FGF-2) was demonstrated to undergo ADP-ribosylation in ARTC1-transfected rat mammary adenocarcinoma (NMU) cells (Boulle, N. et al., 1995; Jones, E.M. and Baird, A., 1997). FGF-2 has a specific extracellular receptor (FGFR), which was initially detected on the surface of adult bovine aortic endothelial and human hepatoma cells. As FGF-2 has a high affinity for heparin, it is localized and possibly sequestered by the heparin sulfates on the cell surface and in the extracellular matrix. Because heparin is an inhibitor of the ADP-ribosylation reaction, the heparin binding of FGF-2 and its ADP-ribosylation are mutually exclusive. Moreover, the ADP-ribosylated site of FGF-2 is located in its receptor-binding domain and, thus, it is possible that ADP-ribosylation modulates the binding of FGF-2 to its receptor and to heparin, regulating its availability to the cell (Boulle, N. et al., 1995; Jones, E.M. and Baird, A., 1997).

Another example of a characterized ARTC1 substrate is the platelet-derived growth factor-BB (PDGF-BB), whereas its structural homolog PDGF-AA is not modified by this reaction (Saxty, B.A. et al., 2001). ADP-ribosylated PDGF-BB loses its ability to stimulate mitogenic and chemotactic responses in human pulmonary

smooth muscle cells (SMCs). Furthermore, it shows a reduced capacity of binding to PDGF receptors in competition-binding experiments, as compared to the unmodified PDGF-BB (Saxty, B.A. et al., 2001). This suggests that PDGF-BB-dependent signaling can be regulated by ARTC1 at the cell surface.

Finally, in murine T-cell lymphoma EL4 cells, overexpressed ARTC1 ADP-ribosylates distinct cell surface molecules, such as lymphocyte-function-associated antigen 1 (LFA-1), cluster of differentiation (CD) 45, CD43 and CD44, resulting in the inhibition of the T-cell receptor trans-membrane signaling (Liu, Z.X. et al., 1999). These effects have been proposed to result from a failure of the T-cell receptors and co-receptors to associate into a functional receptor cluster. Thus, these T-cell responses would be modulated by mono ADP-ribosylation of cell surface proteins (Liu, Z.X. et al.,1999; Nemoto, E. et al.,1996).

All these data suggest that ARTC1 is involved in different processes and, thus, it could assume a role of particular therapeutic relevance. However, with the only exception being HNP-1, all the data reported have been generated using *in vitro* cellular models. Therefore, experimental observation on animal and human models will be crucial for future studies.

1.2.1.2 ARTC2

ARTC2 was originally identified in rat cells as a cell surface alloantigen and was initially indicated as RT6. Its expression is restricted to mature peripheral T-cells, whereas it is expressed only as a small population in mature thymocytes,

appearing to be developmentally regulated (Haag, F. et al., 1990; Koch-Nolte, F. et al., 1999; Koch-Nolte, F. et al., 1996; Koch-Nolte, F. et al., 2008).

The rat *Art2* gene has a single copy composed of eight exons located on chromosome 1. The entire mature protein, composed of 226 amino acids, is encoded by exon 7 (Haag, F.A. et al., 1996). Two allelic variants have been found in rat, Artc2a and Artc2b, which respectively encodes for ARTC2.1 and ARTC2.2. These two allelic variants differ by less than 5% of their amino acid sequences and eight of the ten different amino acids represent a non-conservative change (Haag, F. et al., 1990). The variation of these ten amino acids alters the enzymatic properties of the two proteins: both of them catalyze the hydrolysis of NAD^+ to ADP-ribose and nicotinamide, but only ARTC2.2 can ADP-ribosylate itself.

While the rat carries two strongly divergent alleles of a single copy gene, the mouse *Art2* locus is duplicated, giving rise to the tandem associated gene *Art2a* and *Art2b*, which approximatively differ in 25% in their amino acid sequences (Prochazka, M. et al., 1991). In mice, the two closely related tandem genes are located on chromosome 7 and their products are co-expressed by T-cells and show similar enzymatic activities. My laboratory has reported the molecular cloning and the functional characterization of the first ARTC2 sequence from Chinese hamster ovary (CHO) cells, named (Cricetinae) cARTC2.1 (Stilla, A. et al., 2011). cARTC2.1 has the R-S-EXE active-site motif that is typical of arginine-specific ARTs, with glutamate 209 as the predicted catalytic amino acid. However, cARTC2.1 requires both of the glutamate residues 207 and 209 of the EXE sequence for its activity: although mutation of the catalytic glutamate 209 is enough to strongly

reduce ART activity, only the double mutation, involving both glutamate 207 and glutamate 209, led to the complete loss of activity (Stilla, A. et al., 2011). Unexpectedly, in human and chimpanzee the *Art2* gene contains three premature in-frame stop codons that preclude the expression of the single copy *Art2* gene as a cell surface protein (Haag, F. et al., 1994).

ARTC2 is expressed in resting T-cells and in natural killer cells (Glowacki, G. et al., 2002; Thiele, H.G. and Haag, F., 2001). The presence of ARTC2 on the surface of immune cells would suggest an immunomodulatory activity (Greiner, D.L. et al., 1987). The first relationship between ARTC2 and inflammation was shown for the two murine ARTC2 isoforms that are expressed in T-cells and macrophages (Hong, S. et al., 2009). When activated by NAD^+, ARTC2 catalyses mono-ADP-ribosylation of the purinergic receptor P2X7, that is a member of the P2X family of adenosine triphosphate (ATP)-gated ion channels. Once P2X7 is activated, it causes calcium flux, formation of large membrane pores and exposure of phosphatidylserine (PS), resulting in cell death, which is a crucial component in immune/inflammatory responses. P2X7 could be activated by millimolar concentrations of ATP (Di Virgilio, F. et al., 2001). Interestingly, the same effects can be triggered by much lower (micromolar) concentration of NAD^+ (Seman, M. et al., 2003).

Usually the concentration of extracellular NAD^+ in serum is low (0.1-0.3 μM) and, under basal conditions, ARTC2 is inactive. It activation can only occur when the levels of extracellular NAD^+ increase. Of relevance to the action of ARTC2, intracellular NAD^+ (ca. 500 μM) can be released into the extracellular space under physiopathological conditions caused by tissue injuries, like acute inflammation.

In addition to ARTC2 being prevalently expressed in peripheral lymphoid tissues, Stilla and co-workers first reported that ARTC2 is also expressed and active in the ovarian system, thus demonstrating that the expression of these enzymes is wider than previously believed (Stilla, A. et al., 2011). Moreover, considering the role of ARTC2 in inducing apoptosis in mouse T-cells, it has been investigated whether this was also the case of ovarian cells (Adriouch, S. et al., 2001; Scheuplein, F. et al., 2003). However, experiments on CHO and SKOV-3 cells indicated that cARTC2.1 protein was not involved in apoptosis, since the sensitivity to anisomycin-induced apoptosis was not modified when the cells were transfected with cARTC2.1 (Stilla, A. et al., 2011). Thus, ARTC2's role in apoptosis, which had been well established in mouse T-cells, cannot be extended to the ovarian system.

1.2.1.3 ARTC5

ARTC5 was first cloned from Yac-1 murine lymphoma cells (Okazaki, I.J. et al., 1996b). It is a single copy gene, which maps to mouse chromosome 7 in close proximity to the *Art1*, *Art2a* and *Art2b* genes. Differently from other ARTCs, *Art5* gene lacks the C-terminal hydrophobic GPI-anchor signal and, thus, ARTC5 exists as a secreted protein (Glowacki, G. et al., 2001). The gene transcript is most abundant in testis, but it is also present in cardiac and skeletal muscle. The deduced amino acid sequence is 32% identical to that of mARTC1. hARTC5 has been reported to be an arginine-specific ART, differently from mARTC5, which instead possesses a prominent NAD-glycohydrolase activity (Glowacki, G. et al., 2002).

Even though mARTC5 was found to be primarily a NAD-glycohydrolase enzyme, at a high NAD^+ concentration (1 mM) its ADP-ribosyl-transferase activity increases. The changes in its catalytic activity correlate with auto-ADP-ribosylation of ARTC5, which may suggest that the modification occurs at a critical active site residue (Glowacki, G. et al., 2002). This could be a mechanism for regulating its enzymatic activity.

Furthermore, recent studies have demonstrated that the defensin HNP-1 inhibits hARTC5 auto-ADP-ribosylation and that, even under conditions that promote ART5 activity (e.g. high NAD^+ concentrations), HNP-1 is not significantly modified (Paone, G. et al., 2006).

Despite ARTC5's ability to catalyze auto-ADP-ribosylation, its ADP-ribosylation of other protein substrates remains relatively poor. However, regardless of the lack of identified ARTC5 targets, this enzyme can be responsible for protein ADP-ribosylation in the extracellular environment.

1.2.2 The inactive ARTCs: ARTC3 and ARTC4

ARTC3 and ARTC4 were firstly cloned in human testis and spleen, respectively. Their deduced amino acid sequences show 28% sequence identity to one another, and, with respect to the other gene family members, the highest sequence similarity to ARTC3 is ARTC2 (41%), that of ARTC4 is ARTC1 (39%; Koch-Nolte, F. et al., 1997). The ARTC3 transcript has been found in testis and, at low levels, in intestine, spleen and skeletal muscle (Koch-Nolte, F. et al., 1997). ARTC4 is, instead,

prominently expressed on erythrocytes and, less strongly, on monocytes, splenic macrophages and human umbilical vein endothelial cells (Parusel, I. et al., 2005). The biological functions of both ARTC3 and ARTC4 are still to be elucidated. ART activity on the surface of human monocytes correlates with the presence of ARTC3 in unstimulated monocytes, whereas ARTC4 is expressed only in response to lipopolysaccharide stimulation, as during bacterial infection (Grahnert, A. et al., 2002).

Cell surface ADP-ribosylated proteins on human monocytes are modified on cysteine residues, suggesting that ARTC3 and ARTC4 could be cysteine-specific enzymes (Grahnert, A. et al., 2002). This is consistent with the finding that neither mouse nor human ARTC3 and ARTC4 showed any detectable arginine-specific enzymatic activity, as reported by Glowacki et al. using *in vitro* assays. Indeed, in accordance with this, and in contrast to the other members of the ARTC family, both ARTC3 and ARTC4 lack the motif R-S-EXE in their catalytic site, which is typical of arginine-specific ARTs (Glowacki, G. et al., 2002). Thus, it is possible that these family members may have lost their enzymatic activity or have acquired a different target specificity. Nevertheless, they still maintain some features and functions of the family, similarly to what happens in the largest ARTD family.

1.3 The ADP-ribosyl-transferases diphtheria toxin-like (ARTDs)

The human ARTD enzyme family consists of 17 multidomain proteins that can be divided on the basis of their catalytic activity into polymerases (ARTD1–6), mono-ADP-ribosyl-transferases (ARTD7–17) and the inactives ARTD9 and ARTD13. Poly-

ADP-ribosylation is a PTM that occurs in multicellular organisms, including plants and some lower unicellular eukaryotes, but it is not seen in prokaryotes and yeast (Perina D. et al., 2014). The reaction consists of the addition of multiple ADP-ribose groups on proteins. The first description of poly-ADP-ribosylation dates back to 1963, when Chambon et al reported the formation of a nucleic acid-like polymer from NAD^+. In the following years poly-ADP-ribosylation was intensively studied and research was dominated by studies focusing on the role of this modification and its implication on various cellular processes.

Poly-ADP-ribose (PAR) is a homo-polymer of ADP-ribose units synthesized with β-NAD^+ as a substrate. The chain length of the polymer is heterogeneous and *in vitro* it can reach 200 units. ADP-ribose chains that are shorter in length than 11 units are referred to as oligo-ADP-ribose (Burkle, A., 2005; Diefenbach, J. and Burkle, A., 2005). PAR is irregularly branched with the number of branches increasing with the length of polymer. The average branching frequency is approximately one branch for every 20-50 units of ADP-ribose. Formation of the polymer is obtained through three different steps: initiation reaction (or mono-ADP-ribosylation of the substrate), elongation of the polymer and branching (D'Amours, D. et al., 1999).

The fact that some members of the ARTDs were involved in several critical cellular functions had made these enzymes really attractive as therapeutic targets. So far, a wide range of ARTD inhibitors have been developed in different research areas such as cancer therapy, ischemia, stress response and neurodegenerative diseases (Luo, X. and Kraus, W.L., 2012; Wahlberg, E. et al., 2012). Moreover, the availability

of the crystal structure of the catalytic domain of some ARTDs further improved studies on ARTDs inhibitors (Thorsell, A.G. et al., 2017; Wahlberg, E. et al., 2012).

PARP1 is the founding member of the PARP family and, for many years, it was the only PARP enzyme known. PARP1 is activated by DNA strand breaks and its role in the cellular response to genotoxic and oxidative stress has been widely recognized and studied, with some PARP inhibitors being evaluated in several clinical trials as anticancer therapeutics (Ali, A.A. et al., 2012; Brown, J.S. et al., 2017; Curtin, N.J., 2012; Dulaney, C. et al., 2017; Jungmichel, S. et al., 2013; Kumar, C. et al., 2017; Langelier, M.F. et al., 2012; Martin-Hernandez, K. et al., 2016; Miwa, M. and Masutani, M., 2007; Peralta-Leal, A. et al., 2009). Olaparib was the first PARP inhibitor to be used for the therapy of patients with ovarian tumors and, more recently, it has been approved by US Food and Drug Administration (FDA) for the treatments of this type of cancer (Kim, G., et al., 2015). Moreover, two other PARP inhibitors such as rucaparib and niraparib have recently been approved by FDA for the therapy of patients with ovarian tumors and there are other PARP inhibitors such as talazoparib and veliparib that are currently under clinical trials (Balasubramaniam, S. et al., 2017; Brown, J.S. et al., 2016; Brown, J.S. et al., 2017; Dulaney, C. et al., 2017; Scott, L.J., 2017).

The observation of PARP activity in PARP1$^{-/-}$ mice accelerated the discovery of other PARPs. Firstly, four similar enzymes (PARP2-5) were identified and characterized, and along with PARP1 they constitute the classical *bona fide* PARP family (Jacobson, M.K. and Jacobson, E.L., 1999; Smith, S., 2001). Then, an in-silico analysis of the human genome suggested the existence of other proteins that

share similarities with PARP1 catalytic domains (Otto, H. et al, 2005). To date, 17 members of the PARP family have been identified, which differ from each other in terms of domain organization, transmodification targets, cellular localization, and biological functions (Ame, J.C. et al., 2004; Otto, H. et al. 2005; Schreiber, V. et al., 2006).

However, recent enzymatic data support the view that the earlier proposed name "PARP" and the provided numbering are no longer accurate. Firstly, the term polymerase is commonly used for template-dependent DNA or RNA synthesizing enzymes, but not for enzymes that modify proteins at a defined amino acid (Otto, H. et al., 2005). Moreover, some of the recently identified PARP members were reported to catalyze mono-ADP-ribosylation, and thus do not comply with the name polymerase (Kleine, H. et al., 2008; Otto, H. et al., 2005). Furthermore, some PARP members (e.g. PARP5a and PARP5b) have been shown to be distinct proteins encoded by different genes, rather than splice variants, and therefore should be numbered individually (Hottiger, M.O. et al., 2010).

Thus, for all these reasons, a new classification has been proposed, based on structural and biochemical features of all ARTs. In line with this new nomenclature, enzymes firstly classified as PARP are now named diphtheria-toxin-like ARTs, abbreviated ARTDs, in accordance with the prototype bacterial toxin that their structural aspects resemble, with numbers indicating the different proteins of the family (Hottiger, M.O. et al., 2010).

1.3.1 The ARTDs domains

All ARTDs share a conserved ADP-ribosyl-transferase (ART) domain, which is usually located at the C-terminus of the protein (except in ARTD4). This ART domain represents the catalytic core required for ART activity (Otto, H. et al., 2005; Verheugd, P. et al., 2016).

Besides the ART domain, ARTDs contain many other motifs and domains that differ between all the enzymes and are involved in different functions, such as DNA or RNA binding, protein-protein interactions, cell signaling or enzyme localization (Hottiger, M.O., 2015). The key functional ARTDs motifs and domains are reported in Figure 1.4 and are discussed below.

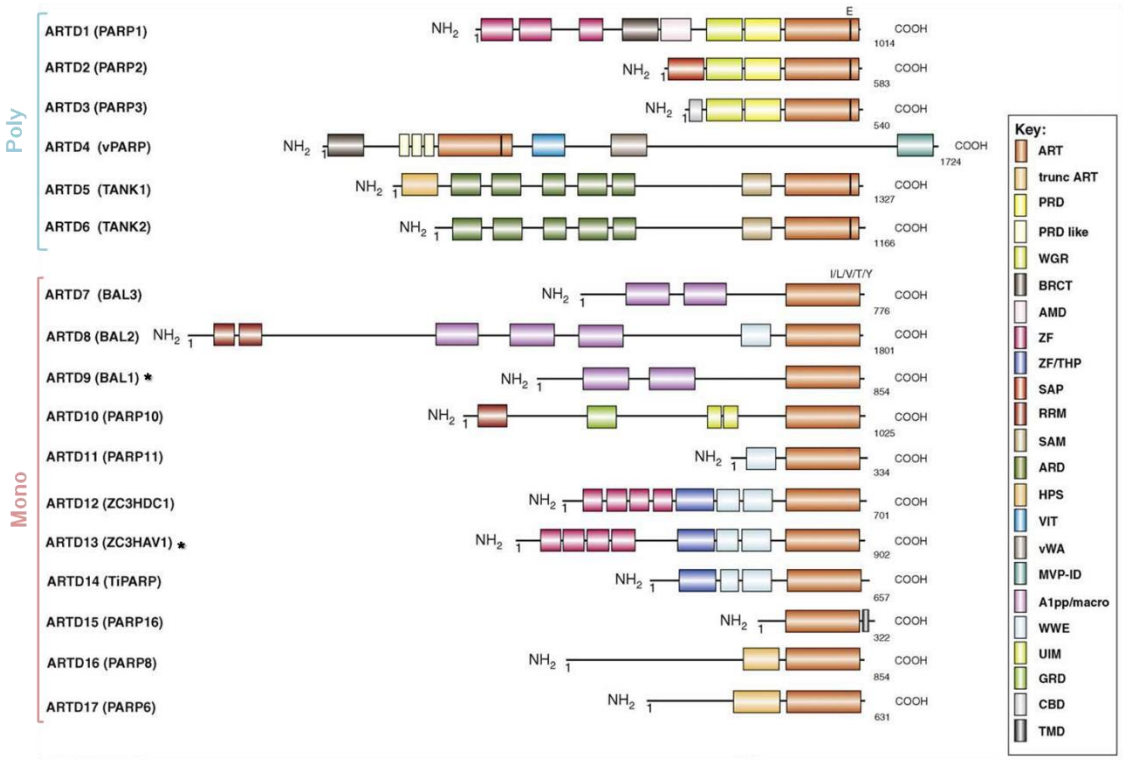

Modified from Hottiger, M.O. et al., 2010

Figure 1.4 The human ARTD family. Schematic comparison of ARTDs based on their domain architecture and their enzymatic activity. The following domains are indicated. ART: ADP-ribosyl-transferase; PRD: PARP regulatory domain; WGR: conserved motif containing W-G-R; BRCT: BRCA1 carboxy-terminal domain; AMD: automodification Domain; ZF: zinc finger; ZF/THP: zinc finger/TiPARP homologous domain; SAP: SAF/Acinus/PIAS-DNA-binding domain; RRM: RNA-binding/recognition motif; SAM: sterile alpha motif; ARD: ankyrin repeat domain; HPS: histidine-proline-serine region; VIT: vault protein inter-alpha-trypsin domain; vWA: von Willebrand type A domain; MVP-ID: Major-vault particle interaction domain; A1pp/macro: A1pp or macro domain; WWE; conserved motif containing W-W-E residues; UIM: ubiquitin interaction motif; GRD: glycine-rich domain; CBD: central binding domain; TMD: trans-membrane domain. Depicted in black within the ART domains are the catalytic glutamates of ARTD1-6. * inactive enzymes

ARTD1-3 are characterized by PRD and WGR domains. The PRD is the PARP regulatory domain and it is thought to be involved in the modulation of the PAR chain branching (Citarelli, M. et al., 2010; Hottiger, M.O. et al., 2010; Langelier, M.F. et al., 2014). The WGR domain represents a motif characterized by the presence of

the conserved amino acid residues tryptophan (W), glycine (G) and arginine (R). It has high affinity for PAR polymers and it has been described as a nucleic acid binding domain (Barkauskaite, E. et al., 2015; Langelier, M.F. et al., 2012). It participates in DNA binding and mediates domain–domain contacts that are essential for DNA-dependent activity (Langelier, M.F. et al., 2014).

ARTD1 also contains three zinc finger (ZF) and one breast cancer type 1 susceptibility protein (BRCA1) carboxy-terminal (BRCT) domains. The ZF domain is a small structural motif usually involved in a wide range of functions, including DNA- or RNA-binding, protein-protein interactions and membrane association (Krishna, S.S. et al., 2003). Specifically, two of the three ZF domains of ARTD1, indicated as ZF-1 and ZF-2, are involved in DNA-binding, acting as DNA nick sensor (Ali, A.A. et al., 2012; Barkauskaite, E. et al., 2015; Langelier, M.F. et al., 2011). The third ZF domain, referred to as ZF-3, is unrelated to ZF-1 and ZF-2, since it is not involved in DNA binding. Instead, it has a role in protein-protein interactions and is crucial for ARTD1 activation and for its DNA-dependent stimulation (Karlberg, T. et al., 2013; Langelier, M.F. et al., 2008; Tao, Z. et al., 2008). In addition to ARTD1, also ARTD12 and ARTD13 contain typical ZF motifs in their N-terminal domains and they have been implicated in RNA-binding (see Chapters 1.3.3.4 and 1.3.4; Barkauskaite, E. et al., 2015; Guo, X. et al., 2004).

The BRCT domain, also present in ARTD4, is a domain predominantly found in cell cycle checkpoint proteins with a role in the DNA damage response (Yu, X. et al., 2003) Studies on ARTD1 BRCT domain suggest it is important for protein-protein

interaction in both DNA repair and cell signaling pathways (Langelier, M.F. and Pascal, J.M., 2013; Loeffler, P.A. et al., 2011; Li, M. et al., 2013).

The vault protein inter-alpha-trypsin (VIT) and the von Willebrand type A (vWA) domains are distinctive features of ARTD4, with probably function in mediating protein-protein interactions (Barkauskaite, E. et al., 2015; Hassa, P.O. and Hottiger, M.O., 2008). Also the major-vault particle interaction domain (MVP-ID) is a unique characteristic of ARTD4, and it is involved in the interaction with the major vault protein, as suggested by name (Kickhoefer, V.A. et al., 1999).

ARTD5 and ARTD6, also known as tankyrases, are characterized by the presence of the sterile alpha motif (SAM) and the ankyrin repeat domains (ARD). SAM is a domain important for mediating multimerization of tankyrases, while ARD is involved in protein-protein interactions (De Rycker, M. et al., 2003; Eisemann, T. et al., 2016; Mariotti, L. et al., 2016; Riccio, A.A. et al., 2016b). Both ARTD5 and ARTD6 contain five ARD in their N-terminal region (Barkauskaite, E. et al., 2015; Eisemann, T. et al., 2016; Smith, S. et al., 1998; Seimiya, H. et al., 2004). Additionally, ARTD5 is characterized by the presence of the HPS domain, a N-terminal domain containing histidine, proline and serine, with a hitherto unclear function (Kaminker, P.G. et al., 2001).

The a1pp or macro domain (A1pp/macro) is specifically found in ARTD7, ARTD8 and ARTD9, which are also known as macro domain containing-mono-ARTDs. Multiple macro domains have been found in these ARTDs, with two in ARTD9 and ARTD7, and three in ARTD8 (Aguiar, R.C. et al., 2005; Barkauskaite, E. et al., 2015). Macro domains have been described as binding modules able to recognize ADP-

ribosylated target, either those mono-ADP-ribosylated or the poly-ADP-ribosylated one, through the binding of the last residue of the poly-ADP-ribose chain (Feijs, K.L. et al., 2013c; Gottschalk, A.J. et al., 2009; Timinszky, G. et al., 2009; see Chapter 1.6.1). Macro domains 2 and 3 of ARTD8 have been shown to recognize mono-ADP-ribosylated substrates (Forst, A.H. et al., 2013). Macro domain 2 of ARTD9 has reported to bind ARTD1-generated poly-ADP-ribose chain at DNA damage sites (Karras, G. I. et al., 2005; Yan, Q. et al., 2013). The function of ARTD9 macro domain 1 of both ARTD8 and ARTD9 still remains to be defined, since they do not bind either poly- or mono-ADP-ribose.

Uniquely among the macro domain containing-mono-ARTDs, but together with ARTD11, ARTD12, ARTD13 and ARTD14, ARTD8 is characterized by the WWE domain (Barkauskaite, E. et al., 2015). It is a domain containing the conserved amino acid sequence tryptophan-tryptophan-glutamate (W-W-E) that has been described to be able to recognize iso-ADPR (Wang, Z. et al., 2012). Structural information about the WWE domain were initially obtained studying ubiquitination-related proteins, another family of proteins characterized by this domain (Zweifel, M.E et al., 2005). However, the determination of the solution structures of ARTD8 and ARTD11 WWE domains demonstrated they have some features resembling that of the ubiquitination-related proteins, but also showing several unique structural features (He, F. et al., 2012; Wei, H. and Yu, X., 2016).

The ubiquitin interaction motif (UIM) is characteristic of ARTD10. This enzyme contains two UIMs that have been reported to interact with K63-poly-ubiquitin chains, promoting mono-ADP-ribosylation of NF-κB (Nuclear Factor-κappaB)

essential modulator (NEMO) and preventing its poly-ubiquitination (Verheugd, P. et al., 2013). As a consequence, NF-κB nuclear translocation is inhibited and this results in impairing the expression of target genes (Verheugd, P. et al., 2013). In addition to this role in inflammation, ARTD10 is also involved in the S-phase repair (Butepage, M. et al., 2015). Indeed, ARTD10's UIMs have been shown to interact with ubiquitinated PCNA (Proliferating Cell Nuclear Antigen) and to be important in maintaining PCNA ubiquitination levels (Nicolae, C.M. et al., 2014).

Comparison of the ART domain of all the ARTDs shows that six diphtheria-toxin-like enzymes are characterized by the presence of a glutamate in the histidine-tyrosine-glutamate (H-Y-E) triad motif (ARTD1–6), the remaining 11 members are characterized by the lack of this glutamate residue, that is replaced by isoleucine (I), leucine (L), threonine (T), valine (V) or tyrosine (Y; ARTD7–17). This glutamate has been demonstrated to be crucial for polymer elongation and, based on its presence, ARTDs have been classified as poly-ARTDs (ARTD1–6), mono-ARTDs (ARTD7,8; ARTD10-12; ARTD14-17) or inactive enzymes (ARTD9 and ARTD13; Figure 1.4; Hottiger, M.O. et al., 2010; Kleine, H. et al., 2008; Otto, H. et al., 2005; Verheugd, P. et al, 2016).

1.3.2 The poly-ARTDs: (ARTD1 to ARTD6)

ARTD1-6 are members of the ARTDs that are typical PARPs, as they all possess the conserved glutamate residue of the H-Y-E triad, which is crucial for polymer elongation (Barkauskaite, E. et al., 2015; Gibson, B.A. and Kraus, W.L., 2012; Hottiger, M.O. et al., 2010; Perina, D. et al., 2014; Verheugd, P. et al., 2016).

ARTD1/PARP1 is the best studied member of this ARTDs group, with a well-defined and detailed structural basis for its DNA damage-dependent activity (Beck, C. et al., 2014; Bock, F.J. and Chang, P., 2016; Langelier, M.F et al., 2012). It is a nuclear protein but there are studies suggesting that ARTD1 could also be present in the mitochondria (Barth, E. et al, 2006; Druzhyna, N. et al, 2000; Scovassi, A.I., 2004).

This protein consists of three modular domains: a N-terminal DNA binding domain consisting of three ZF domains, an automodification domain and a C-terminal ART domain containing the conserved H-Y-E motif (Figure 1.4; Barkauskaite, E. et al., 2015; D'Amours, D. et al., 1999; Hassa, P.O. and Hottiger, M.O., 2008; Karlberg, T. et al., 2013). The DNA binding domain plays a critical role in the recognition of DNA strand aberrations and concurrent activation of ARTD1 (Ali, A.A. et al., 2012; Liu, C. and Yu, X., 2015; Karlberg, T. et al., 2013). The automodification domain is comprised of a BRCA1-carboxy terminus-like module that mediates several protein-ARTD1 and DNA-ARTD1 interactions (Altmeyer, M. et al., 2009; Ciccarone, F. et al., 2017; Langelier, M.F. et al., 2010; Karlberg, T. et al., 2013; Tao, Z et al., 2009).

ARTD1 is responsible for the majority of PARP activity in the cell, and it accounts for approximately 85-90% of mammalian cell poly-ADP-ribosylation activity (Brunyanszki, A. et al., 2016; Karlberg, T. et al., 2013).

ARTD1 is best known for its function in the base excision repair pathway during DNA damage (D'Amours, D. et al., 1999; de Murcia, G. and Menissier de Murcia, J., 1994; Ko, H.L. and Ren, E.C., 2012; Swindall, A.F. et al., 2013; Wei, H. and Yu, X., 2016). It acts as a DNA damage sensor and a signaling molecule binding to both single and double-stranded DNA breaks (Hassa, P.O. and Hottiger, M.O., 2008;

Langelier, M.F. et al, 2011). ARTD1-DNA binding leads to a conformational change of the enzyme, followed by extensive auto-ADP-ribosylation and hetero-ADP-ribosylation of different forms of histones, such as H1, H2B, H3 and H4 (Altmeyer, M. et al., 2009; Hottiger, M.O., 2011; Kim, M.Y. et al., 2005; Liu, C. and Yu, X., 2015; Messner, S. et al., 2010). This causes a complete decondensation of the chromatin structure, allowing access to DNA regions that are normally weakly accessible (Kim, M.Y. et al., 2005; Kraus, W.L. and Hottiger, M.O., 2013).

Apart from its role in DNA repair, ARTD1 is also involved in other complex biological processes such as apoptosis, maintenance of genomic integrity, regulation of replication and differentiation, inflammation and transcriptional regulation (Bock, F.J. and Chang, P., 2016; Hassa, P.O. and Hottiger, M.O., 2008; Kraus, W.L. and Hottiger, M.O., 2013; Malanga, M. and Althaus, F.R., 2005; Koh, D.W. et al., 2005; Schreiber, V. et al., 2006; Yang, Y.G. et al., 2004).

Because of its crucial role in mitosis and cancer, ARTD1 has been at the front line of drug discovery since the 1980s, and the first clinical trial for an ARTD1 inhibitor was initiated in 2003 with rucaparib (Plummer, R. et al., 2008). Since then, other further inhibitors have entered clinical trials with the aim of blocking the mechanism of repair of damaged DNA through ARTD1 inhibition, and thus enhancing the DNA damage caused by chemotherapy and radiotherapy (Brown, J.S. et al., 2017; Curtin, N.J., 2012; Dulaney, C. et al., 2017; Kumar, C. et al., 2017). Currently, several PARP inhibitors such as olaparib, niraparib, talazoparib, veliparib and the same rucaparib are under clinical trials (Brown, J.S. et al., 2016). Some of them are in the last steps of these trials, while olaparib, rucaparib and niraparib

have been recently approved by FDA for the treatment of relapsed ovarian cancer (Balasubramaniam, S. et al., 2017; Scott, L.J., 2017; Kim, G., et al., 2015).

ARTD2/PARP2 is a DNA-dependent nuclear protein which, among all the ARTD members, is the closest relative of ARTD1, since they display the highest sequence homology (69% similarity; Ame, J.C. et al., 2004). Like ARTD1, ARTD2 contains a WGR domain, that is required for DNA-dependent activity, and has the catalytic domain located at the carboxy terminus (Hottiger, M.O. et al., 2010). However, its DNA binding domain is different from that of ARTD1 and, considering that the DNA binding domain of ARTD2 shows no homology to any other ARTDs reported, it may be responsible for the different substrate specificity (Kutuzov, M.M. et al., 2013; Oliver, A.W. et al., 2004).

The main role of ARTD2 is the same of ARTD1 as it acts as a sensor and signaling molecule in response to DNA damage (Beck, C. et al., 2014). Similarly to ARTD1, ARTD2 is activated by DNA nicks and this leads to its auto-ADP-ribosylation and synthesis of long branched chains of PAR (Ame, J.C. et al., 1999; Beck, C. et al., 2014; Ghosh, R. et al., 2016; Langelier, M.F. et al., 2014; Riccio, A.A. et al., 2016a; Schreiber, V. et al., 2002). In addition to its role DNA repair, ARTD2 has other proposed functions in genome integrity, spermatogenesis, adipogenesis and immune cell development (Ali, S.O. et al, 2016; Bai, P. et al., 2007; Dantzer, F. et al., 2006; Robert, I. et al., 2009; Yelamos, J. et al., 2006).

ARTD3/PARP3 is a poly-ARTDs sharing high degree of structural similarity of ARTD catalytic domain and with a conserved glutamate residue as compared to ARTD1 and ARTD2 (Barkauskaite, E. et al., 2015; Hottiger, M.O. et al., 2010). It has been

firstly identified as a core component of the centrosome preferentially located at the daughter centriole throughout all stages of the cell cycle (Augustin, A. et al., 2003). ARTD3 overexpression interfered with the G1/S phase cell cycle progression and it was described to interact with ARTD1 at the centrosome (Augustin, A. et al., 2003). Nevertheless, further studies disputed the centrosomal localization of ARTD3 and suggested that ARTD3 localized to the nucleus and associated with polycomb group proteins involved in gene silencing and DNA repair networks including DNA protein kinases, DNA ligase III and IV, Ku70 and Ku80 and ARTD1 (Boehler, C. et al., 2011; Rouleau, M. et al., 2007). Boehler and colleagues demonstrated ARTD3 cooperates with ARTD1 during the cellular response to DNA double-strand breaks, pertinent to association with Ku and Ligase IV (Boehler, C. et al., 2011).

Initially, auto-ADP-ribosylation and hetero-ADP-ribosylation activities of ARTD3 were described as mono-ADP-ribosyl-transferase activity (Loseva, O. et al., 2010). However, a later report has suggested that ARTD3 possessed poly-ADP-ribosyl-transferase activity (Boehler, C. et al., 2011). In particular, ARTD3 was described to poly-ADP-ribosylate the nuclear mitotic apparatus protein (NuMA) directly and indirectly through ARTD5, suggesting that ARTD3 was required for mitotic spindle integrity during mitosis (Boehler, C. et al., 2011). Collectively, these reports implicate ARTD3 in the maintenance of genomic integrity, mitotic spindle integrity and transcriptional repression.

ARTD4/PARP4/vPARP is the largest member of the ARTD family and has originally been identified as a component of mammalian cytoplasmic ribonucleoprotein

complexes called vault particles that have been proposed to be involved in multidrug resistance of human tumors and to function in intracellular transport (Kickhoefer, V.A. et al., 1999). ARTD4 associates with two essential proteins of the vault particle, major vault protein (MVP) and telomerase-associated protein (TEP1; Kickhoefer, V.A. et al., 1999). ARTD4 is also present in the nucleus where it is not attached to the vault components, and at the mitotic spindle, suggesting that it may play multiple roles not yet identified (Kickhoefer, V.A. et al., 1999).

The structure of ARTD4 is unusual, since it is the only ARTD member to have its catalytic domain located at the N-terminal portion of the protein (Barkauskaite, E. et al., 2015; Hottiger, M.O. et al., 2010; Schreiber, V. et al., 2006). It comprises of five major domains, which are the BRCT motif, the catalytic ARTD domain, the breast cancer vault protein inter-α-trypsin (VIT) domain, the von Willebrand type A (vWA) domain and finally the major vault protein particle interacting domain (MVP-ID; Hottiger, M.O. et al., 2010). BRCT domain is thought to bind phosphorylated DNA damage-sensing proteins (Manke, I.A. et al., 2003). VIT and vWA domains are presumed to mediate protein-protein interactions (Hassa, P.O. and Hottiger, M.O., 2008). MVP-ID is involved in the interaction with the major vault protein, as suggested by its name. MVP mRNA (messenger RNA) levels are shown to be an indicator of the multidrug resistance (MDR), which is a major cause of chemotherapy failure in the cancer patients (Laurencot, C.M. et al., 1997; Liu, C. and Yu, X., 2015; Siva, A.C. et al., 2001; Steiner, E. et al., 2006). Despite this unique feature, ARTD4 is catalytically active and poly-ADP-ribosylates MVP as well as itself

(Barkauskaite, E. et al., 2015; Berger, W. et al., 2009; Butepage, M. et al., 2015; Kickhoefer, V.A. et al., 1999).

ARTD5/PARP5a/Tankyrase-1 and ARTD6/PARP5b/Tankyrase-2 are two closely related ARTD family members sharing 83% sequence identity between each other and 89% sequence identity with the catalytic ARTD domain (Kaminker, P.G. et al., 2001; Kuimov, A.N. et al., 2001; Smith, S. et al., 1998). They differ from other ARTD members because of their unique domain organization, that is composed of a SAM domain, which is required for the tankyrases oligomerization, and the characteristic catalytic ARTD domain (Barkauskaite, E. et al., 2015; Haikarainen, T. et al., 2014; Hottiger, M.O. et al., 2010; Schreiber, V. et al., 2006). Their N-terminal consists of a region comprising of 24 ankyrin repeats, which are segmented into five ARD (ARD I-V) and are used to interact with the target proteins (Haikarainen, T. et al., 2014; Karlberg, T. et al., 2013; Smith, S. et al., 1998; Seimiya, H. et al., 2004). ARTD5 has an additional region at the N-terminal that contains an HPS domain; this additional region most likely has a regulatory function, although it is not well studied and its main function is unknown so far (Haikarainen, T. et al., 2014; Kaminker, P.G. et al., 2001; Karlberg, T. et al., 2013).

Tankyrase-1 localizes to multiple subcellular sites, as it has been found in the cytoplasm as well as in the nucleus (Karlberg, T. et al., 2013; Smith, S. and de Lange, T., 1999; Cook B.D. et al., 2002; Seimiya, H. and Smith, S., 2002). Although tankyrase-1 does not contain an NLS, it is present in the nucleus through its interaction with the telomeric repeat binding factor 1 (TRF1), which contains an NLS (Karlberg, T. et al., 2013; Smith, S. and de Lange, T., 1999; Hsiao, S.J. and Smith, S.,

2008). The intracellular location of tankyrase-2 is less characterized but it has been reported to have a localization similar to that of tankyrase-1 (Haikarainen, T. et al., 2014; Karlberg, T. et al., 2013; Sbodio, J.I. et al., 2002). Tankyrases have been implicated in a diverse range of functions including telomere maintenance, WNT signaling, mitosis and mediation of insulin stimulated glucose uptake (Barkauskaite, E. et al., 2015; Haikarainen, T. et al., 2014).

ARTD5 has first been discovered as a factor that regulated telomere length by binding the negative regulator of telomere length TRF1 and was originally named tankyrase 1 due to its interaction with this factor (Smith, S. et al., 1998). ARTD5 catalyzes auto-poly-ADP-ribosylation and poly-ADP-ribosylation of TRF1, and, a careful analysis of ARTD5 auto-ADP-ribosylation revealed that it synthesizes ADP-ribose polymers with an average length of 20 ADP-ribose units, but polymers lack branching (Haikarainen, T. et al., 2014; Rippmann, J.F. et al., 2002; Smith, S. et al., 1998).

ARTD6 has also been reported to associate with and poly-ADP-ribosylate TRF1, indicating a potential redundant role of ARTD5 and ARTD6 in telomere regulation (Cook, B.D. et al., 2002; Haikarainen, T. et al., 2014; Kaminker, P.G. et al., 2001). ARTD6 also associates with ARTD5 and both enzymes share most of their protein partners including insulin-responsive aminopeptidase (IRAP), NuMA and 182 kDa tankyrase-binding protein (TAB182; Haikarainen, T. et al., 2014; Kaminker, P.G. et al., 2001; Karlberg, T. et al., 2013; Sbodio, J.I. and Chi, N.W., 2002; Sbodio, J.I. et al., 2002; Seimiya, H. and Smith, S., 2002).

Overall, the recent findings about poly-ARTs and their relative targets establish poly-ADP-ribosylation as a protein modification involved in an impressive array of regulatory pathways. A better understanding of the role of these enzymes in both these physiological and pathophysiological processes will be of clinical relevance.

1.3.3 The active mono-ARTDs

As previously mentioned, the mono-ARTs of the ARTD family have amino acid substitutions in their catalytic centers that enables them to attach just mono ADP-ribose moieties to the target proteins (Hottiger, M.O. et al, 2010; Kleine, H. et al, 2008). This subfamily comprises of ARTD7-ARTD17, excluding ARTD9 and ARTD13, which are described as inactive or pseudo ARTDs. ARTD9 and ARTD13 lack both the catalytic glutamate as well as the histidine of the H-Y-E triad and are predicted to be catalytically inactive (Liu, C. and Yu, X., 2015; Otto, H. et al., 2005; Vyas, S. et al., 2014).

The remaining mono-ARTDs do not contain the catalytic glutamate of the H-Y-E motif that is characteristic of polymer forming ARTDs, since it is required for elongation of the ADP-ribose chain (Otto, H. et al, 2005). For instance, the glutamate E988 in human ARTD1 (hARTD1) has been shown to be essential for the ARTD1 elongation reaction and, thus, for the formation of poly-ADP-ribose chains (Marsischky, G.T. et al., 1995; Rolli, V. et al., 1997). Despite this fundamental difference, mono-ARTDs also modify acidic residues and they are proposed to utilize the glutamate of the substrate protein and thus follow the substrate-assisted catalysis mechanism (Kleine, H. et al., 2008).

However, several studies indicate that mono-ARTDs play critical roles in intracellular signaling, such as transcription, immunity, inflammation, and stress response and have been linked to many human diseases, including neurodegenerative and inflammatory diseases, and the onset and progression of cancers (Table 1.3; Fabrizio, G. et al., 2015a; Feijs, K.L. et al., 2013a).

Table 1.3 Active mono-ARTDs.

Family	Nomenclature (Alternative names)	Catalytic motif	Cellular localization	Target	Activators	Physiological roles	Diseases
ARTD	ARTD7 (PARP15/BAL3)	H-Y-L	Stress Granules	Auto-modification	IL4	Stress Granules Assembly	Cancer (DLBCL)
	ARTD8 (PARP14/BAL2/CoaSt6)	H-Y-L	Nucleus (main), Cell periphery, Stress Granules	HDAC2/3, p100	IL4	IL4- and Stat6-dependent transcription	Cancer (DLBCL; B-lymphoma), Inflammation (AAD)
	ARTD10 (PARP10)	H-Y-I	Cytoplasm (main), Nucleus	GSK3β, NEMO, Ran	INF	Inhibits Cell proliferation, Pro-apoptotic	Neurological disease (ALS), Inflammation
	ARTD11 (PARP11)	H-Y-I	Nucleus (main), Cytoplasm (additional)	Unknown	-	Unknown	Unknown
	ARTD12 (PARP12/ZC3HDC1)	H-Y-I	Golgi apparatus, Stress Granules	Unknown	INF	Stress Granules Assembly	Alphaviruses clearance
	ARTD14 (PARP7/TiPARP/RM1)	H-Y-I	Nucleus	PEPCK	INF TCDD	Gluconeogenesis	Unknown
	ARTD15 (PARP16)	H-Y-Y	Endoplasmic reticulum	IREβ1α, PERK, Kapβ1	Stress	Nucleo-cytoplasmic transport, UPR	Inflammation
	ARTD16 (PARP8)	H-Y-I	Nucleus (main), Cytoplasm (additional)	Unknown	-	Unknown	Unknown
	ARTD17 (PARP6)	H-Y-I	Cell membrane (main)	Unknown	-	Inhibits Cell cycle progression	Cancer (colorectal)

Modified from Fabrizio, G. et al., 2015a

1.3.3.1 ARTD7 and ARTD8

ARTD7 (PARP15/BAL3) was originally identified, together with ARTD8 (PARP14/BAL2) as a gene closely related to ARTD9 (PARP9/BAL1; B-aggressive lymphoma 1, see Chapter 1.3.1.7; Aguiar, R.C. et al., 2000; Aguiar, R.C. et al., 2005; Butepage, M. et al., 2015)

These three members of the ARTD family are characterized by the presence of N-terminal macro domains, with two in ARTD9 and ARTD7, and three in ARTD8 (Figure 1.4; Aguiar, R.C. et al., 2005). Thus, these are collectively known as macro domain containing-mono-ARTDs. Macro domains are protein domains known to

bind mono- and poly-ADP-ribose (Forst, A.H. et al., 2013; Han, S. and Tainer, J.A., 2002; Kleine, H. and Luscher, B., 2009). Recently, macro domains 2 and 3 of ARTD8 were reported to recognize and read mono-ADP-ribosylated ARTD10 and substrates of ARTD10 (Forst, A.H. et al., 2013). It has been demonstrated that these two ARTD8 macro domains bind to mono-ADP-ribosylated targets and this association is strictly dependent on the presence of mono-ADP-ribosylation, as they do not associate to poly-ADP-ribosylated proteins (Forst, A.H. et al., 2013). Thus, they have been indicated as mono-ADP-ribosylation reader modules.

Both ARTD7 and ARTD8 demonstrate auto-mono-ADP-ribosylation activity (Aguiar, R.C. et al., 2005).

Little is known about ARTD7, besides that it is localized to stress-granules along with ARTD8, it has been reported to have a transcriptionally repressive function through its N-terminal macro domains and its auto-ADP-ribosylation activity has been suggested to counteract the repressive effect of the macro domains (Aguiar, R.C. et al., 2005).

Whereas ARTD7 remains poorly characterized, ARTD8 is better understood and has been implicated in STAT6 (Signal Transducer and Activator of Transcription 6)-dependent transcriptional control and cytokine-regulated control of cellular metabolism (Cho, S.H. et al., 2011; Goenka, S. et al., 2007). Thus, it is also known as CoaSt6 (Collaborator of Stat6) and as an activator of interleukin 4 (IL-4)– and Stat6–dependent transcription. ARTD8 potentiated IL4-induced STAT6 transactivation via its macro domains and catalytic activity (Goenka, S. and Boothby, M., 2006; Goenka, S. et al., 2007). ARTD8 also catalyses ADP-ribosylation

of p100, a protein that interacts with RNA polymerase II and functions as a bridging factor between Stat6 and the transcription machinery (Yang, J., et al., 2002). However, the functional consequences of this modification remain to be characterized in detail.

Similarly, the role of ARTD8-mediated ADP-ribosylation of the HDAC2 and HDAC3 histones deacetylases remains unclear. However, in the presence of IL-4, the ART activity of ARTD8 is activated, and HDAC2 and HDAC3 are ADP-ribosylated and released from their promoters, allowing the binding of Stat6 and the consequent transcription (Yang, J., et al., 2002). In line with this, a catalytically inactive mutant of ARTD8 did not enhance Stat6-mediated transcription, and ART inhibitors blocked IL-4–dependent transcription (Goenka, S. et al., 2007).

Moreover, in response to IL-4, ARTD8 is also involved in proliferation and survival of B-lymphocytes, with a role in the regulation of the glycolytic activity of these cells (Cho, S.H. et al., 2009; Cho, S.H. et al., 2011). This is in line with the requirement for a major supply of cellular biomass to sustain continuous cell growth and proliferation of cancer cells. ARTD8 also interacts with and stabilizes the phosphoglucose isomerase/ autocrine motility factor (by inhibiting its ubiquitination), a cytosolic and secreted enzyme that is essential for glycolysis and gluconeogenesis and that is involved in tumor progression and metastasis (Yanagawa, T. et al., 2007). Recently, ARTD8 was also identified as a downstream effector of the Jun N-terminal kinase 2 (JNK2)-dependent pro-survival signal by binding to and inhibiting JNK1 pro-apoptotic activity, promoting the survival of myeloma cells (Barbarulo, A. et al., 2013).

Intriguingly, ARTD8 has been found to be localized not only in the nucleus, but also at the cell periphery, together with ARTD9, where it associates with actin fibres (Vyas, S. et al., 2013). Because human actin has been previously reported to be modified not only by the bacterial toxins, but also by a not yet identified endogenous enzyme (Fabrizio, G. et al., 2015a; Lodhi, I.J. et al., 2001), it could be hypothesized that the ART activity of ARTD8 can modify actin, affecting actin polymerization and cell proliferation. Finally, the ART activity of ARTD8 has been seen to be involved in the pathogenesis of asthma using a murine model of allergic airway disease, in line with the regulatory role of ARTD8 on IL-4– and STAT6–dependent transcription and with the roles that IL-4 and STAT6 have in asthma (Mehrotra, P. et al., 2013). Thus, considering the widely studied roles of ARTD8 in cancer and its emerging role in allergic airway diseases, the targeting of ARTD8 activity appears to be of particular therapeutic relevance for lymphoma, myeloma and asthma.

1.3.3.2 ARTD10

ARTD10, also known as PARP10, is the founding member of the mono-ARTDs and was initially discovered through in silico screening of ARTD family members (Ame, J.C. et al., 2004). It is a 150-kDa enzyme that comprises several domains of potential functional relevance. With the exception of the ART catalytic domain, ARTD10 domain structure is unique from the other ARTDs. In addition to the C-terminal ART catalytic domain (amino acids 818-1025), the ARTD10 sequence is characterized by an RNA-recognition motif (RRM; amino acids 11-85), a glycine-

rich domain (amino acids 281-399), a glutamic acid (Glu)-rich region (amino acids 588-697) containing two ubiquitin interaction motifs (UIM; amino acids 650-667, 673-690); and a leucine-rich nuclear export sequence (NES; amino acids 598-607; Figure 1.4). The RRM and the glycine-rich domain are both involved in the RNA binding (Yu, M. et al., 2005).

ARTD10 is predominantly cytosolic under basal conditions, but it can shuttle between the cytoplasmic and the nuclear compartments (Kleine, H. et al., 2012). The nuclear export of ARTD10 is mediated through its NES, while a region that acts as a nuclear localization signal (NLS), that has been mapped in the middle of ARTD10, defines its nuclear import (Kleine, H. et al., 2008).

Besides mono-ADP-ribosylation, ARTD10 undergoes auto-ADP-ribosylation as well as modifying each of the four core histones. It has also been reported to interact with the proto-oncoprotein c-Myc, a key transcriptional regulator of cell proliferation (Kleine, H. et al., 2008; Yu, M. et al., 2005). When overexpressed in various cell lines, ARTD10 acts as an inhibitor of the c-Myc- and H-ras-mediated cell transformation and this role is independent of its ADP-ribosylation activity; neither c-Myc nor its heterodimerization partner Max were ADP-ribosylated by ARTD10 (Yu, M. et al., 2005). However, the catalytic activity of ARTD10 is strictly required to inhibit cell proliferation, since its catalytically inactive mutant is not effective (Herzog, N. et al., 2013). Specifically, the catalytically active ARTD10 inhibits cell proliferation, as revealed by measurements of living cells, and this is a consequence of apoptosis induction, as determined by Annexin V staining and by analysis of cleaved ARTD1 (Herzog, N. et al., 2013).

Although it remains unknown which protein(s) are mono-ADP-ribosylated by ARTD10 to mediate this growth inhibitory phenotype, a possible candidate is the glycogen synthase kinase 3 beta (GSK3β), which is known to regulate cell proliferation and whose kinase activity is inhibited once it is modified by ARTD10 (Feijs, K.L. et al., 2013b; Wu, D. and Pan, W., 2010).

The ARTD10 target GSK3β appears to have a role in neurodegenerative disorders, as its overexpression causes neuronal cell death (Seira, O. and Del Rio, J.A., 2014). GSK3β has been implicated in the fatal neurodegenerative disease amyotrophic lateral sclerosis (ALS), which is characterized by degeneration of motor neurons, resulting in progressive motor paralysis. Mutations in the gene coding for superoxide dismutase (SOD1) are associated with approximately 20% of familial ALS. Different studies have shown that GSK3β inhibition can prevent motor neuron cell death in an *in vitro* ALS model that is characterized by expression of the G93A mutant of human SOD1 (Ahn, S.W. et al., 2012). Thus, through mono-ADP-ribosylation of GSK3β, ARTD10 can act as an inhibitor of cell proliferation and also as a regulator of neuronal cell death.

Recently, ARTD10 has also been reported to have a role in the NF-κB) transcription factor signaling. The NF-κB family is involved in cell proliferation, innate and adaptive immune responses, and further crucial processes, like inflammation and tumorigenesis (DiDonato, J.A. et al., 2012). ARTD10 is a regulator of the NF-κB pathway by mono-ADP-ribosylating NEMO, reducing its poly-ubiquitination and activation of NF-κB (Verheugd, P. et al., 2013). However, unlike the regulation of c-Myc, the regulation of NF-κB is dependent on ARTD10 catalytic activity and on

the UIMs (Verheugd, P. et al., 2013). Moreover, in addition to its role in cell signaling pathways that regulate proliferation and apoptosis, ARTD10 expression can also be induced by LPS and IFNα, which indicates its further involvement in immunological processes (Eckei, L. et al., 2017).

1.3.3.3 ARTD11, ARTD16 and ARTD17

ARTD11, ARTD16 and ARTD17 are three mono-ARTDs that, with the exception of the typical mono-ART catalytic domain, remain to be characterized for the presence of other motifs and domains. ARTD11, also denoted as PARP11, and ARTD16, also referred to as PARP8, are minimally investigated members of the mono-ARTDs. The limited studies available for them indicate they have no known domains outside of their catalytic one, with the exception of the single tryptophan-tryptophan-glutamate (WWE) domain of ARTD11, which it has been reported to bind ADP-ribose (He, F. et al., 2012). Also their functions have not been determined to date.

ARTD17, also known as PARP6, is a mono-ARTD with possible involvement in cancer. It has been described as a negative regulator of cell-cycle progression in HeLa cells, as ARTD17 overexpression was reported to arrest cells in S-phase and this was dependent on the presence of the catalytic domain (Tuncel, H. et al., 2012). Moreover, a role for ARTD17 as tumor suppressor involved in colorectal cancer development has been proposed. The immunohistochemical analysis of human colorectal cancer specimens has shown that ARTD17 expression is inversely correlated with Ki-67, which is a well-known proliferation marker, and is associated

with a good prognosis. Thus, it has been hypothesized that ARTD17 expression levels might be used as a prognostic biomarker for improved survival of patients with colorectal cancer (Tuncel, H. et al., 2012). However, the catalytic activity of ARTD17 has not been evaluated and its potential activity in other cellular functions has not yet been fully determined.

1.3.3.4 ARTD12

ARTD12, also known as PARP12, is a member of the mono-ARTDs whose function is still incompletely characterized. ARTD12 belongs to a subgroup of ARTD family members characterized by the presence of typical ZF motifs in its N-terminal domain, which are known to bind to viral, and also cytoplasmic, RNAs (Guo, X. et al., 2004; Guo, X. et al., 2007; Hall, T.M., 2005; Liang, J. et al., 2008). Thus, it is also referred to as ZC3HDC1, zinc finger CCCH type domain containing 1. ARTD12 exists in two isoforms denoted as long (L) and short (S) ARTD12 (ARTD12L and ARTD12S, respectively; Atasheva, S. et al., 2012). ARTD12L is a protein composed of 711 amino acids containing all the five ZF domains and the ART domain, which is crucial for the catalytic activity. ARTD12S is a protein of only 485 amino acids that contains the same five ZF domains, but lacks the ART domain (Atasheva, S. et al., 2012). ARTD12 is a mono-ADP-ribosyl-transferase with automodification activity and it possesses at least two distinct subcellular locations and related functions. Unlike many other ARTD members, ARTD12 is largely excluded from the nucleus, and appears to localize into distinct cytoplasmic structures in a protein domain-dependent manner (Welsby, I. et al., 2014).

Upon ectopic expression or exposure to oxidative stress, it is recruited to stress-granules (SGs), where ARTD12 blocks mRNA translation through its association with the translational machinery. Both the N-terminal domain and the integrity of the catalytic domain are essential for this function (Leung, A.K. et al., 2011; Welsby, I. et al., 2014). Moreover, ARTD12 associates with both long and short isoforms of ARTD13 (short isoform is missing the catalytic domain), ARTD5 and ARTD7 within these stress granules (Leung, A.K. et al., 2011). Otherwise, under stimulation with lipopolysaccharide (LPS), ARTD12 localizes into structures unrelated to SGs. The association into these structures has been found to correlate with increased NF-κB signaling, suggesting a role for ARTD12 in inflammation (Welsby, I. et al., 2014). ARTD12 has been recently identified as a putative anti-viral gene, belonging to a large family of interferon-stimulated genes (ISGs) whose expression is often induced during viral infections (De Veer, M.J. et al., 2001; Liu, S.Y. et al., 2012). After infection by the alphavirus Venezuelan equine encephalitis virus (VEEV), ARTD12L is up-regulated and exhibits inhibitory effects on replication (Atasheva, S. et al., 2012). The same inhibitory effects on replication of VEEV have also been shown for other alphaviruses and RNA viruses (Atasheva, S. et al., 2012). Interferon stimulation up-regulates *Artd12* gene expression to counteract infections through inhibition of both cellular translation and virus replication. These inhibitions and antiviral activities depend on its binding to polyribosomes, via its RNA-binding domain, and requires its catalytic activity (Atasheva, S. et al., 2014). This process has been suggested to be a cellular defense against invading viral pathogens, although this has not yet been mechanistically investigated (Schoggins, J.W. et al.,

2011). More recently, expression of ARTD12 has also been found elevated in tissues from mice subjected to bacterial superantigen Staphylococcal enterotoxin B (SEB) mediated toxic shock, suggesting a potential role of this protein during immune activation (Ferreyra, G.A. et al., 2014).

1.3.3.5 ARTD14

ARTD14 is a 75-kDa nuclear mono-ARTD that is also known as PARP7 or TiPARP (2,3,7,8-tetrachlorodibenzo-p-dioxin (TCDD)-inducible PARP). Its expression is induced by TCDD, which is a carcinogen and a potent activator of the ligand-activated transcription factor aryl hydrocarbon receptor (AHR; Diani-Moore, S. et al., 2010; Ma, Q. et al., 2001). Once activated by ligand binding, AHR translocates into the nucleus, dimerizes with its binding partner AHR nuclear translocator (ARNT) and acts as a transcription factor (Ma, Q. et al., 2001).

Upon TCCD treatment, a decreased gluconeogenesis is observed, which is at least in part due to repression of AHR-mediated transcription of phosphoenolpyruvate carboxykinase (PEPCK). ARTD14 over-expression reproduces the TCDD effects on glucose metabolism, and it has been suggested that ARTD14 mediates these TCDD effects (Diani-Moore, S. et al., 2010). TCDD-dependent transcriptional induction of ARTD14 leads to ADP-ribosylation of cytosolic and mitochondrial PEPCKs (Diani-Moore, S. et al., 2013). However, as AHR suppression also enhances ADP-ribosylation, it is clear that the complex modulatory effects on ADP-ribosylation by AHR are far from being defined at present (Diani-Moore, S. et al., 2013). Further research has shown that ARTD14 is itself regulating AHR signaling in a negative

feedback loop by acting as a transcriptional repressor (MacPherson, L. et al., 2013). However, it also acts with a different mechanism from that of AHR repressor (AHRR), as the silencing of ARTD14, but not that of AHRR, increases TCDD-induced AHR protein levels, whereas the silencing of both ARTD14 and AHRR enhances AHR transactivation (Macpherson, L. et al., 2014).

Interestingly, over-expression of MACROD1, one of the member of the macro domain family (see Chapter 1.6.1), but not that of MACROD2, is able to reverse the repressive effect of ARTD14, as shown in a reporter gene assay, and interacts with AHR (Ahmed, S. et al., 2015). This evidence suggests that ARTD14-mediated mono-ADP-ribosylation functions as an important PTM in the pathway controlling the response to environmental toxins and that MACROD1 might antagonize the repressive effect of ARTD14 by removing mono-ADP-ribosylation from ARTD14, AHR and other so far unidentified substrates (Butepage, M. et al., 2015).

1.3.3.6 ARTD15

ARTD15, previously known as PARP16, is the smallest member of the ARTD family. It has been the first ARTDs to be found to associate with the endoplasmic reticulum (ER; Di Paola, S. et al., 2012). It is a single-pass transmembrane protein with the N-terminal region (amino acids 1-280) positioned towards the cytoplasm, and the very short C-terminal tail (amino acids 300-322) in the ER lumen. In line with this orientation towards the cytosolic compartment, ARTD15 interacts with and modifies the nuclear transport factor karyopherin-β1/importin-β1 (Kapβ1; Di Paola, S. et al., 2012). Kapβ1 is selectively mono-ADP-ribosylated by ARTD15 and this

modification has been hypothesized to control the nucleo-cytoplasmic shuttling of cellular proteins, as the pivotal role of Kapβ1 is to be a carrier protein regulating the transport of various cargo proteins through the nuclear pore complex (Di Paola, S. et al., 2012). However, it remains open what the consequence of mono-ADP-ribosylation is for the function of Kapβ1.

ARTD15 also demonstrates auto-mono-ADP-ribosylation that could be inhibited with some well-characterized ARTD inhibitors, such as MIBG (meta-iodobenzylguanidine) and PJ34 (N-(6-oxo-5, 6-dihydrophenanthridin-2-yl)-N, Ndimethylacetamide HCl; Di Paola, S. et al., 2012; Karlberg, T. et al., 2012). Furthermore, mono-ADP-ribosylation has not been reported to occur at arginine, glutamate or cysteine residues and could not be reverted by ADP-ribosyl-hydrolase 1 and 3 (ARH1, ARH3; Di Paola, S. et al., 2012). Moreover, ARTD15 is required for activation of two proteins involved in the ER stress response during the unfolded protein response (UPR): the double-stranded RNA-dependent protein kinase (PKR)-like ER kinase (PERK) and the inositol-requiring enzyme 1α (IRE1α; Jwa, M. and Chang, P., 2012). During ER stress, ARTD15 has been found to auto-ADP-ribosylate itself and ADP-ribosylate PERK and IRE1α, increasing their kinase activities and the endoribonuclease activity of IRE1α, which are necessary for a proper execution of the UPR (Jwa, M. and Chang, P., 2012). However, the role of ARTD15 in the UPR needs further investigations. Considering the ability of ARTD15 to modify Kapβ1, PERK and IRE1α, it is emerging as a novel attractive therapeutic target, since it has a role in the regulation of nucleo-cytoplasmic trafficking and in the UPR, cellular processes that are both involved in different

diseases, such as inflammation, neurodegeneration and cancer (Fabrizio, G. et al., 2015a).

A recent study has implicated ARTD15 activity in cystic fibrosis (CF). This study provided evidence that analogs of latonduine, through the modulation of ARTD15 activity, restored one of the most common mutations of the CF transmembrane conductance regulator gene (CFTR; Carlile, G.W. et al., 2016). This CFTR mutation generates a protein that is misfolded and retained in the endoplasmic reticulum. To date, a promising therapeutic approach was represented by the use of latonduine, a marine sponge metabolite identified as a corrector of this mutation. A series of latonduine analogs have further been developed and they have been shown to function as correctors of CFTR mutation by the inhibition of ARTD15 activity and the consequent blocking of IRE1α ribosylation (Carlile, G.W. et al., 2016). The ribosylation of IRE1α has been reported to be essential for its activation during the UPR (Jwa, M. and Chang, P., 2012). Preventing this activation through ARTD15 inhibition and IRE1α activity modulation blocked the increased expression of chaperones which should have helped to process the misfolded CFTR in the ER before transport for proteasomal degradation, thus allowing partially misfolded mutated CFTR to escape the ER quality control and traffic to the plasma membrane (Carlile, G.W. et al., 2016). Indeed, when surface expression of mutated CFTR is restored, it retains some function, however, its stability in the plasma membrane and open probability are reduced compared with wild-type channels (Hwang, T.C. and Sheppard, D.N., 2009; Lukacs, G.L. et al., 1993). These findings, in addition to opening new areas of investigation about IRE1α role in CFTR rescue, also

strengthened the importance of ARTD15-mediated ADP-ribosylation and its emerging role as a therapeutic target for different diseases, including those with protein-trafficking defects.

1.3.4 The inactive ARTDs: ARTD9 and ARTD13

ARTD9 is a nucleo-cytoplasmic shuttling protein that has been identified as a risk-related gene product in aggressive diffuse large B-cell lymphoma (DLBCL), the most common non-Hodgkin lymphoma (Aguiar, R.C. et al, 2000; Camicia, R. et al., 2013; Juszczynski, P. et al., 2006; Shaffer, A.L. 3rd et al., 2012). ARTD9, as for the other members of the macro domain-containing mono-ARTDs family (ARTD7 and ARTD8), has two prototypical macro domains within the N-terminus, which can bind mono- and poly-ADP-ribose (Barkauskaite, E. et al., 2015; Feijs, K.L. et al., 2013c; Karras, G.I. et al., 2005). It has been described to possess transcriptional repressive activity that was dependent on interaction through these macro domains but independent of its catalytic activity, since ARTD9 does not show any ART activity (Aguiar, R.C. et al., 2005; Feijs, K.L. et al., 2013c).

Over-expression of ARTD9 promoted lymphocyte migration, indicating a tumor-promoting role in high-risk DLBCL (Aguiar, R.C. et al., 2000), which has been suggested to be through modulation of interferon gamma (IFNγ) signaling-related gene expression (Juszczynski, P. et al., 2006). It is known that IFNγ is secreted by host-activated tumor-infiltrating T lymphocytes and it induces expression of ARTD9 and its interactor BBAP (B-lymphoma and BAL-associated protein) in DLBCL cell lines. ARTD9 induction, in turn, promotes the transcription of

interferon-controlled genes (Juszczynski, P. et al., 2006). Thus, by inhibiting the host immune response against the lymphoma, ARTD9 can function as a transcriptional activator of tumor genes in an inflammatory environment. Furthermore, ARTD9 has been identified as a novel co-repressor of transcription of interferon response factor 1 (IRF1), a tumor suppressor (Camicia, R. et al., 2013). ARTD9 directly interacts with STAT1β (signal transducer and activator of transcription 1 isoform β) to inhibit IRF1 expression, repressing the anti-proliferative and pro-apoptotic INFγ-STAT1-IRF1-p53 complex (Camicia, R. et al., 2013).

ARTD9 has also been linked to the DNA damage response pathway (Yan, Q. et al., 2013). In response to DNA strand breaks, ARTD9 and its partner BBAP are recruited to DNA damage sites and co-localized with ARTD1 and its product poly-ADP-ribose (Yan, Q. et al., 2013). At the DNA damage sites, ARTD9 and BBAP mediate the specific recruitment of the adaptor protein RAP80 (receptor-associated protein 80) and checkpoint mediators 53BP1 (p53 binding protein 1) and BRCA1 through BBAP-mediated ubiquitination, which limits early and delayed DNA damage and enhances cellular viability (Yan, Q. et al., 2013).

ARTD13, also known as Zinc-finger Antiviral Protein (ZAP/ZC3HAV1) or PARP13, according to previous classification, is a type 1 interferon-inducible host factor that regulates viral RNA transcripts. It was initially identified as zinc finger antiviral protein in a screen for host factors that confer resistance to the retrovirus murine leukemia virus (MLV) infection (Bick, M.J. et al., 2003; Gao, G. et al., 2002; Muller, S. et al., 2007). However, ARTD13 antiviral activities have been later expanded to

other retroviruses (HIV, human immunodeficiency virus) as well as different viral families (Mao, R. et al., 2013; Muller, S. et al., 2007; Zhu, Y. et al., 2011).

ARTD13 binds directly to specific viral mRNAs through its N-terminal zinc finger domains and it recruits cellular mRNA degradation factors to promote degradation of the target viral mRNA and the inability of the virus to replicate efficiently (Guo, X. et al., 2004; Guo, X. et al., 2007; Zhu, Y. and Gao, G. 2008; Zhu, Y. et al., 2011). These antiviral properties are not due to ADP-ribosylation since full-length ARTD13 is not catalytically active, nor is its short isoform (Kleine, H. et al., 2008; Leung, A.K. et al., 2011).

In fact, in humans ARTD13 exists in two major isoforms resulting from alternative splicing: the full length ARTD13.1, and the truncated ARTD13.2 (Hayakawa, S. et al., 2011; Vyas, S. et al., 2013). Both isoforms lack ARTD activity and are unable to ADP-ribosylate target proteins: the catalytic domain of ARTD13.1 lacks amino acid residues required for ADP-ribosylation activity, whereas ARTD13.2 completely lacks the catalytic domain. Three additional isoforms have been predicted based on sequence analyses but their expression in humans has not been experimentally verified (Todorova, T. et al., 2015). The two isoforms have been recently reported to localize to cytoplasmic stress granules along with ARTD5, ARTD7 and ARTD12 and, interestingly when over-expressed, both of them decrease miRNA-mediated silencing (Leung, A.K. et al., 2011). ARTD13 is unique among ARTDs, as it is the only catalytically inactive ARTD shown to be targeted for ADP-ribosylation by other ARTDs (Leung, A.K., et al., 2011; Vyas, S. et al., 2013; Vyas, S. et al, 2014).

In addition to the antiviral functions of ARTD13, it acts as a pro-apoptotic and a pro-inflammatory factor and is a component of the TNF (tumor necrosis factor)-related apoptosis-inducing ligand (TRAIL) mediated immune response to cancer (Todorova, T. et al., 2015). For all these reasons, ARTD13 represents a promising therapeutic target for the treatment of multiple disease states, including viral infections, autoimmune diseases and cancer.

1.4 Sirtuins with ADP-ribosylation activity: SIRT4 and SIRT6

In addition to the previously described families of ART, some members of the sirtuin family have also been reported to carry out protein ADP-ribosylation. Silent information regulator SIR2-like proteins (sirtuins or SIRTs) are a highly conserved class of enzymes found in a variety of phylogenetically distributed species, including archea, eubacteria, yeast, mammals and even viruses (Blander, G. and Guarente, L., 2004; Carafa, V. et al., 2016; Chen, B. et al., 2015; Denu, J.M., 2005; Frye, R.A. et al., 2000; Grubisha, O. et al., 2005). All the members of the sirtuin family share a conserved core domain that comprises approximately 200-275 amino acids, which consists of a NAD^+ binding site and a catalytic domain (Brachmann, C.B. et al., 1995; Frye, R.A., 1999; Sanders, B.D. et al., 2010). Additional N-terminal and/or C-terminal sequences of variable length flank this core domain and these extensions have been identified as targets of PTMs, with a role in regulating sirtuins function (Zhao, K. et al., 2003; Flick, F. and Luscher, B., 2012; Sanders, B.D. et al., 2010).

The mammalian sirtuin family is composed of seven proteins, SIRT1-7 that, according to molecular phylogenetic analysis, can be divided into four classes: class I groups SIRT1, SIRT2 and SIRT3, class II SIRT4, class III SIRT5 and class IV SIRT6 and SIRT7 (Frye, R.A., 2000; Vassilopoulos, A. et al., 2011). Sirtuins from class II and class III seem to have evolved earlier than the other classes, which, in fact, are only present in eukaryotes. Thus, SIRT4 and SIRT5 may be the most ancient mammalian sirtuins (Costantini, S. et al, 2013). The seven mammalian sirtuins have different cellular localizations: SIRT1 and SIRT2 have been detected in the nucleus and cytosol, SIRT3, SIRT4 and SIRT5 in mitochondria, whereas SIRT6 and SIRT7 are predominantly nuclear (Figure 1.5; Gertz, M. and Steegborn, C., 2010; Haigis, M.C. and Sinclair, D.A., 2010; Michan, S. and Sinclair, D., 2007; Michishita, E. et al., 2005; North, B.J. et al., 2003).

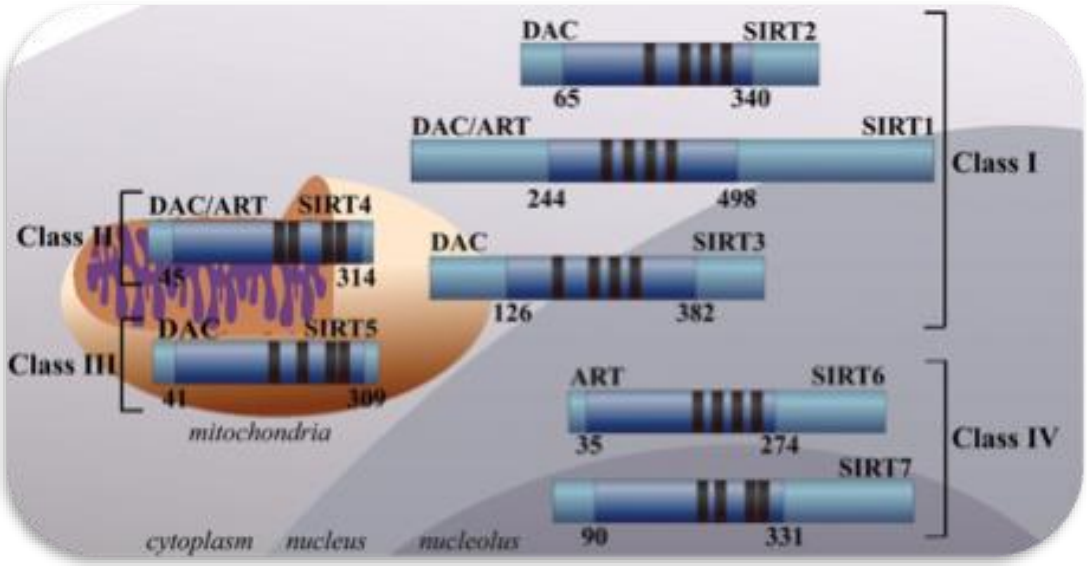

Taken from Karagiannis, T.C. and Ververis, K., 2012

Figure 1.5 Mammalian sirtuin family. Schematic representation of mammalian sirtuins, based on their activity (deacetylases, DAC, or ADP-ribosyl-transferases, ART), their subclasses distribution and their subcellular localization. DAC or ART binding domains are depicted in dark blue, zinc binding domains in black.

The SIRT family regulates a broad range of cellular processes including development, metabolism, DNA repair, DNA recombination, cellular differentiation, transcriptional regulation, apoptosis and lifespan (Blander, G. and Guarente, L., 2004; Carafa, V. et al., 2016; Costantini, S. et al, 2013; Denu, J.M., 2005; Grubisha, O. et al., 2005; Kupis, W. et al., 2016). Most mammalian SIRTs are reported to exhibit *in vivo* and *in vitro* histone deacetylation activity: NAD^+ is used to deacetylate lysine and to simultaneously transfer the acetyl group onto ADP-ribose, generating O-acetyl (OA)-ADP-ribose and releasing nicotinamide (Smith, J.S. et al., 2000; Blander, G. and Guarente, L., 2004; Haigis, M.C. and Sinclair, D.A., 2010; Kupis, W. et al., 2016; Sauve, A.A. and Schramm, V.L., 2004). Interestingly, SIRT1 has been shown to deacetylate ARTD1 and to be functionally connected with it due to the use of their common substrate NAD^+. These enzymes participate in common pathways that are important for different cell fate and metabolic decisions, but with counterbalancing roles (Canto, C. et al., 2015). In addition to their role as deacetylases, some sirtuins are able to catalyze mono-ADP-ribosylation reactions, suggesting that some members of the family may be able to perform more than one biochemical reaction (Ahuja, N. et al., 2007; Haigis, M.C. and Sinclair, D.A., 2010; Kupis, W. et al., 2016; Liszt, G. et al., 2005).

SIRT4 is a mitochondrial sirtuin, which has been reported an activity of cysteine-specific mono-ADP-ribosylation on glutamate dehydrogenase (GDH; Herrero-Yraola, A. et al., 2001; Haigis, M.C. et al., 2006). GDH is involved in the conversion of glutamate to α-ketoglutarate, and the ADP-ribosylated form of GDH results in inhibition of this activity with the consequent reduction of α-ketoglutarate

production (Herrero-Yraola, A. et al., 2001). This SIRT4-mediated modification of GDH is involved in the regulation of insulin secretion in pancreatic β cells (Haigis, M.C. et al., 2006). In SIRT4-deficient pancreatic β cells, GDH activity increases, leading to stimulation of insulin secretion in response to glutamine. Therefore, SIRT4 has an inhibitory effect on amino-acid–stimulated insulin secretion (Haigis, M.C. et al., 2006).

SIRT6 has been reported to have auto-mono-ART activity and to catalyze mono-ADP-ribosylation of ARTD1 in human cells, promoting DNA double-strand break repair by homologous recombination in response to oxidative stress (Mao, Z. et al., 2011; Mao, Z. et al., 2012). SIRT6 has also been associated with aging and cancer: SIRT6 expression diminishes with cellular senescence and its overexpression in non-senescent cells strongly stimulates homologous recombination repair, in an ARTD1-dependent manner (Mao, Z. et al., 2012). Thus, SIRT6 might counteract age-related genomic instability, and the higher incidence of cancer, with age. Moreover, SIRT6 overexpression has been reported to induce apoptosis in different cancer cell lines (Van Meter, M. et al., 2011a). Interestingly, the activity of SIRT6 as tumor suppressor has been associated with its mono-ART activity and not, like other sirtuin members (SIRT1, SIRT2, SIRT3 and SIRT7), to the deacetylase one (Bruzzone, S., et al., 2013; Donadini, A. et al., 2013; Van Meter, M. et al., 2011b). However, although mono-ART activity has been linked with SIRT4 and SIRT6, the relevance of the sirtuins as cellular ARTs is in doubt, as the efficiency of this reaction has been reported to be very low. Sirtuin-mediated ADP-ribosylation needs to be better understood, since it represents an important area of future discovery. A

better characterization of the mechanistic basis of the reaction, the substrate specificity of the ADP-ribosylation activity, and of the relevance of this activity *in vivo* is an ongoing subject of investigation.

1.5 ADP-ribosyl-hydrolases

Both mono- and poly-ADP-ribosylation are reversible reactions: specific hydrolase enzymes are able to cleave these covalent bonds, thereby releasing the target protein. Poly-ADP-ribose (PAR)-glycohydrolase (PARG) can specifically hydrolyze the ribose–ribose bonds in PAR chains, while the ADP-ribosyl-hydrolases (ARHs) cleave the mono-ADP-ribose–protein bond (Lin, W. et al., 1997; Mashimo, M. et al., 2014; Takada, T. et al., 1993; Verheugd, P. et al., 2016). ARHs are enzymes that reverse mono-ADP-ribosylation reactions by catalyzing the removal of ADP-ribose from modified proteins (Figure 1.6; Mashimo, M. et al., 2014; Moss, J. et al., 1992). Considering that ADP-ribosylation of proteins generally leads to loss of function, removal of ADP-ribose could be associated with the reactivation of the target protein. Thus, the molecular characterization of ARHs supports the idea that reversible ADP-ribosylation cycle, controlled by the balance between the transferase and hydrolase activity, could have a role in the regulation of eukaryotic cell functions.

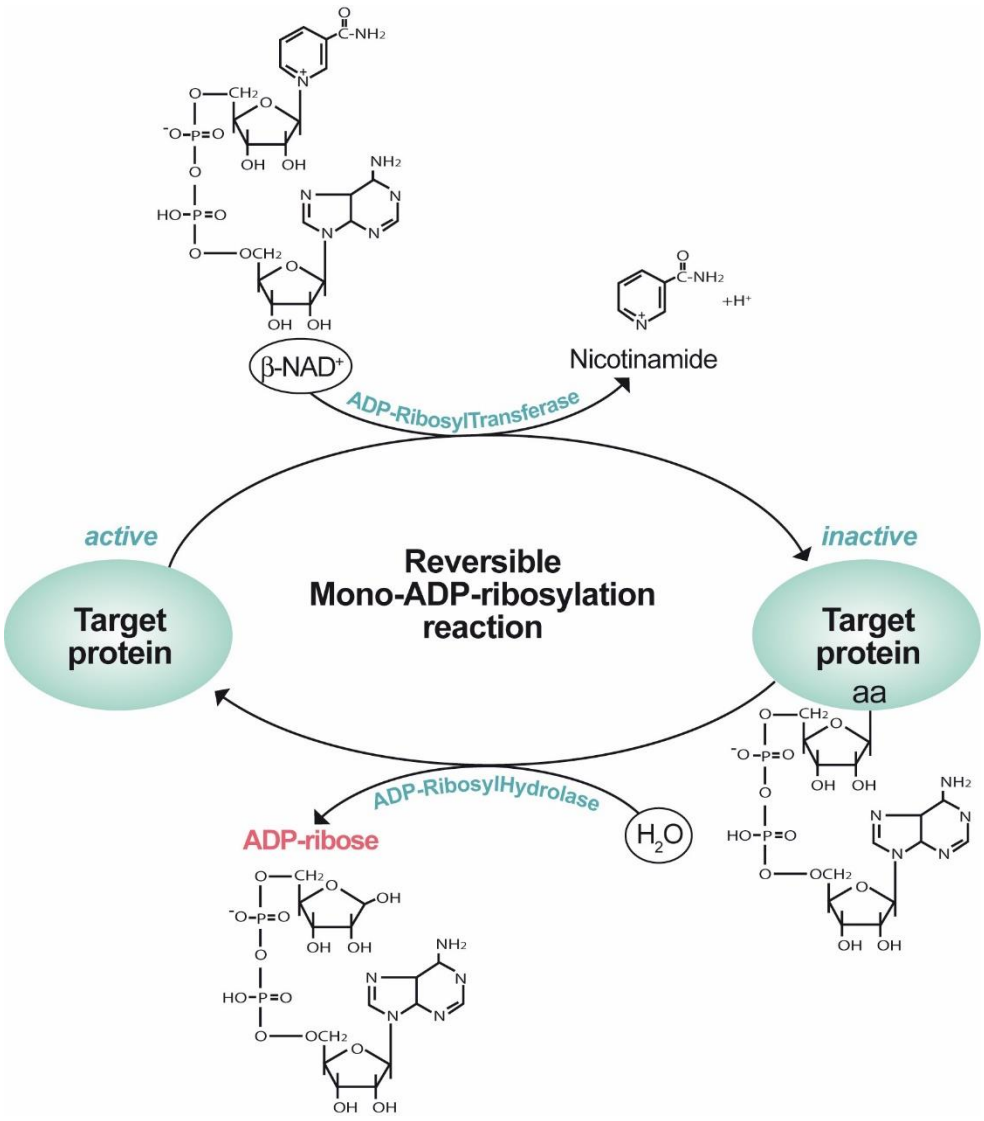

Taken from Fabrizio, G. et al., 2015a

Figure 1.6 Schematic representation of the reversible mono-ADP-ribosylation reaction. Mono-ARTs transfer the ADP-ribose moiety from NAD^+ to a specific amino acid of the target protein, releasing nicotinamide. This modification leads to inactivation of the target protein. Specific hydrolase enzymes are able to cleave the covalent bond between ADP-ribose and the side chain of target protein, restoring normal protein functions.

A well-documented example of the regulatory role of ADP-ribosylation cycle is that of the photosynthetic bacterium *Rhodospirillum rubrum*, where it regulates the function of the enzyme dinitrogenase reductase (Li, X.D. et al., 2009; Lowery, R.G. and Ludden, P.W., 1988; Nordlund, S. and Ludden, P.W., 2004; Nordlund, S. and Hogbom, M., 2013; Wang, H. et al., 2005). This enzyme is reversible mono-

ADP-ribosylated by an ART known as DRAT (dinitrogenase reductase ADP-ribosyl-transferase), which modifies arginine 101 of dinitrogenase reductase (Lowery, R.G., and Ludden, P.W., 1988; Ma, Y. and Ludden, P.W., 2001; Pope, M.R. et al., 1985; Wang, H. et al., 2005). However, the dinitrogenase reductase could be fully reactivated by an ARH known as DRAG (dinitrogenase reductase activating glycohydrolase), as reviewed by Nordlund and Hogbom in 2013 (Nordlund, S. and Hogbom, M., 2013). Thus, *Rhodospirillum rubrum* represents the first example of how a vital biochemical process like nitrogen fixation is tightly regulated through an ADP-ribosylation cycle.

The best characterized ADP-ribosyl-hydrolase is ARH1, which specifically hydrolyzes ADP-ribose-arginine bonds, leading to the release of free mono-ADP-ribose and regeneration of the guanidino group of arginine (Moss, J. et al., 1986; Takada, T. et al., 1993). ARH1 is a soluble 39-kDa protein that in mammalian cells shows prevalently cytosolic activities, although some are also located on the cell surface (Hassa, P.O. et al., 2006; Mashimo, M. et al., 2014). In addition to mammals, ARH1 has also been identified in bacterial and avian systems (Lowery, R.G. and Ludden, P.W., 1988; Moss, J. et al., 1985; Moss, J. et al., 1986, Moss, J. et al., 1992). ARH1 activity exists in a variety of animal species, with the highest specific activities found in rat and mouse brain, spleen and testis (Moss, J. et al., 1992). Despite their functional similarities, ARH1 protein from human, rat and mouse tissues have only limited region of similarity in their deduced amino acids sequences (Moss, J. et al., 1992). In these regions, the conserved aspartate residues (Asp 60 and Asp 61) of rat ARH1 have been demonstrated to be critical for catalytic activity, but not for

ADP-ribose binding (Mashimo, M. et al., 2014; Konczalik, P. and Moss, J., 1999). These active site residues appear to be conserved from bacteria to human and to have a critical role for catalysis (Mashimo, M. et al., 2014; Konczalik, P. and Moss, J., 1999).

It has also been shown that ARH1 activity can counteract the ADP-ribosylation of Gαs that is catalyzed by cholera toxin, and that cellular knock down of ARH1 shows increased sensitivity to the deleterious effects of this toxin. However, during diseases, the extremely efficient ART activity of cholera toxin cannot be reversed by ARH1 (Mashimo, M. et al., 2014; Kato, J. et al., 2011).

Besides ARH1, additional unidentified proteins exhibiting ADP-ribosyl lyase activities have been reported, which are thought to function on glutamate, lysine or cysteine residues, releasing a deoxy form of ADP-ribose (Oka, J. et al., 1984; Okayama, H. et al., 1978; Tanuma, S. and Endo, H., 1990). Enzymatic activities responsible for the hydrolysis of ADP-ribosyl-cysteine have been identified in human and bovine erythrocytes and in mitochondria from bovine liver (Jorcke, D. et al., 1998; Saxty, B.A. and van Heyningen, S., 1995; Tanuma, S. and Endo, H., 1990). In silico screening revealed two Arh-like genes, *Arh2* and *Arh3*, which are homologous to the human *Arh1* gene (Glowacki, G. et al., 2002). Despite their structural similarities, ARH family members have different functions. However, the discovery of ARH2 and ARH3 suggested that the hydrolase family is larger than originally thought. ARH2 is the closest relative of ARH1, with which it shares 45% sequence identity, but does not exhibit any detectable activity on ADP-ribose-arginine, -cysteine, -diphtamide or –asparagine bonds (Koch-Nolte, F. et al., 2008;

Mashimo, M. et al., 2014; Oka, S. et al., 2006). Thus, it is possible that ARH2 is inactive, or is a candidate for glutamate- or aspartate-specific ARH.

ARH3 is an enzyme localized in the nucleus and in mitochondria with unexpected activity, since it is capable of hydrolyzing poly-ADP-ribose and O-acetyl-ADP-ribose, but not mono-ADP-ribose (Mashimo, M. et al., 2014; Oka, S. et al., 2006). The critical aspartate residues of ARH3 (Asp77 and Asp78) are located in a region similar to that required for hydrolase activity in ARH1, but distinct from that of PARG (Mashimo, M. et al., 2014; Oka, S. et al., 2006). Also, the analysis of tridimensional structure indicates the presence of an α-helical protein fold with pseudo two-fold symmetry, confirming the difference from the mixed α-helix/β-sheets secondary structure prediction of PARG (Koch-Nolte, F. et al., 2008; Mashimo, M. et al., 2014; Mueller-Dieckmann, C. et al., 2006).

All these data are consistent with the conclusion that ARH3 might be a functional PARG, but structurally unrelated to the real PARG (Mashimo, M. et al., 2014; Oka, S. et al., 2006).

The characterization of ADP-ribosyl-hydrolase activities strongly support the significance of the mono-ADP-ribosylation reaction and the existence of an ADP-ribosylation cycle, even though the functional interplay of the constituents of such a cycle remains to be demonstrated. Further investigations are necessary, also considering the recent findings about macro domain containing protein that have been reported to be able to remove mono-ADP-ribose from substrate proteins and, thus, reverse mono-ADP-ribosylation reactions (see Chapter 1.6 below).

1.6 ADP-ribose binding modules

Different receptor and adaptor proteins have been described for their special ability to recognize specific signals such as small second messenger molecules and PTMs, thereby participating in various cellular signaling pathways. The molecular recognition is usually carried out by globular protein modules that recognize their ligand substrate with high specificity and act by changing the cellular localization, the local concentration or the specific activity of their target (Till, S. and Ladurner, A.G., 2009).

Considering the recent scientific advances in the PTMs field and the increasing awareness on ADP-ribosylation reactions, it has been of considerable interest to identify and characterize protein binding motifs and/or modules able to bind mono- and poly-ADP-ribose. Recent evidences indicate there are four principal ADP-ribose binding domains and motifs:

i) the Nudix domain,

ii) the poly-ADP-ribose binding peptide motif,

iii) the poly-ADP-ribose binding zinc-finger (PBZ) domain,

iv) the macro domain.

The Nudix domain is a domain containing the consensus sequence $GX_5EX_7REUXEEXGU$, where X is any amino acid and U is a hydrophobic amino acid, typically isoleucine, leucine, or valine. This domain has been found in phosphatases (Bessman, M. J. et al., 1996; Gabelli, S.B. et al., 2001). The poly-ADP-ribose binding peptide motif consists of hydrophobic and positively charged amino acids with the

consensus sequence [HKR]-X-[AIQVY]-[KR]-[AILV]-[FILPV], and lies within histones (H3, H4, H2A and H2B), XRCC1 (X-ray cross complementing group 1 protein), p53 and RNPs (ribonucleoproteins; Gagne, J.P. et al., 2008; Pleschke, J.M. et al., 2000). The PBZ domain is characterized by the following consensus sequence [K/R]XXCX[F/Y]GXXCXBBXXXXHXXX[F/Y]XH, where B is a basic amino acid residue and X any amino acid. The PBZ domain has been found in DNA repair and checkpoint proteins, for example one and two PBZ domains are present in checkpoint with forkhead and ring finger domains (E3 ubiquitin protein ligase; CHFR) and aprataxin and PNKP (polynucleotide kinase/phosphatase) like factor (APLF) proteins, respectively (Ahel, I. et al., 2008; Eustermann, S. et al., 2010; Kanno, S. et al., 2007). The macro domain represents protein modules that have been found in protein across different species (Karras, G.I. et al., 2005). Macro domains regulate different cellular functions that will be discussed in the next paragraph. Collectively, the identification of specific ADP-ribose-binding sites in several proteins that participate in cellular signal network suggests ADP-ribosylation could be involved in protein-protein and protein/DNA interactions, protein localization or protein degradation.

1.6.1 Macro domains

Macro domains are a family of evolutionarily conserved proteins that can interact with ADP-ribose or other NAD derivatives (Forst, A.H. et al., 2013; Neuvonen, M. and Ahola, T., 2009). Members of the macro domain family have been conserved throughout evolution, with homologues identified in viruses (coronaviruses,

alphaviruses), archea (*Archaeoglobus fulgidus*), bacteria (*Escherichia coli*), invertebratres (*Drosophila melanogaster*), anphibians (*Xenopus laevis*), plants (*Arabidopsis thaliana*, *Oryza sativa*) and mammals (humans, mice; Anantharaman, V. et al., 2002; Han, W. et al., 2011; Till, S., and Ladurner, A.G., 2009). In humans, so far, ten human genes encoding 11 members of the macro domain family have been identified, since macroH2A includes the two isoforms macroH2A1.1 and macroH2A1.2 (Table 1.4; Han, W. et al., 2011).

Table 1.4 Human macro domain family proteins.

Member	Other names	Reported functions
MacroH2A1	MacroH2A1.1 MacroH2A1.2	Transcriptional regulation, genome silencing, X-chromosome inactivation
MacroH2A2	H2AFY2	Transcriptional regulation, developmental roles
MACROD1	LRP16	Transcriptional co-activator
MACROD2	C20orf133	Developmental disorders and Kabuki syndrome
MACROD3	GDAP2, FLJ20142, dJ776p7.1	Ganglioside-induced differentiation-associated protein
ALC1	CHD1L, CHDL, FLJ22530	Oncogene, ATP-dependent chromatin remodeler, epithelial–mesenchymal transition (EMT)
PARP-9	BAL, BAL1, DKFZp666B0810	Modulates transcription and promotes B-cell lymphoma migration
PARP-14	BAL2, CoaSt6, KIAA1268, pART8	Transcriptional cofactor and development
PARP-15	BAL3, FLJ40196, FLJ40597, MGC126750, MGC126752, pART7	Transcriptional co-repressor
C6orf130	MGC19570, dJ34B21.3	Serologic marker

Modified from Han, W. et al., 2011

Although the first macro domain was discovered more than 20 years ago, only in the recent years it has been demonstrated that macro domains can bind ADP-

ribose, definitively establishing the connection between macro domains and ADP-ribosylation reactions and opened up new interesting research areas (Karras, G.I. et al., 2005). Macro domains are not identical: their structural differences predetermine macro domain containing protein to act solely as a reader of mono-ADP-ribose or poly-ADP-ribose, or to act as a reader and eraser of the modification as well. A globular macro domain comprises six stranded mixed β-sheets and five α-helices, which form a cleft for the ligand. The binding occurs via stacking interaction with the adenine ring, strengthened through the interactions with the pyrophosphate of ADP-ribose and with specificity provided by hydrogen bonding with the distal ribose (Karras, G.I. et al., 2005; Han, W. et al., 2011; Till, S. and Ladurner, A.G. 2009).

Different macro domains are capable of interacting with monomeric, polymeric, or both forms of ADP-ribose and other NAD derivatives. For example, the macro domain of the histone variant macroH2A1.1 and the chromatin remodeller ALC1 are binding module for poly-ADP-ribose (Feijs, K.L. et al., 2013c; Gottschalk, A.J. et al., 2009; Timinszky, G. et al., 2009). Other macro domains interact with mono-ADP-ribosylated proteins, such as the macro domain of the Af1521 protein from *Archaeoglobus fulgidus*, which represents the first evidence of a macro domain containing protein able to recognize mono-ADP-ribosylated targets (Dani, N. et al., 2009). Recently, other members of the human macro domain containing proteins, such as ARTD8, macroD1, macroD2 and C6orf130 (O-acetyl-ADP-ribose deacetylase, also name TARG1), have been associated to mono-ADP-ribosylation and demonstrated to reverse this reaction (Feijs, K.L. et al., 2013c; Forst, A.H. et al.,

2013; Jankevicius, G. et al., 2013; Rosenthal, F. et al., 2013; Sharifi, R. et al., 2013). Additionally, some macro domains are O-acetyl-ADP-ribose (OAADPr) binding modules able to efficiently catalyze the hydrolysis of OAADPr, which is a metabolite from the sirtuin-mediated NAD^+-dependent deacetylation reactions (Chen, D. et al., 2011; Tong, L. and Denu, J.M., 2010). Thus, all of these macro domain-containing proteins are mono-ADP-ribosyl-hydrolases that can reverse mono-ADP-ribosylation, removing mono-ADP-ribose from modified proteins. These findings define macro domain-containing proteins as the functional antagonists of intracellular mono-ARTs and definitively establishes mono-ADP-ribosylation as a fully reversible PTM (Rosenthal, F. et al., 2013).

Macro domains are involved in different biological processes, since it has been demonstrated they can function in DNA repair, chromatin remodelling, developmental mechanisms depending on poly-ADP-ribose production or acting in concert with sirtuins as potential *in vivo* regulators of cellular OAADPr produced by NAD^+-dependent deacetylation reactions catalysed by these enzymes (Changolkar, L.N. and Pehrson, J.R., 2006; Changolkar, L.N. et al., 2007; Chen, D. et al., 2011; Timinszky, G. et al., 2009).

1.6.2 Macro domains as affinity tools

The demonstration that macro domains have ADP-ribose binding properties opens new possibilities for studying ADP-ribosylation reactions. In fact, during the past years, one of the major difficulties in the analysis of this PTM was the lack of biochemical tools able to easily recognize ADP-ribosylated proteins. The

characterization of the Af1521 macro domain from *Archaeoglobus fulgidus* and the demonstration that it can bind not only ADP-ribose, but also ADP-ribosylated proteins, confirmed that macro domains represent protein–protein interaction domains (Karras, G.I. et al., 2005). This finding prompted researchers to evaluate the possibility to use the macro domain module as an affinity tool to isolate ADP-ribosylated proteins (Dani, N. et al., 2009). Particularly, Dani and colleagues showed that Af1521 can be used as a selective bait for high-affinity purification of mono-ADP-ribosylated proteins. Moreover, when used in combination with mass spectrometry, it is a powerful tool for the identification of mono-ADP-ribosylated target, since it allows identification of a series of previously known ADP-ribosylated protein in addition to a large number of new substrates that need to be individually validated (Dani, N. et al., 2009). Therefore, the use of macro domains as an affinity tool represents an important step toward the discovery of new ART targets for which it is of extreme importance understanding the physiological role and the pharmacological potential associated with this protein modification.

1.7 Mono-ADP-ribosylation substrates

Several proteins have been identified as targets of mono-ADP-ribosylation reactions and their modification has numerous and diverse effects on protein functions and cellular pathways, including DNA damage, RNA metabolism, chromatin organization, transcription, protein trafficking, signal transduction, stress responses and cell cycle regulation (Di Girolamo, M. et al., 2005; Feijs, K.L. et al., 2013a; Gibson, B.A. and Kraus, W.L., 2012; Scarpa, E.S. et al., 2013). For most

of these ADP-ribosylated substrates the modified amino acids have been identified, while the specific enzymes that are responsible for these modifications are still not known. An example of an orphan ART substrate is that of the G-protein β subunit, whose functional, enzymatic mono-ADP-ribosylation has been found both in isolated plasma membranes from different cell lines (including Swiss 3T3, CHO and HL60 cells), and in intact cells (Lupi, R. et al., 2000). Specifically, mono-ADP-ribosylation of the β subunit occurs on arginine 129 (Arg129), a critical amino acid residue located in the β common-effector-binding surface (Chen, Y. et al., 1997; Weng, G. et al., 1996; Yan, K. and Gautam, N., 1997; Yan, K. et al., 1996). The reaction is catalyzed by an unknown plasma membrane-associated mono-ART, with an intracellular catalytic site. Interestingly, the modified β subunit can be de-ADP-ribosylated by a cytosolic ARH, which regenerates a native βγ dimer by releasing the bound ADP-ribose (Lupi, R. et al., 2000). Mono-ADP-ribosylation of this Arg129 residue prevents β subunit-dependent modulation of effectors such as type 1 adenylyl cyclase (AC), phosphoinositide 3-kinase (PI3K) and phospholipase C (PLC; Lupi, R. et al., 2000; Lupi, R. et al., 2002). Thus, the ADP ribosylation/de-ribosylation cycle seems to correspond to a functional activation/inactivation cycle of the βγ dimer, modulating its function.

Of note, it is of particular interest that the mono-ADP-ribosylation of the β subunit has been shown to be regulated by hormonal control: it can be increased upon activation of specific G-protein coupled receptors (GPCRs) such as thrombin, serotonin and cholecystokinin receptors (Lupi, R. et al., 2002). Our group has reported that β subunit mono-ADP-ribosylation is differentially modulated by

GPCRs and, particularly, that hormone stimulation of the thrombin receptor induces β subunit mono-ADP-ribosylation, thus affecting G-protein signaling (Di Girolamo, M. et al., 2005). Conversely, hormone stimulation of the gonadotropin-releasing hormone receptor (GnRHR) inhibits β subunit mono-ADP-ribosylation and simultaneously activates the ADP-ribosylation factor 6 (ARF6; Dani, N. et al., 2011). This activation of ARF6, in turn, acts as a competitive inhibitor for the β subunit modification, becoming the preferred substrate of the endogenous mono-ART (Dani, N. et al., 2011).

The demonstration that the β subunit is physiologically modified by mono-ADP-ribosylation is of extreme interest both because of the central role that the βγ dimer plays in signal transduction pathways downstream of GPCRs, and because this was the first *in vivo* demonstration of a PTM for the G-protein β subunit.

An intracellular ADP ribosylation/de-ribosylation cycle has also been described for the mitochondrial protein GDH. Cysteine-specific ADP-ribosylation of GDH causes substantial inhibition of its enzymatic activity in intact Hep-G2 cells (Herrero-Yraola, A. et al., 2001). Further studies have identified SIRT4 as the enzyme responsible for the mono-ADP-ribosylation of GDH. Specifically, SIRT4 ADP-ribosylates GDH and reduces its activity by 50% in β cells during calorie-sufficient conditions, opposing the effects of calorie restriction (Haigis, M.C. et al., 2006). During calorie restriction there is an increase in GDH activity accompanied by a downregulation of SIRT4, a finding that contrasts with the expectation of the increase in sirtuins activity. The downregulation of SIRT4 could depend on the reduction in the NAD/NADH ratio observed during calorie restriction (Haigis, M.C.

et al., 2006). The lower NAD/NADH ratio may downregulate SIRT4 activity and reduce the ADP-ribosylation of GDH that, thus, shows increased activity. Due to the central position of GDH in metabolism, where it lies as the crossroads of several important pathways, a tight control of its catalytic activity is essential.

Another yet-to-be identified cellular ART modifies the elongation factor 2 (EF-2): its ADP-ribosylated form has been detected in a wide variety of eukaryotic cell types and it has been proposed to serve as a mechanism for regulating cellular protein synthesis (Fendrick, J.L. et al., 1992).

Also the cytoskeletal proteins desmin, actin and tubulin have been described as target of intracellular mono-ADP-ribosylation. Desmin is a muscle-specific intermediate filament protein and it has been described as a substrate for an endogenous arginine specific mono-ART that, however, has not yet been molecularly characterized (Huang, H.Y. et al., 1993). ADP-ribosylated desmin cannot assemble into intermediate filaments *in vitro* and, when incubated with ARH, the self-assembly properties of the protein are restored (Zhou, H. et al., 1996).

Actin is another intracellular target of mono-ADP-ribosylation: it can be mono-ADP-ribosylated by arginine-specific ART in homogenates of various cells and tissue. Mono-ADP-ribosylation of non-muscle actin inhibits its ability to polymerize in chicken heterophils, affecting some of the actin-mediated functions such as the release of azurophilic granules (Terashima, M. et al., 1996). Moreover, it has been reported that in HL-60 cells mono-ADP-ribosylation of actin is involved in the modification of the cytoskeleton and can lead to apoptosis (Lodhi, I.J. et al., 2001).

Also tubulin can be a target of mono-ADP-ribosylation as it has been initially demonstrated by an *in vitro* analysis (Raffaelli, N. et al., 1992). Because ribosylation of tubulin blocks its self-assembly properties, it has been proposed that the ADP-ribosylation sites could be essential for tubulin assembly (Terashima, M. et al., 1999). More recently, Dani and colleagues confirmed the fact that tubulin is a target of mono-ADP-ribosylation demonstrating it was one of the proteins identified by mass spectrometry after a GST (glutathione S-transferase)-mAf1521 pull-down assay (Dani, N. et al., 2009).

Additionally, the transcriptional corepressor C-terminal binding protein, brefeldin A (BFA)-induced ADP-ribosylated substrate (CtBP1/BARS) is another target that can be modified by mono-ADP-ribosylation (Di Girolamo, M. et al., 1995; Feng, Y. et al., 2003). CtBP1/BARS functions as both a transcriptional corepressor and as a modulator of Golgi structure and upon BFA stimulation, it results in mono-ADP-ribosylation catalyzed by an unknown intracellular mono-ART (De Matteis, M.A. et al., 1994; Di Girolamo, M. et al., 1995). The ADP-ribosylation of CtBP1/BARS causes its inactivation. Specifically, it loses its catalytic activity and its ability to promote the fission of Golgi tubules (Weigert, R. et al., 1999). Specific inhibitors of BFA-induced ADP-ribosylation are able to prevent the toxic effect of BFA on the Golgi complex, supporting the functional role of this reaction (Weigert, R. et al., 1997).

Moreover, the ARF6 has been identified as a new target of mono-ADP-ribosylation, that specifically occurs on arginine 110 (Arg110; Dani, N. et al., 2011). ARF6 is involved in the regulation of plasma-membrane related processes, and in the reorganization of the cortical actin cytoskeleton (D'Souza-Schorey, C. and

Chavrier, P., 2006; Donaldson, J.G., 2003; Honda, A. et al., 1999). Moreover, it is emerging as a key component of tumor invasion and metastasis, and its mono-ADP-ribosylation seems to contribute to the regulation of these ARF6-mediated functions (Dani, N. et al., 2013). Thus, ARF6 can be regarded as a promising target for therapeutic intervention in cancer. The molecular chaperone GRP78/BiP has also been reported to undergo intracellular mono-ADP-ribosylation. Its mono-ADP-ribosylation and the specific role of this modification will be detailed discussed in the next paragraphs.

1.8 GRP78/BiP

The 78 kDa glucose-regulated protein GRP78, also known as BiP (immunoglobulin heavy chain-binding protein), is a molecular chaperone initially described in 1977 (Shiu, R.P. et al.,1977). It is also referred to as HSPA5, Heat Shock Protein family A (HSP70) member 5, since it is a member of the 70 kDa Heat Shock Family of Stress Proteins (HSP70; Daugaard, M. et al., 2007; Murphy, M.E., 2013). Although it shares about 60% amino acid sequence homology with HSP70, including the ATP-binding site required for its role as a chaperone in protein folding, there are two distinct aspects that differ between GRP78/BiP and HSP70 (Daugaard, M. et al., 2007; Murphy, M.E., 2013). Firstly, GRP78/BiP has a signal peptide sequence that targets it to the ER, whereas HSP70 does not contain this sequence and is cytosolic, and translocating to the nucleus upon stress (Daugaard, M. et al., 2007; Murphy, M.E. 2013). Secondly, GRP78/BiP is not affected by heat shock conditions that,

instead, greatly elevated the expression of HSP70 and other members of the heat shock protein family (Murphy, M.E., 2013; Wooden, S.K. and Lee, A.S., 1992).

GRP78/BiP, which primarily resides in the lumen of the ER, has a central role in ER-mediated cellular processes (Lee, A.S., 2001). It functions as a facilitator of proper protein folding, preventing intermediates from aggregating and targeting misfolded proteins for proteaosomal degradation (Flynn, G.C. et al., 1991; Ellgaard, L. and Helenius, A., 2003; Romisch, K., 2005). In addition, it has a role in binding of calcium for storage at high concentrations in the ER lumen and it serves as an ER stress signaling regulator, controlling the activation of transmembrane ER stress sensors (Ni, M. and Lee, A.S., 2007).

Specific mono-ADP-ribosylation of GRP78/BiP was demonstrated in 1994 (Ledford, B.E. and Leno, G.H., 1994). The mono-ADP-ribosylation of GRP78/BiP was detected in response to nutritional stress, a condition that depletes the ER of proteins, resulting in a reduction of translation activity. Laitusis and co-workers have hypothesized that this ADP-ribosylation is related to the rate of protein synthesis and processing (Laitusis, A.L. et al., 1999). According to this model, in cells with high rate of protein synthesis GRP78/BiP is in its active state, complexed with protein-folding intermediates and not available for the ADP-ribosylation. A physiological, or induced, decrease of protein synthesis results in the accumulation of the active, free form of the chaperone that is mono-ADP-ribosylated and, thus, inactivated. Hence, the modification of GRP78/BiP by mono-ADP-ribosylation could be a system to balance the amount of the active, functional chaperone with both protein processing and synthesis.

Although GRP78/BiP mono-ADP-ribosylation has been known for long time, the enzyme responsible for this modification has not yet identified. It was previously postulated that an arginine-specific enzyme of the ARTC family would be needed to modify GRP78/BiP and it has been recently reviewed by Fabrizio et al. in 2015 (Di Girolamo, M. et al., 2005, Fabrizio, G. et al., 2015b). Moreover, it has been demonstrated that mono-ADP-ribosylation of GRP78/BiP occurs on two arginine residues (R470, R492) in the substrate binding domain of the chaperone and analysis of the mutated protein is in line with the concept that this PTM can interfere with substrate binding (Chambers, J.E. et al., 2012).

1.8.1 GRP78/BiP and Unfolded Protein Response (UPR)

The ER represents one of the major signal-transducing organelle, providing a highly selective quality control system to ensure correct protein folding and assembly, and recognizing unfolded proteins that can be repaired or targeted for proteasomal degradation. A number of biochemical, physical and pathological stimuli, such as ER calcium depletion, glucose deprivation, oxidative stress and DNA damage can disrupt ER homeostasis and lead to accumulation of unfolded or misfolded proteins in the ER, causing the so called "ER stress". Eukaryotic cells have evolved a coordinated cellular response to adapt to adverse conditions in order to maintain homeostasis and survive. One such coping mechanism is the activation of the UPR (Gardner, B.M. et al., 2013; Grootjans, J. et al., 2016; Kaufman, R.J., 1999; Strzyz, P., 2016; Welihinda, A.A. et al., 1999).

Activation of the UPR has three main consequences, ultimately resulting in enhancement of ER protein folding capacity through expansion of the ER and increased expression of chaperones and foldases, an initial transient inhibition of protein synthesis to temporarily stop production of new proteins, and induction and activation of the ER-associated degradation (ERAD) system that retro-translocates terminally misfolded proteins from the ER for proteasome-dependent degradation (Olzmann, J.A. et al., 2013; Ni, M. and Lee, A.S. 2007; Qi, L. et al., 2017). If the ER stress conditions are not resolved and still continuing persisting, an ER stress-induced cell death arises. Generally, ER stress-associated cell death occurs through caspase activation, although caspase-independent necrosis and autophagy have also been observed (Hitomi, J. et al., 2004; Nakagawa, T. et al., 2000; Ullman, E. et al., 2008). The UPR in mammalian cells is regulated by three ER transmembrane proteins: activating transcription factor 6 (ATF6), inositol-requiring 1 alpha (IRE1α), and double-stranded RNA-dependent protein kinase (PKR)-like ER kinase (PERK; Brewer, J.W., 2014; Hetz, C., 2012; Mori, K., 2000). Each sensor is composed of an ER luminal domain sensitive to accumulation of misfolded proteins, an ER transmembrane domain that can target proteins for localization to the ER membrane, and a cytosolic functional domain (Figure 1.7; Schroder, M. and Kaufman, R.J., 2005).

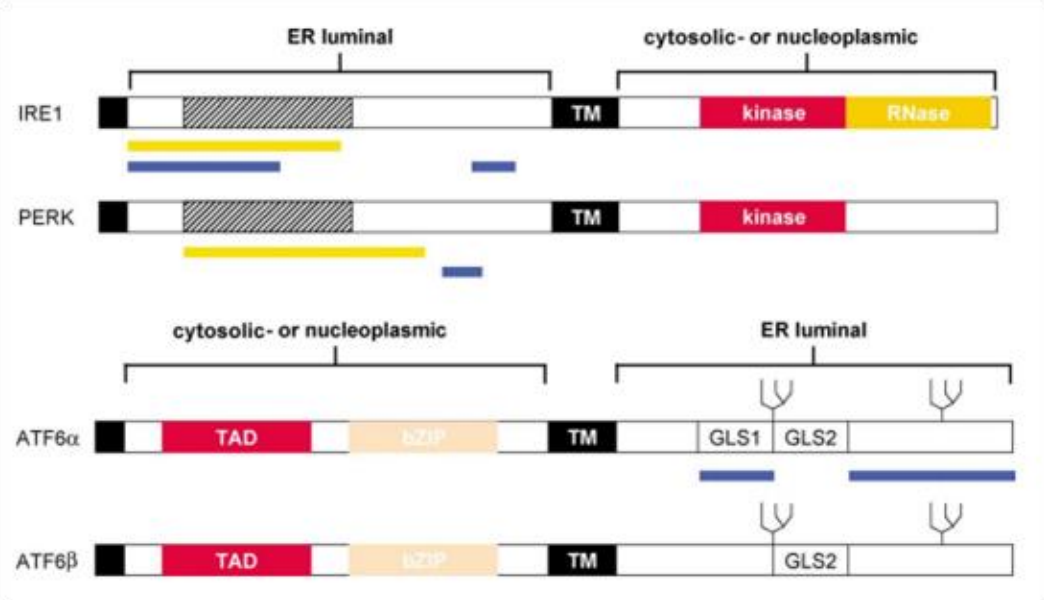

Modified from Schroder, M. and Kaufman, R.J., 2005

Figure 1.7 Architecture of the ER stress sensors. Schematic representation of the principal domains of the ER stress sensors IRE1α, PERK and ATF6. The orange bars represent regions sufficient for signal transduction or oligomerization. The blue bars represent regions binding to GRP78/BiP. A black box represents the signal peptide and the hatched box depicts the region of limited homology between IRE1 and PERK. The following domains are indicated. bZIP: basic leucine zipper; GLS1 and GLS2: Golgi localization sequences 1 and 2; TAD: transcriptional activation domain; TM: transmembrane domain.

GRP78/BiP is a key regulator of UPR. In addition to GRP78/BiP that actively binds nascent polypeptide chains, there is some GRP78/BiP that interacts with the luminal domain of ATF6, IRE1α and PERK, keeping them inactive (Bertolotti, A. et al., 2000; Chen, X. et al., 2002; Shen, J. et al., 2002). Importantly, the peptide-binding site of GRP78/BiP that associates with the receptors is the same that binds to hydrophobic patches of misfolded or unfolded ER peptides (Rutkowski, D.T. and Kaufman, R.J., 2004).

During ER stress, the GRP78/BiP that binds the UPR-signaling proteins is recruited to the misfolded nascent proteins that are accumulating in the ER and, thereby, it releases its binding of ATF6, IRE1α and PERK. Once released, these three protein

sensors become functional, initiating the UPR (Figure 1.8; Brewer, J.W., 2014; Hetz, C., 2012; Merksamer, P.I. and Papa, F.R., 2010; Ron, D. and Walter, P., 2007). The first pathway to be activated, within minutes, is PERK, followed by ATF6 and, lastly, by IRE1α (Novoa, I. et al., 2003).

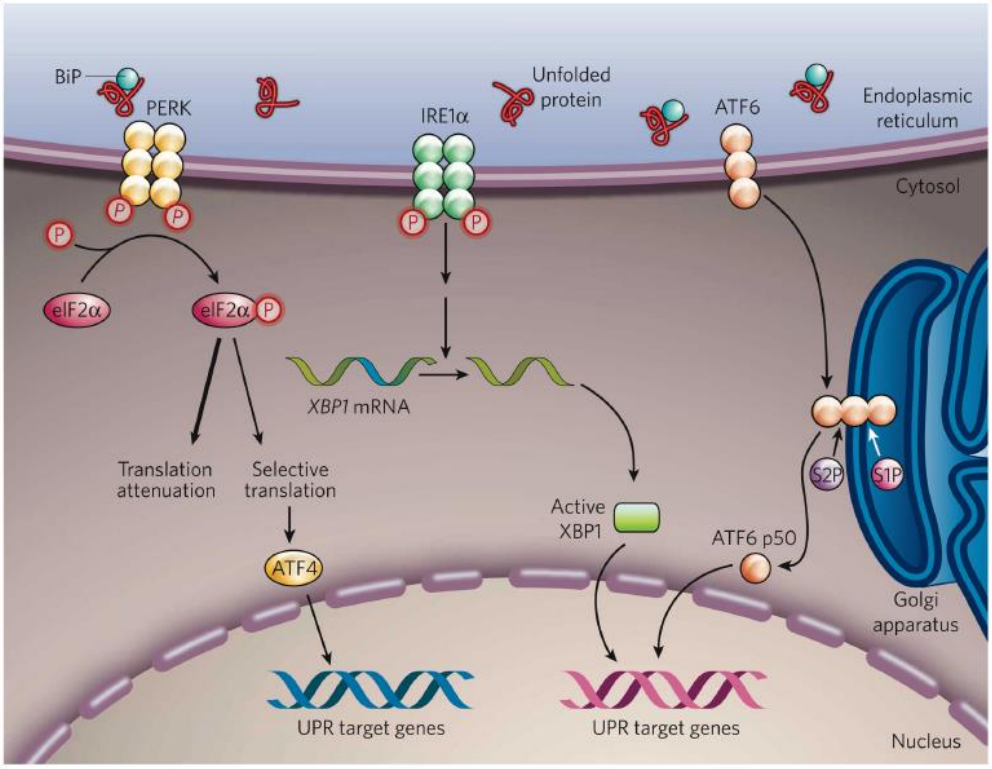

Modified from Zhang, K. and Kaufman, R.J., 2008

Figure 1.8 The mammalian UPR pathways. During ER stress GRP78/BiP preferentially binds to unfolded or misfolded proteins, thus driving the equilibrium of GRP78/BiP binding away from IRE1α, PERK and ATF6. These three proteins are the initiators of the three main signaling cascades of the UPR.

Despite disparate signaling mechanisms, each signaling pathway activates transcription factors that mediate the induction of a variety of UPR response genes. These UPR signaling pathways are examined in the next paragraphs.

1.8.1.1 PERK

PERK is the first pathway to be activated, within minutes from UPR starting (Brewer, J.W. et al., 2014; Novoa, I. et al., 2003). PERK is a type I ER-resident transmembrane protein that, under normal conditions, is bound to GRP78/BiP. Following ER stress, GRP78/BiP dissociates, thereby allowing PERK to autophosphorylate and dimerize, also inducing transphosphorylation (Bertolotti, A. et al., 2000; Brewer, J.W. et al., 2014; Cui, W. et al., 2011; Liu, C.Y. et al., 2000). Once activated, PERK phosphorylates the α subunit of eukaryotic translation initiation factor (eIF2α) on serine 51 (Brewer, J.W. et al., 2014; Cui, W. et al., 2011; Harding, H.P. et al., 1999; Shi, Y. et al., 1998; Wek, R.C. et al., 2006). This interferes with global mRNA binding of ribosomal 60s and 40s subunits and results in global translational attenuation and reduction of protein synthesis, thus reducing ER workload (Brostrom, C.O. and Brostrom, M.A., 1998; Harding, H.P. et al., 1999; Hinnebusch, A.G., 1994; Liu, Z. et al., 2015; Wek, R.C. et al., 2006)

Although in general phosphorylation of eIF2α attenuates mRNA translation, translation of certain mRNAs with short open reading frames in the 5′-UTR is enhanced by phosphorylation of eIF2α (Harding, H.P. et al., 2000; Liu, Z. et al., 2015; Wek, R.C. et al., 2006). ATF4 is an example of such mRNA and its expression results in upregulation of UPR target genes encoding proteins involved in amino acid biosynthesis, antioxidative stress response, and ER stress-induced apoptosis (Harding, H.P. et al., 2003; Liu, Z. et al., 2015).

Activation of PERK by ER stress is reversible: activated PERK can be rapidly dephosphorylated upon restoration of ER homeostasis. Also eIF2α phosphorylation is a controlled mechanism: the C/EBP (CCAAT-enhancer-binding protein) homologous protein (CHOP), which is a pro-apoptotic transcription factor, is activated by ATF4; CHOP upregulates the growth arrest and DNA damage inducible gene 34 (GADD34) which dephosphorylates eIF2α, thus acting as a negative feedback loop and relieving the cell of the translational repression during prolonged ER stress (Chambers, J.E. et al., 2015; Liu, Z. et al., 2015; Marciniak, S.J. et al., 2004; Novoa, I. et al., 2001).

1.8.1.2 ATF6

After PERK activation and reduction of protein synthesis, ATF6 cleavage occurs next most rapidly. The relative delay is caused by the need for nuclear translocation of ATF6 and the induction of transcription and protein synthesis. ATF6 is comprised of two transmembrane basic leucine zipper (bZIP) transcription factors, ATF6α and ATF6β, which under normal conditions are held in the ER in a complex with GRP78/BiP (Yoshida, H. et al., 2000). When ER stress occurs and GRP78/BiP dissociates from ATF6, it translocates to the Golgi apparatus where the full length 90 kDa ATF6 is proteolytically processed by two Golgi resident enzymes: site-1 protease (S1P) and site-2 protease (S2P; Shen, J. and Prywes, R. 2004; Hetz, C. et al., 2012; Ye, J. et al., 2000). This releases a 50 kDa cytosolic bZIP transcription factor, which translocates into the nucleus and binds to several different promoter elements of ER stress response genes (Haze, K. et al., 1999; Hetz, C. et al., 2012;

Kokame, K. et al., 2001; Wang, Y. et al., 2000; Yoshida, H. et al., 1998). Among these target genes are XBP1, CHOP, as well as ER chaperones such as GRP78/BiP, which allow the ER to cope with the increased protein folding demand following UPR/ER stress (Haze, K. et al., 1999; Hetz, C. et al., 2012; Yoshida, H. et al., 2000).

1.8.1.3 IRE1α

IRE1α is a type 1 transmembrane serine/threonine receptor protein kinase that can also function as an endonuclease (Chen, Y. and Brandizzi, F., 2013; Tirasophon, W. et al., 1998; Tirasophon, W. et al., 2000). In response to ER stress and to subsequent release from GRP78/BiP, IRE1α homodimerizes and becomes autophosphorylated, leading to activation of its kinase and endoribonuclease functions (Chen, Y. and Brandizzi, F., 2013; Shamu, C.E. and Walter, P., 1996; Welihinda, A.A. and Kaufman, R.J., 1996). The endoribonuclease activity is responsible for promoting increased splicing of X-box binding protein 1 (XBP1) mRNA, a process by which a 26-nucleotide sequence of XBP1 mRNA is excised leading to a shift in its reading frame to create spliced XBP1 (XBP1s; Jiang, D. et al., 2015; Lee, K. et al., 2002). Unlike the unspliced XBP1 protein, which is rapidly degraded, XBP1s encodes a bZIP transcription factor with a potent transactivation domain (Jiang, D. et al., 2015; Lee, A.H. et al., 2003; Poothong, J. et al., 2017). XBP1s translocates to the nucleus where it leads to expression of a number of UPR target genes including genes involved in folding, secretion, degradation and ER translocation of proteins (Jiang, D. et al., 2015; Lee, A.H. et al., 2003; Yoshida, H. et al., 2001; Poothong, J. et al., 2017). Compared to activation of PERK and ATF6, there is a delay in the IRE1α pathway

due to the fact that the substrate XBP1 mRNA is expressed at low levels in non-stressed cells, but is upregulated by ATF6 in the presence of ER stress (Lee, K. et al., 2002; Oslowski, C.M. and Urano, F., 2011).

1.8.2 Additional GRP78/BiP localizations

GRP78/BiP is generally regarded as an ER resident chaperone protein. However, recent evidence suggests that GRP78/BiP can be actively translocated to other cellular locations and be secreted, thus assuming additional functions that control cellular signaling, proliferation, invasion, apoptosis, inflammation and immunity, with implications in cancer progression and therapeutic resistance (Figure 1.9; Lee, A.S., 2014).

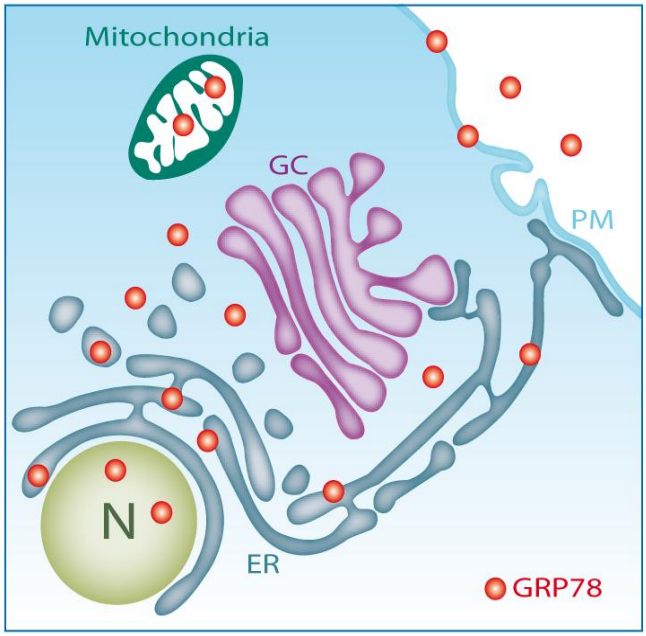

Cellular localization	Functions	References
ER	• Chaperone activity • Ca^{2+} binding activity • Target protein degradation • Regulation of ER stress and UPR	Flynn, G.C. et al., 1991; Ellgaard, L. and Helenius, A., 2003; Ni, M. and Lee, A.S. 2007; Romisch, K., 2005.
Cytoplasm	• Regulation of ER stress signaling pathway • Suppression of ER stress induced apoptosis • Suppression of lead-induced neurotoxicity	Ni, M. et al., 2009; Ni, M. et al., 2011; Qian, Y. et al., 2000; Qian, Y. et al., 2005.
Nucleus	• Cross-link to DNA • Suppression of DNA damage induced apoptosis	Ni, M. et al., 2011.
Mitochondria	• Regulation of energy balance during ER stress	Sun, F.C. et al, 2006; Shu, C.W. and Huang, C.M., 2008.
Cell surface	• Receptor for pro-survival growth signaling • Receptor for pro-apoptotic signaling	Shin, B.K. et al., 2003; Zhang, Y. et al., 2010.

Figure 1.9 Different GRP78/BiP localizations and functions. In addition to its main ER localization, GRP78/BiP can be actively translocated to other cellular locations, assuming additional functions. N = nucleus; ER = Endoplasmic reticulum; PM = plasma membrane.

A cytosolic novel isoform named GRP78va, deriving from ER stress-induced alternative pre-mRNA splicing, has been found at high levels in leukaemic cell lines and in leukaemia patient samples, specifically enhancing PERK signaling to promote cell survival under conditions of ER stress (Ni, M. et al., 2009; Ni, M. et al., 2011). However, it is still uncertain which client proteins the cytosolic GRP78/BiP

interacts with. Moreover, a cytosolic distribution of GRP78/BiP in astroglia cells has been shown to protect these cells against neurotoxicity (Qian, Y. et al., 2000; Qian, Y. et al., 2005). A nuclear form of GRP78/BiP has also been observed, specifically after its ectopic over-expression or its induction by ER stress, and it has been proposed it might have a role in the DNA cross-linking and in protecting the DNA damage-induced apoptosis (Ni, M. et al., 2011).

ER stress also promotes GRP78/BiP relocalization to the mitochondria, which are physically and functionally interconnected with the ER. Immunoelectron microscopy experiments confirmed the GRP78/BiP localization to the mitochondrial membrane compartment and demonstrate that this event occurs during UPR activation (Sun, F.C. et al, 2006). Mitochondria-associated GRP78/BiP has been shown to bind to the proto-oncogene serine/threonine-protein kinase RAF1, contributing to the maintenance of mitochondrial permeability and protecting against ER-stress-induced apoptosis (Shu, C.W. and Huang, C.M., 2008).

ER stress, or ectopic expression of GRP78, has also been associated with an additional atypical form of GRP78/BiP, that has been shown to preferentially localize on the cell surface of stressed endothelial cells and cancer cells (but not in either non-stressed or non-cancer cells), where it can act as a receptor that regulates different cellular activities (Zhang, Y. et al., 2010). First evidence of cell surface GRP78/BiP was reported in 1998, and was induced by thapsigargin treatment of human rabdomyosarcoma cells (Delpino, A. et al., 1998). Further studies indicated that there are numerous cancer cell lines whose global profile of

the cell surface proteome revealed the presence of GRP78/BiP and that, among other chaperone proteins, it is present in relatively high abundance (Shin, B.K. et al., 2003).

The understanding of how an ER resident protein such as GRP78/BiP can localize to the cell surface is an interesting aspect to be elucidated. It has been shown that the murine tumor cell DnaJ-like protein-1 (MTJ-1), as well as being a transmembrane protein, also acts as a co-chaperone to GRP78/BiP within the ER (Chevalier, M. et al., 2000). Silencing the MTJ-1 gene expression by small interfering RNA (siRNA) abolishes cell surface localization of GRP78/BiP, thus suggesting that MTJ-1 is essential for transport to the cell surface (Misra, U.K. et al., 2005). Another specific protein that in the prostate cancer cell line PC-3 has been reported to be able to transport GRP78/BiP to the cell surface is the tumor suppressor prostate apoptosis response 4 (PAR-4, also known as PAWR; Burikhanov, R., et al., 2009). However, it has been proposed that, since GRP78/BiP is expressed to such high levels in tumors, it may oversaturate the ER protein retrieval mechanism, resulting in co-trafficking to the cell surface with its client proteins (Li, J. and Lee, A.S., 2006; Luo, B. and Lee, A.S., 2013).

Cell surface GRP78/BiP acts as a multifunctional receptor impacting both cell proliferation and viability. A well-documented example of this function is represented by cell surface GRP78/BiP in prostate cancer cells, which acts as a high-affinity receptor for the activated form of the plasma proteinase inhibitor alpha-2-macroglobulin (α2M*; Misra, U.K. et al., 2002). The binding of α2M* to cell surface GRP78/BiP can promote cellular proliferation by triggering the extracellular

signal-regulated kinase (ERK) and the serine/threonine-protein kinases (AKT) activation, increasing DNA and protein synthesis (Misra, U.K. and Pizzo, S.V., 2012). Another pro-proliferative mechanism associated with GRP78/BiP is the interaction of cell surface GRP78/BiP with Cripto-1 (also known as teratocarcinoma-derived growth factor 1), a GPI-anchored oncoprotein that is developmentally regulated (Shani, G. et al., 2008). Cell surface GRP78/BiP is a necessary mediator of Cripto proliferative signaling in human cancer and disruption of cell surface GRP78/BiP and Cripto complex has been associated with blocking of different Cripto activation pathways (Kelber, J.A. et al., 2009).

1.8.3 GRP78/BiP and cancer

GRP78/BiP expression levels are highly induced in a variety of cancer cells and solid tumors, including breast, lung, prostate and ovarian cancers, melanoma and glioma cells (Bini, L. et al., 1997; Chatterjee, S. et al., 1994; Fernandez, P.M. et al., 2000; Koomagi, R. et al., 1999; Xing, X. et al., 2006). These findings correlate with the high proliferative rates of cancer cells and the observation that the knockdown of GRP78/BiP by siRNA inhibits tumor cell invasion *in vitro* as well as tumor growth and metastasis aggressiveness in xenograft models, suggesting an important role of GRP78/BiP in cancer progression (Fu, Y. and Lee, A.S., 2006; Gutierrez, T. and Simmen, T., 2014; Tan, J.S. et al., 2016; Urra, H. et al., 2016; Zhang, J. et al., 2006). The first evidence that GRP78/BiP is required for tumor growth came from the observation that fibrosarcoma cells with GRP78/BiP knockdown were unable to form tumors or they quickly regressed *in vivo* (Jamora, C. et al., 1996). Increasing

evidence has suggested an important cytoprotective role for GRP78/BiP in cancer as well as conferring drug resistance. In head and neck cancer (HNC) cell lines, GRP78/BiP is highly expressed and its knockdown by siRNA significantly reduced cell growth and colony formation, inhibiting migration and invasive ability (Chiu, C.C. et al., 2008). Over-expression of GRP78/BiP in gastric cancer correlates with tumor size, depth of invasion, lymphatic and venous invasion, lymph node metastasis and stage of disease (Zheng, H.C. et al., 2008). Moreover, its over-expression is inversely correlated with patient survival and its knockdown in gastric cancer xenograft mouse model inhibits tumor growth and metastasis (Zhang, J., et al., 2006). In hepatocellular carcinoma high GRP78/BiP expression correlates with increasing histological grade (Shuda, M. et al., 2003). Also in prostate tumors GRP78/BiP expression is markedly higher than that in benign prostate tissue, and the degree of GRP78/BiP expression correlates with increased risk of recurrence and reduced survival (Daneshmand, S. et al., 2007). In patients with diffuse large B-cell lymphoma, over-expression of GRP78/BiP is associated with worse overall survival (Mozos, A. et al., 2011).

However, while the majority of evidence indicates GRP78/BiP as a prognostic marker for poor outcomes in solid tumors, a few exceptions do exist. There is no evidence of a correlation between GRP78/BiP and pathological stage in lung cancer: patients with positive GRP78/BiP expression tend toward better prognosis (Uramoto, H. et al., 2005). Also in neuroblastoma, GRP78/BiP expression is higher in more differentiated tumors and correlates with better survival for patients with both well and poorly differentiated tumors (Hsu, W.M. et al., 2005). Finally, in

primary resected oesophageal adenocarcinoma, GRP78/BiP appears to be more elevated in the early stages of tumor as compared to the more advanced ones or to the normal oesophageal squamous epithelium. Moreover, survival analysis suggests a trend to better survival from oesophageal cancer in patients with higher levels of GRP78/BiP (Langer, R. et al., 2008).

1.8.3.1 GRP78/BiP as a novel therapeutic target

GRP78/BiP over-expression has been widely reported in many human cancers and associated with aggressive properties. Interfering with its activity in those tumors can reverse the malignant phenotypes, suggesting that GRP78/BiP might become a really attractive target for new drug development. Recently, specific GRP78/BiP inhibitors acting at multiple levels have been identified but the most interesting challenge is represented by the cell surface expression of GRP78/BiP, since it is primarily found in malignant but not normal cells and, thus, offers the opportunity for cancer-specific therapy and drug delivery with minimal harmful effects on normal cells.

Agents that inhibit the synthesis, the stability or the activity of GRP78/BiP already exist and they are able to simultaneously suppress its function, but the main problem is to minimize their toxicity to normal organs. A study on heterozygous knockout mouse models revealed that a 50% decrease in GRP78/BiP expression has no effect on normal organs but significantly impedes tumor growth (Dong, D. et al., 2011). Thus, these agents that selectively block the induction of GRP78/BiP

should only affect tumors that require a high level of the chaperone, saving normal organs.

An alternative strategy is represented by the gene therapy directed against the GRP78/BiP promoter. Because GRP78/BiP promoter is highly active in aggressive solid tumors, it could be used to direct expression of suicide genes, immunosuppressors and tumor suppressors. An example of GRP78/BiP promoter-driven suicide gene therapy activated by photodynamic therapy has been reported and it has been shown to cause regression of sizable human breast cancer tumor in mouse xenograft models in combination with ganciclovir (Dong, D. et al., 2004).

Alternatively, a selective destruction of GRP78/BiP at the protein level might be possible using the bacterial toxin Subtilase cytotoxin (SubAB). It consists of a binding pentamer of B units and an active A subunit; this A subunit (SubA) is a subtilase-like serine protease that, when transported to the ER, selectively attacks GRP78/BiP. SubA cleaves GRP78/BiP at a single site (Leucine 416 and Leucine 417) in an exposed loop connecting the ATPase and the substrate-binding domain of the molecule, thereby inactivating it (Montecucco, C. and Molinari, M., 2006; Paton, A.W. et al., 2006). The selective cleavage of GRP78/BiP by SubA releases PERK, IRE1α and ATF6 leading to overwhelming activation of the UPR and subsequent apoptosis (Matsuura, G. et al., 2009; Wolfson, J.J. et al., 2008).

Another way to effectively inactivate GRP78/BiP in cancer cells is to target its ATP-binding domain, since the ATPase catalytic activity of GRP78/BiP is necessary for its anti-apoptotic function (Reddy, R.K. et al., 2003). Recently, a number of novel

naturally occurring compounds have been demonstrated to down-regulate GRP78/BiP, including (-)-epigallocatechin gallate (EGCG), honokiol and aspirin (also known as salicylate; Ermakova, S.P. et al., 2006; Deng, W.G. et al., 2001). These compounds are able to directly bind to the ATP binding domain of the chaperone and, thus, inhibit its ATPase activity, sensitizing cancer cells to chemotoxic agents (Martin, S. et al., 2013).

Furthermore, GRP78/BiP inhibition of protein refolding activity could be achieved through the use of an unconjugated peptide derived from the co-chaperone BAG1 (BCL2 associated athanogene 1), that binds to the substrate binding domain of GRP78/BiP and inhibit its functionality (Maddalo, D. et al., 2012). Prostate cancer cells that stably express this peptide showed reduced growth and apoptosis in xenograft models in a manner dependent on binding to GRP78/BiP (Maddalo, D. et al., 2012).

Moreover, GRP78/BiP can be also inactivated by acetylation. It has been shown that GRP78/BiP is acetylated after histone deacetylase (HDAC) inhibition and, once acetylated, it dissociates from the three UPR stress sensors, causing UPR activation (Kahali, S. et al., 2010). Vorinostat is a drug already approved by FDA for the use in some types of cancer and, since it is an HDAC inhibitor, it could be used to interfere with GRP78/BiP activity (Kahali, S. et al., 2010; Manal, M. et al., 2016). In addition, several synthetic peptides containing GRP78/BiP-binding motifs fused to cell-death inducing peptides or cytotoxic drugs have been shown to induce apoptosis in many cancer cells *in vitro*, including human prostate and breast cancer cells, human melanoma, chemotherapy-resistant B lineage acute

lymphoblastic leukemia cells and multidrug resistant gastric cells (Miao, Y.R. et al., 2013).

Recently, a high affinity GRP78/BiP-specific mouse monoclonal IgG (immunoglobulin G) antibody (MAb159) was identified as a promoter of endocytosis and degradation of cell surface GRP78/BiP, thereby activating apoptosis (Liu, R. et al., M, 2013). Ab159 induces cancer cell death and suppresses the growth of colon and lung xenografts, the metastatic growth of human breast and melanoma xenografts and the growth of prostate cancer and leukemia in genetically engineered mouse models (Liu, R. et al., M, 2013). Another mouse monoclonal IgG antibody targeting the carboxyl-terminal domain of GRP78/BiP, C107, has been tested for its ability to induce apoptosis in melanoma cells *in vitro* and slow their growth as xenografts in mice (de Ridder, G.G., 2012). Also a human monoclonal IgM antibody (PATSM6) isolated from a patient with gastric cancer has been reported to simultaneously bind multiple GRP78/BiP molecules on the surface of tumor cells, inducing apoptosis in human multiple myeloma cells and suppressing human melanoma growth both *in vitro* and in xenografts (Hensel, F. et al., 2013; Rasche, L. et al., 2013; Rauschert, N., et al. 2008). It has also been reported that autoantibodies against GRP78/BiP from ovarian cancer patients promote apoptosis and decrease the invasiveness of ovarian cancer cells (Cohen, M. and Petignat, P., 2011). Moreover, autoantibodies against GRP78/BiP from prostate cancer patients are able to block cell surface GRP78/BiP signaling, potentially reducing the risk of cancer-related thrombotic events (Al-Hashimi, A.A. et al., 2010).

Overall, the existence of specific inhibitors and targeting agents directed against GRP78/BiP appears to hold great therapeutic promise. Their clinical efficacy, as well as a better understanding of the mechanisms of the stress-induced relocalization of GRP78/BiP from the ER to the cell surface and the other organelles, a broad identification of its interactive partners, and a deep characterization of the role of GRP78/BiP as a cancer prognostic marker, will greatly advance the knowledge of GRP78/BiP in cancer biology.

1.9 Conclusions

ADP-ribosylation is a reversible PTM catalyze by different classes of enzymes: ARTCs, ARTDs and some member of the sirtuin family. These include both mono- and poly-ADP-ribosylation, that, moreover, can be reversed by enzymes, such as ARHs, PARGs and macro domain containing proteins, which cleave the covalent bond to release the target protein. All these reactions have been established as important resources in the regulation of the biological activity of several proteins. Additionally, the role of this modification has been linked to different human diseases, such as inflammation, diabetes, neurodegeneration, and cancer, thus revealing the need for the development of specific ART inhibitors. Though the modification was discovered over 50 years ago, it has been only in the recent years that knowledge about ADP-ribosylation has been greatly improved.

Thanks to several proteomics techniques it has been possible to identify the ADP-ribosylation sites of previously known substrates. Moreover, novel ADP-ribosylated targets with central roles in signal transduction and intracellular

trafficking have been identified, as well as the discovery of a large number of new enzymes that can catalyze this PTM.

As a further confirmation of this being a challenging and exciting time in the field of ADP-ribosylation, a database of ADP-ribosylated proteins named "ADPriboDB" (http://ADPriboDB.leunglab.org) has been created very recently, as published on July 2016 by Vivelo and colleagues (Vivelo, C.A. et al., 2016). It is the first publicly available database containing information about ADP-ribosylated proteins collected from 1975 to 2015, with the aim of facilitating researchers finding and using this cumulative information about ADP-ribosylation reactions.

However, further improved understanding of how these enzymes are regulated and how the reaction they catalyze impacts upon different cellular functions are required. A better awareness of the basic biology of ADP-ribosylation in human physiology and pathology would have obvious clinical relevance for the treatment of various diseases. Considering the importance of ADP-ribosylation, the general aim of this study was to investigate the cellular role of GRP78/BiP mono-ADP-ribosylation. Specifically, the enzyme involved in the modification of the chaperone was identified, and the cellular localization of this enzyme was characterized. Then, the cellular role of this long-known GRP78/BiP mono-ADP-ribosylation in processes such as UPR and cancer was explored. Moreover, some aspects of the interaction between the mono-ART ARTD10 and its target GAPDH (glyceraldehyde 3 phosphate dehydrogenase) were investigated.

Chapter 2

2.1 Materials

2.1.1 Chemicals

All chemicals used for the work presented here were of high quality and are listed in Table 2.1 along with their suppliers.

Table 2.1 List of chemicals used in this study.

Name	Supplier
β-Mercaptoethanol	Fluka
Acetic acid	Carlo Erba
Acrylamide stock solution: 40% (w/v) acrylamide/bis-acrylamide (37.5:1)	Sigma-Aldrich
Agarose	Sigma-Aldrich
Amersham ECL Western Blotting Detection Reagent	GE Healthcare Life Sciences
Amersham Hyperfilm ECL	GE Healthcare Life Sciences
Amersham Low Molecular Weight Calibration Kit for SDS Electrophoresis	GE Healthcare Life Sciences
Ammonium chloride (NH_4Cl)	Sigma-Aldrich
Ammonium persulfate (APS)	Sigma-Aldrich
Ampicillin	Sigma-Aldrich
Annexin-V (FITC conjugated)	BD Biosciences
Bacto Agar	BD Biosciences
BigDye Terminator v3.1 Cycle Sequencing Kit	Applied Biosystems
Bio-Rad Protein Assay	Bio-Rad
Bovine serum albumin (BSA)	Sigma-Aldrich
Bromophenol blue	Sigma-Aldrich

Calcium chloride ($CaCl_2$)	Carlo Erba
Chloroform	Carlo Erba
cOmplete Mini EDTA-free Protease Inhibitor Cocktail Tablets	Roche Life Science
Coomassie Brilliant Blue G	Sigma-Aldrich
Cycloheximide (Chx)	Sigma-Aldrich
DEPC-treated water	Ambion
Dimethyl pimelimidate (DMP)	Pierce
Dimethyl sulfoxide (DMSO)	Sigma-Aldrich
Disodium phosphate (Na_2HPO_4)	Sigma-Aldrich
DL-Dithiothreitol (DTT)	Sigma-Aldrich
DNA ladder 100bp	Nippon genetics
DRAQ5	Cell Signaling
Dulbecco's modified Eagle's medium (DMEM)	Gibco/Lonza
Ethanol	Carlo Erba
Ethanolamine (C_2H_7NO)	Sigma-Aldrich
Ethidium bromide	Sigma-Aldrich
Ethylenediaminetetraacetic acid (EDTA)	Sigma-Aldrich
Ethylene glycol-bis(2-aminoethylether) N,N,N′,N′-tetraacetic acid (EGTA)	Sigma-Aldrich
FastGene Gel/PCR Extraction Kits	Nippon genetics
Fetal bovine serum (FBS)	Gibco/Lonza
Formaldehyde	Sigma-Aldrich
GenElute Plasmid Miniprep Kit	Sigma-Aldrich
Glutathione-sepharose resin	GE Healthcare Life Sciences
Glycerol	Merk
Glycine	Sigma-Aldrich
Hanks' Balanced Salt Solution without calcium and magnesium ($HBSS^{=}$)	Gibco

Hepes	Sigma-Aldrich
High-Capacity cDNA Reverse Transcription Kit	Applied Biosystems
Hoechst Stain solution	Sigma-Aldrich
Hydrogen chloride (HCl)	Carlo Erba
Isopropanol	Carlo Erba
Isopropyl-β-D-thiogalactoside (IPTG)	Sigma-Aldrich
jetPEI	Polyplus
jetPRIME	Polyplus
KAPA Taq PCR Kit	Kapa Biosystems
Kodak BioMax XAR Film	Sigma-Aldrich
Lysozyme	Sigma-Aldrich
L-Glutamine	Gibco
L-Glutathione reduced (GSH)	Sigma-Aldrich
Magnesium chloride ($MgCl_2$)	Sigma-Aldrich
MagPurix Cultured Cell DNA Extraction Kit	Zinexts
Methanol	Carlo Erba
Minimal Essential Medium (MEM)	Gibco/Lonza
Minimal Essential Medium Non-Essential Amino Acids (MEM NEAA)	Life Technologies
Monosodium phosphate (NaH_2PO_4)	Sigma-Aldrich
MOPS	Sigma-Aldrich
Mowiol 4-88	Calbiochem
Nitrocellulose membrane	Perkin Elmer
N,N,N′,N′-Tetramethylethylenediamine (TEMED)	Sigma-Aldrich
Nuclease free water	Ambion
NucleoSEQ	Macherey-Nagel
Paraformaldehyde	Electron Microscopy Sciences

Penicillin-streptomycin (P/S)	Life Technologies
Phosphate-buffered saline (PBS)	Gibco
Ponceau Red	Sigma-Aldrich
Potassium acetate (CH_3CO_2K)	Sigma-Aldrich
Potassium chloride (KCl)	Merk
Potassium dihydrogen phosphate (KH_2PO_4)	Sigma-Aldrich
Power SYBR Green PCR Master Mix	Applied Biosystems
Propidium iodide	BD Biosciences
Protein-A sepharose resin (CL-4B)	GE Healthcare Life Sciences
Puromycin	Sigma-Aldrich
Qiagen Plasmid Maxi Kit	Qiagen
QuikChange Site-Directed Mutagenesis Kit	Stratagene
Ribonuclease inhibitor	Takara
Roswell Park Memorial Institute 1640 Medium (RPMI)	Gibco/Lonza
Rubidium chloride (RbCl)	Sigma-Aldrich
Running buffer 10X	Bio-Rad Laboratories
Saponin	Sigma-Aldrich
Silver nitrate ($AgNO_3$)	Sigma-Aldrich
Skim milk powder	Fluka
Sodium azide (NaN_3)	Sigma-Aldrich
Sodium carbonate ($Na_2C_2O_3$)	Sigma-Aldrich
Sodium chloride (NaCl)	Carlo Erba
Sodium dodecyl sulphate (SDS)	Sigma-Aldrich
Sodium hydroxide (NaOH)	Carlo Erba
Sodium tetraborate ($Na_2B_4O_7$)	Sigma-Aldrich
Sodium thiosulfate ($Na_2S_2O_3$)	Sigma-Aldrich
Thapsigargin	Sigma-Aldrich

Transfer buffer 10X	Bio-Rad Laboratories
Triethanolamine ($C_6H_{15}NO_3$)	Sigma-Aldrich
Tris(hydroxymethyl)aminomethane (Tris)	Sigma-Aldrich
Triton X-100	Bio-Rad Laboratories
TRIzol reagent	Invitrogen
Trypsin-EDTA (0.5%), no phenol red	Gibco
Tryptone Peptone	BD Biosciences
Trypan Blue	Sigma-Aldrich
Tween-20	Sigma-Aldrich
Yeast Extract	BD Biosciences
3MM filter paper	Whatman

2.1.2 Oligonucleotides

All oligonucleotides used in the studies presented in this thesis, and their application, are listed in Table 2.2.

Table 2.2 List of oligonucleotides used in this study.

Name	5′-3′ Sequence	Application
ARTC1fwE240G	TCCCTGGAGAGGAAGGGGTGCTGATCCCC	Site-directed mutagenesis
ARTC1revE240G	GGGGATCAGCACCCCTTCCTCTCCAGGGA	Site-directed mutagenesis
ARTC1fwE238/240G	TCCCTGGAGGGGAAGGGGTGCTGATCCCC	Site-directed mutagenesis
ARTC1revE238/240G	GGGGATCAGCACCCCTTCCCCTCCAGGGA	Site-directed mutagenesis
ARTC1 qRT For	GGCCTCATGGAAGCACTTCA	(qRT)-PCR

ARTC1 qRT Rev	GAGAAGAGGTCTCGTCGTGTGA	(qRT)-PCR
ATF4 qRT For	TTGAGGATAGTCAGGAGCGT	(qRT)-PCR
ATF4 qRT Rev	TGGAACACACAGCTACAGCA	(qRT)-PCR
CHOP qRT For	ACCAAGGGAGAACCAGGAAACG	(qRT)-PCR
CHOP qRT Rev	TCACCATTCGGTCAATCAGAGC	(qRT)-PCR
GAPDH qRT For	CAACTTTGGTATCGTGGAAGGAC	(qRT)-PCR
GAPDHqRT Rev	ACAGTCTTCTGGGTGGCAGTG	(qRT)-PCR
GRP78 For	TAGCATCTGAGCTGGCTCCT	PCR
GRP78 Rev	GTGTCAGGCGATTCTGGTCA	PCR
GRP78/BiP qRT For	ACGTGGAATGACCCGTCTGT	(qRT)-PCR
GRP78/BiP qRT Rev	AACCACCTTGAACGGCAAGA	(qRT)-PCR
XBP1 qRT For	TTACGAGAGAAAACTCATGGC	(qRT)-PCR
XBP1 qRT Rev	GGGTCCAAGTTGTCCAGAATGC	(qRT)-PCR
siGENOME Human HSPA5 siRNA SMARTpool	CCACCAAGAUGCUGACAUU GAAAGGAUGGUUAAUGAUG CGACUCGAAUUCCAAAGAU CAGAUGAAGCUGUAGCGUA	Gene silencing
siRNA1ARTC1	AUGCAUGAGACACGGGACA dTdT	Gene silencing
siRNA2ARTC1	ACACGGAGUUCCAGGCCAA dTdT	Gene silencing
siRNA3ARTC1	GCCCUGGCCUCCUUUGAUG dTdT	Gene silencing
siRNA4ARTC1	GCGAGUACAUCAAAGACAA dTdT	Gene silencing

All oligonucleotide sequences were purchased from Sigma-Aldrich; siGENOME Human HSPA5 siRNA reagent was from Dharmacon.

2.1.3 Antibodies

All the primary antibodies used in this study were raised against the following proteins: actin, ART1, ATF6, calnexin, calreticulin, flag, GAPDH, giantin, GRP78/BiP,

GST, lamp-1, protein disulfide isomerase (PDI), tubulin and WGA. The secondary antibodies used were anti-mouse and anti-rabbit. Their specific supplier, animal host, dilution and application (WB: Western Blotting; IF: immunofluorescence) are listed in Table 2.3.

Table 2.3 List of antibodies used in this study.

Name	Supplier	Animal host	Dilution	Application
Anti-Actin	Sigma-Aldrich	Mouse	1:2000	WB
Anti-ART1	Sigma-Aldrich	Rabbit	1:500	WB
Anti-ART1	AbCam	Rabbit	1:70	IF
Anti-ATF6	Imgenex	Mouse	1:100	IF
Anti-Calnexin	BD Biosciences	Mouse	1:50	IF
Anti-Calreticulin	AbCam	Mouse	1:100	IF
Anti-Flag	Sigma-Aldrich	Mouse	1:5000	WB
Anti-Flag	Sigma-Aldrich	Rabbit	1:500	IF
Anti-GAPDH	Santa Cruz	Mouse	1:1000 1:50	WB IF
Anti-Giantin	Giuseppe Di Tullio (FMNS)	Mouse	1:100	IF
Anti-GRP78/BiP	BD Biosciences	Mouse	1:1000	WB
Anti-GRP78/BiP	Santa Cruz	Rabbit	1:100	IF
Anti-GST	Giuseppe Di Tullio (FMNS)	Rabbit	1:1000 1:10000	WB IF
Anti-HA	Cell Signalling	Rabbit	1:600 1:1000	IF WB
Anti-Lamp1	Sigma-Aldrich	Mouse	1:100	IF
Anti-Mouse	Calbiochem	Goat	1:10000	WB

Anti-Mouse (Alexa Fluor 488)	Thermo Fisher Scientific	Goat	1:400	IF
Anti-Mouse (Alexa Fluor 546)	Thermo Fisher Scientific	Goat	1:400	IF
Anti-PDI	Stressgen	Mouse	1:100	IF
Anti-Rabbit	Calbiochem	Goat	1:10000	WB
Anti-Rabbit (Alexa Fluor 488)	Thermo Fisher Scientific	Goat	1:400	IF
Anti-Rabbit (Alexa Fluor 546)	Thermo Fisher Scientific	Goat	1:400	IF
Anti-Tubulin	Sigma-Aldrich	Mouse	1:2000	WB
Anti-WGA	Thermo Fisher Scientific	/	1:200	IF

2.1.4 Solutions and buffers

All solutions and buffer used were freshly prepared and are listed in Table 2.4.

Table 2.4 List of solutions and buffers used in this study.

Name	Contents
Annexin-V binding buffer	10 mM Hepes/NaOH (pH 7.4), 10 mM NaCl, 2.5 mM $CaCl_2$
Binding buffer	50 mM Tris-HCl (pH 7.4), 100 mM NaCl, 1.5 mM $MgCl_2$, 10% FBS; 0.5 mM DTT (before use)
Blocking buffer A	3% milk (w/v) in 1X PBS
Blocking buffer B	10% FBS (v/v) in 1X PBS
Cell lysis buffer	20 mM Tris (pH 7.5), 150 mM NaCl, 1 mM EDTA, 1 mg EGTA, 1% Triton X-100; 1 mM DTT (before use), 1 protease inhibitor cocktail tablet per 10 mL of lysis buffer (before use)
Destaining solution	30% (v/v) methanol, 10% (v/v) acetic acid, 40% (v/v) H_2O

Developing solution	0.04% (v/v) formaldehyde in 2% (w/v) $Na_2C_2O_3$
Fixing solution	50% (v/v) methanol, 5% (v/v) acetic acid, 45% (v/v) H_2O
GST-eluition buffer	20 mM Tris-HCl (pH 8), 150 mM NaCl, 1 mM EDTA, 1 mM DTT, 10 mM GSH
GST-lysis buffer	20 mM Tris-HCl (pH 8), 150 mM NaCl, 1 mM EDTA, 1 mM DTT
GST-washing buffer	1X PBS, 1 mM DTT
IF Blocking solution	0.05% saponin, 0.5% BSA, 50 mM NH_4Cl in PBS
LB agar	LB medium plus 1.5% (w/v) agar: autoclaved 15 min at 121°C
LB medium	1% Tryptone Peptone, 0.5% Yeast extract, 1% NaCl, autoclaved 15 min at 121 °C
Mowiol 4-88 solution	20 mg Moviol, 80 mL 1X PBS, 40 mL glycerol, pH 6-7
Paraformaldehyde 4%	Paraformaldehyde 8%, PBS 10X, H_2O
1X PBS	1.5 mM KH_2PO_4, 8 mM Na_2HPO_4, 2.7 mM KCl, 137 mM NaCl, pH 7.4
Ponceau Red staining solution	0.1% (w/v) Ponceau Red in 5% (v/v) acetic acid
RF1 buffer	100 mM RbCl, 50 mM $MnCl_2$, 30 mM CH_3CO_2K, 10 mM $CaCl_2$, 15% (v/v) glycerol, pH 5.8
RF2 buffer	RbCl 10 mM, MOPS 10 mM, $CaCl_2$ 75 mM, glycerol 15% (v/v), pH 6.8
RIPA buffer	100 mM Tris-HCl (pH 7.5), 1% Igepal, 0.5% deoxycholate, 0.1% SDS; 1 protease inhibitor cocktail tablet per 10 mL of RIPA buffer (before use)
Sample buffer 4X	250 mM Tris-HCl (pH 6.8), 40% (v/v) glycerol, 0.02% (w/v) Bromophenol blue, 8% (w/v) SDS; 20% (v/v) β-Mercaptoethanol (before use)
Sensitizing solution	0.02% $Na_2S_2O_3$ (w/v) in H_2O
Silver Nitrate solution	0.1% (w/v) $AgNO_3$ in water
Staining solution	50% (v/v) methanol, 40% (v/v) H_2O, 10% (v/v) acetic acid, 0.1% (w/v) Coomassie Brilliant Blue G

T-PBS	0.05% (v/v) Tween-20 in 1X PBS
1X TAE	40 mM Tris (pH 7.6), 20 mM acetic acid, 1 mM EDTA
Trypan Blue solution	0.4% (w/v) Trypan Blue in PBS
WB Blocking solution	1% (w/v) BSA or 5% (w/v) milk in T-PBS

2.1.5 Software

The following software were used in this study:

- Excel (Microsoft), version 2016 for Windows;
- FinchTV (Geospiza Inc.), version 1.4.0;
- GraphPad PRISM (GraphPad software Inc.), version 4.0 for Windows;
- ImageJ (NIH), version 1.43;
- LSM510 (Carl Zeiss Inc.), version 3.2 SP3;
- Primer Express (Applied Biosystems Inc.), version 3.0;
- 7500 Fast System (Applied Biosystems Inc.).

2.2 Methods

2.2.1 Cell culture and treatments

2.2.1.1 Growth conditions and propagation of cell lines

The cell lines used and their respective culture media are listed in Table 2.5.

Table 2.5 List of cell lines used in this study.

Cell line	Culture medium
A2780	RPMI 1640 + 10% FBS + 2 mM L-Glutamine + 100 U/mL P/S
CAOV-3	DMEM + 10% FBS + 2 mM L-Glutamine + 100 U/mL P/S
CHO	DMEM + 10% FBS + 2 mM L-Glutamine + 100 U/mL P/S
HeLa	MEM + 10% FBS + 5 mM NEAA + 2 mM L-Glutamine + 100 U/mL P/S
IGROV-1	RPMI 1640 + 10% FBS + 2 mM L-Glutamine + 100 U/mL P/S
OVCA-432	RPMI 1640 + 10% FBS + 2 mM L-Glutamine + 100 U/mL P/S
OVCAR-3	RPMI 1640 + 10% FBS + 2 mM L-Glutamine + 100 U/mL P/S
OVCAR-5	RPMI 1640 + 10% FBS + 2 mM L-Glutamine + 100 U/mL P/S
SKOV-3	RPMI 1640 + 10% FBS + 2 mM L-Glutamine + 100 U/mL P/S

Chinese Hamster Ovary (CHO) cells and Human cervical cancer (HeLa) cells were from American Type Culture Collection (ATTC, USA). Human ovarian carcinoma cell lines A2780, CAOV-3, IGROV-1, OVCA-432, OVCAR-3, OVCAR-5 and SKOV-3 were obtained from the Mario Negri Institute for Pharmacological Research, kindly provided by Dr. Eugenio Erba.

The cells were cultured in 10 cm^2 petri dishes under controlled atmosphere in the presence of 5% CO_2 at 37°C. All cell culture work was performed under sterile conditions. Cells were subcultured 2-3 times per week at a dilution of 1:3 - 1:10, depending on the cell line. For subculture, cells were washed once with $HBSS^=$ and detached from the petri dish by adding 0.05% Trypsin-EDTA for 5 minutes. After addition of fresh medium to block the protease action, cells were collected into a plastic tube and centrifuged for 5 min at 1200 rpm (revolutions per minute). The

supernatant was aspirated, the cell pellet was resuspended in fresh medium and placed in a new petri dish. All cell lines were routinely tested for Mycoplasma contamination by fluorescence microscopy using Hoechst staining.

2.2.1.2 Cell freezing and recovery

Cells from one 10 cm^2 petri dish were grown to ~80/90% confluency as described above. After the centrifugation, the cell pellet was resuspended into 1 mL of freezing solution. An appropriate freezing solution was used for each cell line, following the recommendations for cryopreservation available on the cell line data sheets. The freezing solutions used for each cell lines are listed in Table 2.6.

Table 2.6 List of cell line freezing solutions used in this study.

Cell line	Freezing solution
A2780	Culture medium + 50% FBS + 10% DMSO
CAOV-3	Culture medium + 5% DMSO
CHO	FBS + 10% DMSO
HeLa	FBS + 10% DMSO
IGROV-1	Culture medium + 10% DMSO
OVCA-432	Culture medium + 10% DMSO
OVCAR-3	Culture medium + 50% FBS + 10% DMSO
OVCAR-5	Culture medium + 10% DMSO
SKOV-3	Culture medium + 10% DMSO

The cells were afterwards transferred into a cryotube and placed directly on ice. After about 24 hours at -80°C, the tubes were transferred in the liquid nitrogen cell storage (-196°C).

For recovery of the cells after freezing, the frozen cells were directly thawed into a 10 cm^2 petri dish with fresh complete medium and 1 mL of FBS. The cells were allowed to attach for one day and then their medium was replaced with fresh complete medium.

2.2.1.3 Cell stress treatments

To evaluate the possible role of hARTC1 in ER stress, the cells were treated with different types of know stressors, which are listed below. For cell stress treatments, cells were seeded in 6-well plates, cultured until ~80/90% confluency and treated with DTT, thapsigargin or subjected to heat shock or hypoxia. DTT is a water-soluble reducing reagent that blocks disulfide-bond formation, thereby quickly leading to ER stress. For DTT treatment, the medium of cells grown for 24 hours was replaced with new medium containing 2 mM DTT. After incubation for 20 minutes, 60 minutes or 120 minutes, cells were collected and analyzed as described below. Thapsigargin is a specific inhibitor of the sarcoplasmic/endoplasmic reticulum calcium-ATPase. Treatment with thapsigargin results in a decrease of ER calcium levels that, in turn, causes the loss of the activity of the calcium-dependent ER chaperones and leads to the accumulation of unfolded proteins, consequently activating ER stress. Thapsigargin is sparingly soluble in aqueous buffer, but it is soluble in organic reagent such as DMSO. For thapsigargin treatment, the medium

of cells grown for 24 hours was replaced with new medium containing 0.3 µM or 1 µM thapsigargin. After incubation for 20 minutes, 60 minutes, 120 minutes, 18 hours or 24 hours, cells were collected and analyzed as described below. For thapsigargin experiments, cells treated with DMSO without thapsigargin were also analyzed, in order to validate thapsigargin specific effect. DMSO did not affect GRP78/BiP protein expression or GRP78/BiP ADP-ribosylation. For heat shock treatment, the medium of cells grown for 24 hours was replaced with new medium and the plate was placed in an incubator with temperature set to 42°C. After 24 hours, the plate was removed from the incubator and cells were collected and analyzed as described below. For hypoxia treatment, the medium of cells grown for 24 hours was replaced with new medium that was preincubated at least for one hour in hypoxic conditions. After addition of this new medium, the plate was placed in an incubator set to 0.1% of O_2, 37°C and 5% of CO_2. After 24 hours, the plate was removed from the incubator and cells were collected and analyzed as described below. Cell stress treatments were analyzed by (qRT)-PCR, Western Blotting, macro-domain far-Western Blotting or immunofluorescence (see Chapters 2.2.3; 2.2.4, 2.2.6; 2.2.7).

2.2.1.4 Cell transfection

2.2.1.4.1 Cell transfection with DNA (plasmids)

To over-express a protein of interest DNA transfection was performed using jetPEI reagent. All the cDNAs used were produced in the laboratory of my supervisor, Dr. Maria Di Girolamo.

Cells were seeded in petri dishes 24 hours prior to transfection. The number of cells seeded varied among the cell lines and was calculated such that the cells would be ~50-70% confluent on the day of the transfection. The transfection mix was prepared according to the manufacturer's protocol using a DNA:jetPEI ratio of 1:2 (w/v) in 150 mM NaCl, with a 15-30 minutes incubation at room temperature prior to addition to the culture. The amount of DNA transfected and the relative volume of jetPEI and NaCl depended on the surface of cell growth are listed in Table 2.7.

Table 2.7 DNA transfection protocol according to the cell culture vessel per well.

Culture vessel	Amount of DNA (µg)	Volume of jetPEI reagent (µL)	Volume of NaCl solution for both DNA and jet PEI (µL)	Total volume of complexes added per well (µL)
24-well	1	2	50	100
12-well	2	4	50	100
6-well	3	6	100	200
10 cm^2 petri dish	10-20	20-40	250	500

Specifically, DNA was diluted in 150 mM NaCl to the final volume recommended for each specific culture vessel. The DNA solution was vortexed gently and spun down briefly. In a separate tube, jetPEI was diluted in 150 mM NaCl to the final volume recommended for each specific culture vessel, vortexed gently and spun down briefly. The jetPEI solution was added to the DNA solution all at once. The obtained DNA/jetPEI mixture was vortexed immediately, spun down briefly and kept for 15 to 30 minutes at room temperature. In the meantime, cell medium was aspirated and replaced with an appropriate volume of serum free medium. Finally, the DNA/jetPEI mixture was added drop-wise to the cells and homogenized by gently swirling the plate. The petri dish was then returned to the cell culture incubator and cells were analyzed as required.

2.2.1.4.2 Cell transfection with siRNAs

To down-regulate a protein of interest siRNA transfection using jetPRIME reagent was performed, following the guidelines mentioned in the instruction manual.

Cells were seeded in petri dishes 24 hours prior to transfection. The number of cells seeded varied among the cell lines and was calculated such that the cells would be ~50-60% confluent one day after the transfection.

To silence hARTC1 cells were transfected with a pool of different siRNAs at 30 nM each (details are given in Chapter 4); to silence GRP78/BiP cells were transfected with 100 nM of siGENOME Human HSPA5 siRNA reagent.

Oligonucleotides used for gene silencing were resuspended in DEPC-treated water using an appropriate volume to have a 20 µM stock concentration. Once

resuspended, aliquots of 20 µL were prepared and stored at -20°C, avoiding multiple freeze-thaw cycles.

The volume of jetPRIME and jetPRIME Buffer needed for complex formation depended on the surface of cell growth and are outlined in Table 2.8.

Table 2.8 siRNA transfection protocol according to the cell culture vessel per well.

Culture vessel	Volume of jetPRIME reagent (µL)	Volume of jetPRIME Buffer (µL)
24-well	2	50
12-well	3	100
6-well	4	200

Specifically, siRNA oligonucleotides were diluted into an appropriate volume of jetPRIME Buffer, depending on the specific culture vessel used. After having mixed the solution by pipetting up and down, jetPRIME reagent was added. The obtained mixture was then vortexed, spun down briefly and incubated for 10 to 15 minutes at room temperature. In the meantime, cell medium was replaced with an appropriate volume of serum free medium. Finally, the transfection mix was added drop-wise to the cells. The petri dishes, gently rocked back and forth, was then returned to the cell culture incubator and analyzed as required.

2.2.2 Cell biology

2.2.2.1 Cell proliferation assay

To determine the effect of hARTC1 on cell proliferation, cells either over-expressing or silenced for hARTC1 were analyzed by direct counting of the cells. Cells were seeded in 12-well plates and counted every 24 hours for 3 days. At the designated time points, the incubation medium was aspirated and cells were detached adding 500 µL of 0.05% Trypsin-EDTA for 5 minutes. After addition of 500 µL of fresh medium, cells were collected into a plastic tube and 10 µL of cell suspension were loaded into a Neubauer chamber. Cell number was determined by twice counting 4 fields with 16 squares each.

The total number of cells/mL was calculated as follow:

$$\text{cells/mL} = \frac{\text{average of total cells count in 4 squares}}{4} \times 10^4$$

2.2.2.2 Cell viability assay

To determine the effect of hARTC1 on cell viability, cells either over-expressing or silenced for hARTC1 were analyzed by Trypan Blue exclusion test. Cells were seeded in 12-well plates. 24 hours later, the incubation medium was aspirated and cells were detached adding 500 µL of 0.05% Trypsin-EDTA for 5 minutes. After addition of 500 µL of fresh medium, cells were collected into a plastic tube. One part of the cell suspension and one part of Trypan Blue solution were put into a new small plastic tube, mixed by pipetting up and down and incubated for five

minutes at room temperature. Afterwards, 10 µL of the composite were loaded into a Neubauer chamber and dead and live cells were determined by twice counting 4 fields with 16 squares each. The numbers of living and dead cells were used to calculate the viability, as well as the total number of cells.

The percent viability was calculated as follow:

$$\text{Cell Viability (\%)} = \frac{\text{average of total viable cells (unstained)}}{\text{average of total cells (stained and unstained)}} \times 100$$

The number of total cells was calculated as described in Chapter 2.2.2.1.

2.2.2.3 Annexin-V/Propidium Iodide dual staining for apoptosis

Analysis of cells undergoing apoptosis was evaluated by binding of FITC-conjugated Annexin-V and uptake of propidium iodide by flow cytometry (FCM) on a BD Facs CANTO flow cytometer.

Cells were seeded in 6-well plates and analyzed every 24 hours for 3 days. At the designated time points, the incubation medium was aspirated and cells were washed twice with $HBSS^{=}$. Cells were detached adding 2 mL of 5 mM EDTA until they were just released from the plate surface. After addition of an equal volume of $HBSS^{=}$ to deactivate EDTA, cells were harvested into a plastic tube and centrifuged at 1100 rpm for 5 minutes at 4°C. The supernatant was removed and cells were resuspended in 1 mL of $HBSS^{=}$. The cellular suspension was transferred into round bottom polystyrene tubes and subsequently centrifuged at 1100 rpm for 5 minutes at 4°C. $HBSS^{=}$ was removed and cell pellet was resuspended in 200

µL of Annexin-V binding buffer containing 5 µL of FITC-conjugated Annexin-V. The sample was vortexed and incubated for 10 minutes at room temperature in the dark. After this time, a volume of 2 mL of Annexin-V binding buffer was added and the sample was centrifuged at 1100 rpm for 5 minutes at 4°C. The supernatant was removed and the pellet was resuspended in 200 µL of Annexin-V binding buffer containing 10 µL of Propidium Iodide (20 µg/mL). After being vortexed, cells were immediately analyzed by flow cytometry.

2.2.3 Biochemistry

The expression of a protein of interest was analyzed by Western Blotting, measuring the protein levels through antibody binding to the specific proteins of interest. Before the immunological detection, sample proteins were extracted from their source using an optimized lysis buffer, separated within a gel through electrophoresis and transferred to a membrane via a "blotting" procedure. After proteins immobilization on the membrane, the proteins of interest were identified using antibodies conjugated for visualization via chemiluminescent mechanism.

2.2.3.1 Preparation of total lysates

Cells were seeded in 6-well plates or in 10 cm^2 petri dishes and treated as required. At the designated time points, the incubation medium was aspirated and cells were washed 3 times briefly with 3-5 mL of cold 1X PBS. In the meantime, cell lysis buffer was prepared as indicated in the Chapter 2.1.4. After aspirating 1X PBS, cell lysis buffer was added to the cells and cells were scraped and transferred into a

1.5 mL Eppendorf tube. During the harvesting of cells, they were always kept on ice. The Eppendorf tube was placed on a rotating wheel for 20 minutes and then sonicated 3 times for 3-4 seconds, with 5 seconds rest in between, using an ultrasonic bath with a 60% amplitude output. Whole cell lysate was centrifuged at 11400 rpm for 10 minutes in a centrifuge chilled to 4°C. The resulting pellet was discarded and the supernatant was aspirated, transferred into a fresh Eppendorf tube and stored at -80°C until use.

2.2.3.2 Sodium dodecyl sulphate-polyacrylamide gel electrophoresis (SDS-PAGE)

2.2.3.2.1 Assembly of polyacrylamide gels

Two 16 x 18 cm glass plates were used for assembling a regular gel. The glass plates were assembled to form a chamber using two 1.5 mm plastic spacers aligned along their lateral edges. The plates were then fixed using two clamps and mounted on a plastic base, which sealed the bottom.

The resolving gel was poured first and was prepared by mixing distilled H_2O, 40% (w/v) acrylamide/bis-acrylamide solution, 1.5 M Tris-HCl pH 8.8, 10% (w/v) SDS, in order to have the selected concentration of acrylamide, 375 mM of Tris-HCl, 0.1% (w/v) SDS. Then, 0.1% (w/v) APS and 0.1% (v/v) TEMED were added. The solution was pipetted and poured in the gap between the plates, leaving ~5 cm for the stacking gel. Soon after pouring, the gel was covered on the top with distilled water to avoid the solution making contact with oxygen, which inhibits the

polymerization. To allow it to gel, it was left standing for 45-60 minutes at room temperature.

After the setting of the resolving gel, the distilled water was removed and the stacking gel was poured next. The stacking gel was prepared by mixing distilled H_2O, 40% (w/v) acrylamide/bis-acrylamide solution, 0.5 M Tris-HCl pH 6.8, 10% (w/v) SDS, in order to have 4% (w/v) of acrylamide, 125 mM Tris-HCl, 0.1% (w/v) SDS. Then, 0.1% (w/v) APS and 0.1% (v/v) TEMED were added. The solution was pipetted and poured onto the resolving gel. A Teflon 15-well comb was immediately placed between the glasses, into the stacking gel. Normally, this gel was allowed to polymerize for 60 minutes at room temperature.

2.2.3.2.2 Sample preparation and running

The concentration of protein in the samples was determined using Bio-Rad Protein Assay. 2 µL of the sample were diluted in 780 µL of sterile water and put into a disposable plastic cuvette. 200 µL of Bradford reagent were added to the sample and mixed well. The absorbance of the sample was measured at 595 nm. The protein concentration of the sample was determined using a calibration curve previously constructed by plotting the absorbance at 595 nm of samples containing known BSA concentrations.

After quantification, samples were prepared for gel electrophoresis using ~60-100 µg of total proteins. An adequate volume of each sample was mixed with 4X sample buffer, adding distilled water to make the total volume to 120-150 µL. After

mixing well, samples were heated at 100°C for 10 minutes in a Multi-Block Heater (Lab-Line, IL, USA), cooled at room temperature and briefly centrifuged.

Before loading, once the gel was polymerized, the comb was removed from gel without disturbing the wells and the wells were washed twice with 1X running buffer, that was prepared from 10X stock by dilution with distilled water.

The heated samples were loaded into the wells and one or two wells were loaded with 20 µL of molecular weight standards which served to follow the running of the samples and for the cutting of the membrane at the given protein molecular weights. Aliquots of highly purified protein standards were prepared reconstituting the lyophilized mixture with 200 µL of 1X sample buffer. After a brief centrifugation, aliquots of 20 µL were prepared and stored at -20°C or immediately use.

The gel was then transferred into the electrophoresis apparatus (Hoefer Scientific Instruments) and the gel chamber was filled with 1X running buffer. A covering lid was placed properly on the gel chamber by connecting corresponding electrodes (black to black and red to red), while the other ends of electrodes were connected to a voltage supply unit. The electrophoresis was carried out under a constant current of 8 mA for overnight runs.

2.2.3.2.3 Silver Staining and gel drying

After electrophoresis, the gel was incubated with fixing solution for 15 minutes at room temperature with gentle shaking. Then it was rapidly washed three times with water and finally placed in water for 1 hour on a shaking platform. The gel was then incubated in sensitizing solution for 1-2 minutes, rapidly washed twice with

water and incubated for 30 minutes at 4°C with chilled silver nitrate solution. After that, the gel was incubated with developing solution. The development was stopped by adding 5% acetic acid solution and washed twice with water before adding 1% acetic acid solution. Finally, the gel was dried with a gel dryer (Hoefer Scientific Instruments) at 80°C for 4 hours.

2.2.3.2.4 Coomassie Brilliant Blue staining

The running gel was carefully transferred to a staining box and rinsed with deionized water. Enough staining solution to cover the gel was poured into the staining box and kept in rocking position for 2 hours to stain the gel. After discarding the used staining solution, the gel was incubated with destaining solution for 1-2 hours under constant shaking, to remove excess stain. The gel was then extensively washed with water to reduce unbound dye background and dried as described above.

2.2.3.3 Western blotting

2.2.3.3.1 Protein transfer onto nitrocellulose

One piece of nitrocellulose membrane, and two pieces of 3MM filter paper, were cut to the size of a gel. Just before SDS-PAGE running was finishing, the Western Blotting "sandwich" was assembled. Firstly, 2-3 sponges were soaked in 1X transfer buffer, facing the positive pole of the transfer chamber. One piece of filter paper was laid on the three sponges and nitrocellulose was laid above the filter paper.

Once the gel had finished running, it was removed from the running rig and glass plates. It was rinsed with 1X transfer buffer and carefully transferred onto the nitrocellulose. After that, another piece of 3MM filter paper was placed on the gel. The excessive transfer buffer and air bubbles in between the gel, the membrane and the filter paper were removed by gently rolling and pressing with a pipette. Another 3 sponges were placed on top and the negative pole of the transfer chamber was used to close off the sandwich.

This blot sandwich was slotted into the blotting apparatus (Hoefer Scientific Instruments) that was subsequently filled with 1X transfer buffer. Transfer was carried out at a constant current of 400 mA for 5 hours.

2.2.3.3.2 Ponceau Red staining

To check protein transfer, the sandwich was disassembled and the nitrocellulose filter was stained with Ponceau Red, a reversible red-coloured protein dye.

Briefly, the membrane was incubated with Ponceau Red solution for 5 minutes at room temperature under constant agitation. At the end of this incubation time, the membrane was rinsed twice with 5% acetic acid and once with water, to remove the excess of unbound dye. After the destaining, the transferred proteins were visualized as red bands on the nitrocellulose membrane.

2.2.3.3.3 Immunostaining

Membrane-immobilized proteins were probed with specific antibodies to identify and quantitate the protein of interest. To perform the probing, the nitrocellulose

membrane was cut into strips with a razor blade. The strips were incubated in blocking solution for 60 minutes at room temperature, to block non-specific binding of the antibodies.

Following the blocking step, the strip was washed 3 times for 5 minutes with T-PBS. Then, it was incubated with a primary antibody directed against the protein of interest, diluted at the appropriate concentration in blocking solution. Incubation with primary antibody was performed for 1 hour at room temperature or overnight at 4°C.

The primary antibody was then discarded and the strip was washed 3 times with T-PBS, for 5 minutes each. After washing, the strip was incubated for 1 hour at room temperature with an appropriate HRP (horseradish peroxidase)-conjugated secondary antibody diluted in blocking solution.

Finally, the strip was washed 3 times for 5 minutes with T-PBS and then incubated with ECL (enhanced chemiluminescence) reagent in the dark, according to the manufacturer instructions. The excess substrate was removed from the strip by holding it upright and touching a piece of blotting paper with the bottom edge of the strip. The drained piece of membrane was placed into an autoradiography cassette, using a plastic wrap to cover it. After gently smoothing out any air pockets, the autoradiography film was placed on the top of the strip. Typically, exposure time ranged from few seconds to several minutes, and usually repeated exposures were done, varying the time, as needed, for optimal detection. To finally visualize the protein band, the film was developed using an auto-processor in a darkroom. Densitometric evaluation was carried out with ImageJ software.

2.2.4 Molecular biology

Different molecular biology experiments were performed, each with a specific aim. Site-directed mutagenesis was used to create a catalytically inactive mutant of the protein of interest. Small- and large-scale DNA preparations were used to obtain the DNA of interest, that would be used for protein expression analysis through DNA transfection. RNA extraction, reverse transcription and quantitative real-time Polymerase Chain Reaction (qRT)-PCR were performed for the measurements of gene transcription. DNA extraction, PCR and DNA sequencing were performed to search for the presence of mutation(s) in a specific sequence of interest.

2.2.4.1 Site-directed mutagenesis

Point mutations were generated using QuikChange Site-Directed Mutagenesis Kit following the protocol supplied by the manufacturer. Single mutagenesis of glutamate 240 to glycine (E240G) or double mutagenesis of both glutamate 238 and glutamate 240 to glycine (E238G/E240G) were performed on the plasmid pME.CD8ART1.

The mutagenic primers were designed to contain the specific mutation in the middle, with 10 to 15 bases of the correct sequences flanking on either side. Primers were normally between 25 and 45 bases in length, terminated in one or more cytosine or guanine bases, had a GC content of more than 40% and a melting temperature (T_m) of 78°C or higher. The primers used are listed in Table 2.1.2.

The PCR reaction was set up in a final volume of 50 µL and contained the following components:

5 µL of 10X reaction buffer (100 mM KCl, 100 mM $(NH_4)_2SO_4$, 200 mM Tris-HCl pH 8.8, 20 mM $MgSO_4$, 1% Triton X-100, 1 mg/mL nuclease-free BSA);

50 ng of plasmid DNA;

125 ng of forward primer (1.5 µL);

125 ng of reverse primer (1.5 µL);

1 µL of supplied dNTP mix;

2.5 U/µL of PfuTurbo DNA polymerase (1 µL);

sterile double distilled water to make the volume to 50 µL.

PCR was carried out using a programmable thermal cycler, with the following cycling conditions: 1 cycle of 95°C for 1 minute; 18 cycles of 95°C for 30 seconds, 55°C for 1 minute and 68°C for 12 minutes; 1 cycle of 68°C for 7 minutes; 4°C for infinity.

Following the amplification reaction, the PCR product was digested by adding 10 U/µL of Dpn I restriction enzyme, which digested the parental, non-mutated, methylated plasmid. The reaction was incubated for 1 hour at 37°C. 16 µL of the Dpn I-treated DNA were used to transform 80 µL of DH5α competent cells.

2.2.4.2 Preparation of competent cells

Escherichia coli DH5α bacterial strain was used to produce competent cells by rubidium chloride method (Kushner, 1978). Bacteria were streaked and incubated overnight on a LB plate. Next day, one single colony was inoculated into 10 mL of

LB and grown overnight at 37°C with shaking at 225 rpm. 1 mL of the overnight saturated culture was inoculated into 9 mL of fresh LB and grown until the optical density (OD) at 600 nm was 0.3. The bacteria were sub-cultured 1:20 into 100 mL pre-warmed LB and grown until the OD at 600 nm reached 0.48. The cells were chilled on ice and centrifuged at 3000 rpm at 4°C for 5 minutes. The obtained supernatant was removed and the pellet gently resuspended in 40 mL of chilled RF1 buffer. The suspension was left on ice for 2 hours, centrifuged as before and gently resuspended in 4 mL of chilled RF2 buffer. Aliquots of 200 µL were prepared in sterile 1.5 mL Eppendorf tubes and stored at -80°C.

2.2.4.3 Transformation of bacteria by heat-shock

Competent DH5α bacteria were thawed on ice and 80 µL added to 15 µL of plasmid, equaling approximately 15 ng of DNA. After gently mixing, the mixture was left on ice for 30 minutes, heat shocked for 120 seconds at 42°C and then returned to ice for 2 minutes. 600 µL LB were added and the mixture was inverted gently before incubating at 37°C for 90 minutes under a constant shaking of 200 rpm. The culture was then plated on LB agar containing 100 µg/mL of ampicilin and incubated overnight at 37°C. The next day, an isolated bacterial colony was picked from the plate and used to inoculate 5 mL of LB containing the appropriate antibiotic. The culture was incubated overnight at 37°C and used for preparation of bacterial glycerol stocks.

2.2.4.4 Preparation of glycerol stocks of bacteria

800 µL of overnight bacterial culture grown in LB medium supplemented with 100 µg/mL of ampicilin were gently mixed with 200 µL of sterile glycerol (20% v/v). After approximately 5 minutes at room temperature, cells were transferred to -80°C for long-term storage.

2.2.4.5 Small-scale preparation of plasmid DNA (miniprep)

Plasmid DNA for small-scale preparation was purified using the GenElute Plasmid Miniprep Kit according to the manufacturer's instructions. All the solutions used were supplied with the kit. A single colony from a plate obtained after transformation of bacteria was inoculated in 2 mL of LB medium containing 100 µg/mL of Ampicilin and shaken overnight at 200 rpm and 37°C. The day after, the overnight culture was transferred into a 2 mL Eppendorf tube and pelleted by centrifugation at 13000 rpm for 5 minutes. The supernatant was removed and the cell pellet was resuspended in 200 µL of Resuspension Solution, vortexing or pipetting up and down to thoroughly resuspend the cells until homogeneous. Cell lysis was achieved by addition of 200 µL Lysis Solution. The content was immediately mixed by gentle inversion until the mixture became clear and viscous and it was allowed to stand at room temperature for 3-5 minutes. Cell debris precipitation was obtained by adding 350 µL of Neutralisation/Binding Solution and gently inverting the tube 4–6. The precipitate was collected by centrifugation at 13000 rpm for 10 minutes. A spin column inserted into a collection tube was

prepared for use by addition of 500 µL of Column Preparation Solution and centrifuged for 1 minute at 13000 rpm. The flow-through liquid was discarded.

The supernatant obtained after addition of Neutralisation/Binding Solution and centrifugation of the mixture was transferred to the spin column and centrifuged at 13000 rpm for 1 minute. The flow through liquid was discarded and 750 µL of Wash Solution were added to the spin column. After centrifugation at 13000 rpm for 1 minute, the flow through liquid was discarded and the column was centrifuged again at 13000 rpm for 1 minute without any additional Wash Solution to remove the excess of ethanol from the spin column.

The spin column was then transferred into a new fresh collection tube and 50 µL of sterile water were added. This was allowed to stand for 1 minute prior to elution of the DNA by centrifugation at 13000 rpm for 1 minute. The resultant eluent containing the DNA was ready for immediate use or storage at –20°C. The concentration and purity of the sample were measured by spectrophotometric analysis. Specifically, 2 µL of DNA were diluted in 198 µL of sterile water (1:100 dilution), put into a 96-well UV compatible plate and analyzed using a spectrophotometer. The DNA concentration and purity were assessed by UV spectroscopy.

The concentration of DNA was calculated from the absorbance at 260 nm using the formula based on the Beer-Lambert law (that predicts a linear change in absorbance with concentration):

$$\text{DNA Concentration in µg/µL} = \frac{\text{A260 x 50 (DNA coefficient) x 100 (dilution factor)}}{1000}$$

Purity was calculated measuring the A260/A280 ratio. A ratio of ~1.8 is generally accepted as "pure" for DNA. The sequence of all the constructs purified were confirmed by automated DNA sequencing performed at the BMR Genomic service (Padua, Italy).

2.2.4.6 Large-scale preparation of plasmid DNA (maxiprep)

Large-scale DNA plasmid preparation was performed using the Qiagen Plasmid Maxi Kit, following the manufacturer's purification protocol. All the solutions used were supplied with the kit. A small amount of bacteria transformed with the plasmid of interest were scraped from the glycerol stock, inoculated in 2 mL of LB medium containing 2 µL of 100 µL/mL ampicilin and grown overnight at 37°C under continuous shaking at 200 rpm for 6-8 hours.

This preculture was used to inoculate 250 mL of LB containing 100 µL/mL ampicillin. After an overnight incubation, the bacteria were collected by centrifugation at 6000 rpm in JA14 rotor for 10 minutes at 4°C. The supernatant was removed and the cell pellet was resuspended in 10 mL of Buffer P1, vortexing or pipetting up and down until no cell clumps remained. 10 mL of Buffer P2 were added to the content, mixed thoroughly by vigorously inverting the sealed tube 4–6 times and incubated at room temperature for 5 minutes. After addition of 10 mL of chilled Buffer P3, the content was mixed immediately and thoroughly by vigorously inverting 4–6 times and incubated on ice for 20 minutes. The sample was centrifuged at 8000 rpm for 60 minutes at 4°C and the supernatant, containing plasmid DNA, was recovered and centrifuged again at 8000 rpm for 15 minutes at

4°C. In the meanwhile, a column was equilibrated by applying 10 mL of Buffer QBT and the column was allowed to empty by gravity flow. The recovered supernatant was applied to the equilibrated column and allowed to enter the resin by gravity flow. After complete passage of the sample through the column, it was washed twice by adding 30 mL of Buffer QC.

When all the Buffer QC has completely passed through the column, DNA was eluted by adding 15 mL of Buffer QF. The eluate was collected into a 50 mL falcon tube.

DNA precipitation was obtained by adding 10.5 mL of room-temperature isopropanol to the eluted DNA. Sample was immediately mixed by inverting the tube 4–6 times and centrifuged at 8000 rpm for 60 minutes at 4°C. The supernatant was carefully decanted and the DNA pellet was washed with 15 ml of room-temperature 70% ethanol. After centrifugation at 18000 rpm for 15 minutes, the supernatant was carefully decanted without disturbing the pellet. The pellet was allowed to air-dry and then redissolved in a suitable volume (300-400 µL) of sterile water. The concentration and purity of the sample were measured by spectrophotometric analysis, as described in Chapter 2.2.4.5. The sample was then aliquoted into sterile 1.5 mL Eppendorf tubes and stored at -20°C.

2.2.4.7 Total RNA extraction

Cells were seeded in 6-well plates and treated as required. At the designated time points, cell medium was removed and cells were washed twice with 1 mL of ice cold $HBSS^{=}$. 1 mL of TRIzol reagent was added per well and, after pipetting several

times, cells were collected into a sterile 1.5 mL Eppendorf tube RNase- and DNase-free. The sample was stored at -20°C until RNA extraction.

To obtain RNA, the sample was thawed and 200 µL of chloroform were added per 1 mL of TRIzol reagent used for the initial homogenization. The sample was mixed by vigorous shaking by hand for 15 seconds and incubated for 3 minutes at room temperature. Following centrifugation of 11400 rpm for 15 minutes at 4°C, the mixture separated into a lower red phenol-chloroform phase, an interphase, and a colorless upper aqueous phase, that exclusively contained RNA. This upper aqueous phase was carefully transferred into a new fresh Eppendorf tube without disturbing the underlying interphase. The volume of the aqueous phase should be about 50-60% of the volume of TRIzol reagent used.

The subsequent precipitation of the RNA from the aqueous phase was obtained by adding 1 mL of isopropanol per 1 mL of TRIzol reagent used for the initial homogenization. The sample was incubated for 10 minutes at room temperature and centrifuged at 11400 rpm for 10 minutes at 4°C. The precipitated RNA formed a gel-like pellet at the tube bottom of the tube.

After completely removing the supernatant, the RNA pellet was washed with 1 mL of 75% ethanol per 1 mL of TRIzol reagent used for the initial homogenization. The sample was mixed by vigorous shaking by hand for 15 seconds and centrifuged at 9000 rpm for 5 minutes at 4°C. The leftover ethanol was removed as much as possible, without touching the pellet, and the RNA pellet was allowed to air dry. 10-15 µL of DEPC-treated water were added to the pellet and mixed gently by pipetting. RNA concentration and purity were measured by spectrophotometric

analysis. Specifically, 2 µL of RNA were diluted in 198 µL of DEPC-treated water (1:100 dilution), put into a 96-well UV-compatible plate and analyzed using a spectrophotometer.

The concentration of RNA was calculated from the absorbance at 260 nm using the formula based on the Beer-Lambert law (that predict a linear change in absorbance with concentration):

$$\text{RNA Concentration in µg/µL} = \frac{\text{A260 x 40 (RNA coefficient) x 100 (dilution factor)}}{1000}$$

Purity was calculated measuring the A260/A280 ratio. A ratio of ~2 is generally accepted as "pure" for RNA. The obtained RNA was stored at -20°C or used directly for cDNA synthesis.

2.2.4.8 Reverse transcription

Total RNA preparations were retro-transcribed using the High-Capacity cDNA Reverse Transcription Kit, following the manufacturer's instruction. All the components used were supplied with the kit. All steps were carried out on ice, unless otherwise specified. cDNA was generated using 2 µg of total RNA in a total reaction volume of 20 µL.

Firstly, RNA sample was prepared putting 2 µg of total RNA in DEPC-treated water for a reaction volume of 10 µL. Sample was left on ice until addiction of the RT Master Mix.

RT Master Mix (10 µL) was prepared as follows:

- 2 µL of 10X RT Buffer;

- 0.8 µL of 25 x dNTP Mix (100 mM);

- 2 µL of 10 x RT Random Primers;

- 1 µL of MultiScribe Reverse Transcriptase;

- 0.5 µL of RNase Inhibitor (not included in the kit);

- 3.7 µL of DEPC-treated water.

10 µL of RT Master Mix were added to 10 µL of RNA sample, pipetting up and down two times to mix. The tube was sealed, briefly centrifuged to spin down the contents and to eliminate any air bubbles and placed into the thermal cycler.

The reverse transcription was performed using the following conditions: 25°C for 10 minutes; 37°C for 120 minutes; 85°C for 5 minutes; 4°C for infinity. After setting the reaction volume to 20 µL, sample was loaded into the thermal cycler and the reverse transcription run was started. The resulting cDNA was used immediately for (qRT)-PCR, or the cDNA was stored at -20°C until use.

2.2.4.9 Quantitative real-time Polymerase Chain Reaction (qRT)-PCR

cDNA obtained from retro transcription reactions were used to measure expression levels of different genes. The cDNA samples were diluted to 20 ng/µL adding 80 µL of DEPC-treated water to the 20 µL of retro transcription reactions. Gene-specific primers were designed by using Primer Express 3.0 software and are listed in Table 2.1.2. Primers were resuspended using an appropriate volume of DEPC-treated water to have a 100 µM stock concentration. Once resuspended, aliquots were prepared and stored at -20°C, avoiding multiple freeze-thaw cycles.

The amplifications were done with the SYBR Green PCR Master Mix. For each reaction, the following mixture was used:

- 5 µL of Power SYBR Green PCR Master Mix;
- 1.2 µL of primers at the concentration of 150 nM;
- 0.8 µL of DEPC-treated water;
- 3 µL of cDNA (60 ng).

PCR assays were performed in 96-well optical reaction plates using the ABI 7500HT machine (Applied Biosystem). Instrument settings were as follow: 95°C for 10 minutes, followed by 40 cycles at 95°C for 15 seconds and then 1 minute at 60°C. The experiments were carried out in triplicate for each data point. Baseline values of amplification plots were set automatically and threshold values were kept constant to obtain normalized cycle times and linear regression data.

The relative quantification in gene expression was determined using the ΔΔCt method, obtaining the fold changes in gene expression normalized to an internal control gene, and relative to one calibrator. The housekeeping gene GAPDH was used as internal control to normalize all data, while the choice of the calibrator varied among the different experiments and it is specified in the text where relevant.

2.2.4.10 Automated genomic DNA extraction

Samples of frozen cells were directly thawed and centrifuged at 10000 rpm for 5 minutes. The supernatant was removed and the cell pellet was washed once with 1 mL of 1X PBS. Samples were vortexed and, after resuspending the cell pellet using

1 mL of 1X PBS, they were centrifuged a second time for 5 minutes at 6000 rpm. 400 µL of provided Buffer BL2 and 20 µL of provided proteinase K solution were added to each sample, that were subsequently mixed by vortexing. Afterwards, samples were incubated at 56°C in a thermomixer set at 800 rpm overnight, until they were completely lysed. Lysis time varies depending on the type and quantity of samples, without influencing the preparation; considering each sample derived from one 10 cm^2 petri dish, an overnight lysis was used. Subsequently, DNA extraction was performed using the automated extractor MagPurix (Zinexts).

2.2.4.11 DNA quantification

DNA concentration and purity were estimated using a NanoDrop Spectrophotometer (Thermo Scientific). For quantification, 1 µL of sterile double distilled water was applied to the pedestal to calibrate the instrument. Then, each DNA sample was mixed, 1 µL was applied to the pedestal and reading was measured. After quantification of all samples, their concentration was adjusted as appropriate for subsequent analysis. Specifically, samples were diluted in sterile double distilled water to a final concentration of 50 ng/µL.

2.2.4.12 Standard PCR

Samples were subjected to standard PCR amplification using the KAPA Taq PCR Kit. After having properly thawed and mixed all the reagents needed, a PCR mix containing the appropriate volume of all reaction components was prepared. The

forward and reverse primers that were used for the PCR were designed using Primer-BLAST and are listed in Table 2.1.2.

The PCR reaction was set up in a final volume of 25 µL and contained the following components:

- 2.5 µL of 10X provided reaction buffer;
- 1 µL of genomic DNA;
- 1 µL of primer mix (forward plus reverse);
- 0.5 µL of supplied dNTP mix;
- 0.1 µL of KAPA Taq DNA Polymerase;
- sterile bidistilled water to make the volume to 25 µL (19.9 µL).

PCR amplification was performed in a programmable thermal cycler, using the following cycling conditions: 1 cycle of 95°C for 5 minutes; 40 cycles of 95°C for 30 seconds, 67°C for 30 seconds and 72°C for 30 seconds; 1 cycle of 72°C for 7 minutes; 4°C for infinity.

2.2.4.13 Agarose gel electrophoresis

The amplification products were analyzed by electrophoresis. 5 µL of the PCR product, mixed with 3 µL of Bromophenol blue, were loaded on a 2% agarose gel in 1X TAE buffer. 0.5 µL/mL ethidium bromide were added to the gel to make visualization of the DNA via UV light possible. The gel was run for 15 minutes at 200 mV in 1X TAE buffer. A DNA ladder of 100 bp was used to determine the size of the amplified products.

2.2.4.14 Purification of PCR products

The Fastgene Gel/PCR Extraction Kit was used for the purification of the PCR products. All buffers were provided with the kit. One volume of sample (20µL) was mixed with five volumes of Binding Buffer GP1 by vortexing. A FastGene GP Column was placed into a collection tube and the sample mixture from previous step was applied into the column. After centrifugation at 13000 rpm for 30 seconds, the flow-through was discarded and the column was placed back into the collection tube. 600 µL of Wash Buffer GP2 were added to the column and it was centrifuged at 13000 rpm for 30 seconds. The flow-through was discarded and the column was placed back into the collection tube. An additional centrifugation of 2 minutes at 13000 rpm was performed to dry the column matrix. The FastGene GP Column was transferred into a new microcentrifuge tube and 20 µL of Elution Buffer GP3 were added to the centre of the column matrix. This was allowed to stand for 2 minutes until Elution Buffer was absorbed by the matrix. Elution of purified DNA was obtained with another centrifugation at 13000 rpm for 2 minutes.

2.2.4.15 DNA sequencing and analysis

Sequencing was carried out using the BigDye Terminator v.3.1 Cycle Sequencing kit, following the standard protocol.

For each reaction, this specific mixture was prepared:

- 0.1 µL of provided Big Dye Solution;

- 0.1 µL of provided Big Dye Buffer;

- 0.6 µL of primer reverse;

- 2 µL of PCR product;

- sterile double distilled water to make the volume to 20 µL (17.2 µL).

The sequencing reactions were run for 2 hours, using the following cycling conditions: 96°C for 1 minute; 25 cycles at 96°C for 10 seconds, 50°C for 5 seconds and 60°C for 4 minutes; 4°C for infinity.

Each reaction was purified with NucleoSeq and the final sequencing was obtained using the automatic sequencer ABI PRISM 3130 XL Genetic Analizer (Applied Biosystems). Sequence results were then visualized using the FinchTV software version 1.4.0 and compared to the actual NCBI (National Center for Biotechnology Information) reference sequences of the gene of interest *human Grp78/BiP*.

2.2.5 Co-immunoprecipitation experiments

Co-immunoprecipitation experiments were performed to validate the specific protein-protein interaction between ARTD10 and GAPDH. To perform co-immunoprecipitation, an antibody against a target protein (HA-ARTD10) was coupled to Sepharose beads through protein A, then the complexes containing the target protein were immunoprecipitated with the antibody-coupled beads by centrifugation. Protein components in the complexes were then separated by SDS-PAGE and visualized by Western Blotting using antibodies specific to the different components (anti-HA and anti-GAPDH).

For the experiment, semi-confluent transiently transfected cells were incubated with RIPA buffer (500 µL/10 cm^2 petri dish). The cells were scraped off the plate and broken by shearing (14 times) through a 25-gauge syringe needle. During the harvesting of the cells they were always kept on ice. The obtained lysates were then collected and centrifuged at 13000 rpm for 15 minutes at 4°C. The protein concentration of the supernatants was measured using Bio-Rad Protein assay kit, following the procedure described in Chapter 2.2.3.2.2. After quantification, samples were incubated with 2 µg of anti-HA antibody for each 500 µg of lysate. Incubation was overnight at 4°C under constant shaking (200 rpm). The day after, the samples were incubated with 40 µL of a 50% slurry of protein-A Sepharose resin for 1 hour at 4°C, with constant rotation (200 rpm). The resin was washed three times with RIPA buffer, and then boiled in loading buffer. The samples were then analyzed Western Blotting using antibodies raised against GAPDH or the HA tag.

2.2.6 Immunofluorescence microscopy

Immunofluorescence experiments were performed to analyze the localization of the proteins of interest using markers for different cellular compartments, and to quantify the amount of the specific protein in these different cellular compartments. For immunofluorescence, cultured cell lines were fixed onto glass slides and then probed using two different antibodies. The first one bound to the target protein, but was not fluorescently labeled itself (primary antibody). The second one (secondary antibody) specifically recognized the primary antibody

and carried a fluorescent dye. The fluorescent dyes used were Alexa Fluor dyes: Alexa Fluor 488 was used for green-fluorescence, while Alexa Fluor 546 was used for red-fluorescence. Depending on the host species of the primary antibody, Alexa 488- or Alexa 546-conjugated goat anti-rabbit or anti-mouse antibodies were used. For DNA staining, the cell permeable far-red fluorescent DNA dye DRAQ5 (1,5-bis{[2-(di-methylamino)ethyl]amino}-4, 8-dihydroxyanthracene-9,10-dione) was used.

2.2.6.1 Cell fixation and immunolabeling

Cells were seeded onto 24-well glass slides and left for 24 hours to attach. Cells were then transfected for the indicated time or left untreated and immediately fixed. For fixation, the medium was completely removed carefully from the wells and cells, after being washed 5 times with 1X PBS, were incubated with 300 µL of 4% paraformaldehyde for 10 minutes at room temperature. After washing 5 times with 1X PBS, cells were permeabilized with 300 µL of IF blocking solution for 20 minutes at room temperature. IF blocking solution was then removed, cells washed 5 times with 1X PBS and stained with the primary antibodies solution. Appropriate primary antibodies (Table 2.1.3) were prepared by diluting in IF blocking solution. 8 µL spots of antibodies solution were incubated with each glass slide. After a 1 hour incubation at room temperature in the dark, cells were washed 5 times with 1X PBS and stained with the secondary antibodies solution. 8 µL spots of secondary antibodies diluting in IF blocking solution (Table 2.1.4) were incubated with each slide for 1 hour at room temperature in the dark. Glass slides were then

rinsed 5 times with 1X PBS and mounted using Mowiol 4-88 solution. They were left to dry overnight and stored at 4°C until analysis by confocal microscopy.

2.2.6.2 Immunofluorescence analysis with confocal microscopy

Immunofluorescence samples were observed using a laser scanning confocal microscopy (Zeiss LSCM 510) equipped with 40X and 63X oil emersion objectives. Optical confocal sections were taken at 1 Airy unit with a resolution of 512x512 or 1024x1024 pixels and exported as TIFF files.

2.2.6.3 Co-localization analysis

Co-localization was analyzed using LSM510-3.2 software. To assess the co-localization the background immunofluorescence was removed by adjusting the threshold levels and the histo and co-localization functions of the above software were used. The software provided two co-localization coefficients that range from 0 (no co-localization) to 1 (complete co-localization). The co-localization coefficients indicated the amount of pixels of the channel A that co-localized with pixels from channel B and *vice versa*. Finally, the co-localization extent was expressed as a percentage of co-localizing immunofluorescent pixels relative to the total immunofluorescence per channel.

2.2.7 GST-Af1521 macro domain affinity tool

The Af1521 macro domain from *Archaeoglobus fulgidus* was used as an affinity probe for recognizing ADP-ribosylated targets, taking advantage of the previous

demonstration of its high affinity for ADP-ribose and its ability to bind not only ADP-ribose, but also ADP-ribosylated proteins (Karras, G.I. et al., 2005). Dani and colleagues demonstrated it could be used in pull-down experiments in combination with mass spectrometry, allowing identification of mono-ADP-ribosylated target (Dani, N. et al., 2009). In addition to pull-down experiments, the macro domain Af1521 was used for the setting up of biochemical and immunofluorescence techniques, revealing as a useful tool for the identification of ADP-ribosylated proteins.

2.2.7.1 GST-Af1521 macro domain purification

pGEX4T1 vector containing GST-Af1521 macro domain (wild-type) and GST-Af1521 (G42E) macro domain (mutant) were produced in our laboratory by Annalisa Stilla, by sub-cloning His-Af1521 macro domain (wild-type) and His-Af1521 (G42E) macro domain (mutant) kindly provided by Dr. Ladurner A. (EMBL Genome Biology Unit, Heidelberg, Germany).

For purification, a small amount of DH5α *Escherichia coli* strain harbouring the GST-Af1521 macro domain (wild-type) or the GST-Af1521 (G42E) macro domain (mutant) were scraped from the glycerol stock (see Chapter 2.2.4.4) and inoculated in 100 mL of LB containing 100 µg/mL of Ampicilin. The culture was grown overnight at 37°C under continuous shaking (200 rpm). This culture was diluted 1:20 in 500 mL of the same medium and grown under the same conditions, constantly monitoring the OD at 600 nm. As soon as the OD approximately reached 0.6, the fusion protein was induced for about 3 hours and 30 minutes at

37°C with 0.5 mM IPTG. The total bacterial culture was harvested by centrifugation at 600 rpm for 15 minutes at 4°C. The resulting bacterial pellet was re-suspended (40 mL/L of culture) in GST-lysis buffer in the presence of protease inhibitors and 0.5 mg/mL lysozyme. The suspension was incubated for 30 minutes on ice under continuous shaking and then stored at -80°C overnight. In parallel, 1 mL of the induced and non-induced cultures was taken to confirm the protein expression. Samples were collected by centrifugation and lysed with sample buffer. 25 µL of the lysates were fractionated on polyacrilamide gel that was subsequently stained with Coomassie brilliant blue, as described in Chapter 2.2.3.2.4.

The following day, the bacterial suspension was thawed at room temperature and 1% Triton X-100 and 1 mM fresh DTT were added. The suspension was incubated for 20 minutes on ice under continuous shaking and then lysed by sonication on ice (5-7 pulse of 10 seconds each). The lysate was then centrifuged at 15000 rpm for 15 minutes at 4°C. The supernatant was recovered and added to 1 mL of glutathione-sepharose resin previously equilibrated in lysis buffer. The suspension was incubated for 2-3 hours at 4°C under gentle agitation and then pelleted at 200 rpm for 8 minutes at 4°C to sediment the matrix. After discarding the supernatant, the resin was packed into a 10 mL column and washed 5-10 times with GST-washing buffer. Protein elution was started by adding 300 µL of GST-elution buffer, followed by 6 elution with 1 mL of GST-elution buffer. The purified protein was then dialyzed (1:200 v/v) against 1X PBS. The resulting protein concentration was measured using Bio-Rad Protein assay kit, following the

procedure described in Chapter 2.2.3.2.2. The protein was then aliquoted and stored at -80°C.

2.2.7.2 GST-Af1521 macro domain cross-linking

For cross-linking, the resin was washed twice with a 10-fold volume of 0.2 M Sodium tetraborate pH 8.6, the supernatant was removed and the resin was incubated with a 10-fold volume of 0.2 M Sodium tetraborate pH 8.6. It was centrifuged and subsequently incubated with a 2-fold volume of triethanolamine added with 20 mM DMP for 1 hour at room temperature. After this step, the supernatant was discarded and washed once with a 10-fold volume of 0.2 M ethanolamine pH 8.2. Then, the cross-linking reaction was quenched by incubating the resin with 0.2 M ethanolamine pH 8.2 for 1 hour at room temperature. The resin was washed 3 times with 10-fold volume of 1X PBS and once with a 10-fold volume of 0.1 M glycine pH 2.5. These washes were repeated 3 times. Finally, the resin was washed 3 times with 1X PBS and stored in 1X PBS plus 0.02% NaN_3 at 4°C. For every step, a small amount of resin (7 µL) was taken to check the cross-linking procedure by SDS-PAGE analysis.

2.2.7.3 GST-Af1521 macro domain pull-down assay

2-10 mg of total lysates for each sample, solubilized with 700 µL of RIPA buffer, were incubated with a glutathione-sepharose resin for 2 h at 4 °C, for the preclearing step. The supernatant underwent a two-step pull-down; the first with 50 µg of macro domain mutant (G42E) covalently cross-linked to a resin, which

cannot recognize ADP-ribosylated proteins. In this way, all the proteins that non-specifically recognize the cross-linked Af1521 macro domain were eliminated. After an overnight incubation at 4°C, the supernatant of the first pull-down was incubated overnight at 4°C with 50 µg of macro domain wild-type. The beads were collected with centrifugation at 200 rpm for 5 minutes and washed 3 times with 1 mL of RIPA buffer. Proteins that remained bound to the resin were eluted at 100°C for 5 min with sample buffer and subjected to SDS-PAGE. The eluted proteins analyzed by gels underwent Coomassie brilliant blue staining or silver staining, and the bands of interest were analyzed by MALDITOF-MS (matrix-assisted laser desorption/ionization time-of-flight-mass spectrometry) or by LC-MS/MS (liquid chromatography tandem-mass spectrometry).

2.2.7.4 GST-Af1521 macro domain far-Western Blotting

For far-Western Blotting, cell lysates were prepared as described in Chapter 2.2.3.1. Samples were separated by SDS-PAGE using an 8% polyacrylamide gel and subsequently blotted onto nitrocellulose filter, as described previously. After protein transfer onto nitrocellulose, the membrane was initially incubated with blocking buffer A for 1 hour at room temperature, followed by an overnight incubation at 4°C with blocking buffer B. The day after, the solution was discarded and the filter was incubated with binding buffer containing 50 ng/mL of purified GST-macro domain (wild-type or mutant) for 1 hour at room temperature. The binding buffer was discarded and the filter was washed 3 times with T-PBS, 5 minutes each. The membrane was then incubated with a polyclonal anti-GST

antibody for 3 hours at room temperature. Following 3 washes of 5 minutes each with T-PBS, the filter was incubated with an HRP-conjugated anti-rabbit antibody for 90 minutes at room temperature. Finally, the membrane was washed 3 times with T-PBS for 5 minutes each and incubated with ECL reagent in the dark for ECL-based detection with autoradiography films, following the same procedure described in Chapter 2.2.3.3.3.

2.2.7.5 GST-Af1521 macro domain immunofluorescence

Cells were seeded onto 24-well glass slides and left for 24 hours to attach. Cells were then transfected for the indicated time or left untreated and immediately fixed and permeabilized. The procedures used for fixation and permeabilization were the same of that described in Chapter 2.2.5.1. After that, cells were incubated with 60 ng/µL of purified GST-macro domain (wild-type or mutant) diluting in IF blocking solution for 1 hour at room temperature, in the dark. Cells were then washed and incubated with a primary anti-GST antibody and then with a specific secondary antibody, following the protocol described previously for immunofluorescence cells labeling. The primary and secondary antibodies used with the appropriate dilutions are listed in Table 2.1.3

After mounting the glass slides with Mowiol 4-88 solution, they were left to dry overnight and stored at 4°C until analysis by confocal microscopy.

2.2.8 Statistical analysis

For analysis of mRNA copy number and protein levels, all quantitative data were expressed as mean±standard deviation (SD) of three or more separate experiments (unless otherwise specified).

All statistical analyses were performed using the GraphPad PRISM software version 4.0.

For cell stress treatments and cell transfection experiments, Unpaired Student's t-tests were performed on the means and the p values were calculated. A p-value less than 0.05 or 0.01 was considered to be statistically significant, as specified in each figure. For ovarian cancer cell lines screening, the D'Agostino and Pearson omnibus normality test was used to check the uniform distribution of the values.

For co-localization analysis, values were expressed as mean±standard error of the mean (SEM) of three or more separate experiments (unless otherwise specified). They were analyzed by one-way analysis of variance (ANOVA) and a p-value less than 0.0001 was considered to be statistically significant.

Chapter 3

Mono-ADP-ribosylation of GRP78/BiP by hARTC1 expressed within the endoplasmic reticulum

3.1 Introduction

ARTCs comprise a small group of proteins that are either GPI-anchored enzymes localized at the external side of the plasma membrane, or are secreted into the extracellular compartment (Glowacki, G. et al., 2002; Koch-Nolte, F. et al., 2008). Rat, mouse and human ARTCs have been well studied and characterized. Rat (r) and mouse (m) have six functional enzymes (ART1, ART2.1 and ART2.2, ART3, ART4 and ART5), with the *Artc2* gene that is duplicated. Human (h) ARTC family is composed of only four proteins (hARTC1, hARTC3, hARTC4 and hARTC5), since *Artc2* is a pseudogene containing three premature in-frame stop codons that preclude its expression. Two of these four hARTCs, hARTC1 and hARTC5, are active enzymes, whereas hARTC3 and hARTC4 are inactive proteins that lack any enzymatic activity due to the presence of mutations in their active site motif. Among these active hARTCs, hARTC5 lacks the GPI-anchor signal sequence and is secreted, thus hARTC1 represents the only active, non-secreted member of the family.

Several reports suggest that hARTC1 is localized to the plasma membrane, as it has been demonstrated to be involved in the modification of arginine residues of soluble or plasma-membrane-associated protein targets such as integrin α7, HNP-

1 and of other cell surface molecules (LFA-1, CD45, CD43 and CD44; Paone, G. et al., 2002; Seman, M. et al., 2003; Zolkiewska, A. and Moss, J., 1993; for a detailed description of substrates target of mono-ADP-ribosylation hARTC1-mediated see Introduction, Chapter 1.2.1.1). However, there is also a report indicating that hARTC1 can also have an intracellular localization, anchored to the membrane of the sarcoplasmic reticulum of rabbit skeletal muscle (Soman, G. et al., 1984).

The first aim of my study was to precisely define the cellular localization of hARTC1 in mammalian cells. To this end, I performed immunofluorescence experiments to analyze the localization of both over-expressed and endogenous protein, using markers for different cellular compartments. Moreover, once the specific cellular localization of hARTC1 was identified, additional substrate proteins that could be ADP-ribosylated were sought. Indeed, there is a large number of proteins, both extracellular and intracellular, that have been demonstrated to undergo mono-ADP-ribosylation. However, the enzyme(s) responsible for their modification still remains to be identified. Interestingly, most of these targets have been reported to have a role in cell signaling and metabolism and the enzymatic activities involved in their modifications have been shown to be both cytosolic and membrane associated. Thus, it could be possible that hARTC1 is involved in some of these previously reported mono-ADP-ribosylation reactions.

To identify one or more novel possible targets of hARTC1 several different approaches were used, including immunofluorescence and biochemical experiments, which took advantage of a previously described tool that is able to recognize ADP-ribosylated targets. Within this study, this tool was employed for

the development of novel techniques that, in addition to allowing identification of new targets of hARTC1-mediated mono-ADP-ribosylation, represent a relevant technological advance for the study of ADP-ribosylation reactions.

3.2 Results

3.2.1. hARTC1 is an ER-resident protein

3.2.1.1 Study of over-expressed hARTC1 cellular localization in HeLa cells

Previous reports have indicated that hARTC1 is involved in the modification of plasma membrane-associated proteins, suggesting it is localized to the cell membrane as is the case with its closest functional homologue ARTC2, which has been well described to be GPI-anchored to the cell membrane of T cells. To obtain information about the cellular localization of hARTC1, I analyzed cells by immunofluorescence. For these experiments, I used HeLa cells transfected with hARTC1. Furthermore, considering the established information about ARTC2 localization, I also used cells transfected with the hamster cARTC2.1, employed as a marker for a plasma membrane localized ARTCs. Indeed, cARTC2.1 was previously cloned in my laboratory and characterized as a typical GPI-anchored, plasma membrane-associated, arginine-specific ART enzyme (Stilla, A. et al., 2011). Both hARTC1 and ARTC2.1 expression constructs were previously produced in our laboratory, using the eukaryotic expression vector pME.CD8LF with the Flag-tag at the N-terminus.

Specifically, HeLa cells were transiently transfected with Flag-tagged hARTC1 wild-type (hARTC1 wt) or with Flag-tagged cARTC2.1 wild-type (cARTC2.1 wt). After 24 hours of transfection cells were fixed with 4% PFA and stained with antibodies. Both hARTC1 wt- and cARTC2.1 wt-transfected cells were stained with anti-Flag antibody to visualize the over-expressed proteins. Wheat germ agglutinin (WGA) was used for plasma membrane staining. WGA is a 36 kDa protein that selectively recognizes sialic acid and N-acetylglucosaminyl sugar residues, which are predominant components of the plasma membrane. Thus, it is one of the most widely used markers for membrane labeling.

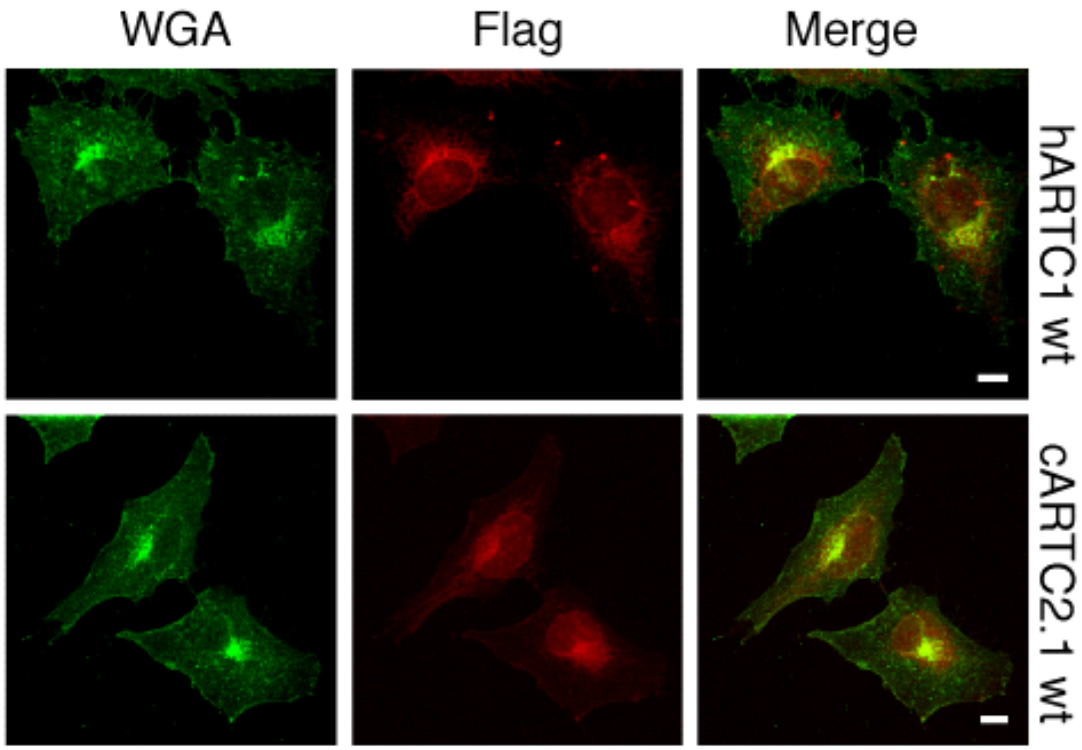

Modified from Fabrizio, G. et al., 2015b

Figure 3.1 hARTC1 wt and cARTC2.1 wt co-localization with WGA, a plasma membrane marker. Representative immunofluorescence images of HeLa cells transiently transfected with Flag-hARTC1 wt or Flag-cARTC2.1 wt, stained with anti-Flag (red) and anti-WGA (green) antibodies, as indicated. The WGA intracellular localization is due to cell permeabilization. The scale bar represents 10 μm. The data shown are representative of at least three independent experiments.

Of note, the analysis of cells by confocal microscopy revealed that hARTC1 wt had a prevalent intracellular localization, with only a minimal co-localization with WGA (Figure 3.1, hARTC1 wt). On the contrary, a substantial amount of the cARTC2.1 wt co-localized with the plasma membrane, as expected (Figure 3.1, cARTC2.1 wt).

To further evaluate the cellular localization of hARTC1, multiple immunofluorescence experiments were performed, analyzing the co-localization of the over-expressed hARTC1 wt and cARTC2.1 wt with various organelle markers. For each experiment, HeLa cells were transiently transfected for 24 hours with hARTC1 wt or with cARTC2.1 wt, fixed with 4% PFA and permeabilized. Cells were then stained using an anti-Flag antibody to visualize the over-expressed proteins, whereas organelles were labeled with appropriate fluorescent markers.

Firstly, a possible co-localization with the ER was investigated. The ER was labeled using two alternative markers: calnexin and calreticulin (Figure 3.2). These proteins are well known to be ER resident, but while calnexin is an abundant 90 kDa chaperone localized to the membrane of the ER, calreticulin is a 48 kDa protein located in the lumen of the reticulum. Both calnexin and calreticulin are widely used as ER markers (Williams, D.B., 2006; https://www.ncbi.nlm.nih.gov/gene/811).

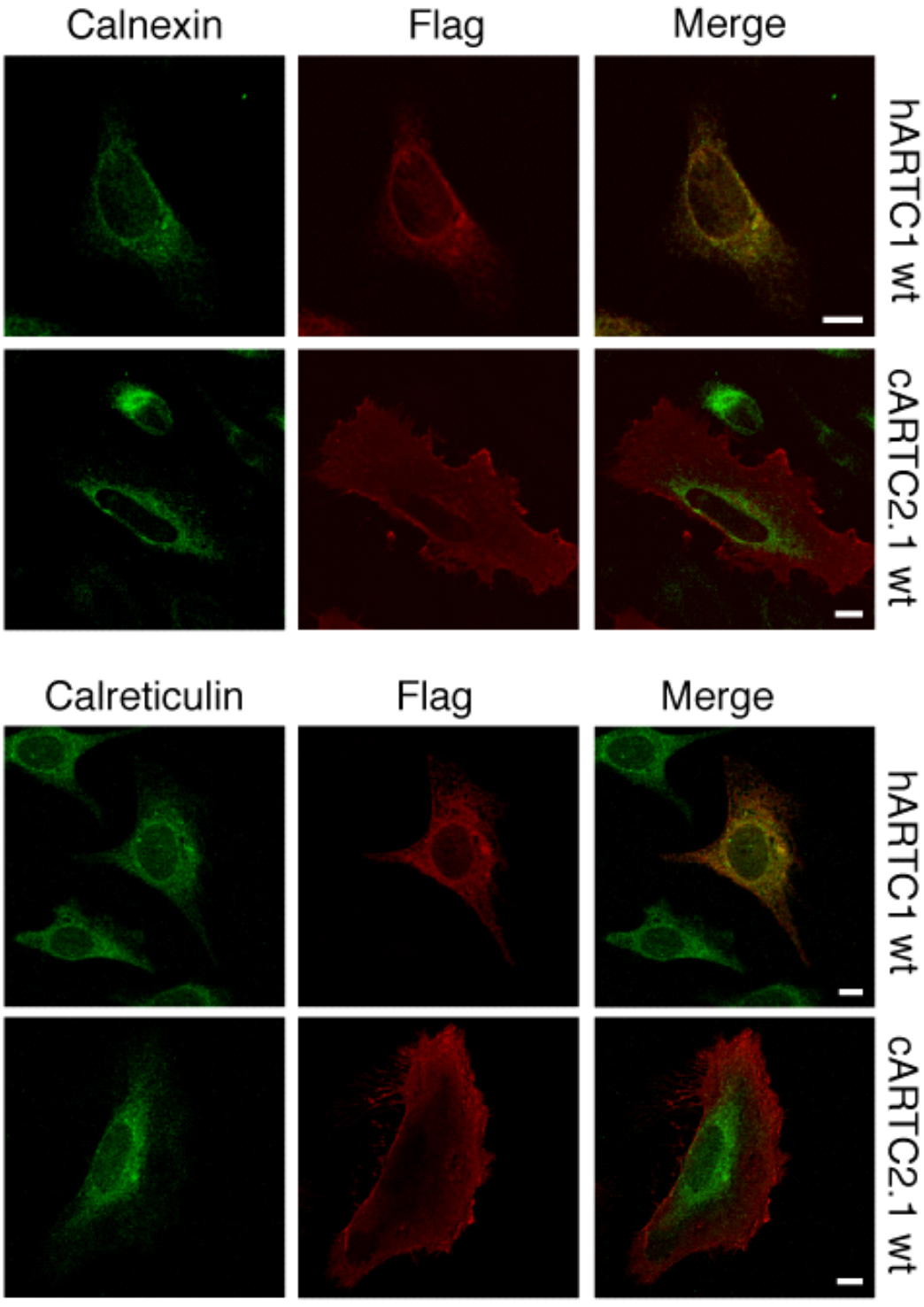

Modified from Fabrizio, G. et al., 2015b

Figure 3.2 hARTC1 wt and cARTC2.1 wt co-localization with ER markers. Representative immunofluorescence images of HeLa cells transiently transfected with Flag-hARTC1 wt or Flag-cARTC2.1 wt, stained with an anti-Flag antibody (red) and antibodies raised against calnexin or calreticulin (green), as indicated. The scale bar represents 10 μm. The data shown are representative of at least three independent experiments.

The analysis of cells by confocal microscopy revealed that hARTC1 wt was mainly located at the ER, as it substantially co-localized with both the ER markers calnexin and calreticulin (Figure 3.2, hARTC1 wt). This was not the case for cARTC2.1 wt for which, instead, little co-localization with the ER was detectable (Figure 3.2, cARTC2.1 wt).

To complete the analysis of the cellular localization of the enzymes, the expression of hARTC1 wt and cARTC2.1 wt was compared with the additional organelle markers giantin and lamp1. Giantin is one of the most commonly used Golgi markers, as it is a resident Golgi protein, specifically located to the cis/medial-Golgi apparatus (Linstedt, A.D. and Hauri, H.P., 1993). Lamp1 is a protein primarily localized at lysosomal membranes and, thus, typically used as a lysosomal marker (https://www.ncbi.nlm.nih.gov/gene/3916).

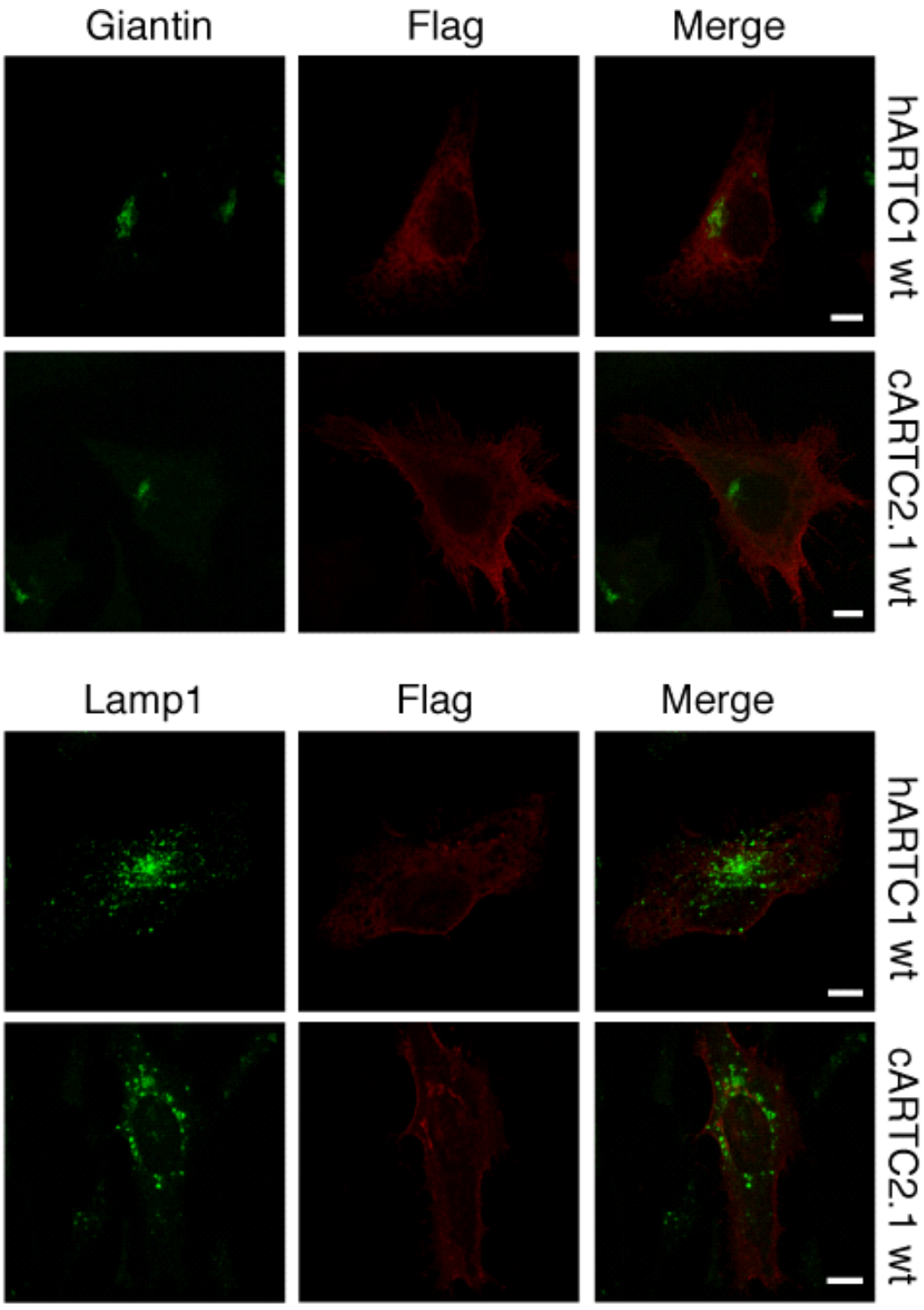

Modified from Fabrizio, G. et al., 2015b

Figure 3.3 hARTC1 wt and cARTC2.1 wt co-localization with Golgi and lysosomal markers. Representative immunofluorescence images of HeLa cells transiently transfected with Flag-hARTC1 wt or Flag-cARTC2.1 wt, stained with an anti-Flag antibody (red) and antibodies raised against giantin and lamp1 (green), as indicated. The scale bar represents 10 μm. The data shown are representative of at least three independent experiments.

The analysis of cells by confocal microscopy revealed that neither hARTC1 wt nor cARTC2.1 wt were localized in the Golgi apparatus or on lysosomes, since no co-localization was detectable with the correspondent organelle markers (Figure 3.3). Since the confocal microscopy analysis revealed an unexpected hARTC1 wt intracellular localization, which seemed to mostly co-localize with the ER markers, and was different from cARTC2.1 wt, a more detailed analysis was performed, evaluating, for each experiment, the amount of co-localization between the Flag-tagged enzymes and the different cellular markers (Figure 3.4). For co-localization assessment, I used the LSM510-3.2 software, as specified in Chapter 2.2.6.3 of the *Materials and Methods*. Co-localization was expressed as a percentage of co-localizing immunofluorescence over the total immunofluorescence per channel (Figure 3.4).

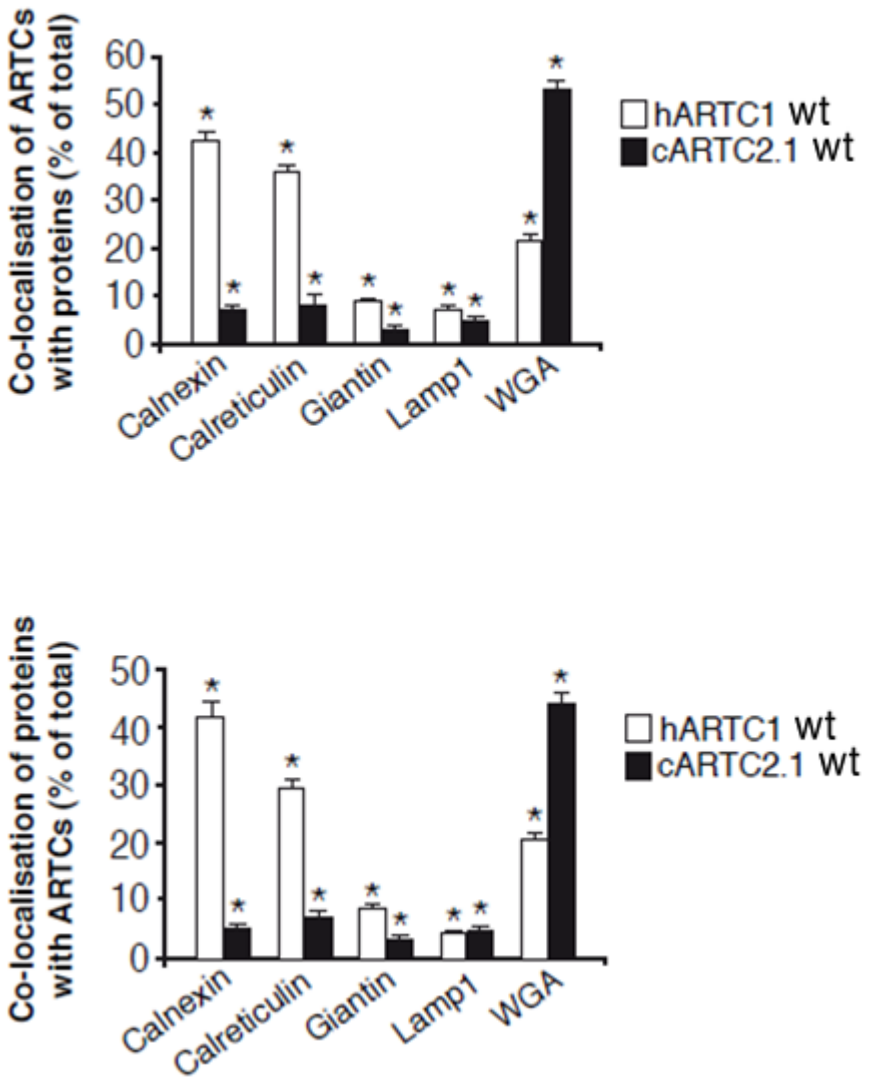

Modified from Fabrizio, G. et al., 2015b

Figure 3.4 Quantification of co-localization of hARTC1 wt and cARTC2.1 wt with specific organelle markers. Co-localization of ARTCs with specific organelle markers is shown in the upper panel, while that of organelle markers with ARTCs is shown in the lower panel. The column graphs show the percentage of overlapping red (Flag-tagged ARTCs) and green (organelle markers) pixels. The data were obtained from three independent experiments, with at least 50 cells per experiment (mean±SEM). * indicates significantly different from the co-localization coefficient 0, which correspond to immunofluorescence of non-transfected cells of the same sample ($p < 0.0001$).

Co-localization analysis indicated that main location of hARTC1 wt was at the ER, with a 42±1.7% co-localization with the ER protein marker calnexin and 36±1.2% with the other ER protein marker calreticulin (Figure 3.4, white bars). Additionally,

hARTC1 wt was partly localized to the plasma membranes, with about 21±0.5% co-localization with WGA, and only to a lower extent could it be found in the Golgi apparatus (9±0.5% co-localization with giantin) or on lysosomes (7±0.4% co-localization with lamp1; Figure 3.4, white bars). In contrast, only 10% of cARTC2.1 wt co-localized with the ER proteins calnexin and calreticulin (8±0.4% and 9±0.6%, respectively), whereas most of cARTC2.1 wt co-localized with the plasma membrane (53±0.8% co-localization with WGA), as expected (Figure 3.4, black bars). Only a minimal co-localization was seen with the Golgi marker giantin (3±0.3%) or with the lysosomal marker lamp1 (5±0.2%; Figure 3.4, black bars). Thus, quantification analysis confirmed that hARTC1 wt was prevalently localized to the ER, as it co-localized with two different ER markers (calnexin and calreticulin), whereas there was very little co-localization with other intracellular compartments (Fabrizio, G. et al., 2015b).

Immunofluorescence experiments (Figure 3.2), and the corresponding quantitative analysis (Figure 3.4), reveal an ER cellular localization for hARTC1. However, it was possible that the detected fluorescence within the ER compartment was due to newly synthesized proteins that transiently passed through the ER. To exclude this possibility, additional immunofluorescence experiments were performed, exposing cells transfected with the ARTCs to cycloheximide (chx), a well-known treatment used for protein synthesis inhibition. To address this point, HeLa cells were transiently transfected for 24 hours with hARTC1 wt, cARTC2.1 wt, and also with a Flag-tagged cARTC2.1 double mutant E207G/E209G (cARTC2.1 dm) and with Flag-tagged hARTC4 (hARTC4). HeLa cells expressing these constructs were

incubated for 3 hours in the absence (Figure 3.5, control) or in the presence of chx (Figure 3.5, chx), and then analyzed by immunofluorescence microscopy. To visualize the over-expressed proteins, the cells were stained with an anti-Flag antibody. At the same time, the ER compartment was stained with an antibody against protein disulfide isomerase (PDI), which is one of the most abundant ER-associated endogenous proteins. The co-localization of the different ARTC enzymes with PDI was quantified using the Zeiss LSM510-3.2 software, as described in the *Materials and Methods*.

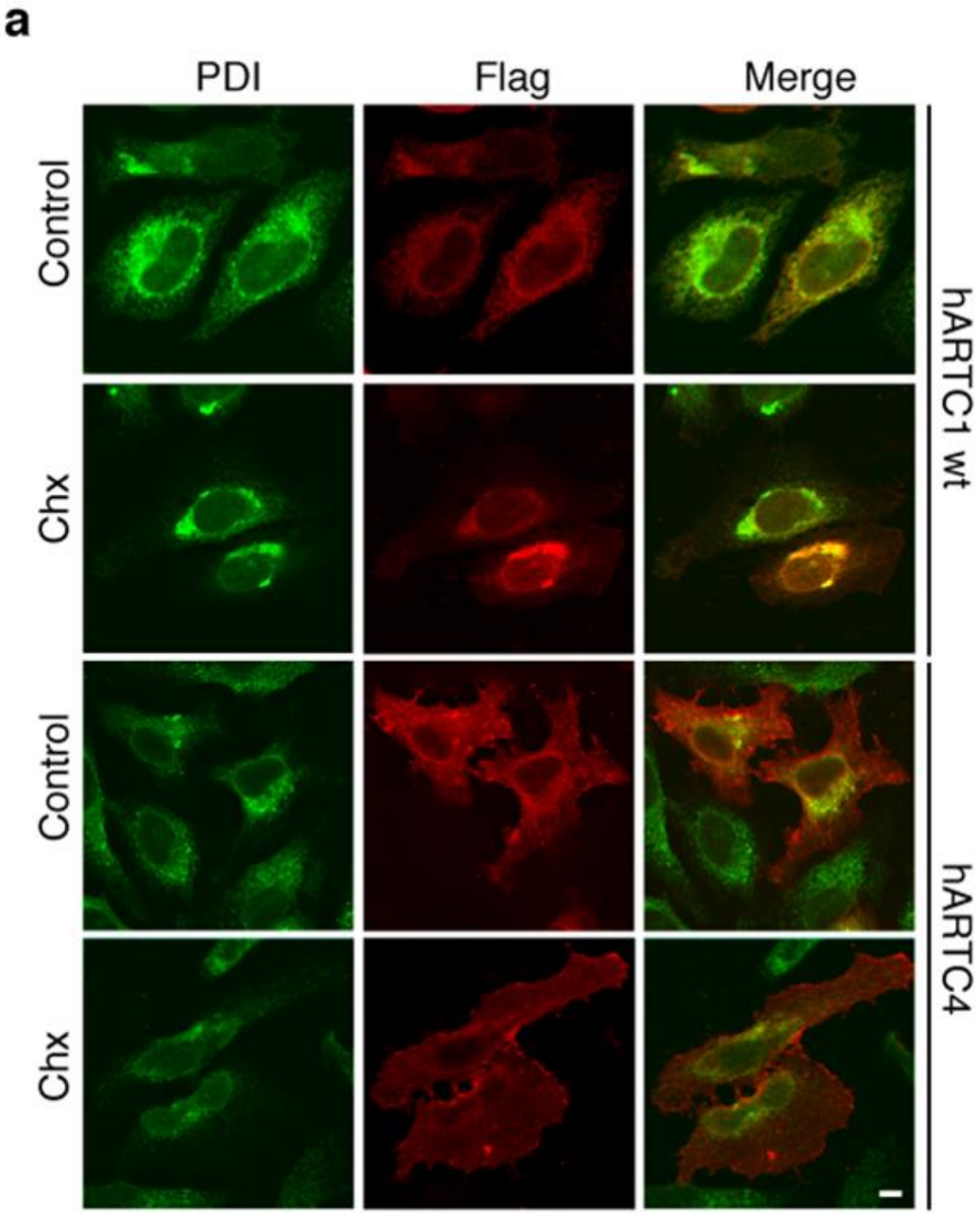
a
PDI
Flag
Merge
Control
Chx
Control
Chx
hARTC1 wt
hARTC4

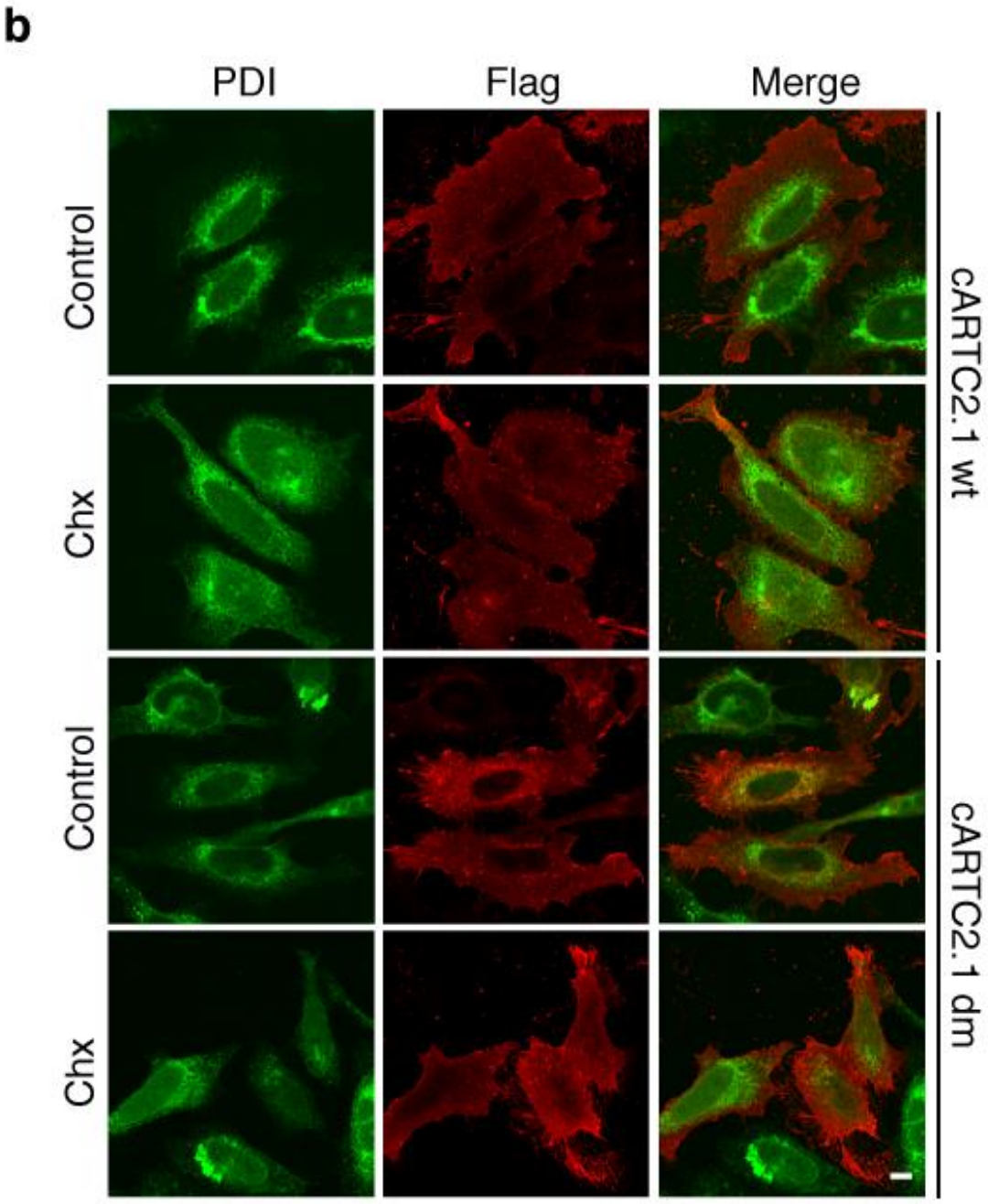
b
PDI
Flag
Merge
Control
Chx
Control
Chx
cARTC2.1 wt
cARTC2.1 dm

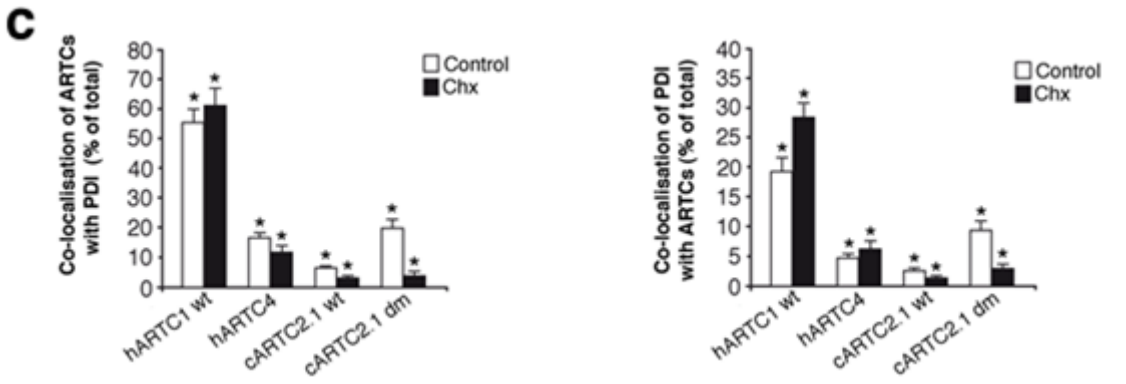

Modified from Fabrizio, G. et al., 2015b

Figure 3.5 hARTC1 wt is an ER resident protein. (a, b) Representative immunofluorescence images of HeLa cells transiently transfected with the indicated constructs and either untreated (control) or incubated with cycloheximide (chx, 100 μg/mL), stained with anti-Flag (red) or anti-PDI (green) antibodies, as indicated, then analyzed by immunofluorescence. The scale bar represents 10 μm. The data shown are representative of at least three independent experiments. (c) Quantification of the co-localization of ARTC enzymes with PDI, and *vice versa*. The column graphs show averaged data from three independent experiments with at least 50 cells per experiment (mean±SEM). * indicates significantly different from the co-localization coefficient 0, which correspond to immunofluorescence of non-transfected cells of the same sample ($p < 0.0001$).

The analysis of cells by confocal microscopy revealed that hARTC1 wt co-localized with PDI to the same extent in both control and chx-treated cells (Figure 3.5a, hARTC1 wt). In contrast, the minimal co-localization of hARTC4, cARTC2.1 wt and cARTC2.1 dm with PDI that was seen in control cells, was reduced as a consequence of the chx treatment (Figure 3.5a, hARTC4; Figure 3.5b, cARTC2.1 wt, cART2.1 dm). Quantification of data confirmed that 55±4% and 6±1% of hARTC1 wt and cARTC2.1 wt, respectively, co-localized with PDI in transfected, non-treated, control cells (Figure 3.5c). However, when the cells were treated with chx, 61±6% and 3±0.8% of hARTC1 wt and cARTC2.1 wt, respectively, co-localized with PDI (Figure 3.5c). Also, cARTC2.1 dm and hARTC4 showed very little co-localization with PDI (16±2% and 19±3%, respectively), as the relative quantification analysis

revealed, and their minimal co-localization was reduced after chx treatment (11±2% and 3±1%, respectively; Figure 3.5c).

Under conditions that block new protein synthesis, such as the addition of chx to cells, proteins that were not ER-resident would exit the ER compartment and be transported to their final destination. This was the case for hARTC4, cARTC2.1 wt and cARTC2.1 dm. On the contrary, the treatment with chx had no effect on the localization of hARTC1 wt, thus confirming that it was mainly located in the ER (Fabrizio, G. et al., 2015b).

3.2.1.2 Study of endogenous hARTC1 cellular localization in HeLa cells

The experiments described above using over-expressed proteins revealed an unexpected ER cellular localization for hARTC1. The fact that under the same experimental conditions cARTC2.1 wt was correctly localized to the plasma membrane indicates that the transfected HeLa cells were viable and able to transport proteins to their correct destination, and that over-expressed Flag-tagged proteins could be reliably used to examine cellular localization. However, to further exclude the possibility of mis-localization due to hARTC1 wt over-expression, the cellular location of endogenous hARTC1 was characterized. At present, there is no data concerning the cellular localization of endogenous hARTC1, and all the available information about its cellular expression was obtained with the over-expressed enzyme.

An antibody, or another probe, is required to examine the localization of endogenous proteins. Since no commercial antibody directed against

endogenous hARTC1 has yet been tested for immunofluorescence analysis, initial experiments were aimed to characterize commercially available antibodies from different suppliers. In contrast to the different antibodies tested, that from Abcam was the only one revealing an immunofluorescence signal clearly distinguishable from the background. Once the best antibody was characterized by immunofluorescence, the optimal dilution and blocking conditions were determined in order to improve the immunofluorescence signal. The identification of the optimal antibody working conditions was of extreme importance since it allowed, for the first time, the visualization of endogenous hARTC1 expression by confocal microscopy.

After setting up the optimal antibody working conditions, the co-localization between endogenous hARTC1 and the ER protein calnexin was evaluated. Hela cells were fixed with 4% PFA, permeabilized and stained with an anti-ARTC1 antibody and an anti-calnexin antibody.

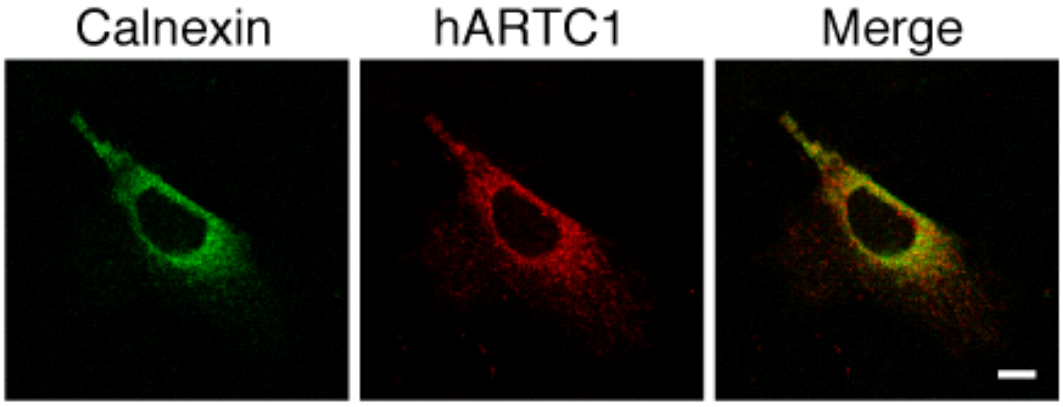

Modified from Fabrizio, G. et al., 2015b

Figure 3.6 Endogenous hARTC1 is located in the ER. Representative immunofluorescence image of non-transfected HeLa cells stained with anti-hARTC1 (red) or anti-calnexin (green) antibodies, as indicated. The scale bar represents 10 μm. The data shown are representative of at least three independent experiments.

The analysis of cells by confocal microscopy indicated that endogenous hARTC1 co-localized with the ER marker calnexin (Figure 3.6).

The immunostaining depicted in Figure 3.6 was evaluated as described earlier to quantitate the co-localization between hARTC1 and the calnexin ER marker.

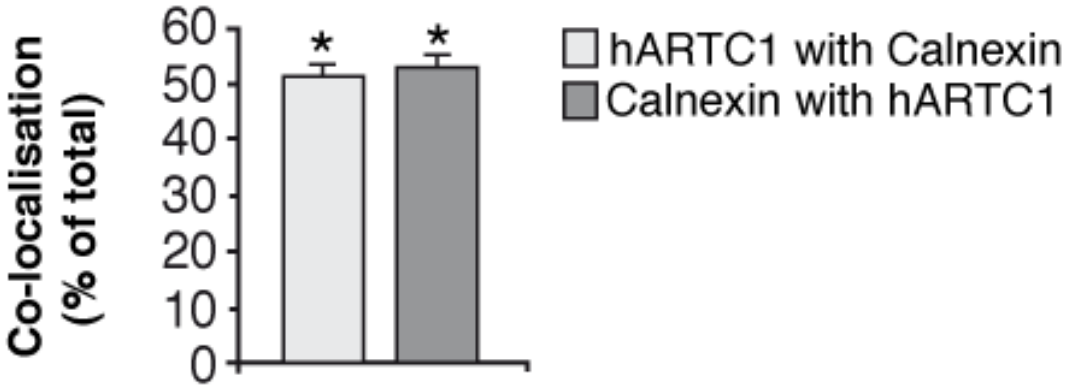

Modified from Fabrizio, G. et al., 2015b

Figure 3.7 hARTC1 co-localization with the ER marker calnexin. The bars indicate co-localization of endogenous hARTC1 with calnexin, and *vice versa*. The data are expressed as percent of hARTC1 that co-localized with calnexin and the percent of calnexin co-localizing with hARTC1, and were obtained from three independent experiments with at least 50 cells per experiment (mean±SEM). * indicates significantly different from the co-localization coefficient 0, which correspond to immunofluorescence of non-transfected cells of the same sample ($p < 0.0001$).

The quantification of the immunofluorescence analysis indicated that 51±2% of hARTC1 co-localized with calnexin (Figure 3.7). This value was consistent with the data obtained using the transfected cells over-expressing hARTC1 wt (Figure 3.4) confirming the main ER localization of the endogenous protein. Altogether, these data demonstrated that hARTC1 is a protein primarily localized to the ER, with only one fifth of the protein associated with the plasma membrane (Fabrizio, G. et al., 2015b). This finding casts new light on the cellular location of hARTC1, and

plausibly suggested that there may be novel ER-resident substrates for hARTC1-mediated ADP-ribosylation.

3.2.2 hARTC1 is the enzyme responsible for GRP78/BiP mono-ADP-ribosylation

The data presented above describing immunofluorescence analysis of hARTC1 in living cells demonstrated that the enzyme has a prevalent intracellular localization, and for the first time reported a quantification of the enzyme's distribution. Since some of the protein (~20% c.f. Figure 3.4) is localized to the plasma membrane, hARTC1 can catalyze mono-ADP-ribosylation of plasma membrane-associated proteins, some of which have been reported (Nemoto, E. et al.,1996; Liu, Z.X. et al., 1999; Zolkiewska, A. and Moss, J., 1993). However, nothing is known about intracellular targets of hARTC1. Due to its substantial intracellular localization, it is reasonable to search for proteins that could be mono-ADP-ribosylated by hARTC1 within cellular organelles. Of note, intracellular ADP-ribosylated proteins are known, but the enzyme(s) responsible for the modification still remain to be identified. It is possible that hARTC1 is involved in some of these previously identified mono-ADP-ribosylation reactions.

In order to identify intracellular substrates of hARTC1, a strategy was employed that took advantage of our previous demonstration that a protein module, named *Archaeoglobus fulgidus* macro domain (mAf1521) which has a high affinity for ADP-ribose (Dani, N. et al., 2009). This peptide can function as a bait to isolate ADP-ribosylated proteins and, thus, it can be used for the identification of novel ADP-ribosylated proteins. This tool was employed in both biochemical and cell

biology approaches, allowing identification of novel targets of hARTC1-mediated ADP-ribosylation. The setting up of new macro domain-based experiments represent an important technological advancement in the study of APD-ribosylation reactions.

3.2.2.1 Macro domain-based pull-down assay

Initial experiments used the macro domain mAf1521 for macro-based GST pull-down assays, as described by Dani and colleagues (Dani, N. et al., 2009). To verify the functionality of this assay, the method was firstly set up by analyzing CHO cells transfected with a wild-type ARTC enzyme, or a mutant, inactive form of the same enzyme. Considering that no hARTC1 mutant was available, these experiments employed cARTC2.1 wt and cARTC2.1 dm. After 24 hours of transfection, cells from each transfection condition were lysed and subjected to two-step pull-down with the GST-tagged macro domains (see *Materials and Methods*): the first pull-down was performed using the GST-tagged mAf1521/G42E mutant, which does not bind ADP-ribosylated proteins. This step allowed removal of protein that was non-specifically bound to the macro domain module. The supernatant from this first step was recovered and underwent a second pull-down with wild-type GST-mAf1521, to specifically retain ADP-ribosylated proteins. The pulled-down proteins obtained following this two-step procedure were separated by 10% SDS-PAGE and revealed by colloidal Coomassie blue staining.

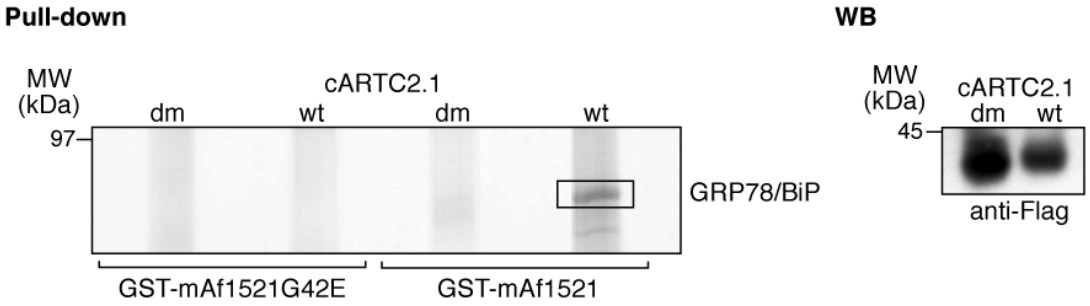

Modified from Fabrizio, G. et al., 2015b

Figure 3.8 Macro domain-based pull-down assay coupled to MALDITOF–MS analysis identifies GRP78/BiP as a substrate of cARTC2.1 wt. Representative pull-down from CHO cells transfected with enzymatically active cARTC2.1. wt or with the enzymatically inactive cARTC2.1 dm. Cell lysates (3 mg protein) underwent a non-specific pull-down step using the GST-tagged mAf1521/G42E mutant (with abrogated binding of mAf1521 ADP-ribosylated proteins). The unbound material underwent a second pull-down with wild-type GST-mAf1521, to specifically retain ADP-ribosylated proteins. This two-step procedure resulted in separation of specific proteins that were revealed by colloidal Coomassie blue staining and identified by MALDI-TOF analysis (NCBI acc. number: AAA52614; score: 209; matched peptide no.: 21; sequence coverage: 35%; molecular mass: 72 kDa; protein scores ≃65 are significant ($p < 0.05$). Western Blotting (WB) showed the levels of expression of the indicated Flag-tagged proteins, as performed by immunoblotting with an anti-Flag antibody. The data shown are representative of at least five independent experiments.

As depicted in Figure 3.8, a specific protein band of ca. 78 kDa was detected in the Flag-cARTC2.1 wt-transfected CHO cells pulled-down with GST-tagged mAf1521 wt. No band was detected in cARTC2.1 dm-transfected cells. As expected, no bands were revealed after the incubation with the mutant macro domain, which does not bind ADP-ribosylated proteins. To confirm transfection of the cells with cARTC2.1 wt and cARTC2.1 dm, Western Blotting was performed, which indicated similar levels of expression for both of the transfected proteins (Figure 3.8).

Having verified the functionality and specificity of the pull-down method, I performed similar experiments using CHO cells transfected with either an empty

vector, hARTC1 wt or cARTC2.1 wt with the latter being employed as internal control.

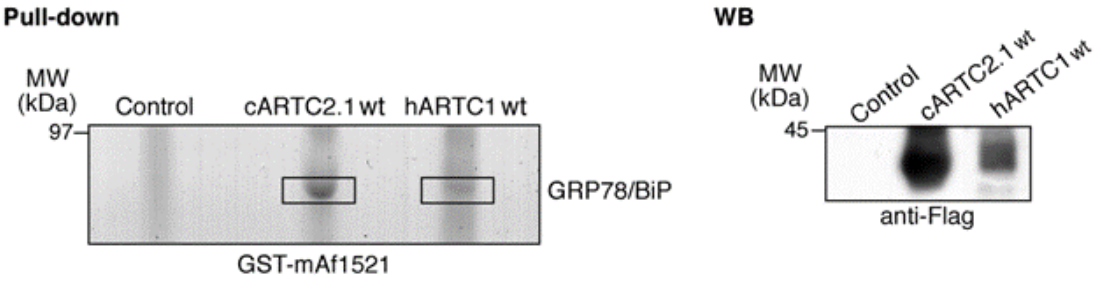

Modified from Fabrizio, G. et al., 2015b

Figure 3.9 Macro domain-based pull-down assay coupled to MALDITOF–MS analysis identifies GRP78/BiP as a substrate of hARTC1 wt. Representative pull-down from CHO cells transfected with an empty vector or with enzymatically active hARTC1 wt or cARTC2.1 wt. Cell lysates (3 mg protein) underwent non-specific pull-down step using the GST-tagged mAf1521/G42E mutant (with abrogated binding of mAf1521 ADP-ribosylated proteins). The unbound material underwent a second pull-down with wild-type GST-mAf1521, to specifically retain ADP-ribosylated proteins. This two-step procedure resulted in separation of specific proteins that were revealed by colloidal Coomassie blue staining and identified by MALDI-TOF analysis (NCBI acc. number: AAA52614; score: 209; matched peptide no.: 21; sequence coverage: 35%; molecular mass: 72 kDa; protein scores ≃65 are significant ($p < 0.05$). Western Blotting (WB) showed the levels of expression of the indicated Flag-tagged proteins, as performed by immunoblotting with an anti-Flag antibody. The data shown are representative of at least five independent experiments.

As depicted in Figure 3.9, no band was pulled-down from cells transfected with the empty vector alone, whereas a protein band of ca. 78 kDa was detected in hARTC1 wt-transfected cells. The transfection of the enzymes was checked with Western Blotting (Figure 3.9, WB). The Western Blotting indicated that both enzymes were expressed in the CHO cells albeit with a higher level of cARTC2.1. The specific band that was pulled-down in cells transfected with the active enzymes was then excised from the gel and subjected to identification by MALDI-TOF–MS analysis. This specific band was identified as the highly conserved ER

chaperone protein GRP78/BiP, thus suggesting that catalytically active cARTC2.1 wt and hARTC1 wt are involved in the previously described ADP-ribosylation of the chaperone (Fabrizio, G. et al., 2015b).

3.2.2.2 Macro domain-based immunofluorescence assay

Taking advantage of the ability of macro domain Af1521 to specifically bind GRP78/BiP in cells transfected with hARTC1 wt and cARTC2.1 wt, it was next investigated whether the same macro domain could be used to visualize ADP-ribosylated proteins by immunofluorescence. To this end, conditions were set up for an immunofluorescence assay using the GST-tagged wild-type (mAf1521) and its non-ADP-ribose binding mutant (mAf1521/G42E). Specifically, HeLa cells were non-transfected and were fixed with 4% PFA, permeabilized and incubated with the wild-type mAf1521 macro domain or the mAf1521/G42E mutant. To detect the macro domain bound to ADP-ribosylated proteins an anti-GST antibody was used.

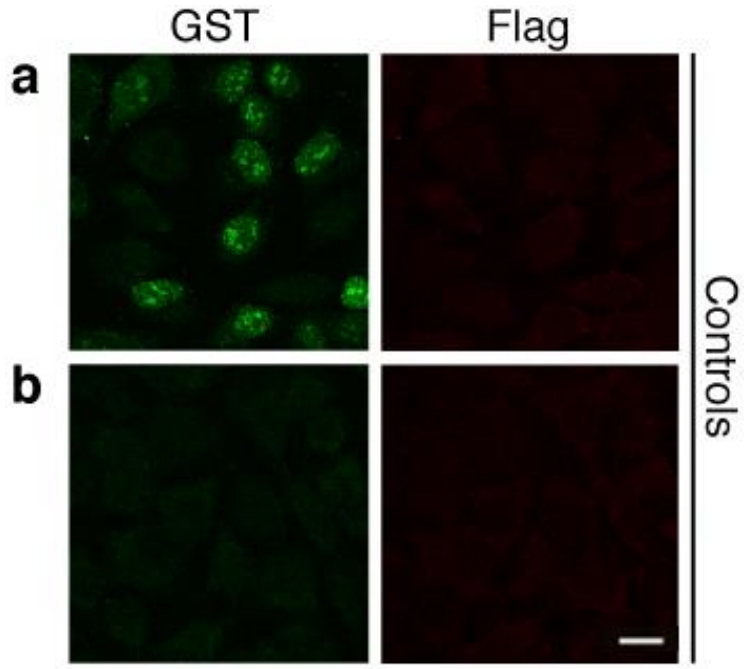

Modified from Fabrizio, G. et al., 2015b

Figure 3.10 The mAf1521 macro module can be used to visualize ADP-ribosylated proteins. Representative immunofluorescence images of non-transfected HeLa cells that were incubated with GST-mAf1521 (a) or GST-mAf1521/G42E (b), stained with anti-Flag and anti-GST antibodies, as indicated, and analyzed by immunofluorescence. The scale bar represents 10 μm. The data shown are representative of at least ten independent experiments.

The analysis of cells by confocal microscopy revealed predominantly nuclear staining for control cells incubated with GST-mAf1521 wild-type (Figure 3.10a), suggesting that in these cells, under basal condition, nuclear ADP-ribosylation could be detected. The specificity of this labelling was confirmed by the lack of cell staining when the GST-tagged mAf1521/G42E mutant macro domain was used (Figure 3.10b). As expected, there was no detectable Flag staining in non-transfected cells. Thus, the use of macro domain in immunofluorescence represented an efficient method allowing visualization of ADP-ribosylated proteins in intact cells (Fabrizio, G. et al., 2015b).

Similar experiment was then performed using HeLa cells transiently transfected for 24 hours with Flag-tagged hARTC1 wt (Figure 3.11a, b), hARTC4 (Figure 3.11c, d), cARTC2.1 wt (Figure 3.11e, f) or cARTC2.1 dm (Figure 3.11g, h). For cell staining, an anti-Flag antibody was used to detect the over-expressed enzymes while an anti-GST antibody was used to detected the GST-tagged mAf1521 and, thus, visualize ADP-ribosylation.

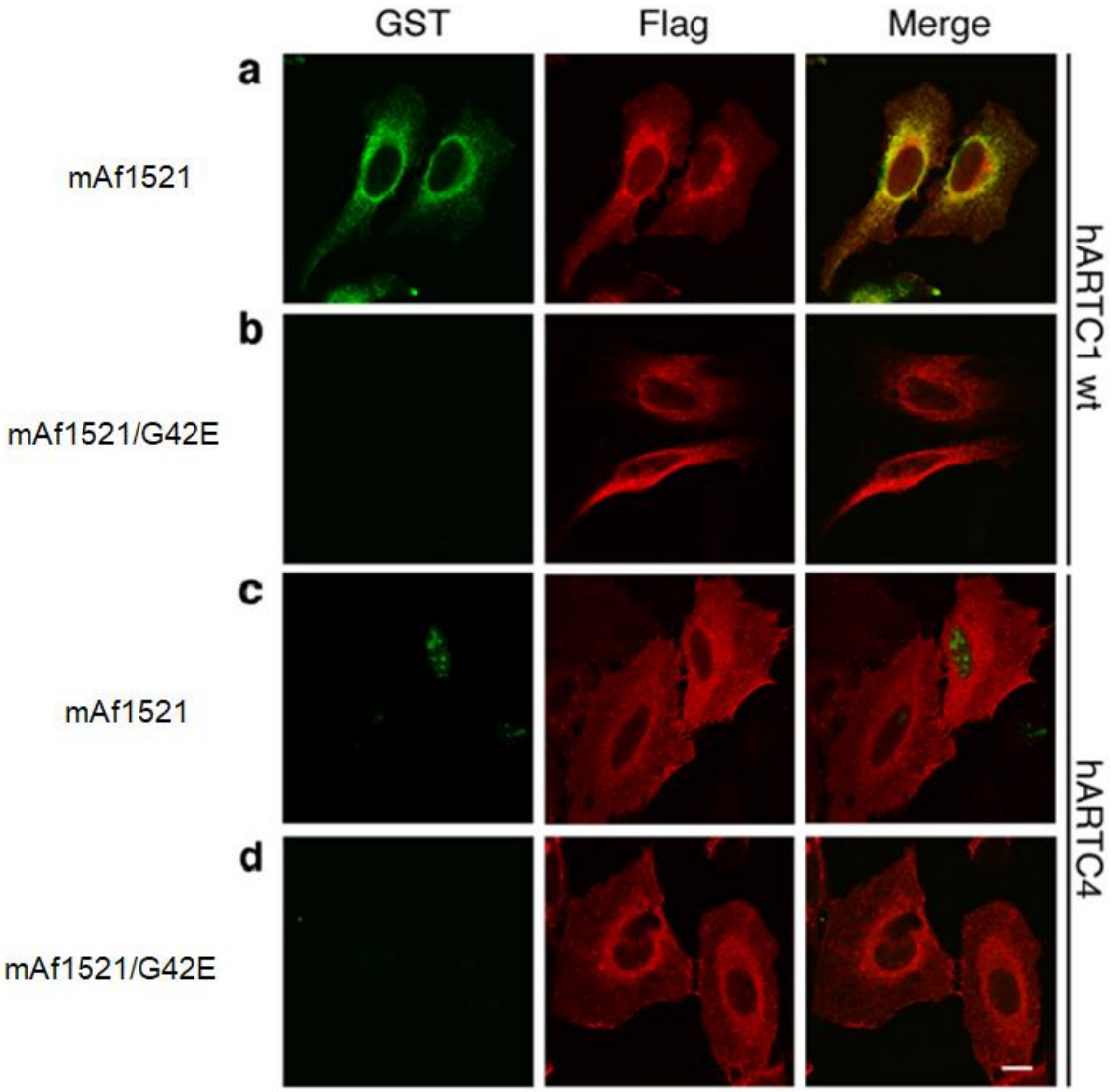

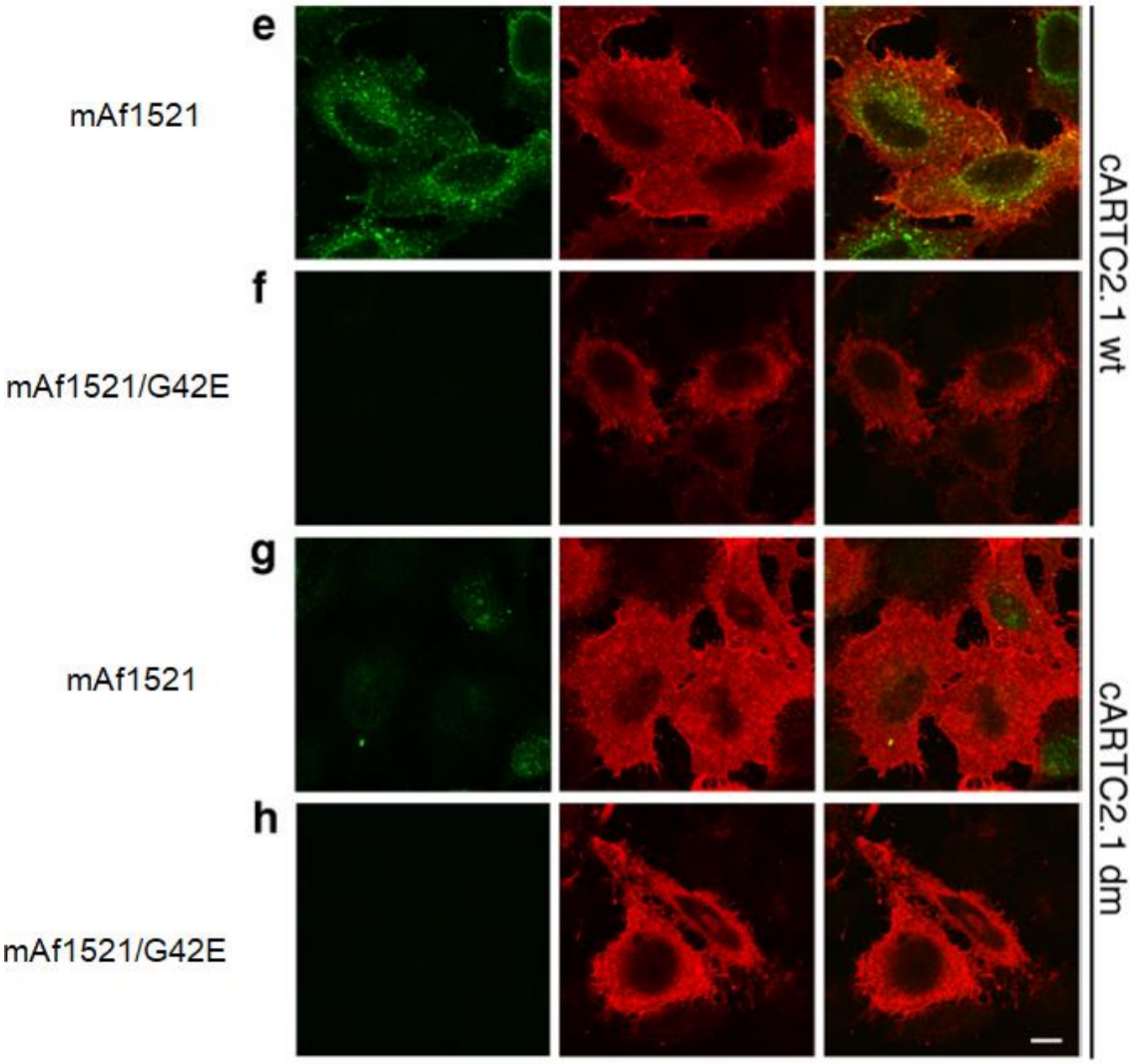

Modified from Fabrizio, G. et al., 2015b

Figure 3.11 The mAf1521 macro module allows visualization of ADP-ribosylated proteins in cells transfected with active ARTCs. Representative immunofluorescence images of HeLa cells transiently transfected with the indicated constructs and incubated with GST-mAf1521 (a, c, e, g) or GST-mAf1521/G42E (b, d, f, h), stained with anti-Flag and anti-GST antibodies, as indicated, and analyzed by immunofluorescence. The scale bar represents 10 μm. The data shown are representative of at least ten independent experiments.

The immunofluorescence images showed clear peri-nuclear staining of hARTC1 wt (Figure 3.11a, b; see also Figures 3.2; 3.5; 3.6), whereas a minimal peri-nuclear staining was seen for hARTC4 (Figure 3.11c, d). As expected, the staining of cARTC2.1 wt and cARTC2.1 dm (Figure 3.11e, f and Figure 3.11g, h, respectively)

showed that they were correctly localized to the cell periphery, as previously reported (Stilla, A. et al., 2011).

Additionally, GST-mAf1521 also revealed a peri-nuclear staining in cells transfected with enzymatically active hARTC1 wt (Figure 3.11a) and cARTC2.1 wt (Figure 3.11e), in line with ADP-ribosylation events occurring within the ER. In contrast, cells transfected with the inactive enzymes, hARTC4 and cARTC2.1 dm, showed nuclear staining with GST-mAf1521 (Figure 3.11c and Figure 3.11g, respectively), as in control cells (Figure 3.10a). Obviously, the mutated mAf1521/G42E peptide that cannot bind ADP-ribosylated proteins showed no staining in any of the transfected cells (Figure 3.11b, d, f, h), as expected.

Of note, cARTC2.1 has been well described as a plasma membrane enzyme, as the staining with anti-Flag antibody also confirmed (Stilla, A. et al., 2011; Figure 3.5b). However, no detectable peripheral staining was observed with GST-mAf1521 in cells over-expressing cARTC2.1. This can be explained considering there is not sufficient extracellular NAD^+ to sustain ADP-ribosylation events in the extracellular compartment where cARTC2.1 is mainly localized. It has been previously demonstrated, that a peripheral ADP-ribosylation staining can only be detected when cells were incubated with NAD^+ (Stilla, A. et al., 2011). However, as a GPI-anchored enzyme, it is transiently present into the ER where it can act as an ART (Figures 3.9 and 3.11).

Altogether, these data provided a technological advance in the study of ADP-ribosylation by immunofluorescence microscopy. A prominent GST-mAf1521-dependent peri-nuclear staining of cells was seen upon transfection with the active

enzymes hARTC1 wt and cARTC2.1 wt, but not with their inactive counterparts. This GST-mAf1521 peri-nuclear staining correlated with hARTC1 wt- and cARTC2.1 wt-mediated ADP-ribosylation occurring at the ER level (Fabrizio, G. et al., 2015b).

To further investigate whether this peri-nuclear staining revealed by immunofluorescence with GST-mAf1521 in cells over-expressing hARTC1 wt and cARTC2.1 wt was due to ADP-ribosylated GRP78/BiP, since it occurred in the same organelle where the chaperone is known to reside, immunofluorescence experiments were performed using HeLa cells transiently transfected for 24 hours with Flag-tagged hARTC1 wt, hARTC4, cARTC2.1 wt and cARTC2.1 dm, as indicated (Figure 3.12). Cells were then incubated with GST-mAf1521 (Figure 3.12a, c, e, g) or with the inactive mutant GST-mAf1521/G42E (Figure 3.12b, d, f, h) and stained with anti-GR78/BiP and anti-GST antibodies, as indicated in the figure.

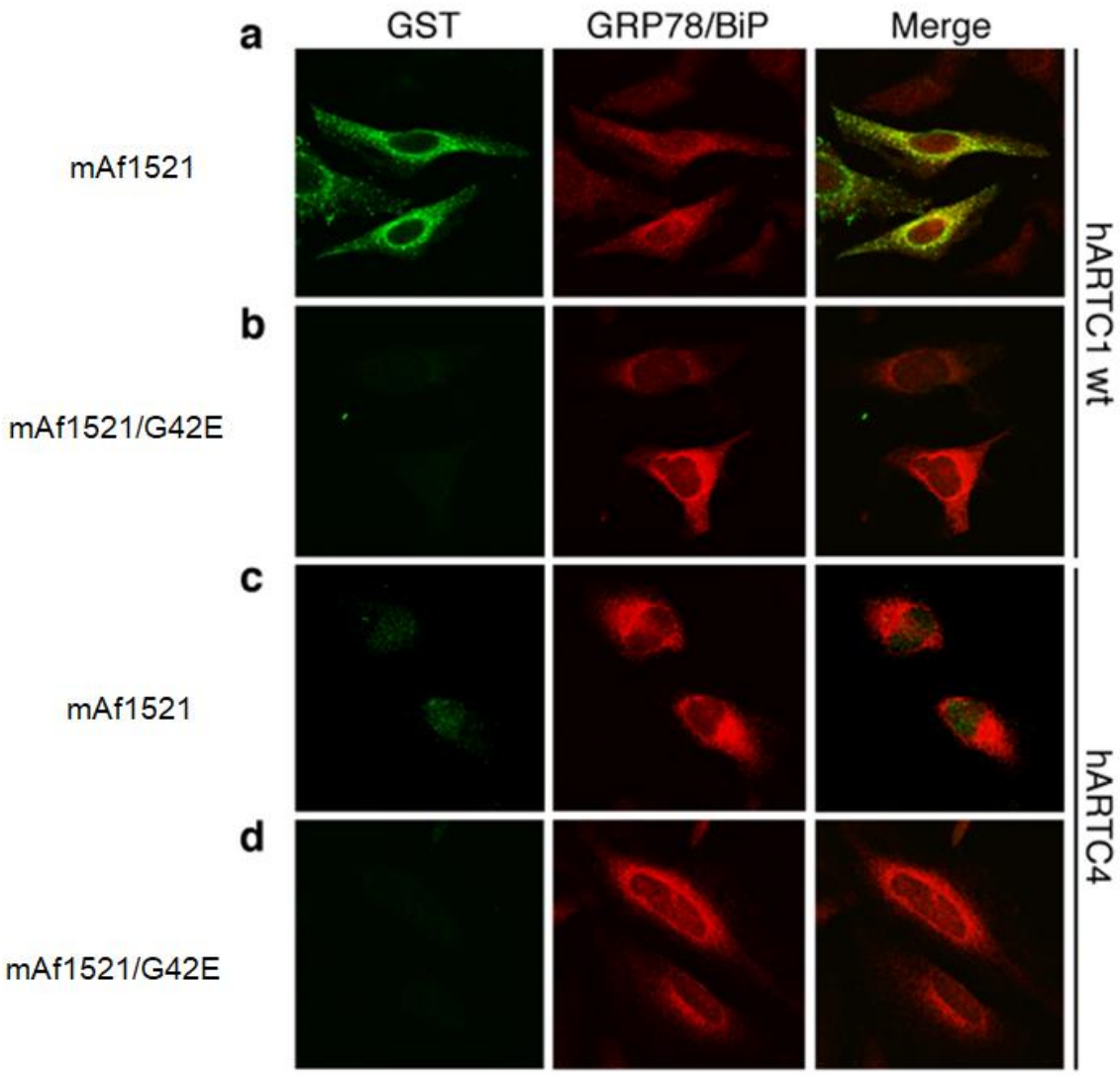
a
GST
GRP78/BiP
Merge
mAf1521
b
mAf1521/G42E
hARTC1 wt
c
mAf1521
d
mAf1521/G42E
hARTC4

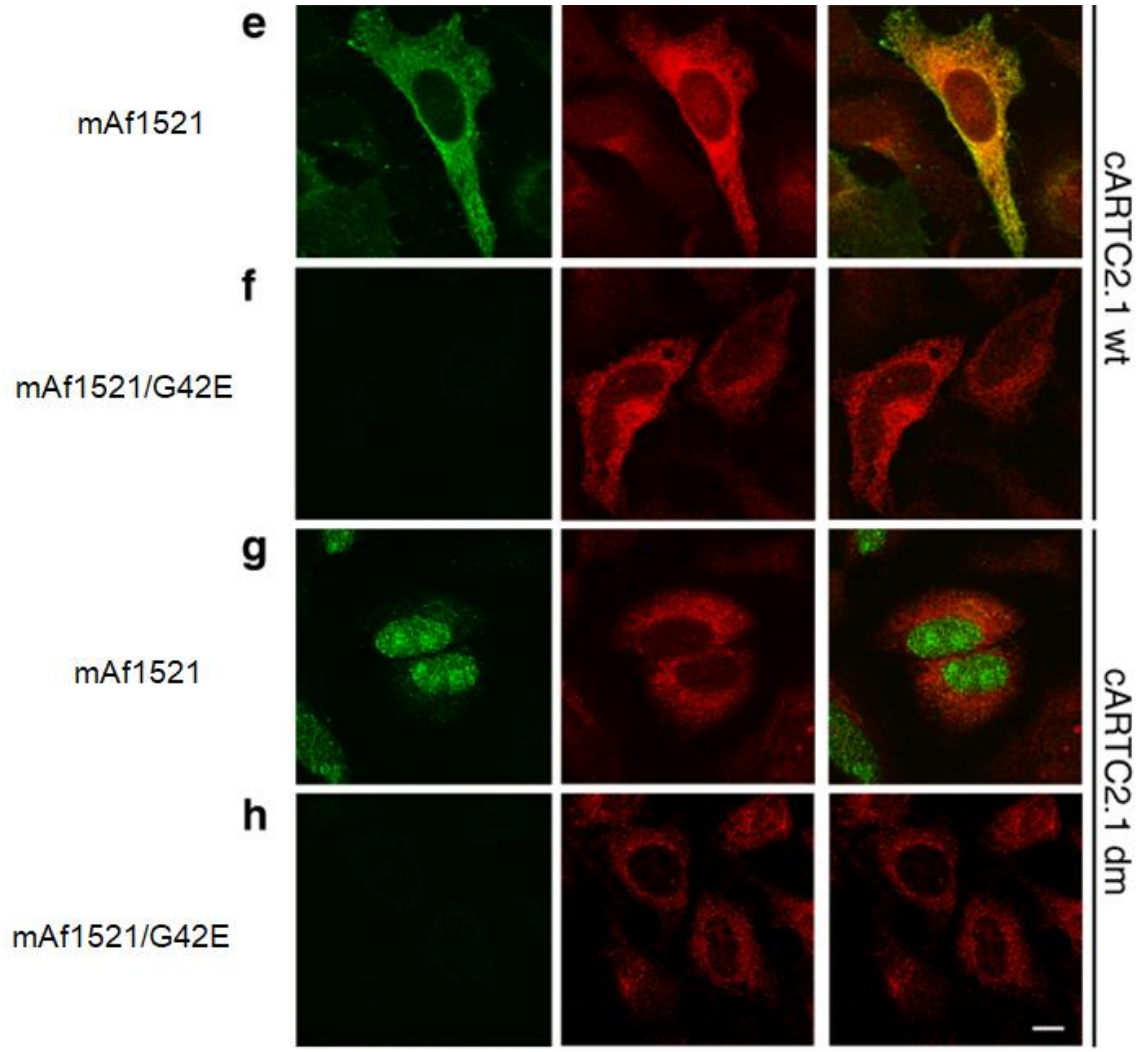

Modified from Fabrizio, G. et al., 2015b

Figure 3.12 The mAf1521 macro module staining co-localizes with GRP78/BiP. Representative immunofluorescence images of HeLa cells transiently transfected with the indicated constructs, incubated with GST-mAf1521 (a, c, e, g) or GST-mAf1521/G42E (b, d, f, h), stained with anti-GST and anti-GRP78/BiP antibodies, as indicated, and analyzed by immunofluorescence. The scale bar represents 10 μm. The data shown are representative of at least five independent experiments.

The immunofluorescence analysis showed that in cells over-expressing the active enzymes hARTC1 wt and cARTC2.1 wt GST-mAf1521 co-localized with GRP78/BiP (Figure 3.12a, e). In contrast, there was no co-localization between GRP78/BiP and GST-mAf1521 when the cells were transfected with the inactive enzymes hARTC4 or cARTC2.1 dm (Figure 3.12c, g). As expected, GST-mAf1521/G42E did

not lead to immunofluorescence with any transfected cells since it does not bind ADP-ribose (Figure 3.12b, d, f, h).

The data described above are consistent with the notion that GRP78/BiP is ADP-ribosylated as a consequence of either hARTC1 wt or cARTC2.1 wt over-expression (Fabrizio, G. et al., 2015b). Of note, cARTC2.1 was physically separated from GRP78/BiP (Figure 3.13c), since it is a cell membrane enzyme (Stilla, A. et al., 2011). However, it induced GRP78/BiP ADP-ribosylation in line with its action as an arginine-specific ART, and with the fact that, as a GPI-anchored protein, it is transiently present into the ER.

Finally, to directly evaluate the co-localization of hARTC1 wt with its target GRP78/BiP, immunofluorescence experiments were performed on cells transfected with the same constructs (Flag-tagged hARTC1 wt, hARTC4, cARTC2.1 wt and cARTC2.1 dm) and then analyzed using an anti-GRP78/BiP antibody in combination with an anti-Flag antibody.

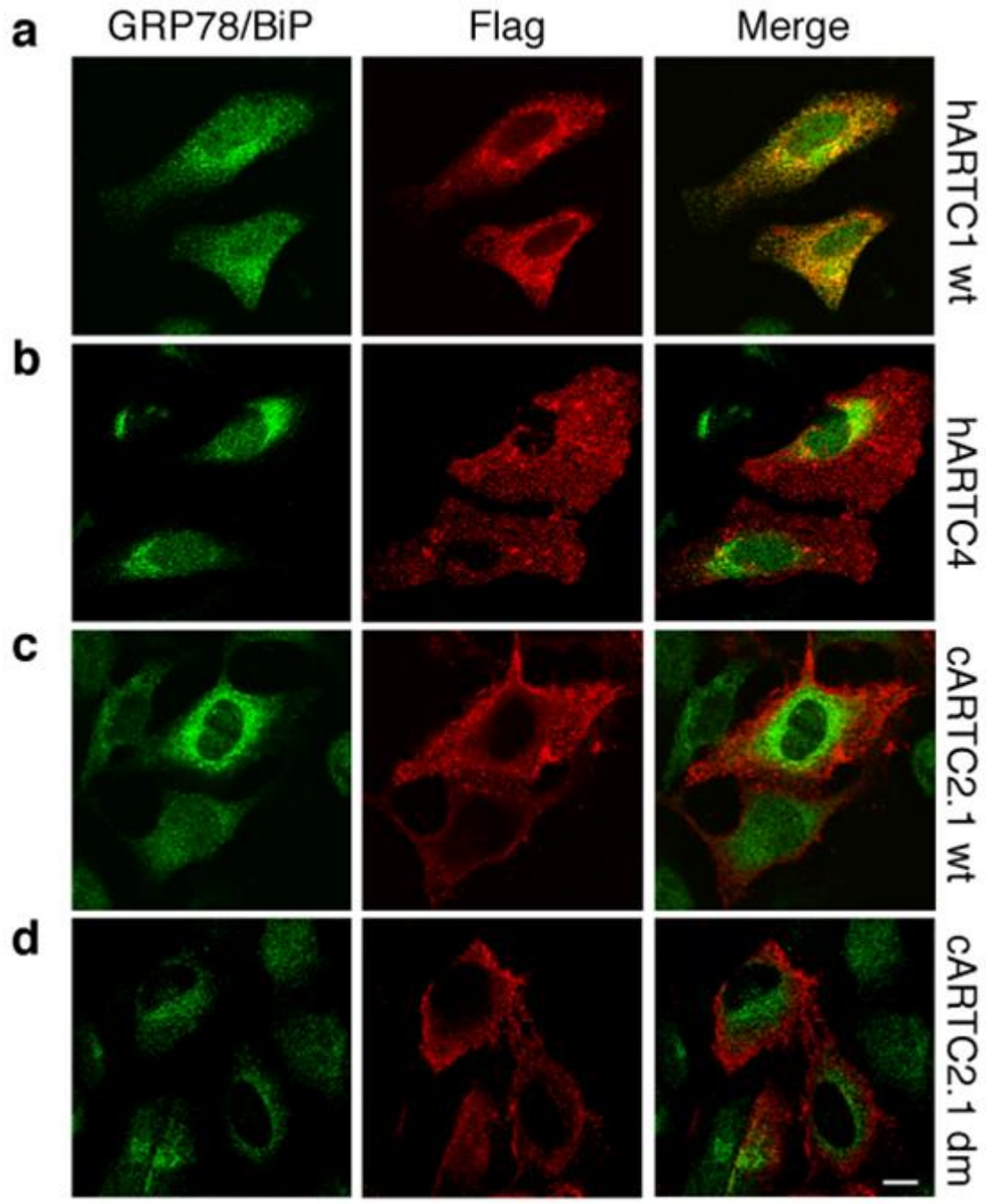

Taken from Fabrizio, G. et al., 2015b

Figure 3.13 hARTC1 wt co-localizes with GRP78/BiP. Representative immunofluorescence images of HeLa cells transiently transfected with the indicated constructs, stained with anti-GRP78/BiP or anti-Flag antibodies, as indicated, and analyzed by immunofluorescence. The scale bar represents 10 μm. The data shown are representative of at least five independent experiments.

As revealed by immunofluorescence images, hARTC1 wt co-localized with GRP78/BiP (Figure 3.13a), consistent with it being an ER-associated enzyme, in

contrast to all of the other ARTCs evaluated under the same experimental conditions (figure 3.13 b, c, d).

3.2.2.3 Macro domain-based far-Western Blotting assay

Taking advantage of the high affinity of the GST-mAf1521 macro domain for ADP-ribosylated substrates, its suitability as a molecular probe in far-Western Blotting was investigated. This is a molecular biological method based on Western Blotting but, instead of an antibody to detect the protein(s) of interest, far-Western Blotting uses a non-antibody protein able to probe for protein(s) of interest. In this way, binding partners of the probe protein may be identified. Different methods can be used to visualize the probe protein: radiolabeling, antibody with tag affinity (like HIS or Flag), or a protein-specific antibody against the probe protein. However, because cell extracts are usually completely denatured due to boiling in detergent before gel electrophoresis, this is only a useful approach for detecting interactions that do not require the native folded structure of the protein of interest.

The ability of the GST-mAf1521 macro domain to recognize ADP-ribosylated proteins immobilized on nitrocellulose was examined. To this aim, lysates obtained from HeLa cells previously transfected with the empty vector (pME.CD8LF), a GPI-GFP construct, or with Flag-tagged hARTC1 wt, hARTC4, cARTC2.1 wt and cARTC2.1 dm, were separated by SDS-PAGE and subsequently transferred to nitrocellulose filters. The filter was then probed with GST-mAf1521, using an anti-GST antibody to reveal it. As shown in Figure 3.14, macro domain labelled numerous bands, each of which corresponded to an ADP-ribosylated substrate.

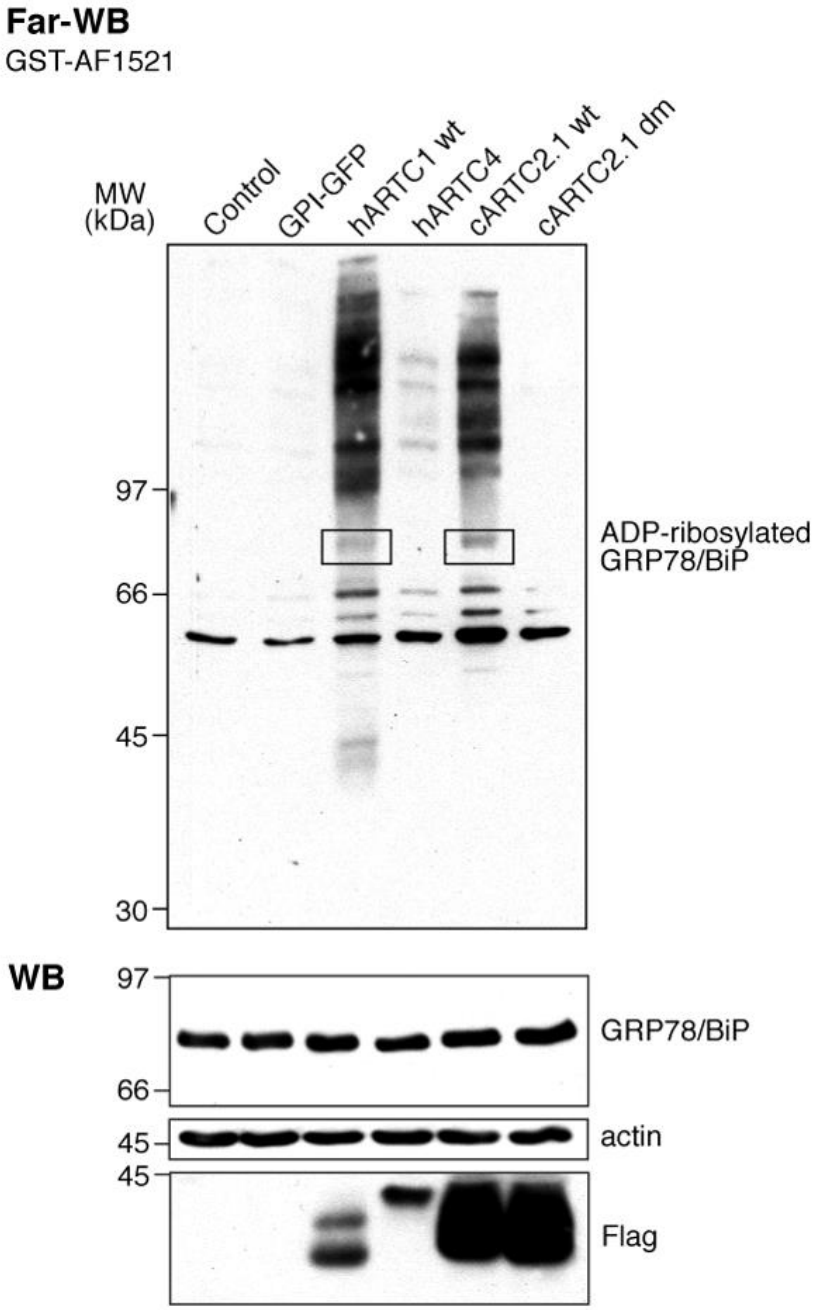

Modified from Fabrizio, G. et al., 2015b

Figure 3.14 GRP78/BiP is ADP-ribosylated by the ARTCs. Representative far-Western Blotting (FAR-WB, top) with GST-tagged mAf1521 of HeLa cells transfected with the empty vector (control) or with the indicated constructs. The solubilized proteins were separated by SDS-PAGE, transferred to nitrocellulose filters and incubated with GST-tagged mAf1521. Representative Western Blotting (WB, bottom) showing that the indicated band in Far-WB was recognized by a specific anti-GRP78/BiP antibody. The levels of expression of the indicated Flag-tagged proteins and the actin loading control are also shown. The data shown are representative of at least three independent experiments.

As shown in Figure 3.14, an evident pattern of ADP-ribosylated proteins was induced by hARTC1 wt and cARTC2.1 wt over-expression, as they both possessed arginine-specific ART activity. In contrast, a very slight protein labeling was obtained after the transfection of the inactive enzymes hARTC4 and cARTC2.1 dm, that were, indeed, comparable to that of the cells transfected with the empty vector (Figure 3.14, Far-WB, control) or with GPI-GFP (Figure 3.14, Far-WB, GPI-GFP). Analysis of the ADP-ribosylated targets of cells transfected with the enzymatically active hARTC1 wt and cARTC2.1 wt, revealed a protein band with the predicted molecular weight of GRP78/BiP (Figure 3.14, Far-WB, ADP-ribosylated GRP78/BiP).

A band at the same apparent molecular weight was also recognized by an anti-GRP78/BiP antibody and, obviously, it was present in all the samples and not just in hARTC1 wt- and cARTC2.1 wt-transfected cells, as the chaperone is ubiquitously expressed (Figure 3.14, WB). Moreover, staining with anti-Flag was performed to check the expression of the transfected enzymes and actin was used a loading control (Figure 3.14, WB).

Thus, the results presented here demonstrated that the GST-mAf1521 macro domain was a powerful tool that was suitable for analysis of ADP-ribosylated substrates in far-Western Blotting and, more importantly, confirmed that mono-ADP-ribosylation of GRP78/BiP was mediated by arginine-specific enzymes of the ARTC family (Fabrizio, G. et al., 2015b).

In order to demonstrate that the band revealed in far-Western Blotting after the transfection of active ARTCs was the mono-ADP-ribosylated GRP78/BiP, siRNA-

mediated knock-down of the chaperone was used. Initially, protocols were optimized to find ideal experimental conditions to silence the chaperone, using a pool of commercially available siRNA. The major difficulty was to efficiently silence one of the most abundant chaperones in the ER, since its silencing resulted in extensive cell death. Thus, it was important to find the optimal conditions to have the best silencing without inducing extensive cell death. The best result was achieved with the "siGENOME Human HSPA5 siRNA reagents" used at 100 nM for 48 hours, as shown in Figure 3.15.

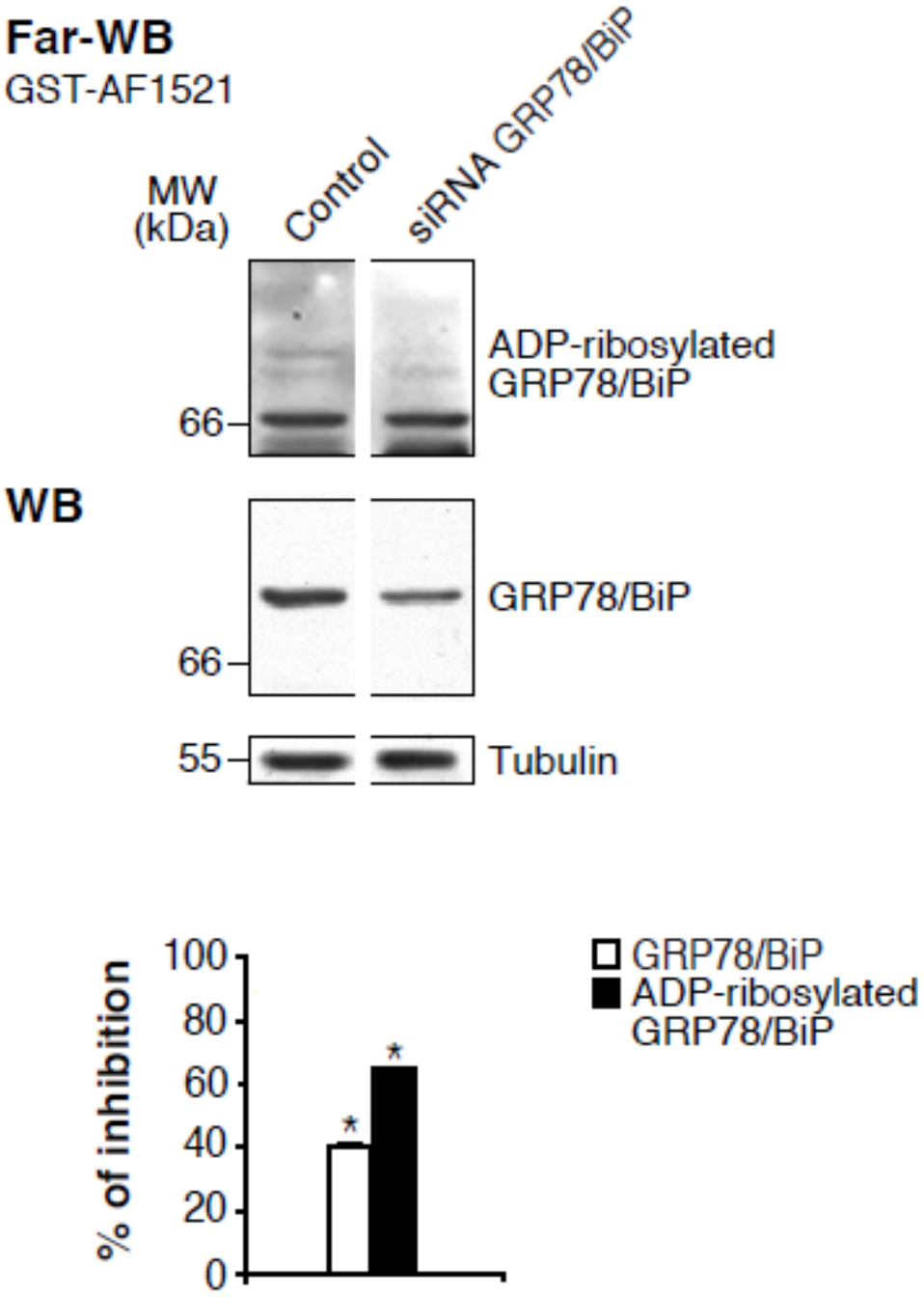

Modified from Fabrizio, G. et al., 2015b

Figure 3.15 Silencing of GRP78/BiP reduces GRP78/BiP mono-ADP-ribosylation. Representative far-Western Blotting (FAR-WB) with GST-tagged mAf1521 of both control and GRP78/BiP-silenced HeLa cells. The solubilized proteins were separated by SDS-PAGE, transferred to nitrocellulose filters, and incubated with GST-tagged mAf1521. Representative Western Blotting (WB) showing GRP78/BiP knock-down and the levels of expression of tubulin, that was used as loading control. Quantification of the reduction of GRP78/BiP (white bar) and that of GRP78/BiP ADP-ribosylation (black bar), expressed as percentage of inhibition. The data shown are representative of at least three independent experiments. *: significantly different from the relevant control ($p < 0.05$).

Western Blotting (WB), as depicted in Figure 3.15, showed a 40% reduction of the GRP78/BiP chaperone after silencing; as already mentioned, a stronger knock-down resulted in extensive cell death. However, this knock-down was sufficient to cause a reduction of the ADP-ribosylated form of the chaperone of about 65%. The demonstration of the reduction of the 78-kDa band revealed by far-WB strongly supported the notion that the protein detected by mAf1521 was, indeed, GRP78/BiP.

These data demonstrated that the GST-mAf1521 macro domain and its ability to bind ADP-ribosylated proteins with high affinity affords a useful tool for analysis of ADP-ribosylation also in far-Western Blotting experiments. Through this novel approach it was possible to demonstrate that hARTC1 is involved in the previously described GRP78/BiP mono-ADP-ribosylation (Fabrizio, G. et al., 2015b).

3.3 Summary

- hARTC1 is located in the ER: both the over-expressed and the endogenous protein co-localize with different ER markers in immunofluorescence experiments.
- hARTC1 and cARTC2.1 are synthetize into the ER as GPI-anchor proteins but, differently from cARTC2.1, which is mainly located in the plasma membrane, half of hARTC1 is ER resident.
- Macro domain is a powerful tool for the study of APD-ribosylation. Macro domain can be used in immunofluorescence allowing visualization of ADP-

ribosylated proteins in intact cells, and in far-Western Blotting to detect specific ADP-ribosylated targets.

- The prime target of hARTC1-mediated mono-ADP-ribosylation is the chaperone GRP78/BiP.

Chapter 4

Study of GRP78/BiP mono-ADP-ribosylation using a catalytically inactive hARTC1 double mutant and siRNA-mediated knock-down of hARTC1

4.1 Introduction

The experiments reported in the previous Chapter demonstrated that hARTC1 wt is an enzyme localized in the ER, where it is involved in the mono-ADP-ribosylation of the chaperone GRP78/BiP. The experiments described in that Chapter were performed using the enzymes cARTC2.1 wt, and its catalytically inactive mutant or the enzyme hARTC4 as the negative controls of hARTC1 wt, both for cellular localization (cARTC2.1 wt and cARTC2.1 dm are localized to the plasma membrane) and activity (cARTC2.1 dm and hARTC4 are inactive enzymes). However, a more specific approach is to use a catalytically inactive mutant of hARTC1 wt. This validates data obtained with other enzymes, and excludes indirect effects mediated by hARTC1 on the ADP-ribosylation of GRP78/BiP. For these reasons, a catalytically inactive mutant version of hARTC1 was generated using site-directed mutagenesis.

Another important experimental approach to study GRP78/BiP mono-ADP-ribosylation by hARTC1 is the use of siRNA-mediated knock-down. Silencing of hARTC1 was therefore used to directly demonstrate that hARTC1 was the enzyme involved in the modification of the GRP78/BiP.

4.2 Results

4.2.1 Study of expression, localization and activity of hARTC1 double mutant

hARTC1 has conserved residues corresponding to the R-S-EXE motif of arginine-specific mono-ADP-ribosyl-transferases (Glowacki, G. et al 2002). In particular, glutamate 240 (E240) is considered a key catalytic amino acid, even though glutamate 238 (E238) is critical for enzyme function (Takada, T. et al., 1995). Mutation of either of these residues has been shown to alter the enzyme's capacity to use arginine as acceptor, supporting the idea that this was the region involved in acceptor recognition (Bourgeois, C. et al., 2003). To test how mutations could alter the substrate specificity, single point and double point mutant versions of hARTC1 were generated. Firstly, experiments to generate a single point hARTC1 mutant by changing the glutamate 240 to glycine (E240G) were performed. Previous work from my laboratory had characterized single point and double point (E207G/E209G) mutant isoforms of hamster ARTC2.1 (Stilla, A. et al., 2011). It was found that the single point mutated protein still had a partial transferase activity, while the double point mutant was completely inactive. In light of these observations, a double mutant (E238G/E240G) was generated, in which both of the glutamic acid residues of the EXE motif were mutated. Unfortunately, attempts to generate the single point mutant hARTC1-E240G failed: no growth on the antibiotic plate was seen after bacterial transformation, even though the positive and negative control of the experiments confirmed that the reaction was properly set up and executed. For the positive control, competent bacteria were

transformed with non-digested plasmid DNA and plated on selection media; it allows measurement of the efficiency of transformation and served as a standard for comparison with other transformations. For the negative control, competent bacteria without addition of plasmid were plated on positive selection media and no growth was observed. Despite repeated attempts and successful transformations procedure, no colony could be observed on the plate corresponding to single point mutant hARTC1-E240G. The over-expression of the mutant protein could have toxic effects on the bacterial growth. A possible explanation could be that the single mutant protein is expressed, but it interferes with the normal proliferation and homeostasis of the microorganism, resulting in cell death. This toxicity is not exclusive for hARTC1 single point mutant as different enzymes of the ART family have already been described to be deleterious for bacteria, causing unsuccessful transformations. However, the double point mutant (E238G/E240G) of hARTC1 was successfully generated. This double point mutant is hereafter referred to as hARTC1 dm. The doubly mutated hARTC1 enzyme was characterized in terms of expression, activity and cellular localization. The level of expression was evaluated by Western Blotting, catalytic activity was assessed with far-Western Blotting and macro domain-based immunofluorescence experiments, and the cellular localization of hARTC1 dm was examined using immunofluorescence experiments.

4.2.1.1 The hARTC1 (E238G/E240G) dm is not able to mediate GRP78/BiP mono-ADP-ribosylation

To evaluate hARTC1 dm expression and activity, Western Blotting and far-Western Blotting experiments were performed. Specifically, HeLa cells were transfected with the empty vector or with hARTC1 wt or hARTC1 dm for 24 hours. Subsequently, cells were lysed, their protein content measured and separated by SDS-PAGE, transferred to nitrocellulose filters and, then, probed with GST-mAf1521 for far-Western Blotting or with anti-ARTC1, anti-GRP78/BiP and anti-tubulin antibodies for Western Blotting.

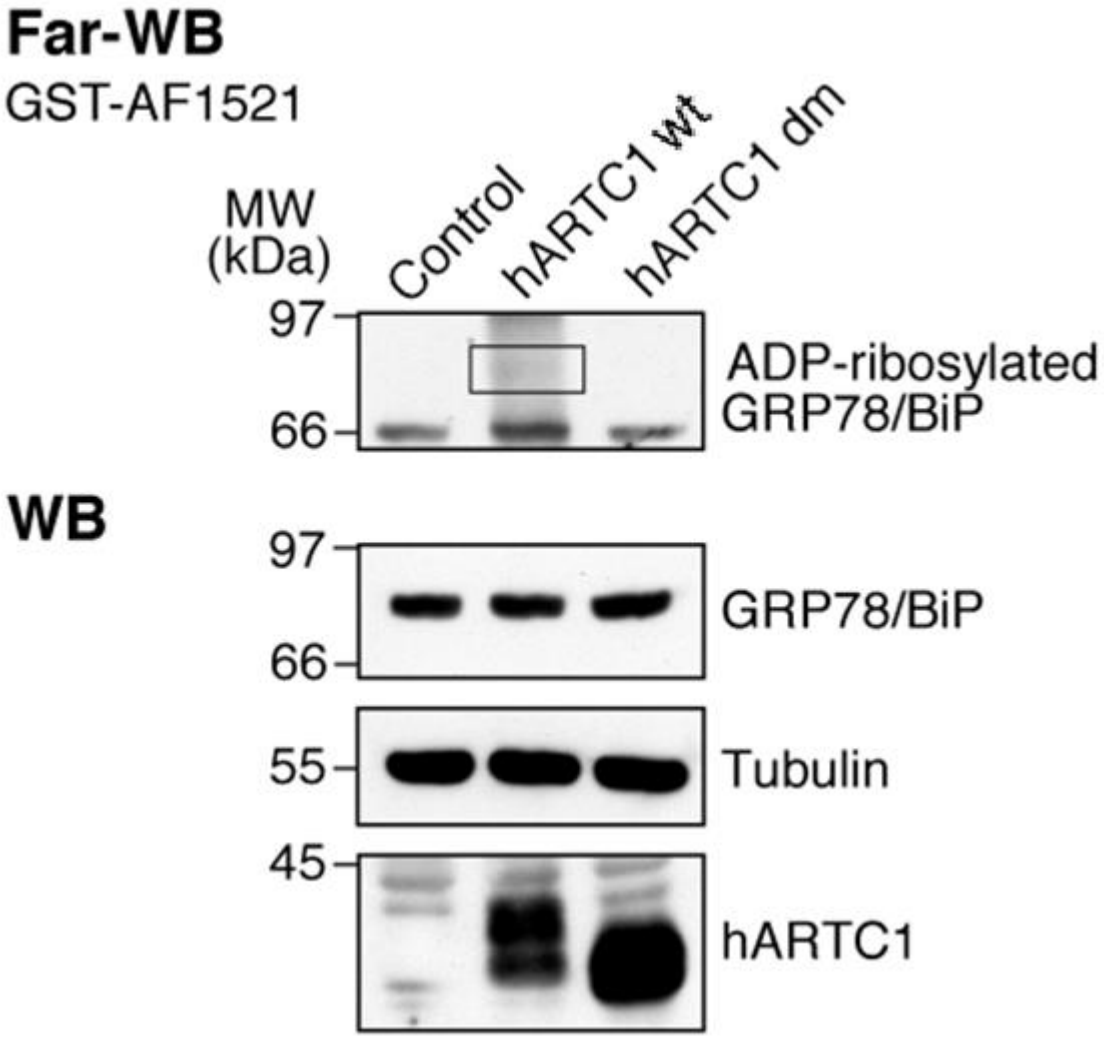

Modified from Fabrizio, G. et al., 2015b

Figure 4.1 hARTC1 dm does not induce GRP78/BiP mono-ADP-ribosylation and is therefore catalytically inactive. Representative far-Western Blotting (FAR-WB, top) with GST-tagged mAf1521 of HeLa cells transfected with an empty vector (control), or with the indicated constructs. The solubilised proteins were separated by SDS-PAGE, transferred to nitrocellulose filters and incubated with GST-tagged mAf1521. Representative Western Blotting (WB, bottom) showing that the indicated band in FAR-WB was recognized by a specific anti-GRP78 antibody. The levels of expression of the indicated hARTC1 proteins are also shown. Tubulin was used as loading control. The data shown are representative of three independent experiments.

As shown in Figure 4.1, hARTC1 dm transfection levels were comparable to that of the wild type protein (Figure 4.1 WB; hARTC1). However, ADP-ribosylated proteins detectable in hARTC1 wt-transfected cells were completely absent in hARTC1 dm-

transfected cells. The lack of band corresponding to GRP78/BiP ADP-ribosylation in cells transfected with hARTC1 dm (Figure 4.1 Far-WB; ADP-ribosylated GRP78/BiP) indicates that hARTC1 dm was an inactive enzyme.

As a further examination of the catalytically inactivity of hARTC1 dm, macro domain-based immunofluorescence experiments were performed using HeLa cells transfected for 24 hours with the Flag-hARTC1 dm. An anti-Flag antibody was used to detect the over-expressed enzyme, and an anti-GST antibody was used to detect the GST-tagged mAf1521 probe to visualize potential ADP-ribosylation (Figure 4.2).

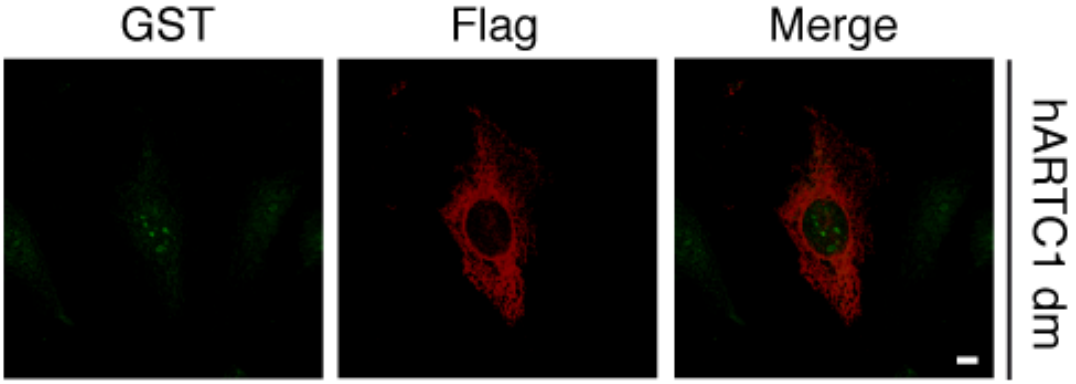

Modified from Fabrizio, G. et al., 2015b

Figure 4.2 The mAf1521 macro module does not allow visualization of ADP-ribosylated proteins in cells transfected with hARTC1 dm. Representative immunofluorescence images of HeLa cells were transiently transfected with Flag-hARTC1 dm, fixed and permeabilized, incubated with GST-mAf1521 and then stained with anti-Flag and anti-GST antibodies. The scale bar indicates 10 µm. The data shown are representative of three independent experiments.

As shown in Figure 4.2, immunofluorescence confirmed that in cells transfected with hARTC1 dm only a modest nuclear staining was detectable with GST-mAf1521, similar to that of control cells (cf. Figure 3.10a) or that of hARTC4- and cARTC2.1 dm-transfected cells (cf. Figures 3.11c, g, respectively). Altogether, these

experiments demonstrated that the double mutant form of hARTC1 was expressed in HeLa cells as an inactive enzyme that could not catalyze ADP-ribosylation reactions (Fabrizio, G. et al., 2015b).

4.2.1.2 The hARTC1 (E238G/E240G) dm is localized to the ER

The cellular location of hARTC1 dm was examined using immunofluorescence experiments. HeLa cells were transfected with hARTC1 dm for 24 hours and stained with an anti-Flag antibody to determine the location of the expressed protein. The cells were also stained with an anti-GRP78/BiP antibody to show the ER.

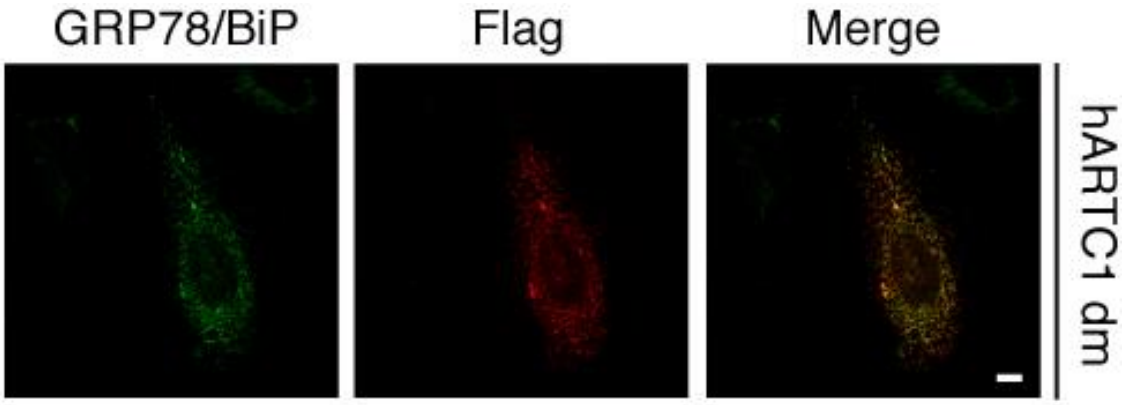

Modified from Fabrizio, G. et al., 2015b

Figure 4.3 hARTC1 dm co-localizes with GRP78/BiP. Representative immunofluorescence images of HeLa cells that were transiently transfected with Flag-hARTC1 dm and stained with anti-GRP78/BiP and anti-Flag antibodies. The scale bar indicates 10 μm. The data shown are representative of three independent experiments.

The analysis of cells by confocal microscopy revealed that, when over-expressed in HeLa cells, Flag-hARTC1 dm co-localized with GRP78/BiP (Figure 4.3). Thus, it appeared to be an ER-resident enzyme exactly as the wild-type counterpart (cf. Figure 3.13a) and in contrast to all of the other ARTCs evaluated under similar experimental conditions (cf. Figure 3.13b, c, d).

This result demonstrated that hARTC1 dm was expressed and correctly localized at the ER compartment albeit catalytically inactive. The results obtained with hARTC1 dm further validate previous data shown in this thesis concerning hARTC1 ER localization and its involvement in GRP78/BiP ADP-ribosylation reaction (Fabrizio, G. et al., 2015b).

4.2.2 Silencing of hARTC1 reduces the level of GRP78/BiP mono-ADP-ribosylation

Silencing of hARTC1 was used to examine the effect of knocking-down the expression of the enzyme and of its consequence for ADP-ribosylation of GRP78/BiP. The working hypothesis was that a reduction of hARTC1 expression accompanied by lower levels of GRP78/BiP modifications would provide a direct demonstration this was the enzyme involved in the chaperone's mono-ADP-ribosylation.

For the silencing of hARTC1 a few commercial tools were available; however, they were not yet being tested by the providers. For this study, a set of 4 siRNAs from Sigma-Aldrich were initially tested but this tool was not able to silence hARTC1. Thus, single siRNA sequences were generated, designing 4 different oligonucleotides that were specific for hARTC1. Then I performed different protocols to optimize the experimental conditions for the best knock-down, including evaluation of different siRNAs combination (single, double, triple or quadruple siRNAs), various siRNA transfection reagents (HiPerFect Transfection Reagent from Qiagen, Lipofectamine 2000 Transfection Reagent from Thermo Fisher Scientific, jetPRIME DNA/siRNA Transfection Reagent form Polyplus), ratio

of transfection reagent to siRNA, cell density at transfection, dose-response and time-course of silencing (48 hours or 72 hours). The best reduction of hARTC1 was achieved with HeLa cells transfected with a pool of three siRNAs (siRNA1ARTC1, siRNA2ARTC1 and siRNA4ARTC1, table 2.1.2) used 30 nM each for 48h, transfected with jetPRIME reagent. hARTC1 knock-down was analyzed by Western Blotting, and the levels of ADP-ribosylated GRP78/BiP by far-Western Blotting.

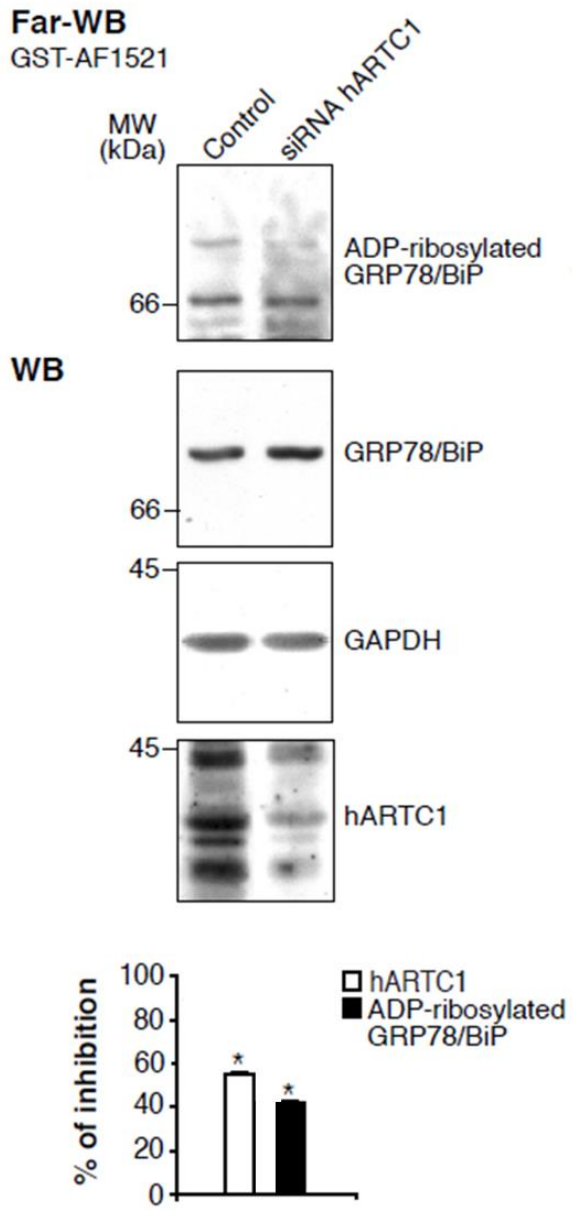

Modified from Fabrizio, G. et al., 2015b

Figure 4.4 Silencing of hARTC1 reduces the basal level of GRP78/BiP mono-ADP-ribosylation. Representative far-Western Blotting (FAR-WB, top) with GST-tagged mAf1521 of both control and hARTC1-silenced HeLa cells. The solubilised proteins were separated by SDS-PAGE, transferred to nitrocellulose filters, and incubated with GST-tagged mAf1521. Representative Western Blotting (WB, bottom) showing hARTC1 knock-down. The anti-ARTC1 antibody revealed at least four major bands that would reflect different degrees of glycosylation of hARTC1. The Western Blotting also showed the levels of expression of GRP78/BIP and of GAPDH, which was used as loading control. The graph (bottom) show the quantification of the reduction of hARTC1 protein expression (white bar; relative to control cells set at 100%), and that of ADP-ribosylated GRP78/BiP (black bar; relative to control cells set at 100%). The data shown are representative of at least three independent experiments. * indicates significantly different from the relevant control ($p < 0.05$).

The Western Blotting shown in Figure 4.4 indicates that the hARTC1 antibody revealed the presence of at least four different major bands. This was reported in the datasheet of this specific commercial antibody from Sigma-Aldrich (see *Materials and Methods*, Table 2.3). The presence of multiple protein bands was consistent with different degrees of glycosylation of the hARTC1 protein, since this modification had previously been reported for ecto-ART enzymes (Zolkiewska, A. et al., 1992). However, application of hARTC1 siRNA led to reductions in the density of all four bands, and quantification of one of them (specifically the one corresponding to the indication "hARTC1" near the bottom panel of Figure 3.19) demonstrated a reduction of band intensity by 55% (relative to control non-transfected cells).

Regarding GRP78/BiP ADP-ribosylation, far-Western Blotting of non-transfected HeLa cells revealed a distinct band corresponding in size to GRP78/BiP that could only be detected after longer exposure (Figures 3.19, control, and 3.15, control). This specific band, however, was reduced by approximately 40% when endogenous hARTC1 was knocked-down by siRNA (Figure 3.19).

Thus, the silencing of hARTC1 was sufficient to inhibit the basal level of ADP-ribosylated GRP78/BiP. This finding provided a direct demonstration that hARTC1 was the enzyme responsible for the modification of the chaperone (Fabrizio, G. et al., 2015b).

4.3 Summary

- A doubly mutated hARTC1 has been generated using site-directed mutagenesis.
- hARTC1 dm is localized at the ER and is expressed as an inactive enzyme that could not generate ADP-ribosylated GRP78/BiP, as evaluated using the macro domain in immunofluorescence and far-Western Blotting experiments.
- The silencing of hARTC1 inhibits the basal levels of GRP78/BiP mono-ADP-ribosylation.

Chapter 5

Expression and activity of hARTC1 are regulated by ER stress but are not involved in the UPR

5.1 Introduction

The molecular chaperone GRP78/BiP has been reported to undergo intracellular mono-ADP-ribosylation, but the enzyme(s) responsible for this modification have not been identified so far (Laitusis, A.L. et al., 1999; Ledford, B.E. and Leno, G.H., 1994). However, due to GRP78/BiP's ER luminal localization, it was previously postulated that, from a topological point of view, an arginine-specific enzyme of the ARTC family would be needed to modify the chaperone (Di Girolamo, M. et al., 2005, Fabrizio, G. et al., 2015b). Consistent with this hypothesis, the data presented in the previous chapters demonstrated that hARTC1 was the enzyme involved in this previously described mono-ADP-ribosylation.

GRP78/BiP is a well-characterized molecular chaperone ubiquitously expressed in mammalian cells (Chen, W.T. and Lee, A.S., 2011). It is best known for binding to hydrophobic patches on nascent polypeptides within the ER, preventing intermediates from aggregating and facilitating the acquisition of proper secondary structure of mature proteins (Gardner, B.M. et al., 2013; Zhu, G. and Lee, A.S., 2015). Along with its role in protein folding, GRP78/BiP has also been demonstrated to be a player in a wide variety of cellular pathways, including ER

stress and UPR (Brewer, J.W., 2014; Hetz, C., 2012; Ni, M. and Lee, A.S., 2007; Zhu, G. and Lee, A.S., 2015).

The role of GRP78/BiP, like the other chaperones, during the processing of nascent proteins in the ER lumen is dependent on ER luminal factors such as calcium concentration, redox homeostasis and oxygen supply (Araki, K. and Nagata, K., 2011; Gorlach, A. et al., 2006; Ushioda, R. et al., 2016). Physiological or pathological conditions that disrupt this fine balance, such as ER calcium depletion, glucose deprivation and oxidative stress, perturb the ER homeostasis and lead to accumulation of unfolded or misfolded proteins in the ER, causing the ER stress (Vincenz-Donnelly, L. and Hipp, M.S., 2017).

The cellular responses to ER stress are multifaceted and include the activation of the UPR pathway, primary aim of which is to sustain cell survival by attenuating protein synthesis and restoring cellular homeostasis (Gardner, B.M. et al., 2013; Grootjans, J. et al., 2016; Kaufman, R.J., 1999; Welihinda, A.A. et al., 1999). The UPR is orchestrated by three ER transmembrane receptors: ATF6, IRE1α and PERK (Brewer, J.W., 2014; Hetz, C., 2012; Mori, K., 2000). In resting cells they are all kept inactivate through their association with GRP78/BiP (Brewer, J.W., 2014; Hetz, C., 2012). Upon ER stress, unfolded proteins accumulate in the ER lumen resulting in the dissociation of GRP78/BiP from ATF6, IRE1α and PERK, subsequently transducing the UPR (Brewer, J.W., 2014; Hetz, C., 2012; Merksamer, P.I. and Papa, F.R., 2010; Ron, D. and Walter, P., 2007). UPR activation leads to an adaptive increase in folding capacity, exemplified by the induction of different genes, including GRP78/BiP (Zhang, K. and Kaufman, R.J., 2008). However, when ER stress

is not mitigated, an ER stress-induced cell death ensues (Iurlaro, R. and Munoz-Pinedo, C., 2016; Logue, S.E. et al., 2013; Sano, R. and Reed, J.C., 2013). Considering the key functions of GRP78/BiP in protein folding and in the ER stress response, the main focus of this Chapter was the study of the biological role of GRP78/BiP mono-ADP-ribosylation in these contexts.

The mono-ADP-ribosylation of GRP78/BiP has been hypothesized to be a way to regulate the availability of the functional chaperone since, when ADP-ribosylated, it is in an inactive state (Laitusis, A.L. et al., 1999; Ledford, B.E. and Leno, G.H., 1994). Under normal conditions, the levels of ADP-ribosylated GRP78/BiP are reported to be low (Laitusis, A.L. et al., 1999). However, during stress conditions, such as amino acid starvation or cell treatment with protein synthesis inhibitors, which cause a reduction in mRNA translation and protein processing, there is an increase in the amount of the modified chaperone. Therefore, it has been suggested that this ADP-ribosylation represents a buffering system that allows the rates of protein processing to be balanced with those of protein synthesis (Laitusis, A.L. et al., 1999). Considering that this study has identified, for the first time, the enzyme involved in GRP78/BiP mono-ADP-ribosylation, further experiments analyzed the functional role of this modification. Firstly, it was investigated whether cell stresses that are well known activators of ER stress and, thus, are reported to induce GRP78/BiP, could also modulate hARTC1 and, consequently, affect GRP78/BiP mono-ADP-ribosylation levels. Secondly, due to GRP78/BiP's role as a master regulator of the UPR, the possible involvement of hARTC1 in this process was examined. Specifically, whether and how the manipulation of hARTC1 gene expression

affected the three GRP78/BiP-interacting sensors was analyzed. Modulating the expression of the enzyme responsible for GRP78/BiP mono-ADP-ribosylation allowed an investigation into the functional role of this post-translational modification and, plausibly revealed hARTC1 as a new, unexpected player of the UPR.

5.2 Results

5.2.1 hARTC1 is an ER stress-sensing protein

Different reports have indicated that GRP78/BiP expression is modulated by various stress-inducing agents or by conditions that adversely affect ER functions, such as oxidative stress, chemical toxicity, inhibition of the ER calcium-ATPase, inhibitors of glycosylation and hypoxia (Beriault, D.R. and Werstucka, G. H., 2013; Oslowski, C.M. and Urano, F. 2011). Therefore, it was examined whether these same stress conditions were also able to modulate hARTC1 levels, thus implicating a hARTC1 in the ER stress response.

Starting from data available within the published literature, HeLa cells were exposed to different stress-evoking treatments already described as GRP78/BiP inducers, whilst changes in mRNA transcript and protein levels were analyzed. Specifically, HeLa cells were subjected to stress treatments with DTT (2 mM for 2 hours), thapsigargin (1 μM for 2 hours, and 0.3 μM for 18 and 24 hours), heat shock (42°C for 24 hours) and hypoxia (induced by 0.1% O_2 for 24 hours; Beriault, D.R. and Werstucka, G. H., 2013; Li, W.W et al., 1993; Negroiu, G. et al., 2000).

For transcript levels, mRNA was extracted from cells subjected to these stress treatments and analysed with (qRT)-PCR, using primers specifically designed for ARTC1, GRP78/BiP and GAPDH (employed as internal control; see Table 2.2).

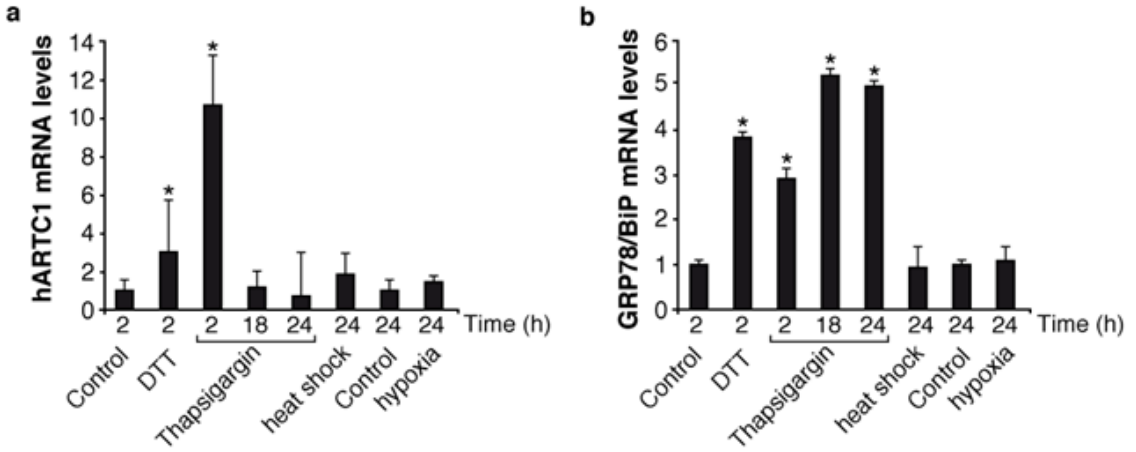

Modified from Fabrizio, G. et al., 2015b

Figure 5.1 hARTC1 and GRP78/BiP mRNA levels are increased by the cell stressors DTT and thapsigargin. The graphs show quantification of the levels of (a) endogenous hARTC1 and (b) GRP78/BiP mRNA transcripts within HeLa cells exposed to different stress-inducing treatments, determined by (qRT)-PCR. The (qRT)-PCR results were normalized to GAPDH mRNA, and then reported as arbitrary units relative to the hARTC1 or GRP78/BiP transcript of non-transfected, non-treated HeLa cells (control, taken as 1.0). Data are presented as mean±SD of three independent experiments, each performed in triplicate. * indicates significantly different from control ($p < 0.01$).

A significant increase of hARTC1 mRNA levels (Figure 5.1a) was observed as a consequence of DTT (3.04±2.76) and thapsigargin (10.73±2.59) treatments, both of which are well-characterized treatments for the induction of ER stress and GRP78/BiP expression. As expected, GRP78/BiP levels increased in HeLa cells treated with DTT (3.82±0.11) and thapsigargin (3.01±0.21), confirming previous reports (Laitusis, A.L. et al., 1999).

GRP78/BiP mRNA levels were increased after 2 hours of treatment with thapsigargin (2.90±0.22), with even higher mRNA levels being observed in cells

treated for 18 hours (5.21±0.13) that were maintained through to 24 hours (4.97±0.11; Figure 5.1b). Conversely, the increase in hARTC1 mRNA was observed after 2 hours of treatment with thapsigargin, but had returned to control levels by 18 hours (1.19±0.87) and 24 hours (0.76±2.30) of treatment (Figure 5.1a).

When other stress treatments were used (heat shock, hypoxia), little or no changes in either hARTC1 (heat shock 1.83±1.21; hypoxia 1.46±0.25) or GRP78/BiP (heat shock 0.92±0.41; hypoxia 1.14±0.16) mRNA levels were observed. Despite the fact that GRP78/BiP is an HSP70 member, and thus is expected to be affect by heat-shock, it has already been reported in the literature that GRP78/BiP expression is not significantly affected by heat shock conditions, as opposed to the other members of the HSP family (Wooden, S.K. and Lee, A.S., 1992).

Thus, hARTC1 and GRP78/BiP transcripts are modulated by the same stresses, even though with different timing (Fabrizio, G. et al., 2015b).

The (qRT)-PCR results were verified by analyzing the changes in hARTC1 and GRP78/BiP protein levels. Specifically, Western Blotting of HeLa cells exposed to the same stress conditions was performed. After being lysed, samples were separated by SDS-PAGE, transferred to nitrocellulose filters and probed with specific antibodies, as described in *Materials and Methods*.

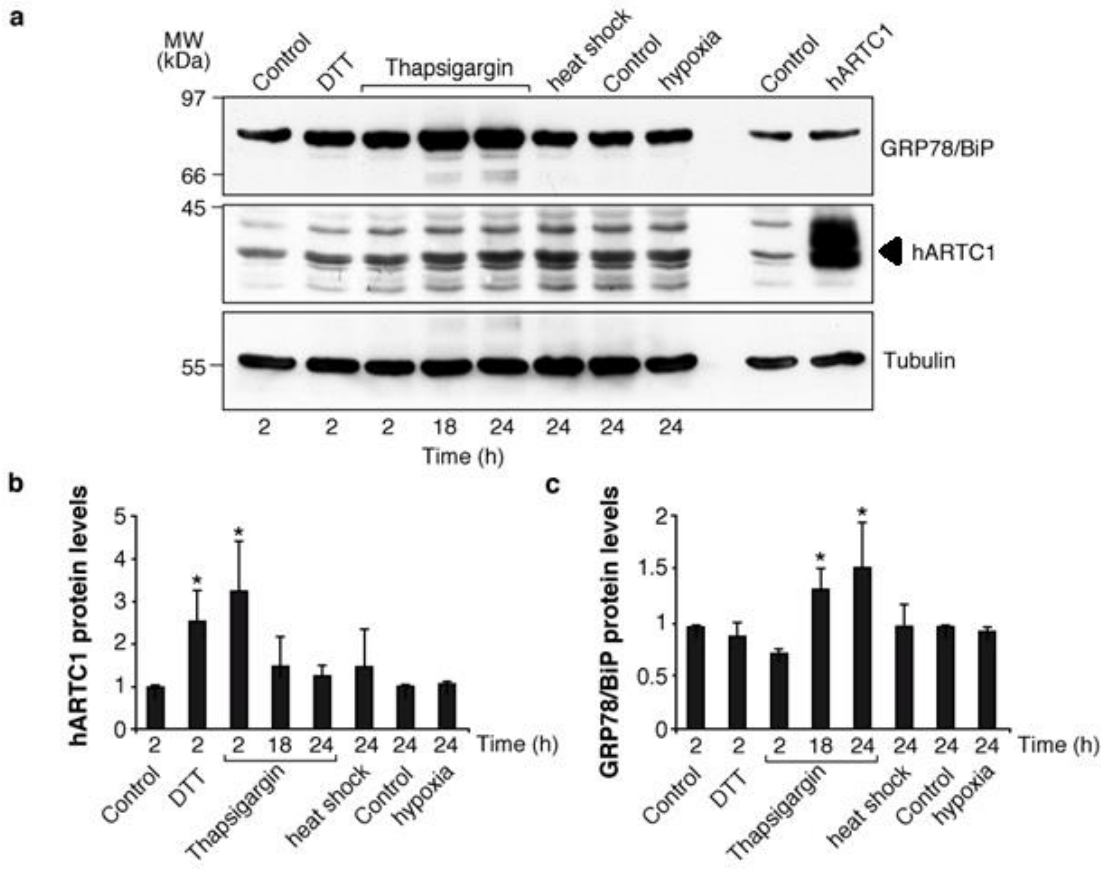

Modified from Fabrizio, G. et al., 2015b

Figure 5.2 hARTC1 and GRP78/BiP protein levels are increased by the cell stressors DTT and thapsigargin. (a) Representative Western Blotting showing endogenous hARTC1 and GRP78/BiP levels in cells exposed to different stress-inducing treatments. Tubulin was used a loading control. The level of expression of hARTC1 following transfection is also shown and was employed for the identification of the hARTC1 protein band of interest. (b and c) Quantification of the protein levels of (b) hARTC1 and (c) GRP78/BiP, normalized to tubulin, and relative to those of non-treated cells (control, taken as 1.0). Data are presented as mean±SD of three independent experiments, each performed in duplicate. * indicates significantly different from the relevant control ($p < 0.05$).

The evaluation of both hARTC1 and GRP78/BiP protein levels under the same incubation conditions confirmed the mRNA analysis (Figure 5.1a, b). Increased levels of hARTC1 and GRP78/BiP were observed as a consequence of the DTT and thapsigargin treatments, but not with the other stressors (Figure 5.2). Quantification of protein bands demonstrated a significant increase of hARTC1 (Figure 5.2b) following 2 hours of treatment with the cell stressors DTT (2.55±0.68)

and thapsigargin (3.22±1.11). Whereas, increased levels of GRP78/BiP (Figure 5.2c) were only observed following long-term treatments with thapsigargin (thapsigargin for 18 hours, 1.33±0.18; thapsigargin for 24 hours, 1.56±0.38). In contrast to the mRNA expression analysis, for which GRP78/BiP was elevated after 2 hours of treatments and continued through the 24 hours, higher protein levels were evident only after 18 and 24 hours (cf. Figure 5.1 and 5.2).

Of note, for the stress treatment experiments two different controls (non-treated, non-transfected cells) were used: the first was employed for the 2-hour DTT and thapsigargin treatments, and the second for the 18- and 24-hours thapsigargin, heat-shock and hypoxia treatments (Figure 5.1). With respect to protein levels, it seemed that both hARTC1 and GRP78/BiP were time-dependently expressed, as shown in Figure 5.2a.

For hARTC1, as shown in the middle panel of Figure 5.2a, multiple bands were visualized, which were consistent with the different degrees of glycosylation of the protein (see also Figure 3.19 and related comments). Densitometric analysis was only performed on one of these band, i.e. the band that increased after hARTC1 transfection (indicated by the arrow in the middle panel of Figure 5.2a). To ensure the quantification of the same band for all experiments, a sample of hARTC1 transfected cells was routinely used as marker for the correct band.

Altogether, the data from mRNA and protein analysis confirmed that under ER stress conditions there was a faster expression of hARTC1 than GRP78/BiP. Conversely, during the long-term ER stress treatments that caused increased

expression of GRP78/BiP, the basal hARTC1 levels were restored (Fabrizio, G. et al., 2015b).

Considering that these data demonstrate that hARTC1 was induced by ER stress treatments known to modulate GRP78/BiP, the next step was to investigate whether these same stress conditions could influence GRP78/BiP mono-ADP-ribosylation. In order to evaluate the effect on mono-ADP-ribosylation, the macro domain-based far-Western Blotting was performed using HeLa cells exposed to both short-term and long-term stress conditions. In both cases, cells were lysed, separated by SDS-PAGE and subsequently transferred to nitrocellulose filters, as described in *Materials and Methods*. Subsequently, the filters were probed with the GST-mAf1521 macro domain, using an anti-GST antibody to reveal its binding (Figures 5.3 and 5.4).

For the short-term stress treatments, GRP78/BiP ADP-ribosylation was analyzed at three different time points (20, 60 and 120 minutes; Figure 5.3). Indeed, both DTT and thapsigargin were reported to cause acute inhibition of translation, and 10 - 20 minutes' treatment was enough to inhibit the synthesis of almost all proteins (Brostrom, C.O. and Brostrom, M.A., 1998).

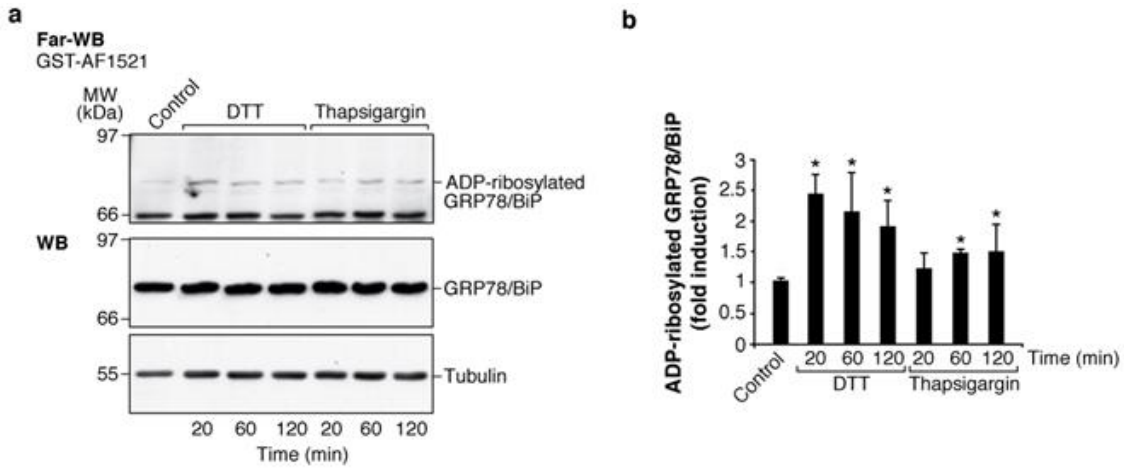

Modified from Fabrizio, G. et al., 2015b

Figure 5.3 ADP-ribosylation of GRP78/BiP is induced by short-term treatment of HeLa cells with DTT and thapsigargin. (a) Representative far-Western Blotting (Far-WB) and (b) relative quantification of ADP-ribosylated GRP78/BiP in HeLa cells that were either untreated (control) or treated for the indicated times with DTT (2 mM) or thapsigargin (1 μM). The indicated band (ADP-ribosylated GRP78/BiP) was also recognized with an anti-GRP78/BiP specific antibody. Tubulin was used as a loading control. Data are representative of at least three independent experiments. * indicates significantly different from the relevant control ($p < 0.05$).

As depicted in Figure 5.3, increased levels of ADP-ribosylated GRP78/BiP were detectable during acute treatments with DTT and thapsigargin. These increased levels of ADP-ribosylated GRP78/BiP were evident after 20 minutes of DTT and thapsigargin addition, and were maintained for 2 hours (Figure 5.3a, Far-WB). Quantification of the relevant band confirmed that there was more than a two-fold induction of GRP78/BiP ADP-ribosylation during the acute stress treatment with DTT (20 minutes, 2.46±0.30; 1 hour, 2.15±0.64), and this was maintained through 2 hours (1.90±0.43; Figure 5.3b). Treatment with thapsigargin did not give a significant increase of GRP78/BiP ADP-ribosylation after 20 minutes of treatment (1.23±0.25), whereas significant increases were detectable after 1 hour (1.48±0.06) and 2 hours (1.50±0.45) of treatment (Figure 5.3b).

For the long-term stress experiments, ADP-ribosylation of GRP78/BiP was analysed in cells exposed to 0.3 μM thapsigargin for 18 and 24 hours. Under these stress treatment conditions, the expression of GRP78/BiP has been well reported to be induced (Figure 5.2; Li, W.W. et al., 1993).

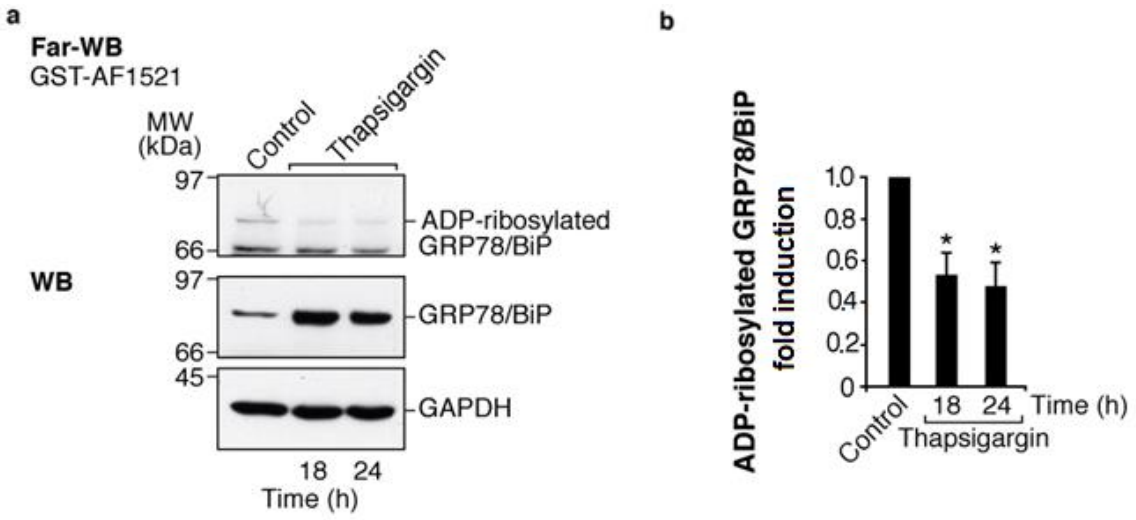

Modified from Fabrizio, G. et al., 2015b

Figure 5.4 ADP-ribosylation of GRP78/BiP is not affected by long-term treatment of HeLa cells with thapsigargin. Representative far-Western Blotting (Far-WB) and relative quantification of ADP-ribosylated GRP78/BiP in HeLa cells that were either untreated (control) or treated for the indicated times with thapsigargin (0.3 μM). The indicated band (ADP-ribosylated GRP78/BiP) was also recognized with an anti-GRP78/BiP specific antibody. GAPDH was used as a loading control. Data are representative of at least three independent experiments. * indicates significantly different from the relevant control ($p < 0.05$).

The long-term stress treatments with thapsigargin were accompanied by the reduction of the ADP-ribosylated form of GRP78/BiP, as evaluated by far-Western Blotting with the mAf1521 macro domain (Figure 5.4a, Far-WB). Quantification of the relevant band indicated a reduction for the 18-hour thapsigargin treatment (0.53±0.10) and for the 24-hour thapsigargin treatment (0.47±0.11; Figure 5.4b). In addition, as expected (Figure 5.2), the expression of GRP78/BiP was increased

(Figure 5.4a, WB). Thus, the long-term stress treatments increased GRP78/BiP expression, but were ineffective in inducing GRP78/BiP ADP-ribosylation.

Altogether these data demonstrated that established activators of ER stress could induce expression of hARTC1 and GRP78/BiP, as well as GRP78/BiP mono-ADP-ribosylation (Fabrizio, G. et al., 2015b). These findings suggested that induction of hARTC1 and the consequent GRP78/BiP mono-ADP-ribosylation could be an early cell response to ER stress conditions, thereby indicating a possible role for hARTC1 in the ER stress response required for cell survival.

5.2.2 hARTC1 does not trigger the UPR

The data reported above indicated that hARTC1 mRNA and protein expression was rapidly increased after the short-term stress treatments with DTT and thapsigargin. In addition to elevated protein levels, these data also indicated an increased enzyme activity that resulted in higher GRP78/BiP ADP-ribosylation levels. Considering that both DTT and thapsigargin are well-characterized inducers of the UPR and that the chaperone GRP78/BiP is a master regulator of this process, the putative role of hARTC1 in the UPR was examined.

To monitor the UPR, the activation of individual UPR signaling pathways, both at mRNA and protein levels was evaluated. Firstly, attempts were made to establish the experimental conditions to detect the UPR activation by Western Blotting. The Western Blotting analysis aimed to monitor PERK pathway, analyzing the autophosphorylation of PERK (using an antibody antiphospho-PERK from Abcam), the amount of eIF2α compared to that of phosphorylated eIF2α (using antibodies

anti-eIF2α and antiphospho-eIF2α from Cell Signaling), the increase of ATF4 (using an antibody anti-ATF4 from Santa Cruz Biotechnologies) and that of CHOP (using an antibody anti-CHOP from Santa Cruz Biotechnologies). Moreover, ATF6 pathway was examined by Western Blotting, evaluating the ATF6 cleavage (using an antibody anti-ATF6 from Santa Cruz Biotechnologies). All these analyses did not allow to measure any UPR activation, even though cells treated with well-known ER stressors were used as controls for the experiments. However, the three UPR signaling pathways were successfully evaluated by (qRT)-PCR using primer sequences specifically designed for human XBP1 (used to analyze IRE1α pathway, see Chapter 1.8.1.3), ATF4 and CHOP (both used to analyze PERK pathway, see Chapter 1.8.1.1). In addition, ATF6 translocation (see Chapter 1.8.1.2) was analyzed by immunofluorescence experiments.

For the evaluation of XBP1, ATF4 and CHOP mRNA transcript levels, cells were subjected to the stress treatments described above that were shown to induce hARTC1 expression and GRP78/BiP mono-ADP-ribosylation. Thus, 2 mM DTT and 1 μM thapsigargin were used for short-term stress experiments (20, 60 and 120 minutes) and 0.3 μM thapsigargin to examine the effects of long-term stress (18 and 24 hours).

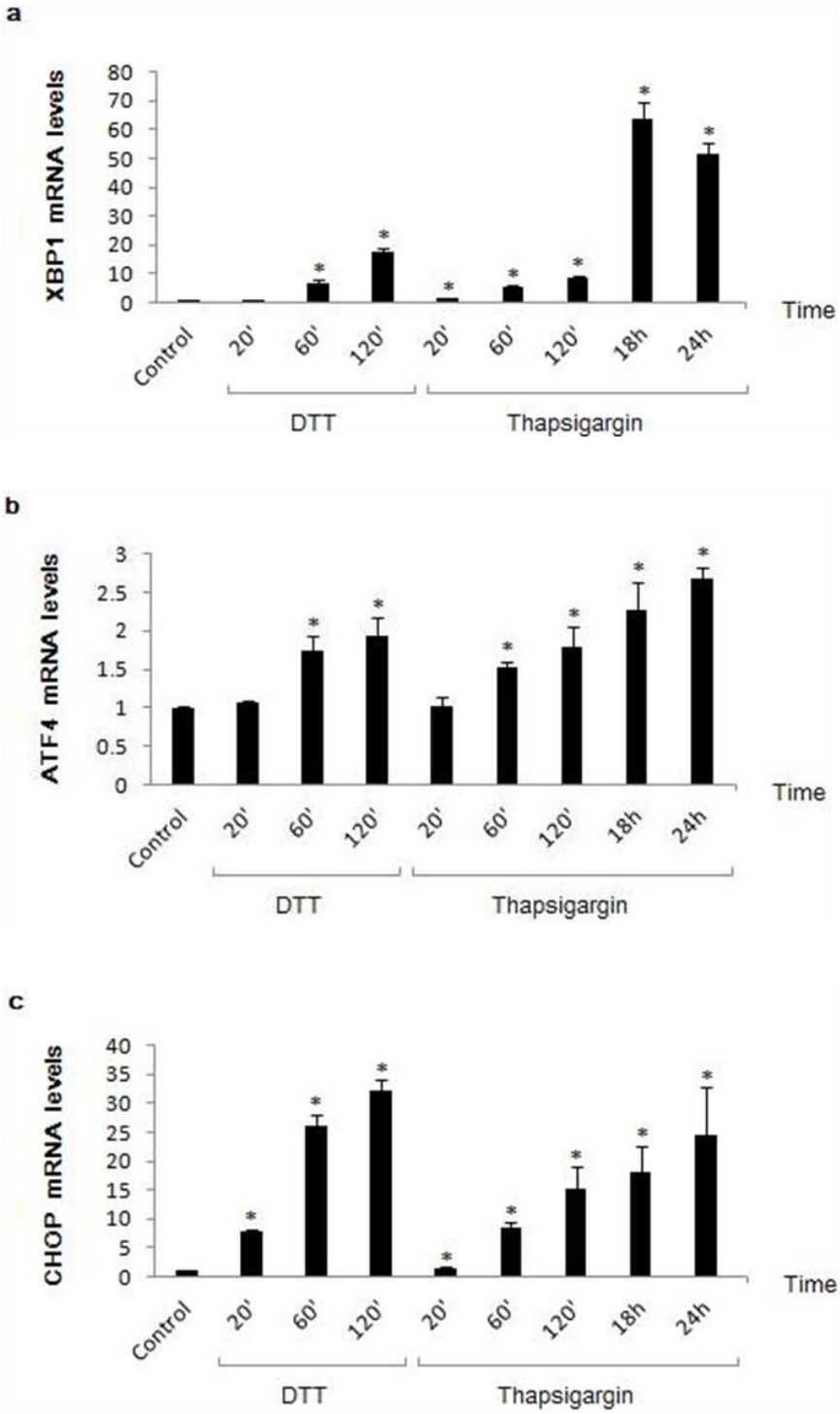

Figure 5.5 XBP1, ATF4 and CHOP are expressed upon treatment with DTT and thapsigargin. Quantification of the mRNA transcript levels of XBP1 (a), ATF4 (b) or CHOP (c) in HeLa cells treated for the indicated time with DTT (2 mM) or thapsigargin (1 μM), determined by (qRT)-PCR, and normalized to GAPDH mRNA. The data are reported using arbitrary units relative to XBP1 (a), ATF4 (b) or CHOP (c) transcript levels in non-treated HeLa cells (taken as 1.0). Data are presented as mean±SD of three independent experiments, each performed in triplicate. * indicates significantly different from the relative control ($p < 0.05$).

There was a time-dependent increase in mRNA transcript expression for all of the three genes analyzed. XBP1, ATF4 and CHOP expression was increased after 20 minutes of treatment with both DTT and thapsigargin, and their levels showed a continued increase at prolonged time treatments (60 and 120 minutes; Figure 5.5). With these experiments, the ability to monitor UPR activation via a (qRT)-PCR was evaluated. The results in Figure 5.5 indicate that (qRT)-PCR provided a sensitive assay for monitoring the expression of key components of cellular UPR caused by established forms of short- and long-term stress. After this validation, the next investigations were designed to determine whether ARTCs could activate the UPR. Indeed, transfection of active ARTCs induced GR78/BiP mono-ADP-ribosylation (Figure 3.14), similar to the effect obtained with short-term DTT and thapsigargin stress treatments. Thus, as DTT and thapsigargin activated the UPR, ARTCs could also have a role in this cellular response.

To this aim, HeLa cells transfected for 24 hours with either active (hARTC1 wt and cARTC2.1 wt) or inactive (hARTC1 dm, hARTC4 and cARTC2.1 dm) ARTCs were analyzed by (qRT)-PCR for XBP1, ATF4 and CHOP mRNA transcript levels. Non-transfected HeLa cells, and cell transfected with a GPI-GFP construct used as a further control, were also analyzed.

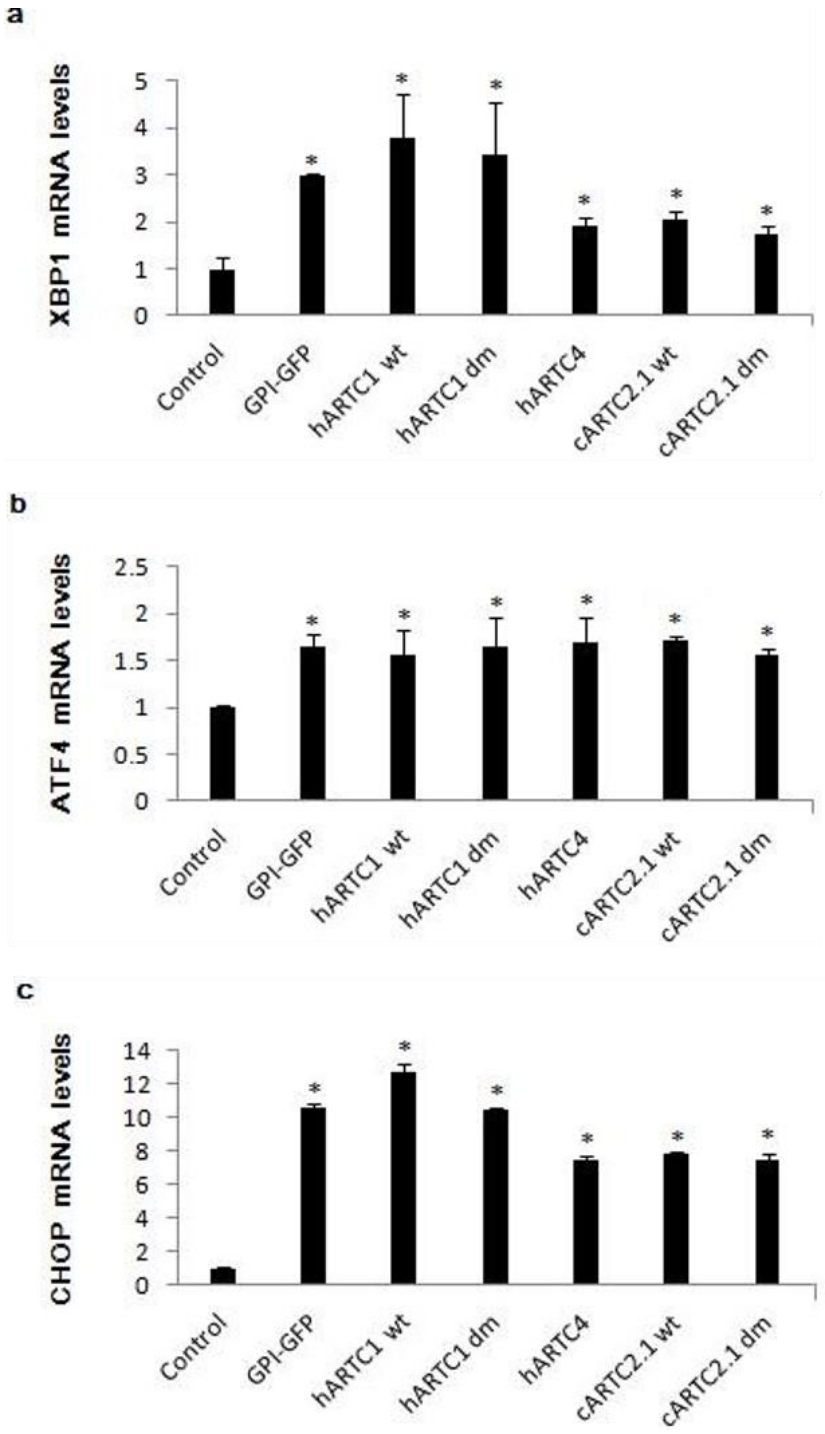

Figure 5.6 XBP1, ATF4 and CHOP mRNA transcripts are increased after transfection of ARTCs. Quantification of the mRNA transcript levels of XBP1 (a), ATF4 (b) or CHOP (c) in HeLa cells transfected with the indicated constructs, determined by (qRT)-PCR, and normalized to GAPDH mRNA. The data are reported using arbitrary units relative to XBP1 (a), ATF4 (b) or CHOP (c) transcript of non-transfected HeLa cells (taken as 1.0). Data are presented as mean±SD of three independent experiments, each performed in triplicate. * indicates significantly different from the relative control ($p < 0.05$).

As shown in Figure 5.6, increased levels of XBP1, ATF4 and CHOP mRNA transcripts were detectable in all the transfected samples. As compared to control cells, transfection of active (hARTC1 wt and cARTC2.1 wt) or inactive (hARTC1 dm, hARTC4 and cARTC2.1 dm) enzymes caused increased XBP1, ATF4 and CHOP mRNA levels (Figure 5.6). However, the transfection of a GPI-GFP construct had similar effects (Figure 5.6). These findings suggested that the activation of the UPR signaling pathways examined was not specifically caused by active ARTCs and their consequent GRP78/BiP mono-ADP-ribosylation, but was due to the transfection of exogenous proteins that passed into the lumen of the ER.

Furthermore, the effect of silencing hARTC1 (achieved as described in Chapter 4.2.2 and checked by Western Blotting) on the UPR signaling pathways was determined by (qRT)-PCR. Thus, XBP1, ATF4 and CHOP mRNA levels were measured in non-transfected HeLa cells and those of cells treated with the transfection reagent only (i.e. mock transfection) or cells silenced for hARTC1.

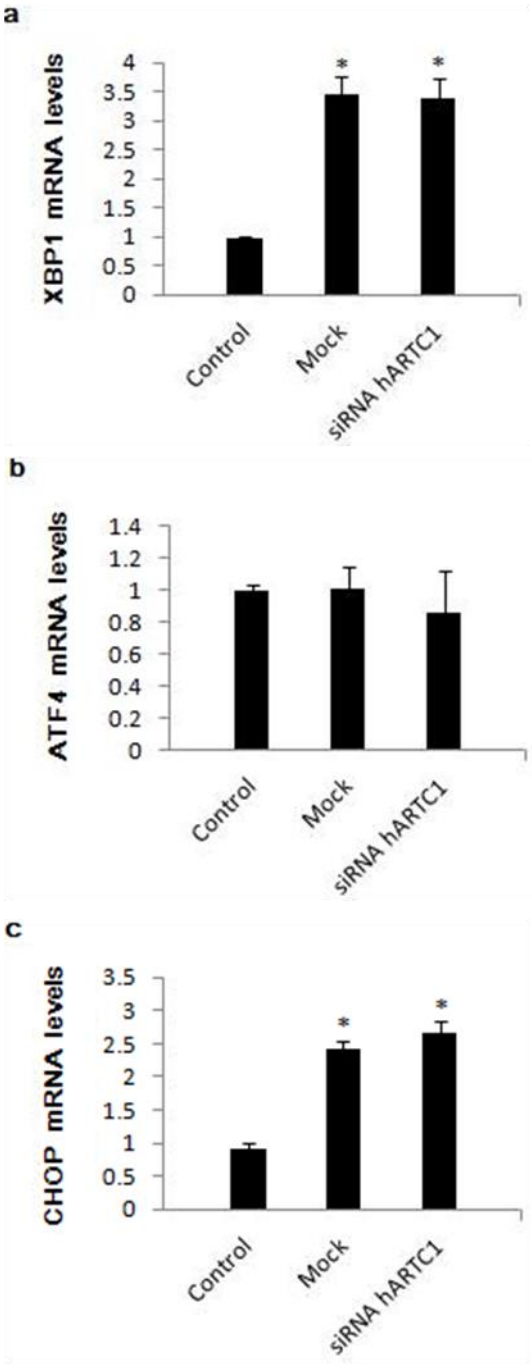

Figure 5.7 XBP1, ATF4 and CHOP mRNA transcripts are increased after mock transfection or silencing of hARTC1. Quantification of the levels of XBP1 (a), ATF4 (b) or CHOP (c) transcripts in mock- or siRNA-transfected HeLa cells, determined by (qRT)-PCR, and normalized to GAPDH mRNA. The data are reported using arbitrary units relative to XBP1 (a), ATF4 (b) or CHOP (c) transcript of non-transfected HeLa cells (taken as 1.0). Data are mean±SD of three independent experiments, each performed in triplicate. * indicates significantly different from the relative control ($p < 0.05$).

Similarly to the transfection experiments (Figure 5.6), a significant increase of XBP1 and CHOP mRNA levels were detected in both mock-transfected and hARTC1-silenced cells (Figure 5.7a, c). ATF4 mRNA levels were, instead, comparable to that of control cells (Figure 5.7b). Even though the increase of XBP1 and CHOP were significantly different from control cells, it seemed they were caused by the transfection reagent/procedure, as they were also elevated in mock-transfected cells. These findings further excluded a possible role for hARTC1 in the UPR.

Finally, to monitor the ATF6 branch of the UPR, the translocation of this protein to the nucleus via the Golgi apparatus was determined by performing immunofluorescence experiments. Firstly, non-transfected HeLa cells, and cells treated with 0.3 μM thapsigargin for 24 hours, were analyzed for nuclear ATF6 localization, to evaluate whether a treatment known to induce the UPR allowed visualization of this translocation.

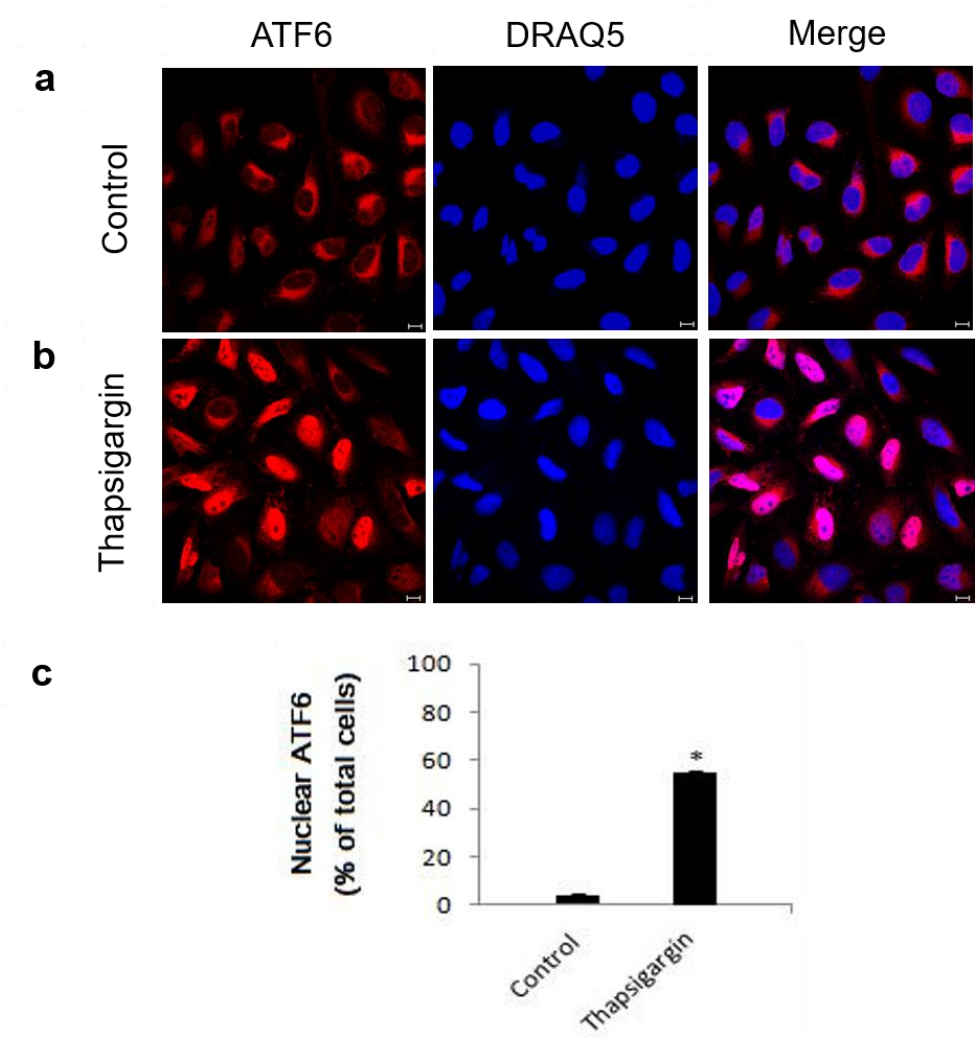

Figure 5.8 ATF6 translocates to the nucleus after thapsigargin treatment. (a, b) Representative immunofluorescence images of non-transfected HeLa cells either untreated (control) or treated with thapsigargin 0.3 μM for 24 hours (thapsigargin). Cells were stained with an antibody anti-ATF6 (red), nuclei were stained with DRAQ5, then analyzed by immunofluorescence. The scale bar represents 10 μm. The data shown are representative of at least three independent experiments. (c) Quantification of ATF6 nuclear localization, expressed as percentages of total cells analyzed. The data shown are means±SD of three independent experiments. * indicates significantly different from the control ($p < 0.01$).

Treatment of cells with thapsigargin caused a significant translocation of ATF6 into the nucleus (56%; Figure 5.8). ATF6 translocation was then evaluated in HeLa cells that were left untreated or were transfected for 24 hours with a GPI-GFP construct or with the ARTCs (hARTC1 wt, cARTC2.1 wt and cARTC2.1 dm).

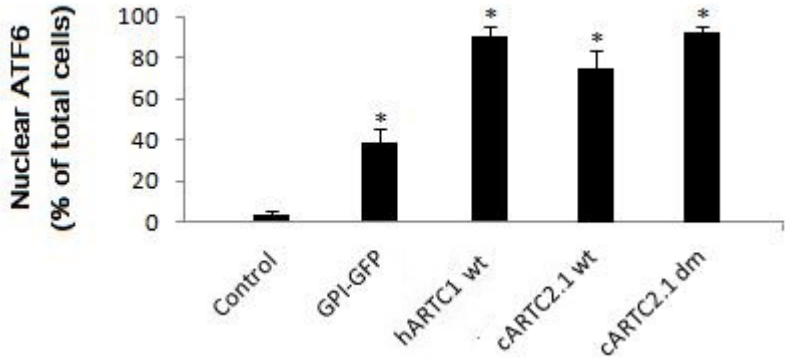

Figure 5.9 ATF6 translocates to the nucleus after ARTCs transfection. Quantification of ATF6 nuclear localization of non-transfected HeLa cells (control) or cells transfected for 24 hours with the indicated constructs, expressed as percentages of total cells analyzed. The data shown are means±SD of three independent experiments. * indicates significantly different from the control ($p < 0.01$).

As shown in the Figure 5.9, upon transfection with any of the constructs it was possible to detect a nuclear ATF6 localization. Quantification of ATF6 nuclear localization, expressed as percentage of the total cells analyzed, confirmed that, as compared to non-transfected control cells, ATF6 nuclear translocation was detectable in almost all the transfected samples (Figure 5.9). Therefore, it was possible that the over-expression of exogenous proteins, independently from their activity (as it was also associated to GPI-GFP transfection), caused the ATF6 nuclear translocation.

Considering the high percentage of transfected cells that displayed nuclear ATF6 translocation, the temporal kinetics of the translocation was investigated. ATF6 translocation of HeLa cells transfected for 6, 9 and 12 hours with GPI-GFP or with the ARTCs (hARTC1 wt, cARTC2.1 wt and cARTC2.1 dm) was determined.

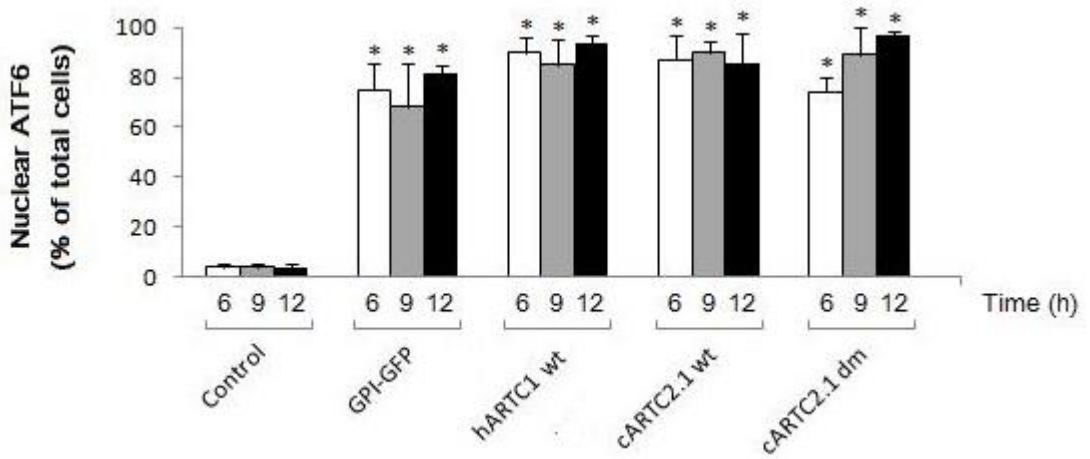

Figure 5.10 ATF6 translocates to the nucleus within 6 hours post transfection with ARTCs. Quantification of ATF6 nuclear localization of non-transfected HeLa cells (control) or cells transfected for 6, 9 and 12 hours with the indicated constructs, expressed as percentages of total cells analyzed. The data shown are means±SD of three independent experiments. * indicates significantly different from the control ($p < 0.01$).

As shown in Figure 5.10, quantification of data confirmed that nuclear ATF6 translocation occurred within occurred within 6 hours of transfection, and was maintained through to 24 hours (Figure 5.10). Considering that the same percentage of cells displaying ATF6 translocation was obtained after the transfection of any of the exogenous proteins indicated in Figure 5.10, it is reasonable to conclude than none of them had a direct effect on the ATF6 branch of the UPR.

Altogether, these data indicate that hARTC1 has no direct role in the UPR pathway. Increased expression of mRNA for the UPR branches analyzed was obtained after the transfection of all exogenous proteins that passed through the ER, and there was no evidence of a change in mRNA expression specifically linked to ARTC transfection or silencing. It is possible that the ADP-ribosylation of GRP78/BiP and

its role as a regulator of the availability of the functional chaperone are involved in a different pathway than in the UPR.

5.3 Summary

- Short-term cells stress treatments with DTT or thapsigargin increase hARTC1 mRNA and protein levels.
- Short-term cells stress treatments with DTT or thapsigargin induce GRP78/BiP ADP-ribosylation.
- Western Blotting does not reveal as a useful approach for monitoring UPR activity. UPR signaling pathways have been successfully evaluated using (qRT)-PCR or immunofluorescence experiments.
- hARTC1, and its activity as GRP78/BiP mono-ART, does not trigger UPR. Indeed, the activation of the UPR signaling pathways is due to the transfection of GPI-anchored proteins that passed into the lumen of the ER and not specifically caused by active ARTCs.

Chapter 6

Study of the biological role of hARTC1

6.1 Introduction

The data reported in Chapters 3, 4 and 5 demonstrated that hARTC1 is able to catalyze the mono-ADP-ribosylation of GRP78/BiP and that the enzyme can act as an ER-stress sensor. Indeed, hARTC1 expression is rapidly increased by well-known ER stresses, such as DTT and thapsigargin. Moreover, these same stresses are able to induce hARTC1-mediated GRP78/BiP mono-ADP-ribosylation.

GRP78/BiP is a central regulator of the ER stress response as it interacts and binds to the three ER transmembrane signaling molecules ATF6, IRE1α and PERK, keeping them inactive (Brewer, J.W., 2014; Hetz, C., 2012). During ER stress, GRP78/BiP is released from these three protein sensors allowing them to become functional and initiate the UPR to restore the ER homeostasis (Zhang, K. and Kaufman, R.J., 2008). However, under severe and prolonged ER stress, the UPR activates unique pathways that lead to cell death through apoptosis or autophagy (Iurlaro, R. and Munoz-Pinedo, C., 2016; Logue, S.E. et al., 2013; Sano, R. and Reed, J.C., 2013). Thus, GRP78/BiP has a crucial role in controlling the balance between cell viability and apoptosis through its ability to maintain the ER stress sensors and the pro-apoptotic machineries in their inactive state.

Therefore, considering that hARTC1 is able to catalyze the mono-ADP-ribosylation of GRP78/BiP, the role of hARTC1 was examined for cellular functions that are

regulated by GRP78/BiP, including cell survival, cell death and cancer. Indeed, the pro-survival role of GRP78/BiP is a characteristic of cancer cells that are constantly subjected to chronic ER stress because of the tumor microenvironment, characterized by nutrient deprivation, acidosis and severe hypoxia (Justus, C.R. et al., 2015; Luo, B. and Lee, A.S., 2013; Wang, M. et al., 2009). In cancer cells the UPR is often activated in order to sustain cell survival and GRP78/BiP is over-expressed in a wide variety of cancer cells including breast, lung, prostate and ovarian cancers, melanoma and glioma cells (Lee, A.S., 2014; Wang, M. et al., 2009; see also Chapter 1.8.3). Of note, recent reports also demonstrated a linkage between hARTC1 and cancer, suggesting that hARTC1 can play a role in invasion, proliferation and apoptosis processes in colon carcinoma (Tang, Y. et al., 2015; Xiao, M. et al., 2013; Xu, J.X. et al., 2017; Yang, L. et al., 2016). Moreover, hARTC1 has been associated with glioma; indeed, it has been reported that hARTC1 expression in glioma tissues is higher than in normal, control brain tissues and that this hARTC1 upregulation could be associated with the aggressiveness of glioma (Li, Z. et al., 2016).

6.2 Results

6.2.1 Study of hARTC1 expression and GRP78/BiP mono-ADP-ribosylation level in ovarian cancer cell lines

To investigate a possible role of hARTC1 in cancer, initial experiments evaluated hARTC1 expression levels in different cancer cell lines (ovary, melanoma, breast,

prostate). Subsequently, attention was focused on ovarian cancer cells, as ovarian cancer is one of the most common cancers in women worldwide (estimated number of new cases in 2017: 1,3%; https://seer.cancer.gov/statfacts/html/cervix.html) and, internationally, it represents the eighth leading cause of cancer death among women (Ginsburg, O. et al., 2017; Torre, L.A. et al. 2017). Currently, the most common front-line treatment uses primary surgery followed by chemotherapy or chemoradiotherapy (the external beam or brachytherapy plus cisplatin are used in the UK). However, this combined therapy is not always sufficient to avoid the disease returning. Therefore, it is of interest explore more effective treatment options for this type of cancer. In recent years, significant research efforts have been made to find new, effective anticancer therapy for ovarian cancer, especially using molecularly-targeted therapy. One of these strategies is focused on the use of PARP inhibitors; to date different PARP inhibitors are under clinical trials for the therapy of patients with ovarian tumors and three of them (Olaparib, Rucaparib and Niraparib) has already been approved by FDA (Balasubramaniam, S. et al., 2017; Brown, J.S. et al., 2016; Brown, J.S. et al., 2017; Dulaney, C. et al., 2017; Scott, L.J., 2017; Kim, G., et al., 2015). Thus, ADP-ribosylation reactions have turned out to be an important target for tumor therapy. The inhibition of ART activity is emerging as a potentially important strategy for ovarian cancer treatment. In addition to the most extensively studied role of the ARTDs in this type of cancer, it would be interesting investigate the role of the ARTCs in this context.

The following ovarian cancer cell lines were chosen for the study: A2780, IGROV-1, OVCAR-3, OVCAR-5, SKOV-3, OVCA-432, CAOV-3. hARTC1 and GRP78/BiP mRNA levels were evaluated with (qRT)-PCR using primers specifically designed for ARTC1, GRP78/BiP and GAPDH (employed as internal control; see Table 2.2).

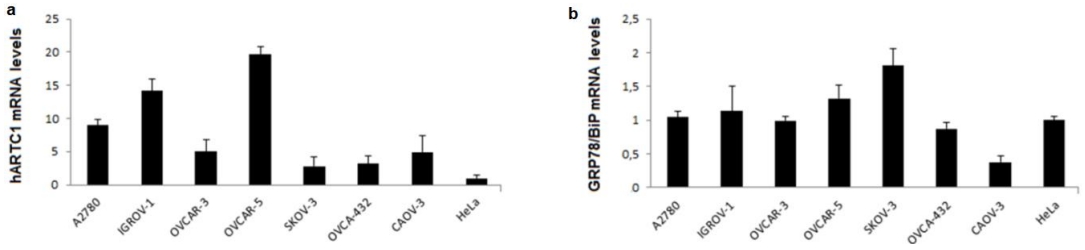

Figure 6.1 hARTC1 and GRP78/BiP mRNA levels in ovarian cancer cell lines. The graphs show quantification of the levels of (a) endogenous hARTC1 and (b) GRP78/BiP mRNA transcripts of different ovarian cancer cell lines, determined by (qRT)-PCR. The (qRT)-PCR results were normalized to GAPDH mRNA, and then reported as arbitrary units relative to HeLa cells (taken as 1.0). Data are presented as mean±SD of three independent experiments, each performed in triplicate. The D'Agostino and Pearson omnibus normality test was used to check the uniform distribution of the values. All data passed the normality requirements.

To compare each cell line, I reported the (qRT)-PCR data as fold induction relative to HeLa cells, which were used for all my previous experiments (Figure 6.1). All the ovarian cell lines showed increased levels of hARTC1 mRNA as compared to HeLa cells (Figure 6.1a). Specifically, A2780, IGROV-1 and OVCAR-5 were associated with 10-fold, or more, higher expression compared to HeLa cells (A2780, 8.97±0.92; IGROV-1, 14.16±1.81; OVCAR-5, 19.63±1.12; Figure 6.1a). The other ovarian cancer cell lines had a more modest expression of hARTC1 mRNA compared to HeLa cells (OVCAR-3, 5.03±1.81; SKOV-3, 2.81±1.40; OVCA-432, 3.16±1.17; CAOV-3, 4.96±2.43; Figure 6.1a).

GRP78/BiP mRNA levels within the ovarian cancer cell lines showed similar levels as compared to HeLa (Figure 6.1b). Among all the cell lines analyzed, the highest

mRNA levels were detected in SKOV-3 cells, which showed a 2-fold induction of GRP78/BiP transcript (1.84±0.35; Figure 6.1b).

Then, hARTC1 protein levels were analyzed in the same cell lines. For this aim, Western Blotting was performed using cell lysates that were separated by SDS-PAGE, transferred to nitrocellulose filters and probed with specific antibodies against hARTC1, GRP78/BiP and GAPDH (used as loading control; see Table 2.3). hARTC1 wt- and hARTC1 dm-transfected cells were also analyzed and used as control for the band of interest (thereby ensuring that the band used for the quantification was the same of all the other previous experiments).

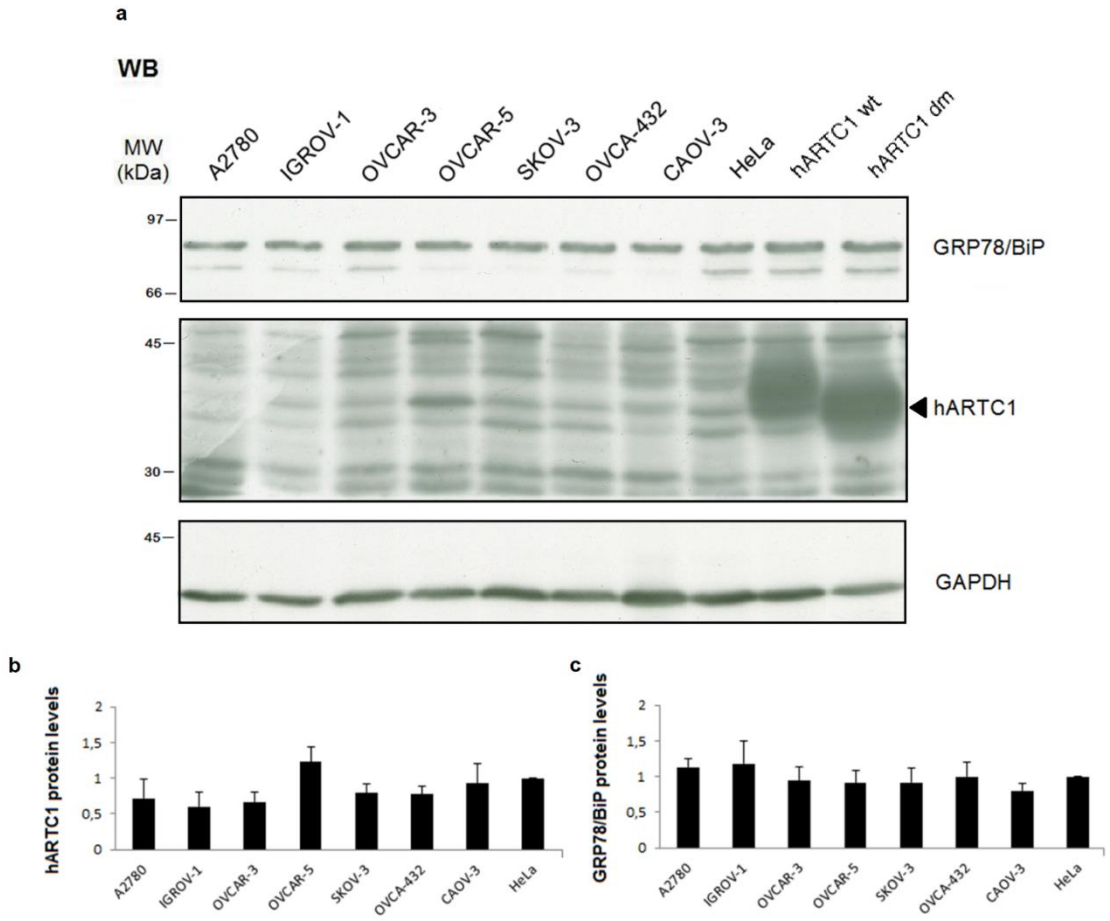

Figure 6.2 hARTC1 and GRP78/BiP protein levels in ovarian cancer cell lines. (a) Representative Western Blotting (WB) of ovarian cancer cell lines and HeLa cells transfected with hARTC1 wt or hARTC1 dm, showing endogenous hARTC1, GRP78/BiP and GAPDH levels. (b and c) Quantification of the protein levels of (b) hARTC1 and (c) GRP78/BiP, normalized to GAPDH, and relative to those of HeLa cells (taken as 1.0). Data are means±SD of at least five independent experiments. The D'Agostino and Pearson omnibus normality test was used to check the uniform distribution of the values; all data passed the normality requirements.

As expected, multiple bands were visualized using the anti-ARTC1 antibody (Figure 6.2a, middle panel). These bands are consistent with the different degrees of glycosylation of the protein (see also Figure 3.19, Figure 5.2 and comments relating to these figures). Densitometric analysis was performed using the band corresponding to that induced by hARTC1 transfection (indicated by the arrow in the middle panel of Figure 6.2a). The highest hARTC1 protein level was detectable in OVCAR-5 cells, in line with the mRNA data (cf. Figures 6.1 and 6.2a). The other

cell lines had similar hARTC1 protein levels, even if the various bands recognized by the anti-ARTC1 antibody were differently modulated (Figure 6.2a, b). The quantification of GRP78/BiP protein levels showed similar levels between all the cell lines and also compared to HeLa cells (Figure 6.2b). In conclusion, the ovarian cancer cell lines analyzed had similar GRP78/BiP and hARTC1 levels; however, hARTC1 seemed to be differently glycosylated in each cell line.

A correlation between hARTC1 and GRP78/BiP mRNA and protein levels for all the ovarian cancer cell lines analyzed is shown in Figure 6.3.

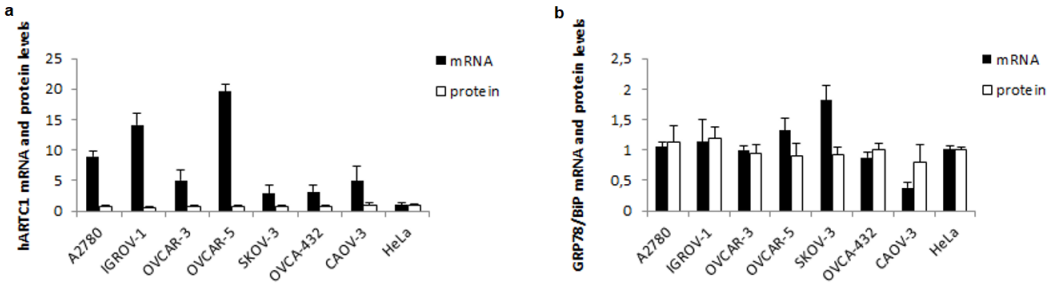

Figure 6.3 hARTC1 and GRP78/BiP mRNA and protein levels in ovarian cancer cell lines. (a) hARTC1 mRNA (black bars) and protein (white bars) levels normalized to GAPDH mRNA or protein levels, and relative to those of HeLa cells (taken as 1.0). (b) GRP78/BiP mRNA (black bars) and protein (white bars) levels normalized to GAPDH mRNA or protein levels, and relative to those of HeLa cells (taken as 1.0). Data are means±SD of at least five independent experiments.

The level of GRP78/BiP mono-ADP-ribosylation in these ovarian cancer cell lines was investigated. For this aim, the macro domain-based far-Western Blotting technique was performed using cells lysates that were separated by SDS-PAGE, transferred to nitrocellulose filters and then probed with GST-mAf1521, using an anti-GST antibody to reveal it.

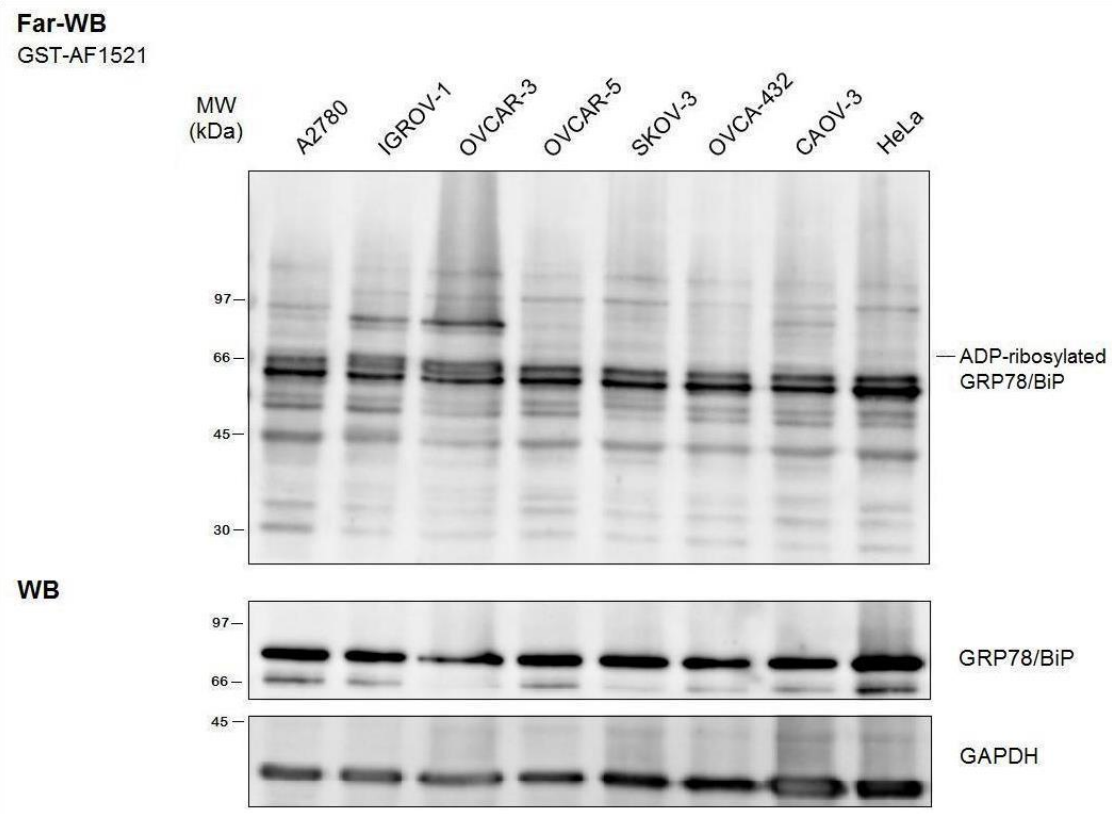

Figure 6.4 GRP78/BiP mono-ADP-ribosylation profile of ovarian cancer cell lines. Representative far-Western Blotting (FAR-WB) with GST-tagged mAf1521 of ovarian cancer cell lines. The indicated band (ADP-ribosylated GRP78) was also recognized with an anti-GRP78 specific antibody. The Western Blotting (WB) also showed the levels of expression of GRP78/BiP and of GAPDH, used as loading control. Data are representative of at least three independent experiments.

As depicted in Figure 6.4, some of the ovarian cell lines showed a protein band following incubation with the anti-GST antibody at the molecular weight of GRP78/BiP that was also recognized by an anti-GRP78/BiP antibody. As reported above, GRP78/BiP protein level, normalized to GAPDH, were similar between all the cell lines (cf Figures 6.2 and Figure 6.4). On the contrary, the levels of ADP-ribosylated GRP78 varied and, compared to HeLa, the highest levels were found in A2780, OVCAR-5 and SKOV-3 cell lines (Figure 6.4). Considering that GRP78/BiP protein levels were confirmed to be similar between all the cell lines, one possibility could be that the lower levels of GRP78/BiP ADP-ribosylation in some of the cell

lines depended on the presence of mutation(s) in the consensus site(s) for ADP-ribosylation of the chaperone.

To search for the presence of mutation(s), GRP78/BiP DNA sequencing analysis was performed for all the ovarian cell lines used. Firstly, an appropriate pair of primers were designed that specifically matched with the nucleotide sequence of the chaperone, flanking both the identified mutation sites of ADP-ribosylation: the arginine (R) residues 470 and 492 (see Table 2.2; Chambers, J.E. et al., 2012). Then, the DNA was extracted from the cell lysates and subjected to PCR amplification using these specific primers. The PCR products were subsequently purified and sequenced. Sequence results were visualized using a specific software (see Chapter 2.2.4.15) and were compared to the NCBI reference sequences of the gene of interest "*human Grp78/Bip*".

a

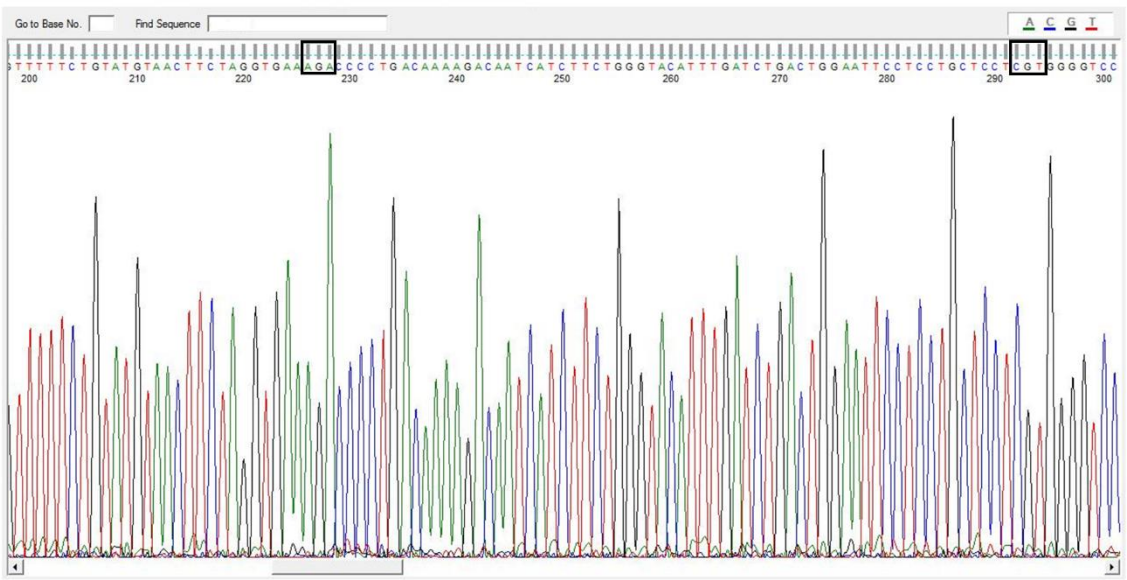

b

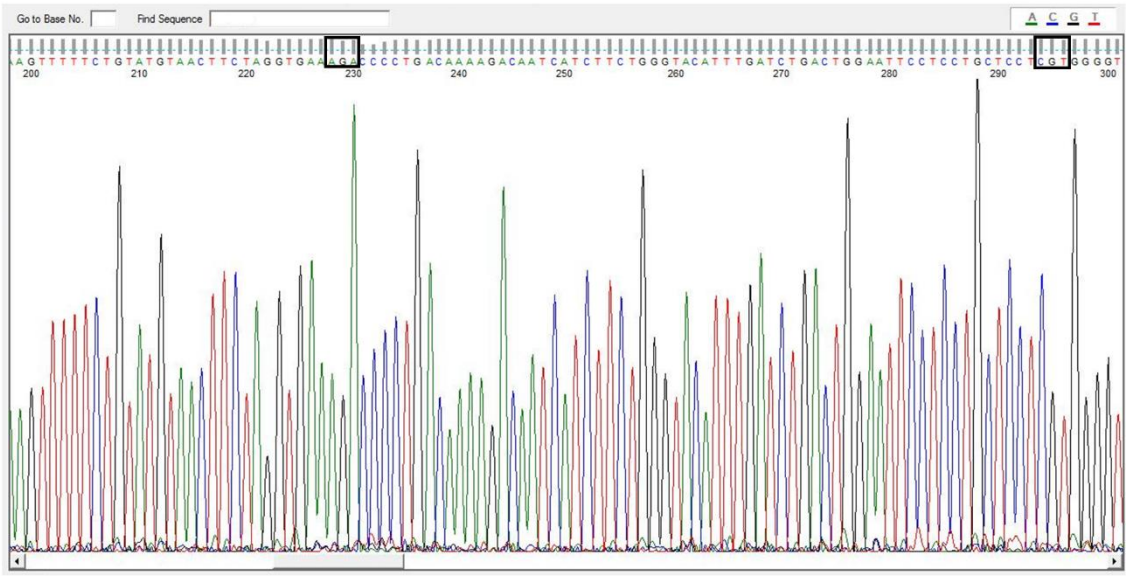
Go to Base No.
Find Sequence
A C G T

c

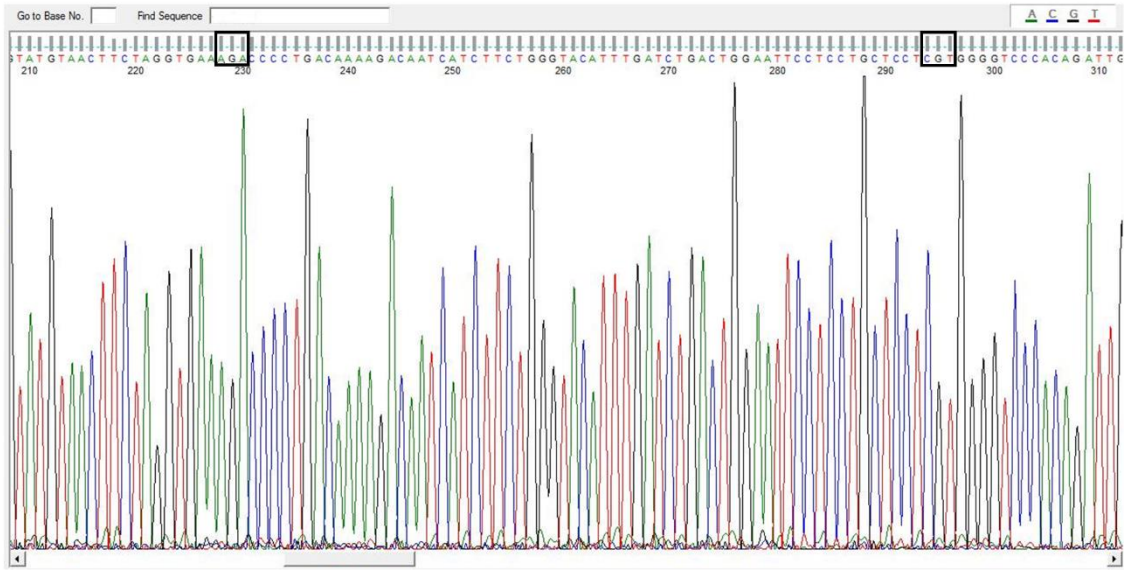
Go to Base No.
Find Sequence
A C G T

d

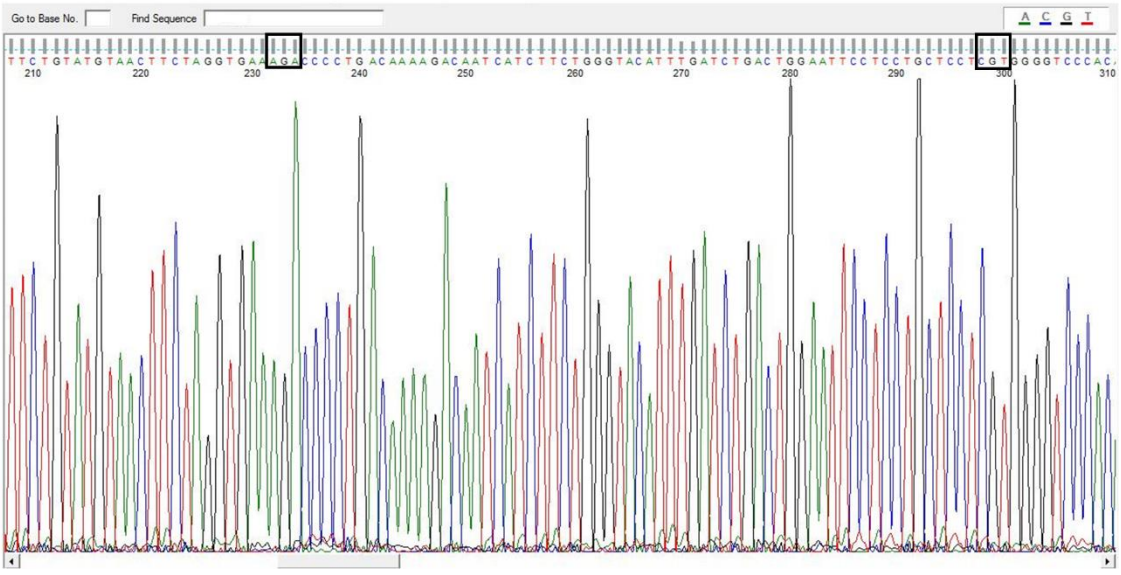
Go to Base No.
Find Sequence
A C G T

e

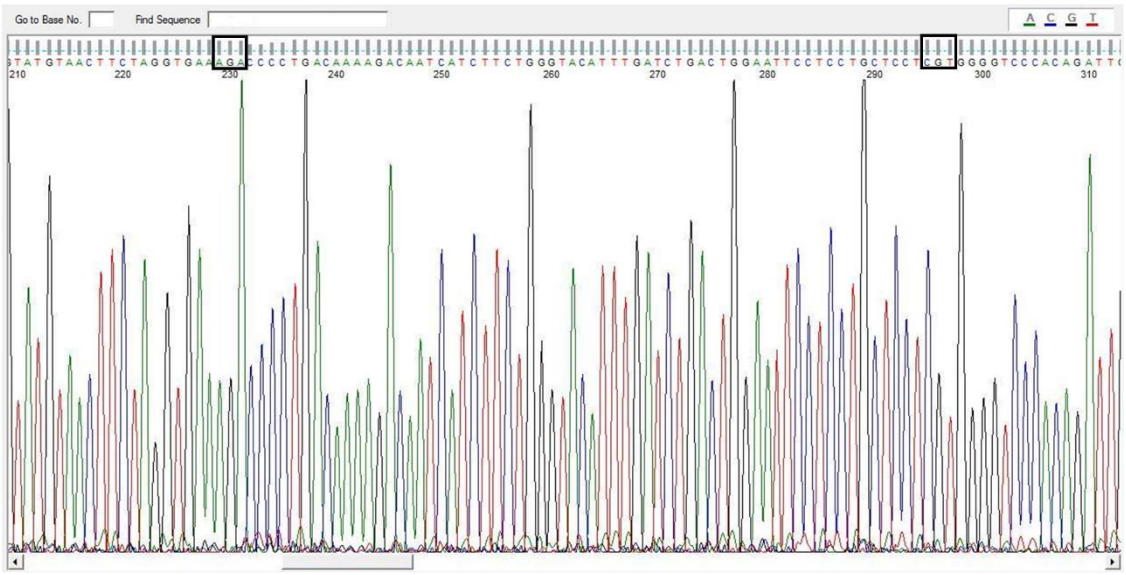
Go to Base No.
Find Sequence
A C G T

f

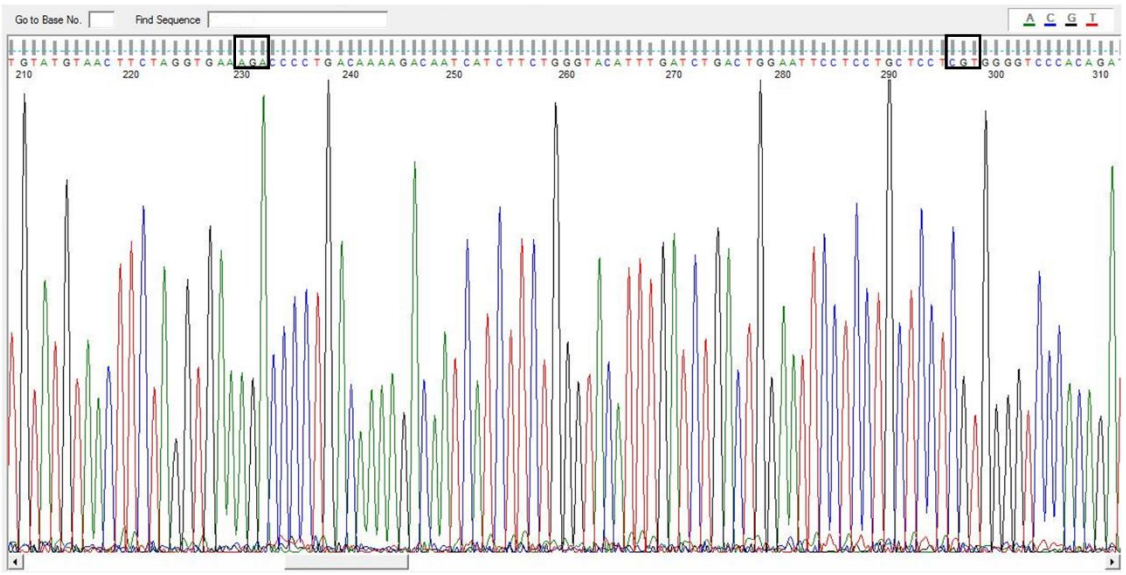
Go to Base No.
Find Sequence
A C G T

g

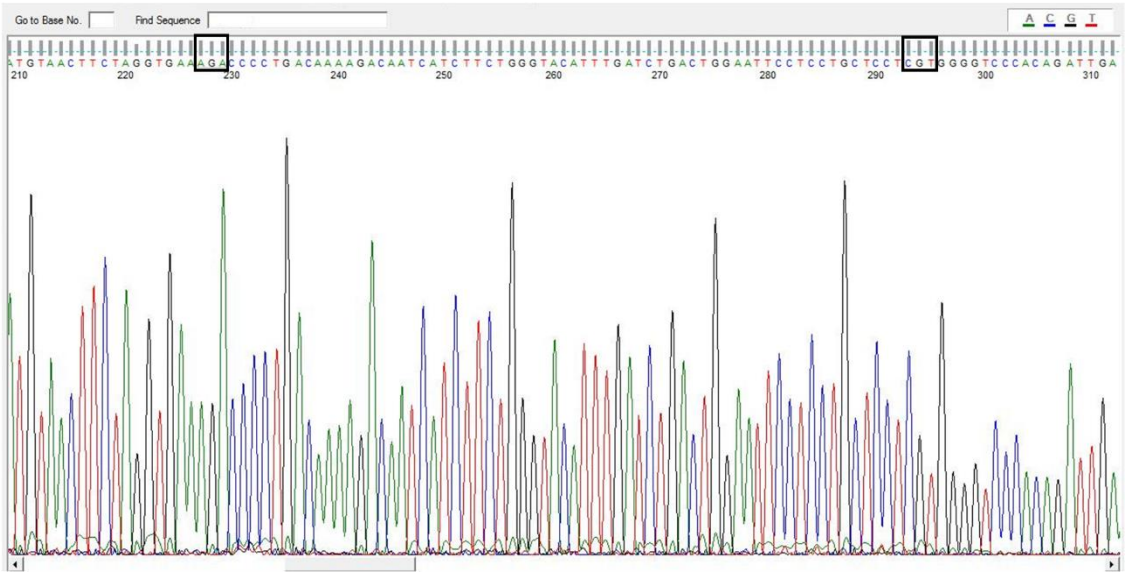
Go to Base No.
Find Sequence
A C G T

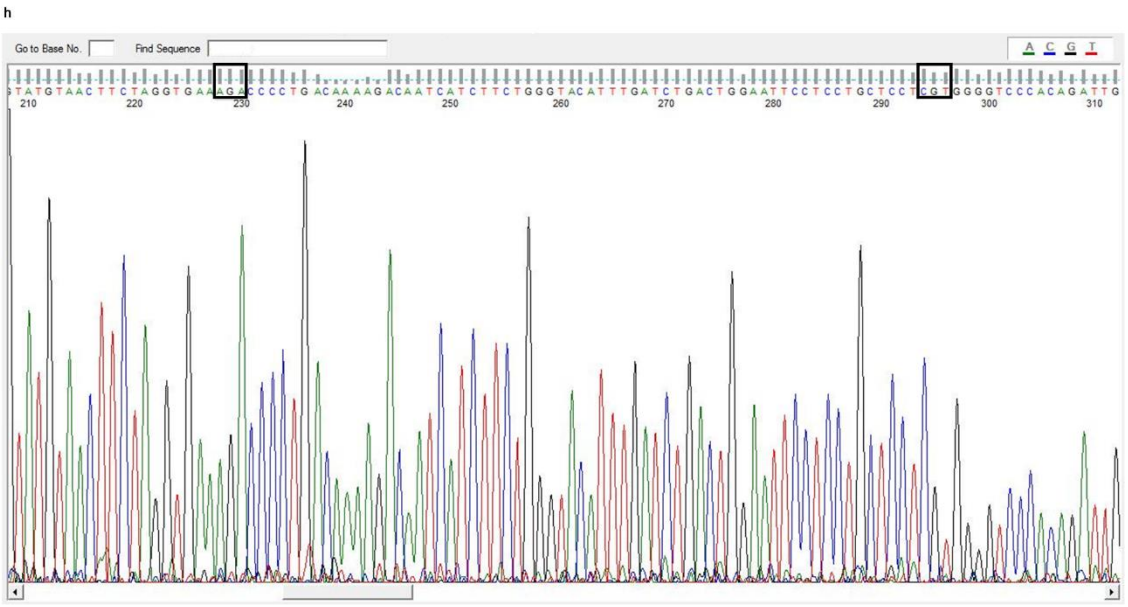

Figure 6.5 Ovarian cancer cell lines do not contain mutations within their GRP78/BiP mono-ADP-ribosylation sites. Analysis of the DNA sequences spanning the identified mono-ADP-ribosylation sites of *Grp78/BiP* for (a) A2780, (b) IGROV-1, (c) OVCAR-3, (d) OVCAR-5, (e) SKOV-3, (f) OVCA-432, (g) CAOV-3 and (h) HeLa cell lines. The sites of ADP-ribosylation correspond to the nucleotidic triplet AGA and CGT. Sequence results were visualized using the FinchTV software.

The identified amino acid sites of ADP-ribosylation are both localized in the substrate-binding domain of the chaperone and R470 is encoded by the corresponding nucleotidic triplet AGA, whereas R492 by the triplet CGT (Chambers, J.E. et al., 2012). The analysis of the purified Grp78/Bip nucleotide sequences from ovarian cancer cell lines demonstrated that none of them had any mutation in either of these ADP-ribosylation sites, since each cell lines had the AGA and CGT triplets in the positions corresponding to these amino acids residues (Figure 6.5). Thus, the different ADP-ribosylated GRP78/BiP levels were not associated with the mutation of the identified ADP-ribosylation sites. Further investigations are needed to understand the reasons for the different ADP-ribosylated states of GRP78/BiP within the ovarian cancer cell lines analyzed.

6.2.2 hARTC1 over-expression in HeLa cells inhibits cell proliferation

GRP78/BiP has a central role in the ER stress response, as it can activate both pro-survival and pro-death signaling; promoting cell survival when the cell can resolve the stress, or cell death when the stress is greater/chronic and the cell fails to restore ER homeostasis. Generally, ER stress-associated cell death occurs through apoptosis. However also other types of cell death have been observed (Hitomi, J. et al., 2004; Nakagawa, T. et al., 2000; Ullman, E. et al., 2008; Wu, J. and Kaufman, R.J., 2006).

Some members of the ARTCs (ARTC2.1 and ARTC2.2) have already been reported to have a role in the apoptotic process. Particularly, mouse ARTC2s, expressed on peripheral T cells, induced P2X7 activation by ADP-ribosylation and led to cell death by apoptosis (Adriouch, S. et al., 2001; Seman, M. et al., 2003). P2X7 is a direct target of ARTC2-mediated ADP-ribosylation and, once activated, results in T cell apoptosis (Adriouch, S. et al., 2001; Seman, M. et al., 2003). Here, it was investigated whether hARTC1 was also implicated in cell death.

Initial experiments used cytometric analysis with annexin-V/propidium iodide (PI) double staining in order to discriminate between necrosis and apoptosis. When cells undergo apoptosis, they expose phosphatidylserine (PS) on their surface and, as the apoptotic process progresses, cell membrane integrity is eventually lost. Thus, in the early stages of apoptosis cells maintain plasma membrane integrity, whereas those cells in the late stages of apoptosis, or are already dead, do not. Annexin-V is a calcium-dependent phospholipid binding protein with high affinity

for PS that binds to cells with exposed PS. PI is a fluorescent dye that intercalates into double-stranded nucleic acid. It is excluded from viable cells, but can enter into dead or dying cells with ruptured plasma membranes. Thus, viable cells with intact membranes exclude PI, whereas membranes of dead and damaged cells are permeable to PI. Cells that stain negative for both Annexin-V and PI are alive and not undergoing measurable apoptosis. Cells that stain positive for Annexin-V and negative for PI are undergoing apoptosis. Cells that stain positive for both Annexin-V and PI are in the end stage of apoptosis. Cells that stain positive for PI and negative for Annexin-V are undergoing necrosis.

For analysis, HeLa cells were left untreated (control) or were treated with the transfection reagent only (mock transfection) or with hARTC1 wt and its catalytically inactive mutant hARTC1 dm. Moreover, as a further positive control, HeLa cells were treated with puromycin, a well-known inducer of apoptosis. Cell death was evaluated after 24, 48 and 72 hours following transfection or treatment with puromycin.

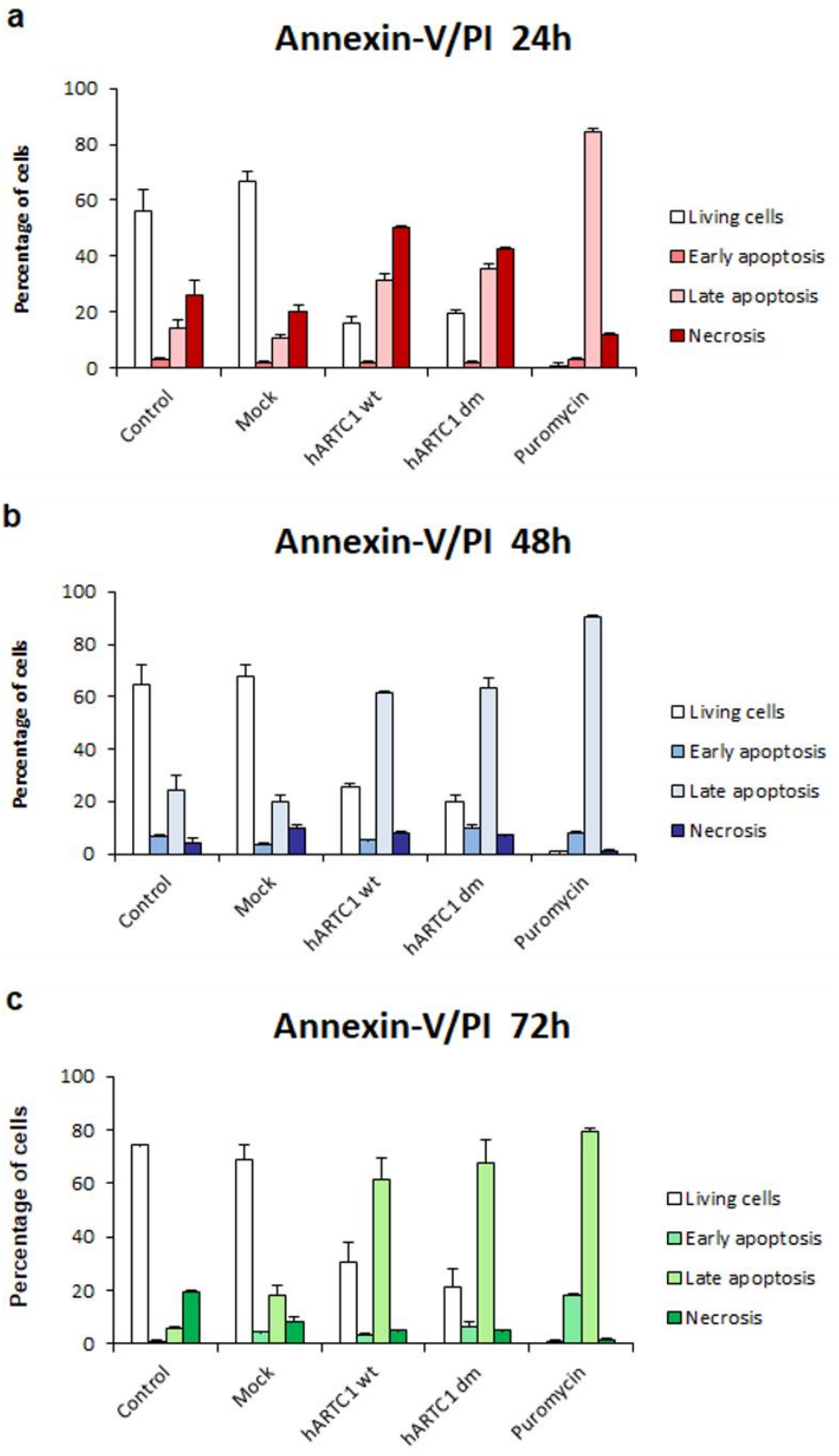

Figure 6.6 Characterization of hARTC1-induced cell death. Flow cytometric analysis of annexin-V and propidium iodide double staining of HeLa cells transiently transfected with the indicated constructs or treated with puromycin (10 μg/mL) for 24h (a), 48h (b) and 72h (c). The results are presented as percentage values (%). The data shown are representative of at least two independent experiments.

As depicted in Figure 6.6a, cells transfected for 24 hours with either hARTC1 wt or hARTC1 dm showed the same percentage of living cells, as well as the same percentage of apoptosis (including early and late apoptosis) and the same abundant percentage of necrosis. Mock-transfected cells were quite similar to control cells, whereas puromycin treated cells were prevalently apoptotic, as expected. After 48 hours of transfection, control and mock-transfected cells still continuing being similar. Puromycin-treated cells showed predominant apoptosis at each of the time points analyzed (Figure 6.6b). On the contrary, hARTC1 wt- and hARTC1 dm-transfected cells showed an increase in the apoptotic process (Figure 6.6b). Finally, 72 hours after transfection the situation was almost the same of that of 48 hours (Figure 6.6c).

Altogether these data indicated that both necrosis and apoptotic cell death were associated with hARTC1 transfection. After 24 hours of transfection the percentage of necrosis and apoptosis were quite similar. Whereas, after 48 and 72 hours of transfection the apoptotic cell death was mainly detectable. However, independently from the type of cell death revealed, this seemed to be an effect due to the transfection of the ARTCs, but not associated with their ADP-ribosylation activity, as it was also registered in hARTC1 dm-transfected cells that, as an inactive enzyme, was demonstrated to not be able to catalyze ADP-ribosylation (see Chapters 3 and 4).

Cell viability assays were performed using the Trypan Blue exclusion test, analyzing whether the over-expression of hARTC1 wt and that of the inactive hARTC1 dm affected cell viability. Specifically, non-transfected (control) HeLa cells, cells treated

with the transfection reagent only (mock transfection), or cells transfected with either hARTC1 wt or with the inactive hARTC1 dm were analyzed. After 24 hours of transfection, cells were stained with Trypan Blue, a molecule that is cell membrane impermeable and, therefore, only enters cells with compromised membranes. Upon entry into the cell, Trypan Blue binds to intracellular proteins thereby rendering the cells a bluish color. Thus, it allowed direct identification and enumeration of live (unstained) and dead (blue) cells in a given population. Cell viability was expressed as the percentage of dead cells within a population (see Chapter 2.2.2.2).

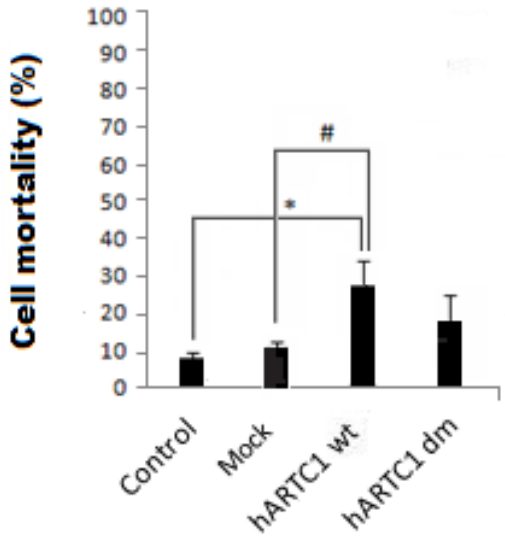

Figure 6.7 hARTC1 induces cell death. Cell mortality determined by Trypan Blue exclusion assay of HeLa cells transiently transfected with the indicated constructs, or with no vector (mock). The data represent means ±SD of at least ten independent experiments. *: indicates significantly different from the control ($p < 0.01$). #: indicates significantly different from mock ($p < 0.05$). The Unpaired Student's t-tests was performed for statistical analysis.

As indicated in Figure 6.7, transfection of the active hARTC1 (hARTC1 wt) enzyme induced significant cell death (27±6.9%) as compared to control samples (control, 7±1.5%; mock, 12±1.5%). This was not the case of the catalytically inactive hARTC1

dm, for which the increase of cell mortality was not statistically significant as compared to control samples (control or mock) or to hARTC1 wt (17±6.8%; Figure 6.7).

The number of percentage of dead cells was calculated as the number of stained (blue) cells over the number of total (stained and unstained) cells. A closer analysis of these data indicated that the number of dead cells was the same for all the samples, whereas the number of living cells varied among them. Indeed, there was a reduction of total cells number in hARTC1 wt transfected cells. The transfection of hARTC1 wt, but not that of hARTC1 dm, was associated to a 50% of reduction of living cells This reduction is most likely caused by the inhibition of cells proliferation (Figure 6.8).

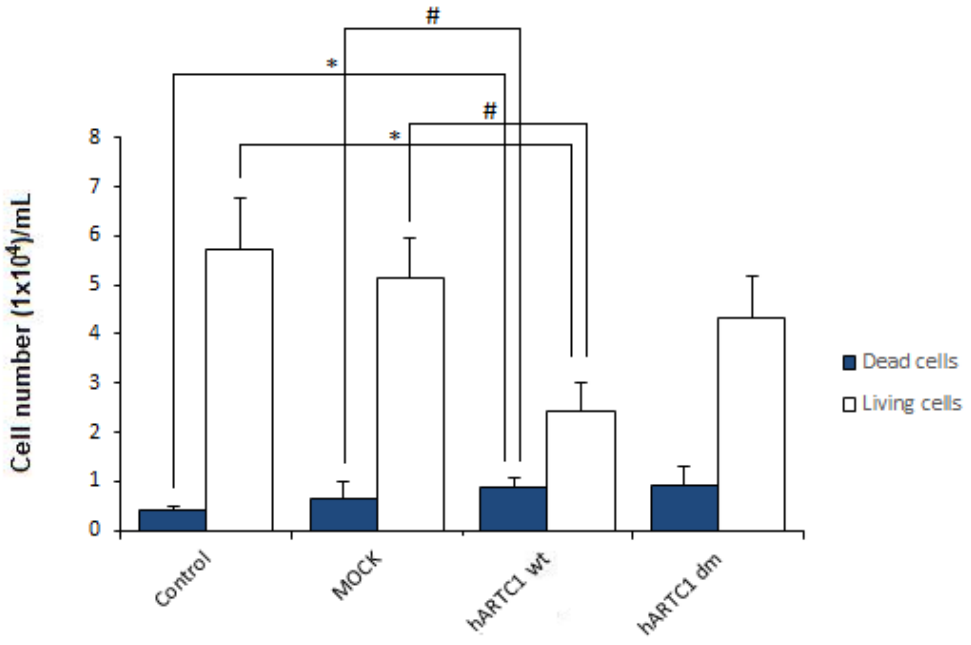

Figure 6.8 hARTC1 reduces the number of living cells. The number of dead (blue) and living (white) cells was determined by Trypan Blue exclusion assay of HeLa cells transiently transfected with the indicated constructs. The results are presented as number of cells/mL. The data shown are representative of at least ten independent experiments. *: indicates significantly different from the control ($p < 0.01$). #: indicates significantly different from mock ($p < 0.05$). The Unpaired Student's t-tests was performed for statistical analysis.

Considering that hARTC1 transfection did not cause an increase of dead cells, but affected the number of living cells, as evaluated by Trypan Blue exclusion assay, the possible role of hARTC1 wt and that of its catalytically inactive mutant hARTC1 dm in cell proliferation was investigated.

To this aim, cell proliferation was measured using non-transfected (control) HeLa cells, cells treated with the transfection reagent only (mock transfection), or transfected with either hARTC1 wt or hARTC1 dm. Cell proliferation was analyzed by direct counting of the cells every 24 hours for 3 days, thus, also verifying a possible time-dependent role. Data were reported by comparison with control cells counted at the same time taken as 1.0 (see Chapter 2.2.2.1).

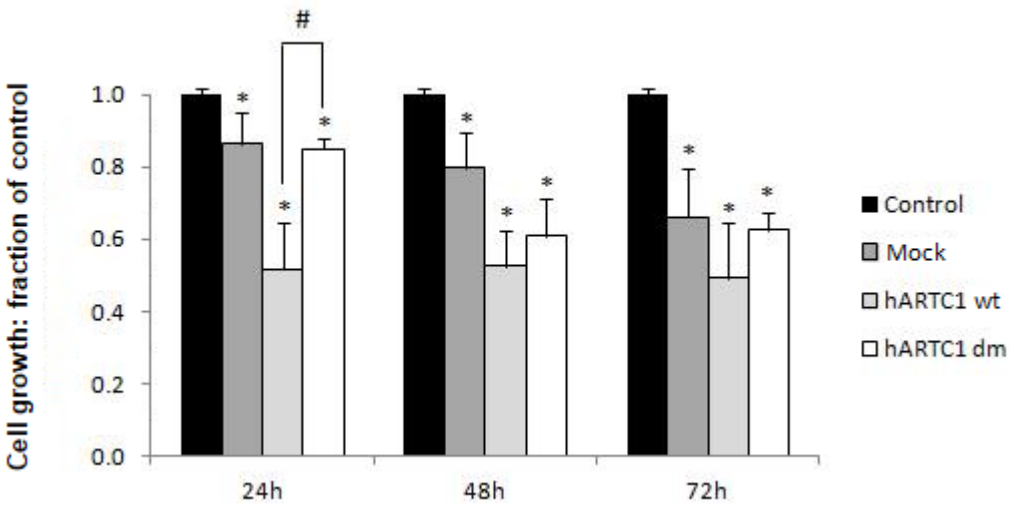

Figure 6.9 hARTC1 inhibits cell proliferation. Cell proliferation was measured by direct counting of HeLa cells transiently transfected with the indicated constructs for 24h, 48h and 72h. The results are normalized to control cells, with control cell numbers taken as 1.0. The data represent mean±SD of at least five independent experiments. * indicates significantly different from the control ($p < 0.01$). # indicates significantly different from hARTC1 dm ($p < 0.05$).

As shown in Figure 6.9, a 50% inhibition of cell proliferation was detectable 24 hours after transfection with hARTC1 wt, as compared to control cells (control and mock), or to hARTC1 dm over-expressing cells. A similar reduction in cell

proliferation was also revealed after 48 and 72 hours of transfection, but this was not statistically significant as compared to hARTC1 dm over-expressing cells. Therefore, transfection of hARTC1 wt, but not that of its catalytically inactive mutant hARTC1 dm, inhibited HeLa cell proliferation at 24 hours from transfection.

Overall, hARTC1 transfection caused a modest induction in cell death, but this was not dependent on the enzyme catalytic activity, as similar effects were seen following hARTC1 dm transfection. However, hARTC1 inhibits cell proliferation and, interestingly, this was dependent on the enzyme catalytic activity, at least in the short-term. This finding suggests that mono-ADP-ribosylation hARTC1-mediated can have a role in cell proliferation.

6.3 Summary

- The ovarian cancer cell lines analyzed do not contain mutation(s) in the identified ADP-ribosylation sites of GRP78/BiP. Further investigations are needed to understand the reasons for the different ADP-ribosylated GRP78/BiP levels detected in these ovarian cancer cell lines.
- Over-expression of hARTC1 inhibits cell proliferation.

Chapter 7

ARTD10 recruits GAPDH into cytosolic cell bodies

7.1 Introduction

Mono-ADP-ribosylation has been identified as a PTM involved in various cellular functions, including cell cycle regulation, apoptosis, metabolism, signal transduction, cell proliferation and cancer (Butepage, M. et al., 2015; Fabrizio, G. et al.2015a; Feijs, K.L. et al., 2013). Among the different ARTD enzymes with a role in cell proliferation, ARTD10 has been one of the most investigated (Verheugd, P. et al., 2013; Yu, M. et al., 2005). ARTD10 was the first ARTD to be characterized as a mono-ART and it has been demonstrated to be a highly dynamic protein, with a cytosolic localization under basal conditions, but able to shuttle between the cytoplasm and the nucleus (Kleine, H. et al., 2012). ARTD10 forms "bodies" that can be primarily detected in the cytoplasm. These bodies are able to move and tend to fuse over time, while also forming *de novo* and disappearing (Kleine, H. et al., 2012).

Different reports indicate that ARTD10 plays important roles in the regulation of several cellular processes, including the control of cell proliferation and of NF-κB signaling (Carter-O'Connell, I. et al., 2016; Kaufmann, M. et al., 2015; Venkannagari, H. et al., 2016). ARTD10 was initially isolated as a partner of the oncoprotein c-Myc, potentially underpinning why its overexpression interfered with cell proliferation (Yu, M. et al., 2005). Although it remains unknown which protein(s) are mono-

ADP-ribosylated by ARTD10 to mediate this growth inhibitory phenotype, a candidate is GSK3β, which is known to regulate cell proliferation and whose kinase activity is inhibited once it is modified by ARTD10 (Feijs, K.L. et al., 2013b; Wu, D. and Pan, W., 2010). Moreover, ARTD10 has been described as a regulator of the NF-kB signaling pathway, which also plays a role in cell proliferation in addition to its essential functions in immune and inflammatory responses (Verheugd, P. et al., 2013). By mono-ADP-ribosylating the NF-kB essential modulator NEMO, ARTD10 inhibits its poly-ubiquitination and its downstream signal pathway, thus causing a reduced activation of NF-κB target genes (Verheugd, P. et al., 2013). Interestingly, the catalytic activity of ARTD10 was strictly required to inhibit cell proliferation, as only wild type ARTD10, but not the catalytically inactive ARTD10-G888W mutant, was able to mediate this function (Herzog, N. et al., 2013).

Recently, in our laboratory, the glyceraldehyde 3-phosphate dehydrogenase (GAPDH) was identified as a novel substrate of ARTD10 (Mayo, E. et al., manuscript in preparation; title: ARTD10 induces ADP-ribosylation of GAPDH, and recruits GAPDH into cytosolic membrane-free cell bodies; list of authors: Mayo, E., Fabrizio, G., Scarpa, E.S., Stilla, A., Dani, N., Chiacchiera, F., Kleine, H., Attanasio, F., Luscher, B., Di Girolamo, M.). GAPDH is a 37 kDa glycolytic enzyme involved in controlling the energy production. GAPDH functions are important for different cellular pathways that affect cell structure, gene expression, signal transduction thereby linking metabolic activity to various cellular processes, including cell survival and proliferation (Zhang, J.Y. et al., 2015). Importantly, glucose metabolism has been reported to have a central role in both cell proliferation and carcinogenesis as the

majority of human tumors have high levels of GAPDH expression (Colell, A. et al., 2009; Guo, C. et al., 2013; Zhang, J.Y. et al., 2015). The activity of GAPDH has been described to be tightly regulated at both transcriptional and post-translational levels. ADP-ribosylation represents one of the PTMs that have been previously reported to regulate GAPDH activity. GAPDH was already known to be a substrate of poly-ADP-ribosylation by ARTD1, which elicited large cellular energy deficits and accelerated cell death (Du, X. et al., 2003; Seidler, N.W., 2013). Our experiments provide evidence that ARTD10 is involved in the mono-ADP-ribosylation of GAPDH.

7.2 Results

7.2.1 ARTD10 interacts and co-localizes with GAPDH in cytosolic cell bodies

The Luscher's group described the existence of ARTD10-dependent bodies (Kleine, H. et al., 2012). We have confirmed the formation of cell bodies in cells overexpressing ARTD10. Interestingly, using electron microscopy experiments we have observed that these bodies were membrane-free (Mayo, E. et al., manuscript in preparation; title: ARTD10 induces ADP-ribosylation of GAPDH, and recruits GAPDH into cytosolic membrane-free cell bodies; list of authors: Mayo, E., Fabrizio, G., Scarpa, E.S., Stilla, A., Dani, N., Chiacchiera, F., Kleine, H., Attanasio, F., Luscher, B., Di Girolamo, M.). Moreover, previous data obtained using immunoprecipitation experiments and MALDI-TOF-MS analysis demonstrated that GAPDH was an ARTD10 interactor. In this context, immunofluorescence experiments were

performed to verify whether the formation of cell bodies was a specific consequence of ARTD10 mono-ART activity, thus excluding that other active ARTDs (i.e. ARTD15 and ARTD16) could also form them. The localization of GAPDH within these cytosolic cell bodies was also analyzed.

Immunofluorescence experiments were performed using HeLa cells transiently transfected with HA-tagged ARTD10 wild-type (referred to as ARTD10), HA-tagged catalytically inactive mutant ARTD10 G888W (referred to as ARTD10-G888W), HA-tagged ARTD16 (referred to as ARTD16), or with FLAG-tagged ARTD15 (referred to as ARTD15). After fixation with 4% PFA and incubation with IF blocking solution (see Chapter 2.1.4, Table 2.4), the transfected cells were stained with anti-HA or anti-FLAG antibodies to visualize the over-expressed proteins and with an anti-GAPDH antibody to check GAPDH distribution.

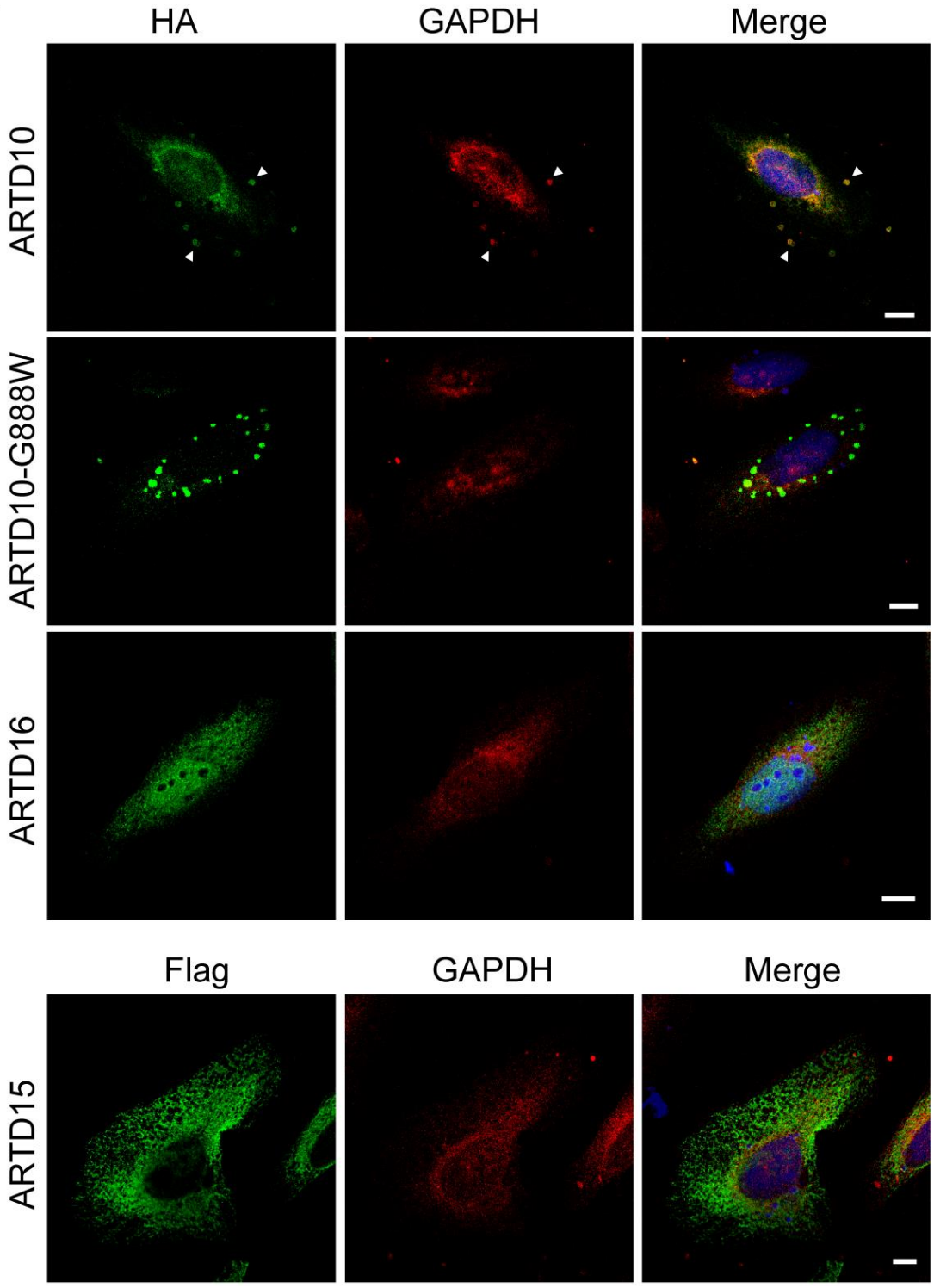

Figure 7.1 GAPDH co-localizes with ARTD10-positive bodies in ARTD10-transfected cells. The panels show representative immunofluorescence images of HeLa cells transiently transfected with HA-tagged ARTD10, ARTD10-G888W, ARTD16 or with FLAG-tagged ARTD15, stained with anti-HA (green) or anti-FLAG (green) and anti-GAPDH (red) antibodies, as indicated. The scale bars represent 10 μm. The data shown are representative of at least three independent experiments.

The analysis of cells using confocal microscopy revealed that upon transfection with the full-length enzyme, ARTD10 mainly localized to the cytosol and concentrated in punctate structures that resembled protein aggregates (Figure 7.1; ARTD10). Interestingly, GAPDH was also recruited into these cytoplasmic cell bodies, where it co-localized with ARTD10 (Figure 7.1; ARTD10). Of note, the catalytically inactive ARTD10-G888W was also able to induce the formation of cell bodies; however, only a minimal co-localization with GAPDH could be visualized (Figure 7.1; ARTD10-G888W). Indeed, quantification analysis confirmed that 45±2% of GAPDH co-localized with ARTD10-positive cell bodies in ARTD10-transfected cells, while only 19±3% of GAPDH co-localized with catalytically inactive ARTD10-G888W-positive cell bodies. ARTD15- and ARTD16-transfected cells did not form cytoplasmic bodies and the enzymes did not co-localize with GAPDH (Figure 7.1; ARTD16; ARTD15). Thus, ARTD10 transfection was able to induce formation of cell bodies, independently from the catalytic activity. The formation of these cell bodies was specific for ARTD10 as the other ARTDs did not cause cell bodies to form. ARTD10 and GAPDH co-localize into these cytoplasmic cell bodies. Since minimal co-localization was detected in ARTD10-G888W transfected cells the ability to recruit GAPDH in the cytosolic bodies is, at least in part, dependent on the catalytic activity of ARTD10.

To further verify the presence of a direct binding between GAPDH and ARTD10, immunoprecipitation experiments were performed using different HA-tagged enzymes, and the precipitated material was probed for GAPDH. HeLa cells were transfected with catalytically active, and catalytically inactive, HA-ARTD10. Cells

were also transfected with HA-ARTD16, which was used as a negative control, considering it was shown to not form cell bodies when over-expressed in HeLa cells and to not co-localize with GAPDH (Figure 7.1, ARTD16). Following transfection and lysate collection, samples were incubated with an anti-HA antibody, then separated by SDS-PAGE and analyzed by Western Blotting using antibodies raised against GAPDH or the HA-tag.

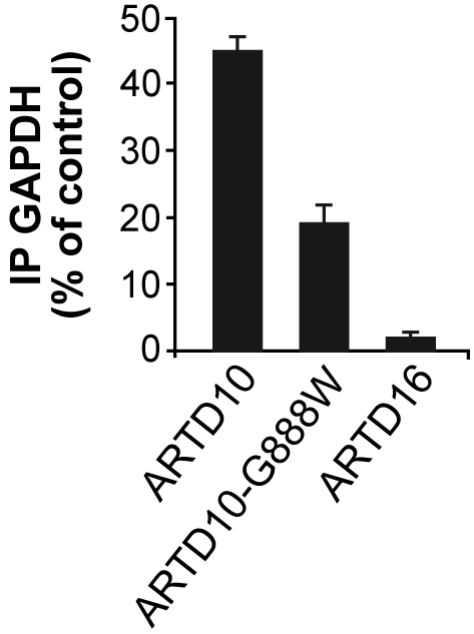

Figure 7.2 ARTD10 interacts with GAPDH. Quantification of GAPDH immunoprecipitation in HeLa cells transiently transfected with HA-tagged ARTD10, ARTD10-G888W and ARTD16, expressed as percentage of control, which correspond to the total amount of GAPDH (supernatant+resin). Data are representative of two independent experiments.

As shown in figure 7.2, GAPDH was co-immunoprecipitated with endogenous ARTD10. Moreover, the quantification of the immunoprecipitated GAPDH indicated that the catalytically inactive ARTD10-G888W could also bind GAPDH, although to a lower extent compared to the catalytically active enzyme (Figure

7.2). No detectable GAPDH was co-immunoprecipitated by ARTD16 under the same experimental conditions (Figure 7.2). Thus, these data exclude the possibility of a non-specific interaction and indicated that ARTD10 and GAPDH can interact and they are part of the same complex.

Altogether, these data demonstrate that the catalytic activity of ARTD10 is not strictly required for formation of cell bodies, consistent with other reports suggesting that different ARTD10 domains are important for their formation (Forst, A.H. et al., 2013; Kleine, H. et al., 2012). These other domains could also be essential for the interaction with GAPDH and its recruitment in the cytosolic bodies. However, the catalytic activity appeared to be important for maintaining GAPDH in the cytosolic bodies, as a more prominent GAPDH recruitment was detected after ARTD10 transfection (45%), in contrast to that of the catalytically inactive ARTD10-G888W (19%). Further studies will be crucial in understanding how these structures, and ARTD10-mediated mono-ADP-ribosylation of GAPDH, are regulated and how they are involved in different of cell functions, including cell proliferation.

7.3 Summary

- ARTD10 transfection induces formation of cytosolic cell bodies.
- GAPDH co-localizes with ARTD10 in these cytosolic cell bodies.
- ARTD10 catalytic activity is important for GAPDH recruitment into the cytosolic cell bodies.

Chapter 8

Final discussion

The present study investigated mono-ADP-ribosylation reactions, mainly exploring hARTC1-mediated mono-ADP-ribosylation, its cellular target(s) and the possible role in different cellular processes. Moreover, some aspects of the interaction between the mono-ART ARTD10, and its target GAPDH, were also investigated.

ADP-ribosylation is a reversible PTM comprising the transfer of single or multiple ADP-ribose moieties from NAD^+ to a substrate, forming a mono- or poly-ADP-ribosylated protein. The reaction is catalyzed by different classes of enzymes, including ARTCs, ARTDs and some members of the sirtuin family. ARTCs encompass extracellular membrane-bound or secreted proteins that modify other membrane-bound proteins or secreted factors (Glowacki, G. et al., 2002; Koch-Nolte, F. et al., 2008). Rat (r), mouse (m) and human (h) ARTCs have been well studied and characterized. Human ARTC family is composed of only four functional members, which are either active mono-ARTs (hARTC1, hARTC5) or inactive proteins (hARTC3, hARTC4). The gene encoding for ARTC2, which is duplicated in mouse and rat, is instead a pseudogene in humans (Koch-Nolte, F. et al., 1997; Prochazka, M., et al., 1991; Haag, F. et al., 1994). All ARTCs are ecto-enzymes anchored to the cell membrane; the only exception is hARTC5, which lacks the signal sequence typical of GPI-anchored membrane proteins and, thus, is a secreted enzyme (Glowacki, G. et al., 2002; Okazaki, I.J. and Moss, J., 1999; Stilla, A. et al., 2011).

Together with ARTC2, ARTC1 has been the most studied member of the ARTC family in rodents. Different ARTC1 substrates have been identified, including soluble or plasma-membrane-associated protein targets such as integrin α7 and various cell surface molecules (LFA-1, CD45, CD43 and CD44), suggesting ARTC1 involvement in different cellular processes (Paone, G. et al., 2002; Seman, M. et al., 2003; Zolkiewska, A. and Moss, J., 1993). Despite the numerous mono-ADP-ribosylated substrates identified in rodents, few information is available about ARTC1 in humans. The human defensin HNP-1 has been described as a target of hARTC1-mediated mono-ADP-ribosylation (Paone, G. et al., 2002). Once ADP-ribosylated, HNP-1 functions results altered, as it loses its antimicrobial and cytotoxic activities (Paone, G. et al., 2002). ADP-ribosylated HNP-1 has been found, *in vivo*, in bronchoalveolar lavage fluids of smoker patients, supporting the idea that the modified form is produced during the inflammatory response when it loses its antimicrobial activity (Paone, G. et al., 2002). Thus, hARTC1 has been proposed to have a regulatory role in airway inflammation (Paone, G. et al., 2002). More recently, hARTC1 has been linked to cancer, suggesting its potential role in invasion, proliferation, aggressiveness and apoptosis processes (Li, Z. et al., 2016; Tang, Y. et al., 2015; Xiao, M. et al., 2013; Xu, J.X. et al., 2017; Yang, L. et al., 2016). Despite the substantial progress made with regard to hARTC1-mediated mono-ADP-ribosylation in humans, its biological role is not well characterized. Therefore, one of the aim of this study was to investigate mono-ADP-ribosylation reactions mediated by hARTC1, searching for new possible substrate(s) of mono-ADP-ribosylation and their potential functional role(s).

The experiments carried out in the first part of the present study demonstrated that hARTC1 is mainly located in the ER. Both the over-expressed and the endogenous protein localized to a tubular membrane network consistent with the ER, as they co-localized with typical ER marker proteins such as calnexin, calreticulin, PDI and GRP78/BiP (Figures 3.2; 3.5; 3.6; 3.13). The use of other ARTCs with known cellular localization (e.g. cARTC2.1 wt and dm, described by Stilla, A. et al. as plasma membrane enzymes) provided a control of these experiments (Stilla, A. et al., 2011; Figures 3.2; 3.5; 3.6; 3.13). Importantly, the ER localization of hARTC1 was not affected by cycloheximide. Indeed, cycloheximide treatment blocks new protein synthesis and, thus, proteins that are not ER-resident exit the ER compartment reaching their final destination. The results obtained here demonstrated that this was the case for hARTC4, cARTC2.1 wt and cARTC2.1 dm (Figure 3.5a, b). On the contrary, the treatment with cycloheximide had no effect on the localization of hARTC1 (Figure 3.5a), thus confirming to be ER localized. As a further validation of the ER localization, quantifications of the percentage of co-localization between the ARTCs and the different cellular markers were performed in several independent experiments, supporting the finding that hARTC1 is an ER localized protein (Figures 3.4; 3.5c; 3.7). This finding was unexpected since ARTC1 has always been hypothesized to be an ecto-enzyme, based on various observations. Indeed, ARTC1 sequence contains a stretch of hydrophobic amino acids that is a typical feature of GPI-anchored membrane proteins (Glowacki, G. et al., 2002). Moreover, numerous plasma membrane-associated proteins have been identified as targets of ARTC1-mediated mono-ADP-ribosylation (Paone, G. et al.,

2002; Seman, M. et al., 2003; Zolkiewska, A. and Moss, J., 1993). Finally, its closest homolog ARTC2 has been well-described as a plasma membrane-localized enzyme (Koch-Nolte, F. et al., 1999; Stilla, A. et al., 2011). The only observation that counteracts this hypothesis comes from a report by Soman G. et al (1984) asserting that ARTC1 can have an intracellular localization. Indeed, in this paper it was reported that in rabbit skeletal muscle, 70% of the ARTC1 activity is intracellularly localized, anchored to the membrane of the sarcoplasmic reticulum (Soman, G. et al., 1984). In line with this description about ARTC1 activity in the sarcoplasmic reticulum, the results reported here demonstrated the intracellular localization of hARTC1 providing, for the first time, a quantification of the enzyme's distribution. The experiments of the present study demonstrated that some of the enzyme (~20% c.f. Figure 3.4) is localized to the plasma membrane, where it may catalyze mono-ADP-ribosylation of some of the previously reported plasma membrane-associated proteins. However, the majority of the enzyme was found to be localized to the ER (~50% c.f. Figures 3.4; 3.5; 3.7), where it may be involved in the mono-ADP-ribosylation of new and undiscovered intracellular targets. Indeed, there is a large number of intracellular proteins that have been demonstrated to undergo mono-ADP-ribosylation, but for which the enzyme(s) responsible for the modification still remains to be identified. Interestingly, most of these mono-ADP-ribosylated targets have been reported to have a role in cell signaling and metabolism, and the enzymatic activities involved in their modifications have been shown to be both cytosolic and membrane associated. Thus, it is plausible that hARTC1 could be involved in some of these previously described intracellular

mono-ADP-ribosylation reactions. To verify this hypothesis, new cellular target(s) of hARTC1 were investigated.

The approaches adopted for substrates analysis were based on the use of Af1521 macro domain, a protein module that we have been previously demonstrated to have high affinity for ADP-ribosylated proteins and has been successfully used to pull down ADP-ribosylated proteins (Dani, N. et al., 2011). In the work described here, the macro domain-based pull-down assay demonstrated that the over-expression of either arginine-specific hARTC1 wt or cARTC2.1 wt led to GRP78/BiP mono-ADP-ribosylation (Figures 3.8; 3.9). GRP78/BiP mono-ADP-ribosylation was already known, but the physiological relevance of this modification (as it regulated the availability of the functional chaperone), and the enzyme(s) involved have not yet been characterized (Laitusis, A.L. et al., 1999).

In the study reported here, new macro domain-based assays were set up utilizing the high affinity of Af1521 macro domain for ADP-ribosylated targets. Specifically, the innovative approaches were the application of macro domain in immunofluorescence and far-Western Blotting experiments. These new macro domain-based assays confirm that GRP78/BiP is a target of hARTC1, highlighting the technological importance of this tool in the study of APD-ribosylation reactions.

The use of macro domain in immunofluorescence assays represents a novel method that allowed, for the first time, the visualization of ADP-ribosylated proteins in living cells. With this approach, in cells under basal conditions only nuclear ADP-ribosylation was detected (Figure 3.10a). The use of a double mutant

form of the macro domain, which has been shown to not bind ADP-ribosylated proteins, provided a suitable negative control (Figure 3.10b). However, in cells over-expressing hARTC1 it was possible to detect a peri-nuclear staining of ADP-ribosylated that co-localized with GRP78/BiP, making it highly likely that this modification occurred in living cells. Furthermore, these studies demonstrated that the ADP-ribosylation was catalyzed by active ARTCs, as it was only observed in cells transfected with cARTC2.1 wt, but not in those transfected with the inactive enzymes cARTC2.1 dm, hARTC4 and hARTC1 dm (Figures 3.11a, c, e, g; 3.12a, c, e, g; 3.13; 4.2). An unexpected finding was that the macro domain nuclear staining was not detectable when cells overexpressed the active ARTCs (Figures 3.11a, e; 3.12a, e). A possible explanation is that when an active enzyme is overexpressed, it consumes most of the cellular NAD, which is therefore not available for nuclear reactions mediated by the endogenous enzyme(s).

As a further demonstration that hARTC1 contributes to GRP78/BiP mono-ADP-ribosylation, the use of macro-domain-based far-Western Blotting allowed direct visualization of ADP-ribosylated proteins in cells transfected with the active ARTCs. Among the numerous protein bands that correspond to different ADP-ribosylated targets, a protein band with the molecular weight of GRP78/BiP was visualized only in cells transfected with the enzymatically active cARTC2.1 wt and hARTC1 wt, but not in cARTC2.1 dm-, hARTC4- or hARTC1 dm-transfected cells (Figures 3.14; 4.1). The same band was also recognized by an anti-GRP78/BiP antibody (Figures 3.14; 3.15; 4.1) and, as further confirmation that it corresponded to the ADP-ribosylated form of the chaperone, it was reduced by 65% in cells where GRP78/BiP expression

was silenced (Figure 3.15). Moreover, silencing hARTC1 also reduced the basal level of ADP-ribosylated GRP78/BiP by 40% (Figure 4.4). As a proof for the specificity of the reaction, a doubly mutated hARTC1 (hARTC1 dm) was generated. When overexpressed in HeLa cells, the mutant protein was correctly expressed and localized to the ER with a similar distribution to hARTC1 wt protein, colocalizing with GRP78/BiP (Figure 4.3). However, hARTC1 dm, although over-expressed at comparable levels to hARTC1 wt (Figure 4.1), was not able to catalyze ADP-ribosylation reactions, as no band corresponding to GRP78/BiP could be visualized using the macro domain-based far-Western Blotting assay (Figure 4.1) and only a modest nuclear staining was detectable with the macro domain-based immunofluorescence experiments, similar to control and to hARTC4- and cARTC2.1 dm-transfected cells (Figure 4.2).

Altogether, these data demonstrate that hARTC1 is an intracellular enzyme, is mainly located in the ER, and is responsible for GRP78/BiP mono-ADP-ribosylation. This modification has been known for some time, and it has been described as a way to regulate the availability of the functional chaperone (Laitusis, A.L. et al., 1999; Ledford, B.E. and Leno, G.H., 1994). Indeed, when GRP78/BiP is ADP-ribosylated it is in an inactive state and this modification occurs in response to nutritional stress and to environmental conditions that can result in reduced protein synthesis, and thus in a reduced flux of proteins into the ER (Laitusis, A.L. et al., 1999). Therefore, it has been hypothesized that GRP78/BiP mono-ADP-ribosylation could be a system for balancing the rate of protein processing with those of protein synthesis. (Laitusis, A.L. et al., 1999; Ledford, B.E. and Leno, G.H.,

1994). The identification of the enzyme responsible for GRP78/BiP mono-ADP-ribosylation is of extreme interest since it allows to study the regulation of the activity of an important ER chaperone such as GRP78/BiP.

Indeed, GRP78/BiP is an ER-resident protein with multiple essential roles that are crucial for contribution to quality control for protein homeostasis in the ER. Efficient GRP78/BiP functions rely on numerous factors such as calcium concentration, redox homeostasis and oxygen supply (Araki, K. and Nagata, K., 2011; Gorlach, A. et al., 2006; Ushioda, R. et al., 2016). Under conditions that perturb the ER homeostasis, such as ER calcium depletion, glucose deprivation and oxidative stress, cells trigger the ER stress response to cope with this imbalance, activating the UPR (Vincenz-Donnelly, L. and Hipp, M.S., 2017). The UPR aims to restore ER homeostasis by temporarily attenuating new proteins translation, increasing the expression of proteins involved in protein folding and maturation, such as chaperones and foldases, inducing the degradation of misfolded proteins through the ER-associated degradation (ERAD) complex (Gardner, B.M. et al., 2013; Grootjans, J. et al., 2016; Kaufman, R.J., 1999; Strzyz, P., 2016; Welihinda, A.A. et al., 1999; Zhang, K. and Kaufman, R.J., 2008). If this fails, ER activates the death signaling pathways (Iurlaro, R. and Munoz-Pinedo, C., 2016; Logue, S.E. et al., 2013; Sano, R. and Reed, J.C., 2013).

Different stress-inducing agents or conditions that adversely affect the ER functions such as oxidative stress, chemical toxicity, inhibition of the ER calcium-ATPase, inhibitors of glycosylation and hypoxia have been reported to modulate GRP78/BiP expression (Beriaulta, D.R. and Werstucka, G. H., 2013; Oslowski, C.M.

and Urano, F. 2011; Toth, M.E. et al., 2015). The present study shows that the same stress treatments reported to stimulate GRP78/BiP expression can also induce hARTC1 expression and activity, and consequently, the ADP-ribosylation of the chaperone. Indeed, both mRNA and protein analysis revealed that hARTC1 expression was rapidly induced by short term treatments of cells with the stressors DTT and thapsigargin, but not with hypoxia or heat shock (Figures 5.1; 5.2). This activation, in turn, resulted in increased levels of ADP-ribosylated GRP78/BiP (Figure 5.3). Of note, it is possible that the increased levels of modified GRP78/BiP were underestimated, considering that this is a reversible reaction, and, therefore, the modified GRP78/BiP might have become the substrate of a specific hydrolase that could have regenerated the non-modified form.

Both DTT and thapsigargin are well-characterized inducers of ER stress, as they affect correct protein folding. In contrast, neither hypoxia nor heat-shock have been demonstrated to affect translation. Specifically, treatment with DTT results in the ER retention of newly synthesized proteins that cannot fold correctly as they cannot form disulfide bonds, whereas the treatment with thapsigargin inhibits the ER calcium-ATPase, thereby causing depletion of the ER calcium, which is associated with a slowed rate of protein processing (Taniyama, Y. et al., 1991; Thastrup, O., 1990). DTT and thapsigargin have been reported to inhibit translation with rapid timing: 10 minutes treatments are sufficient to inhibit the synthesis of almost all proteins (Brostrom, C.O. and Brostrom, M.A., 1998). However, cells can adapt to this translational inhibition. During longer-term exposure to stress treatments protein translation is recovered (Brostrom, C.O. and Brostrom, M.A.,

1998). The results of the present study demonstrated that, as a consequence of longer-term exposure stress treatments, GRP78/BiP is expressed at high levels and its mono-ADP-ribosylated form is not present (Figure 5.4). The induction of GRP78/BiP expression required a minimum of 2 hours, and plateaued within 12–18 hours, depending on the cell type (Brostrom, C.O. and Brostrom, M.A., 1998). These increased levels of GRP78/BiP, and of other chaperones, enhance the ER protein folding capability. Thus, GRP78/BiP is a central mediator of both acute inhibition of translation initiation and its subsequent recovery. The results obtained in this study are broadly consistent with the previously reported observations showing that the ADP-ribosylated form of GRP78/BiP accumulated when the protein flow through the ER was decreased (Laitusis, A.L. et al., 1999). Indeed, when the protein flow through the ER was decreased the cells do not require the chaperone activity as a facilitator of the folding of newly synthesized proteins. The ER stressors DTT and thapsigargin initially depress protein synthesis, rendering GRP78/BiP unnecessary. However, when translation is restored, as during longer term exposure to chemical disruptors, GRP78/BiP activity is required. A reversible PTM such as mono-ADP-ribosylation could allow the rapid regulation of the activity of GRP78/BiP, based on the needs of the cell. In line with these considerations, Chambers and colleagues suggested that cells can quickly adapt to fluctuations in the load of unfolding protein by shifting the amount of GRP78/BiP between active state, and a latent ADP-ribosylated pool (Chambers, J.E. et al., 2012). Indeed, when ADP-ribosylated, GRP78/BiP is inactive with respect to binding polypeptides. This was demonstrated by experiments showing that

mutations that mimic the negative charge of ADP-ribose can destabilize the chaperone binding to its substrate without affecting its ability to hydrolyze or exchange nucleotides (Chambers, J.E. et al., 2012). Thus, the ADP-ribosylation of GRP78/BiP has been proposed to be a way to inactivate the chaperone, avoiding its degradation and allowing the cell to rapidly reactivate it through de-ribosylation (Chambers, J.E. et al., 2012).

GRP78/BiP is a master regulator of the UPR as it is directly associated with the three UPR signaling proteins ATF6, IRE1α and PERK (Brewer, J.W., 2014; Hetz, C., 2012; Mori, K., 2000). In resting cells, the three UPR sensors are kept inactivate through their association with GRP78/BiP (Brewer, J.W., 2014; Hetz, C., 2012). When unfolded proteins accumulate in the ER lumen, for example during ER stress GRP78/BiP is reported to bind to misfolded proteins resulting in its dissociation from ATF6, IRE1α and PERK that become functional, thereby transducing the UPR (Brewer, J.W., 2014; Hetz, C., 2012; Merksamer, P.I. and Papa, F.R., 2010; Ron, D. and Walter, P., 2007). Since DTT and thapsigargin are well-characterized inducers of the UPR it is possible that the increased levels of ADP-ribosylated GRP78/BiP and of hARTC1 detected during cellular treatments with these stresses are associated with the release of the three UPR chaperone interactors. If this is the case, then ADP-ribosylation of GRP78/BiP could also be regarded as a facilitator of the UPR. For the study described here, the evaluation of UPR activation was approached with different techniques. Although evaluation by protein analysis failed, both (qRT)-PCR and immunofluorescence experiments have proven to be functional UPR assays. However, whilst the experiments confirmed that the ER

stressors DTT and thapsigargin are UPR inducers (Figure 5.5), no correlation between GRP78/BiP mono-ADP-ribosylation hARTC1-mediated and UPR activation was detected, since hARTC1 transfection did not trigger the UPR (Figures 5.6; 5.7; 8.1).

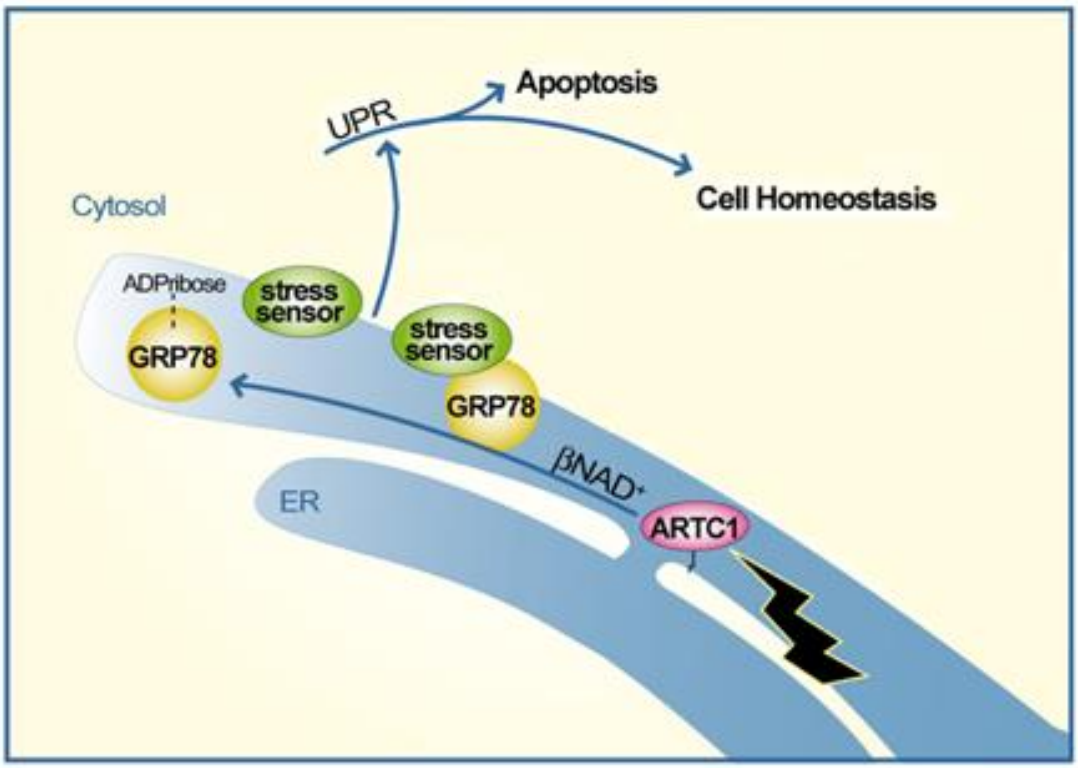

Figure 8.1 Schematic representation of GRP78/BiP mono-ADP-ribosylation mediated by hARTC1 occurring at the ER level.

As no correlation with the UPR was found, other possible roles of hARTC1-mediated mono-ADP-ribosylation were investigated, considering the different cellular functions that are regulated by GRP78/BiP such as cell survival, cell death and cancer. GRP78/BiP has been described as a disease-associated protein, whose expression may serve as a useful biomarker for pathology mechanisms. Indeed, different reports demonstrated it possess distinct functions in addition to that of being a chaperone residing in the ER, as it can be actively translocated to other

cellular locations and assume novel functions controlling signaling, proliferation, invasion, apoptosis, inflammation and immunity (Lee, A.S., 2014). Among these functions, it has been linked to cancer progression and therapeutic resistance, demonstrating it is over-expressed in a wide variety of cancer cells including breast, lung, prostate and ovarian cancers, melanoma and glioma cells (Lee, A.S., 2014 and reference therein; Wang, M. et al., 2009). Recently, hARTC1 has also been associated with cancer, suggesting it can play a role in invasion, proliferation, aggressiveness and apoptosis processes (Li, Z. et al., 2016; Tang, Y. et al., 2015; Xiao, M. et al., 2013; Xu, J.X. et al., 2017; Yang, L. et al., 2016). In the study reported here different ovarian cancer cell lines were examined, analyzing hARTC1 expression and GRP78/BiP mono-ADP-ribosylation. Ovarian cancer is one of the most common types of cancer among women, representing the eighth leading cause of cancer death (Ginsburg, O. et al., 2017; Torre, L.A. et al. 2017). The most common front-line treatment uses primary surgery followed by chemotherapy or chemoradiotherapy. However, this combined therapy is not always sufficient to avoid the disease returning. Thus, more effective treatment options are being explored, especially using molecularly-targeted therapy. One possibility is the use of PARP inhibitors, which represent a good strategy in the management of ovarian cancer. Currently, different trials with PARP inhibitors are in progress, and three of them (Olaparib, Rucaparib and Niraparib) have already been approved by FDA for the therapy of patients with ovarian tumors (Balasubramaniam, S. et al., 2017; Brown, J.S. et al., 2016; Brown, J.S. et al., 2017; Dulaney, C. et al., 2017; Scott, L.J., 2017; Kim, G., et al., 2015). Thus, ADP-ribosylation reactions have turned out to be

important for tumors: the inhibition of ART activity is emerging as a potentially important strategy for ovarian cancer treatment. In addition to the most extensively studied role of the ARTD1 in this type of cancer, it is interesting investigate the role of the ARTCs in this context. Studying the mono-ADP-ribosylation of target proteins with a well-documented role in cancer progression, such as GRP78/BiP, would be extremely useful for understanding how this modification affects protein function(s) in this context.

The various ovarian cancer cell lines chosen for this study were screened for hARTC1 and GRP78/BiP, showing comparable mRNA and protein levels, without any significant difference (Figures 6.1; 6.2). However, using the macro domain-based far-Western Blotting assay, different levels of GRP78/BiP ADP-ribosylation were detected (Figure 6.4). One possible explanation for the lack of significant variation of GRP78/BiP ADP-ribosylation is that GRP78/BiP has mutation(s) in its identified ADP-ribosylation sites and, thus, cannot be modified. Specifically, the amino acid sites of ADP-ribosylation are the arginine (R) residues 470 and 492, both localized in the substrate-binding domain of the chaperone (Chambers, J.E. et al., 2012). However, the sequencing analysis did not show the presence of altered nucleotides, as all the sequence relative to the analyzed cell lines were perfectly overlapped with the corresponding NCBI sequence of *human Grp78/BiP* (Figure 6.5). Thus, the different levels of GRP78/BiP ADP-ribosylation revealed by the far-Western Blotting assay are not associated with the mutation of the ADP-ribosylation sites. Further investigations are needed to understand the reasons the

different ADP-ribosylation states of GRP78/BiP in the ovarian cancer cell lines analyzed.

Interestingly, hARTC1-mediated mono-ADP-ribosylation has been demonstrated to have a role in cell proliferation. The experiments carried out in the last part of this study show that the over-expression of hARTC1 wt, but not that of its catalytically inactive mutant hARTC1 dm, have no effect of cell viability, but can affect cell proliferation, resulting in 50% inhibition during the first 24h of transfection (Figures 6.7; 6.8; 6.9).

In Summary: the collected results demonstrate that hARTC1 is an enzyme mainly localized to the ER, in contrast to the previously characterized ARTC proteins. There, hARTC1 is involved in the mono-ADP-ribosylation of GRP78/BiP, whose modification has been proposed to serve as a rapid regulation of the chaperone activity. In line with this hypothesis, hARTC1 was activated during the short-term treatment with ER stressors, resulting in acute ADP-ribosylation of GRP78/BiP paralleling translational inhibition. Indeed, protein synthesis depression caused by ER stress treatments is a condition which makes GRP78/BiP unnecessary; however, when translation is restored and unfolded protein accumulates in the ER, GRP78/BiP activity is required. A reversible, post-translational modification, such as mono-ADP-ribosylation, allows the rapid regulation of the activity of GRP78/BiP based on the needs of the cell. These findings identify hARTC1 as a novel, previously unsuspected, player in GRP78/BiP-mediated ER stress responses (Figure 8.1). The mono-ADP-ribosylation of the chaperone does not result in the release of GRP78/BiP interactors ATF6, IRE1α and PERK, since hARTC1 over-expression did

not trigger the UPR. However, hARTC1 over-expression inhibited cell proliferation, thus linking hARTC1-mediated mono-ADP-ribosylation to this process. The over-expression of hARTC1 and the consequent GRP78/BiP mono-ADP-ribosylation resulted in the accumulation of the inactive, mono-ADP-ribosylated form of the chaperone that is therefore not available for assisting protein synthesis. It could be hypothesized that this situation causes an inhibition of cell proliferation that is maintained until the cells can restore the pool of active GRP78/BiP, through its de-ribosylation or new chaperone synthesis, as confirmed by the fact that cell proliferation re-start after 48 hours of transfection. To evaluate all these hypotheses further investigations are required. However, these findings open new insights into mono-ADP-ribosylation reactions and how they regulate the biological activity of proteins with key role in central processes such as ER stress response, cell proliferation and cancer.

In addition to hARTC1 mono-ADP-ribosylation, a section of this study focused on mono-ART ARTD10, which was the subject of a research project carried out in our laboratory. ARTD10 is a 150 kDa enzyme belonging to the ARTDs, characterized as a mono-ART (Kleine, H. et al., 2008). Different reports linked ARTD10 to cell proliferation and identified various target of ARTD10 with a potential role in this process (Carter-O'Connell, I. et al., 2016; Kaufmann, M. et al., 2015; Venkannagari, H. et al., 2016; Verheugd, P. et al., 2013; Yu, M. et al., 2005). However, it remains unknown which protein(s) are mono-ADP-ribosylated by ARTD10 to mediate the growth inhibitory phenotype (Yu, M. et al., 2005). Previous and not yet published data of our laboratory identified GAPDH as a novel substrate of ARTD10 (Mayo, E.

et al., manuscript in preparation; title: ARTD10 induces ADP-ribosylation of GAPDH, and recruits GAPDH into cytosolic membrane-free cell bodies; list of authors: Mayo, E., Fabrizio, G., Scarpa, E.S., Stilla, A., Dani, N., Chiacchiera, F., Kleine, H., Attanasio, F., Luscher, B., Di Girolamo, M.). Specifically, we reported that ARTD10 interacts with and mono-ADP-ribosylates the glycolytic enzyme GAPDH and this modification occurs in membrane-free cytosolic cell bodies (Mayo, E. et al., manuscript in preparation; title: ARTD10 induces ADP-ribosylation of GAPDH, and recruits GAPDH into cytosolic membrane-free cell bodies; list of authors: Mayo, E., Fabrizio, G., Scarpa, E.S., Stilla, A., Dani, N., Chiacchiera, F., Kleine, H., Attanasio, F., Luscher, B., Di Girolamo, M.). Indeed, the experiments reported in this study confirmed that the transfection of ARTD10 induce the formation of cell bodies in which GAPDH co-localizes with ARTD10 (Figure 7.1). The presence of these cell bodies was independent from the catalytic activity of ARTD10, as also the catalytically inactive ARTD10-G888W was able to induce their formation (Figure 7.1). However, ARTD10 catalytic activity was essential for recruiting GAPDH into these cell bodies (Figures 7.1; 7.2). These observations are in agreement with the previous description of ARTD10 as a predominantly cytosolic enzyme under basal conditions, able to form discrete and dynamic "bodies" in the cytoplasm (Kleine, H., et al., 2012). Moreover, the catalytic activity of ARTD10 has been reported to be strictly required to inhibit cell proliferation, as only ARTD10 but not the catalytically inactive ARTD10-G888W mutant is able to mediate this function (Herzog, N. et al., 2013). However, despite these important data about ARTD10 as the enzyme that modifies and recruits GAPDH into cytosolic bodies, further studies are necessary

to evaluate if, and how, mono-ADP-ribosylation mediated by ARTD10 has any effect on GAPDH glycolytic activity.

List of abbreviations

AAD	Allergic airway disease
AC	Adenylyl cyclase
ADP	Adenosine diphosphate
AHR	Aryl hydrocarbon receptor
AHRR	AHR repressor
AKT	Serine/threonine-protein kinase
ALS	Amyotrophic lateral sclerosis
AMD	Automodification domain
ANOVA	One-way analysis of variance
APLF	Aprataxin and PNKP like factor
ARD	Ankyrin repeat domain
ARF6	ADP-ribosylation factor 6
Arg	Arginine
ARH	ADP-ribosyl-hydrolase
ARNT	AHR nuclear translocator
ART	ADP-ribosyl-transferase
ARTC	ADP-ribosyl-transferase clostridia toxin-like
ARTD	ADP-ribosyl-transferase diphtheria toxin-like
Asp	Aspartate
ATF6	Activating transcription factor 6
ATP	Adenosine triphosphate
ATTC	American Type Culture Collection
BAG1	BCL2 associated athanogene 1
BAL	B-aggressive lymphoma
BALF	Bronchoalveolar lavage fluids
BBAP	B-lymphoma and BAL-associated protein

BFA	Brefeldin A
BiP	Immunoglobulin heavy chain-binding protein
BRCA1	Breast cancer type 1 susceptibility protein
BRCT	BRCA1 carboxy-terminal
bZIP	Basic leucine zipper
c	Cricetinae
C/EBP	CCAAT-enhancer-binding protein
CBD	Central binding domain
CD	Cluster of Differentiation
cDNA	Complementary DNA
CF	Cystic fibrosis
CFTR	CF transmembrane conductance regulator
CHFR	Checkpoint with FHA and RING finger
CHO cells	Chinese hamster ovary cells
CHOP	C/EBP homologous protein
Chx	Cycloheximide
CoaSt6	Collaborator of Stat6
Cripto-1	Teratocarcinoma-derived growth factor 1
CtBP1/BARS	BFA-induced ADP-ribosylated substrate
DAC	Deacetylase
DLBCL	Diffuse large B-cell lymphoma
dm	Double mutant
DNA	Deoxyribonucleic acid
dNTP	Deoxyribonucleotide triphosphate
DRAG	Dinitrogenase reductase activating glycohydrolase
DRAT	Dinitrogenase reductase ADP-ribosyl-transferase
ECL	Enhanced chemiluminescence
EF-2	Elongation factor 2

EGCG	(-)-epigallocatechin gallate
eIF2α	Eukaryotic translation initiation factor 2 α
EMBL	European Molecular Biology Laboratory
ER	Endoplasmic reticulum
ERAD	ER-associated degradation
ERK	Extracellular signal-regulated kinase
FAR-WB	Far-Western Blotting
FCM	Flow cytometry
FDA	Food and Drug Administration
FGF-2	Fibroblast growth factor 2
FGFR	Fibroblast growth factor receptor
FMNS	Fondazione Mario Negri Sud
GADD34	DNA damage inducible gene 34
GAPDH	Glyceraldehyde 3 phosphate dehydrogenase
GDH	Glutamate dehydrogenase
Glu	Glutamic acid
GnRHR	Gonadotropin-releasing hormone receptor
GPCRs	G-protein coupled receptors
GPI	Glycosylphosphatidylinisotol
GRD	Glycine-rich domain
GRP78	Glucose-regulated protein 78 kDa
GSK3β	Glycogen synthase kinase 3 beta
GST	Glutathione S-transferase
h	Human
HDAC	Histone deacetylase
HeLa cells	Human cervical cancer cells
Hep-G2 cells	Human hepatoma G2 cells
HIV	Human immunodeficiency virus

HL-60 cells	Human promyelocytic leukemia cells
HNC cell lines	Head and neck cancer cell lines
HNP-1	Human neutrophil peptide 1
HPS	Histidine-proline-serine
HRP	Horseradish peroxidase
HSP70	Heat shock family of stress proteins 70 kDa
HSPA5	Heat shock protein family A member 5
IF	Immunofluorescence
IFN	Interferon
Ig	Immunoglobulin
IL	Interleukin
IRAP	Insulin-responsive aminopeptidase
IRE1α	Inositol-requiring enzyme 1α
IRF1	Interferon response factor 1
ISGs	Interferon-stimulated genes
JNK2	Jun N-terminal kinase 2
Kapβ1	karyopherin-β1/importin-β1
kDa	Kilodalton
LC-MS/MS	Liquid chromatography tandem-MS
LFA-1	Lymphocyte-function-associated antigen 1
LPS	Lipopolysaccharide
LSCM	Laser scanning confocal microscopy
m	Mouse
MAb159	Mouse monoclonal IgG antibody
MALDITOF-MS	Matrix-assisted laser desorption/ionization time-of-flight-MS
MDR	Multidrug resistance
MIBG	Meta-iodobenzylguanidine
MLV	Murine leukemia virus

mRNA	Messenger RNA
MS	Mass spectrometry
MTJ-1	Murine tumor cell DnaJ-like protein-1
MVP	Major vault protein
MVP-ID	Major-vault particle interaction domain
NAD	Nicotinamide adenine dinucleotide
NCBI	National Center for Biotechnology Information
NEMO	NF-κB essential modulator
NES	Nuclear export sequence
NF-κB	Nuclear Factor-κappaB
NLS	Nuclear localization signal
NMU cells	Rat mammary adenocarcinoma cells
NuMA	Nuclear mitotic apparatus protein
O-A-ADP-ribose	O-acetyl-ADP-ribose
OD	Optical density
PAR	Poly-ADP-ribose
PAR-4/PAWR	Prostate apoptosis response 4
PARG	Poly-ADP-ribose-glycohydrolase
PARP	Poly-ADP-ribose-polymerase
PBZ	Poly-ADP-ribose binding zinc-finger
PCNA	Proliferating cell nuclear antigen
PDGF	Platelet-derived growth factor
PDI	Protein disulfide isomerase
PEPCK	Phosphoenolpyruvate carboxykinase
PERK	PKR-like ER kinase
PI	Propidium iodide
PI3K	Phosphoinositide 3-kinase
PJ34	N-(6-oxo-5,6-dihydrophenanthridin-2-yl)-N, N dimethylacetamide HCl

PKR	Double-stranded RNA-dependent protein kinase
PLC	Phospholipase C
PNKP	Polynucleotide kinase/phosphatase
PRD	PARP regulatory domain
PS	Phosphatidylserine
PTM	Post-translational modification
r	Rat
Ran	Ras-related nuclear protein
RAP80	Receptor-associated protein 80
RNA	Ribonucleic acid
RNP	Ribonucleoprotein
Rpm	Revolutions per minute
RRM	RNA-binding/recognition motif
S1P	Site-1 protease
S2P	Site-2 protease
SAM	Sterile alpha motif
SAP	SAF/Acinus/PIAS-DNA-binding domain
SD	Standard deviation
SDS-PAGE	Sodium dodecyl sulphate-polyacrylamide gel electrophoresis
SEB	Staphylococcal enterotoxin B
SEM	Standard error of the mean
SGs	Stress-granules
siRNA	Small interfering RNA
Sirtuin or SIRT	Silent information regulator SIR2-like protein
SMCs	Smooth muscle cells
SOD1	Superoxide dismutase
STAT1β	Signal transducer and activator of transcription 1 isoform β
STAT6	Signal Transducer and Activator of Transcription 6

SubA	Sub AB subunit A
SubAB	Subtilase cytotoxin
TAB182	Tankyrase-binding protein 182 kDa
TCDD	2,3,7,8-tetrachlorodibenzo-p-dioxin
TEP1	Telomerase-associated protein
TiPARP	TCDD-inducible PARP
Tm	Melting temperature
TMD	Trans-membrane domain
TNF	Tumor necrosis factor
TRAIL	TNF-related apoptosis-inducing ligand
TRF1	Telomeric repeat binding factor 1
UIM	Ubiquitin interaction motif
UPR	Unfolded protein response
v/v	Volume/volume
VEEV	Venezuelan equine encephalitis virus
VIT	Vault protein inter-alpha-trypsin
vWA	Von Willebrand type A
w/v	Weight/volume
WB	Western Blotting
WGA	Wheat germ agglutinin
wt	Wild-type
XBP1	X-box binding protein 1
XBP1s	Spliced XBP1
XRCC1	X-ray cross complementing group 1 protein
ZAP/ZC3HAV1	Zinc-finger Antiviral Protein
ZF	Zinc finger
ZF/THP	Zinc finger/TiPARP homologous domain
α2M*	Alpha-2-macroglobulin

(qRT)-PCR	Quantitative real-time Polymerase Chain Reaction
53BP1	p53 binding protein 1

References

Adriouch, S., Ohlrogge, W., Haag, F., Koch-Nolte, F. and Seman, M. (2001) Rapid induction of naive T cell apoptosis by ecto-nicotinamide adenine dinucleotide: requirement for mono(ADP-ribosyl)transferase 2 and a downstream effector. *J Immunol* 167, 196–203.

Aguiar, R.C., Takeyama, K., He, C., Kreinbrink, K. and Shipp, M.A. (2005) B-aggressive lymphoma family proteins have unique domains that modulate transcription and exhibit poly(ADP-ribose) polymerase activity. *J Biol Chem* 280, 33756-33765.

Aguiar, R.C., Yakushijin, Y., Kharbanda, S., Salgia, R., Fletcher, J.A. and Shipp, M.A. (2000) BAL is a novel risk-related gene in diffuse large B-cell lymphomas that enhances cellular migration. *Blood* 96, 4328-4334.

Ahel, I., Ahel, D., Matsusaka, T., Clark, A.J., Pines, J., Boulton, S.J. and West, S.C. (2008) Poly(ADP-ribose)-binding zinc finger motifs in DNA repair/checkpoint proteins. *Nature* 451, 81-85.

Ahmed, S., Bott, D., Gomez, A., Tamblyn, L., Rasheed, A., Cho, T., MacPherson, L., Sugamori, K.S., Yang, Y., Grant, D.M., Cummins, C.L. and Matthews, J. (2015) Loss of the Mono-ADP-ribosyltransferase, Tiparp, Increases Sensitivity to Dioxin-induced Steatohepatitis and Lethality. *J Biol Chem* 290, 16824-16840.

Ahn, S.W., Kim, J.E., Park, K.S., Choi, W.J., Hong, Y.H., Kim, S.M., Kim, S.H., Lee K.W. and Sung, J.J. (2012) The neuroprotective effect of the GSK-3β inhibitor and influence on the extrinsic apoptosis in the ALS transgenic mice. *J Neurol Sci* 320, 1-5.

Ahuja, N., Schwer, B., Carobbio, S., Waltregny, D., North, B.J., Castronovo, V., Maechler, P. and Verdin, E. (2007) Regulation of insulin secretion by SIRT4, a mitochondrial ADP-ribosyltransferase. *J Biol Chem* 282, 33583-33592.

Alawneh, A.M., Qi, D., Yonesaki, T. and Otsuka, Y. (2016) An ADP-ribosyltransferase Alt of bacteriophage T4 negatively regulates the Escherichia coli MazF toxin of a toxin-antitoxin module. *Mol Microbiol* 99, 188-198.

Al-Hashimi, A.A., Caldwell, J., Gonzalez-Gronow, M., Pizzo, S.V., Aboumrad, D., Pozza, L., Al-Bayati, H., Weitz, J.I., Stafford, A., Chan, H., Kapoor, A., Jacobsen, D.W., Dickhout, J.G. and Austin, R.C. (2010) Binding of anti-GRP78 autoantibodies to cell surface GRP78 increases tissue factor procoagulant activity via the release of calcium from endoplasmic reticulum stores. *J Biol Chem* 285, 28912-28923.

Ali, A.A., Timinszky, G., Arribas-Bosacoma, R., Kozlowski, M., Hassa, P.O., Hassler, M., Ladurner, A.G., Pearl, L.H. and Oliver, A.W. (2012) The zinc-finger domains of PARP1 cooperate to recognize DNA strand breaks. *Nat Struct Mol Biol* 19, 685–692.

Ali, S.O., Khan, F.A., Galindo-Campos, M.A. and Yelamos, J. (2016) Understanding specific functions of PARP-2: new lessons for cancer therapy. *Am J Cancer Res* 6, 1842–1863.

Allured, V.S., Case, L.M., Leppla, S.H. and McKay, D.B. (1985) Crystallization of the protective antigen protein of Bacillus anthracis. *J Biol Chem* 260, 5012-5013.

Altmeyer, M., Messner, S., Hassa, P.O., Fey, M. and Hottiger, M.O. (2009) Molecular mechanism of poly(ADP-ribosyl)ation by PARP1 and identification of lysine residues as ADP-ribose acceptor sites. *Nucleic Acids Res* 37, 3723–3738.

Ame, J.C., Rolli, V., Schreiber, V., Niedergang, C., Apiou, F., Decker, P., Muller, S., Hoger, T., Menissier-de Murcia, J. and de Murcia, G. (1999) PARP-2, A novel mammalian DNA damagedependent poly(ADP-ribose) polymerase. *J Biol Chem* 274, 17860–17868.

Ame, J.C., Spenlehauer, C. and de Murcia, G. (2004) The PARP superfamily. *Bioessays* 26, 882-893.

Anantharaman, V., Koonin, E.V. and Aravind, L. (2002) Comparative genomics and evolution of proteins involved in RNA metabolism. *Nucleic Acids Res* 30, 1427-1464.

Araki, K. and Nagata, K. (2011) Protein folding and quality control in the ER. *Cold Spring Harb Perspect Biol* 3, a007526.

Atasheva, S., Akhrymuk, M., Frolova, E.I. and Frolov, I. (2012) New PARP gene with an anti-alphavirus function. *J Virol* 86, 8147-8160.

Atasheva, S., Frolova, E.I. and Frolov, I. (2014) Interferon-stimulated poly(ADP-Ribose) polymerases are potent inhibitors of cellular translation and virus replication. *J Virol* 88, 2116-2130.

Augustin, A., Spenlehauer, C., Dumond, H., Menissier-De Murcia, J., Piel, M., Schmit, A. C., Apiou, F., Vonesch, J.L., Kock, M., Bornens, M. and De Murcia, G. (2003) PARP-3 localizes preferentially to the daughter centriole and interferes with the G1/S cell cycle progression. *J Cell Sci* 116, 1551-1562.

Bai, P., Houten, S.M., Huber, A., Schreiber, V., Watanabe, M., Kiss, B., de Murcia, G., Auwerx, J. and Menissier-de Murcia, J. (2007) Poly(ADP-ribose) polymerase-2 [corrected] controls adipocyte differentiation and adipose tissue function through the regulation of the activity of the retinoid X receptor/peroxisome proliferator-activated receptor-gamma [corrected] heterodimer. *J Biol Chem* 282, 37738-37746.

Balasubramaniam, S., Kim, G.S., McKee, A.E. and Pazdur, R. (2017) Regulatory considerations on endpoints in ovarian cancer drug development. *Cancer* 123, 2604-2608.

Barbarulo, A., Iansante, V., Chaidos, A., Naresh, K., Rahemtulla, A., Franzoso, G., Karadimitris, A., Haskard, D.O., Papa, S. and Bubici, C. (2013) Poly(ADP-ribose)

polymerase family member 14 (PARP14) is a novel effector of the JNK2-dependent pro-survival signal in multiple myeloma. *Oncogene* 32, 4231-4242.

Barkauskaite, E., Jankevicius, G. and Ahel, I. (2015) Structures and Mechanisms of Enzymes Employed in the Synthesis and Degradation of PARP-Dependent Protein ADP-Ribosylation. *Mol Cell* 58, 935-946.

Barth, E., Radermacher, P. and Szabo, C. (2006) The world according to poly(ADP-ribose) polymerase (PARP)--update 2006. *Intensive Care Med* 32, 1470-1474.

Bazan, J.F. and Koch-Nolte, F. (1997) Sequence and structural links between distant ADP-ribosyltransferase families. *Adv Exp Med Biol* 419, 99-107.

Beck, C., Robert, I., Reina-San-Martin, B., Schreiber, V. and Dantzer, F. (2014) Poly(ADP-ribose) polymerases in double-strand break repair: focus on PARP1, PARP2 and PARP3. *Exp Cell Res* 329, 18-25.

Berger, W., Steiner, E., Grusch, M., Elbling, L. and Micksche. M. (2009) Vaults and the major vault protein: novel roles in signal pathway regulation and immunity. *Cell Mol Life Sci* 66, 43-61.

Beriault, D.R. and Werstuck, G.H. (2013) Detection and quantification of endoplasmic reticulum stress in living cells using the fluorescent compound, Thioflavin T. *Biochim Biophys Acta* 1833, 2293-2301.

Bertolotti, A., Zhang, Y., Hendershot, L.M., Harding, H.P. and Ron, D. (2000) Dynamic interaction of BiP and ER stress transducers in the unfolded-protein response. *Nat Cell Biol* 2, 326-332.

Bessman, M.J., Frick, D.N. and O'Handley, S.F. (1996) The MutT proteins or "Nudix" hydrolases, a family of versatile, widely distributed, "housecleaning" enzymes. *J Biol Chem* 271, 25059-25062.

Bick, M.J., Carroll, J.W., Gao, G., Goff, S.P., Rice, C.M. and MacDonald, M.R. (2003) Expression of the zinc-finger antiviral protein inhibits alphavirus replication. *Journal of virology* 77, 11555-62.

Bini, L., Magi, B., Marzocchi, B., Arcuri, F., Tripodi, S., Cintorino, M., Sanchez, J.C., Frutiger, S., Hughes, G., Pallini, V., Hochstrasser, D.F. and Tosi, P. (1997) Protein expression profiles in human breast ductal carcinoma and histologically normal tissue. *Electrophoresis* 18, 2832-2841.

Blander, G. and Guarente, L. (2004) The Sir2 family of protein deacetylases. *Annu Rev Biochem* 73, 417-435.

Bock, F.J. and Chang, P. (2016) New directions in poly(ADP-ribose) polymerase biology. *FEBS J* 283, 4017-4031.

Boehler, C., Gauthier, L.R., Mortusewicz, O., Biard, D.S., Saliou, J.M., Bresson, A., Sanglier-Cianferani, S., Smith, S., Schreiber, V., Boussin, F. and Dantzer, F. (2011) Poly(ADP-ribose) polymerase 3 (PARP3), a newcomer in cellular response to DNA damage and mitotic progression. *Proc Natl Acad Sci U S A* 108, 2783-2788.

Boulle, N., Jones, E.M., Auguste, P. and Baird, A. (1995) Adenosine diphosphate ribosylation of fibroblast growth factor-2. *Mol Endocrinol* 9, 767-775.

Bourgeois, C., Okazaki, I., Cavanaugh, E., Nightingale, M. and Moss, J. (2003) Identification of regulatory domains in ADP-ribosyltransferase-1 that determine transferase and NAD glycohydrolase activities. *J Biol Chem* 278, 26351-26355.

Brachmann, C.B., Sherman, J.M., Devine, S.E., Cameron, E.E., Pillus, L., Boeke, J.D. (1995) The SIR2 gene family, conserved from bacteria to humans, functions in silencing, cell cycle progression, and chromosome stability. *Genes Dev* 9, 2888-28902.

Brewer, J.W. (2014) Regulatory crosstalk within the mammalian unfolded protein response. *Cell Mol Life Sci* 71, 1067-1079.

Brostrom, C.O. and Brostrom, M.A. (1998) Regulation of translational initiation during cellular responses to stress. *Prog Nucleic Acid Res Mol Biol* 58, 79–125.

Brown, J.S., Kaye, S.B., Yap, T.A. (2016) PARP inhibitors: the race is on. *Br J Cancer* 14, 713-715.

Brown, J.S., O'Carrigan, B., Jackson, S.P. and Yap, T.A. (2017) Targeting DNA Repair in Cancer: Beyond PARP Inhibitors. *Cancer Discov.* 7, 20-37.

Brunyanszki, A., Szczesny, B., Virag, L. and Szabo, C. (2016) Mitochondrial poly(ADP-ribose) polymerase: The Wizard of Oz at work. *Free Radic Biol Med* 100, 257-270.

Bruzzone, S., Parenti, M.D., Grozio, A., Ballestrero, A., Bauer, I., Del Rio, A. and Nencioni, A. (2013) Rejuvenating sirtuins: the rise of a new family of cancer drug targets. *Curr Pharm Des* 19, 614-623.

Burikhanov, R., Zhao, Y., Goswami, A., Qiu, S., Schwarze, S.R. and Rangnekar, V.M. (2009) The tumor suppressor Par-4 activates an extrinsic pathway for apoptosis. *Cell* 138, 377-388.

Burkle, A. (2005) Poly(ADP-ribose). The most elaborate metabolite of NAD+. *FEBS J* 272, 4576-4589.

Butepage, M., Eckei, L., Verheugd, P. and Luscher, B. (2015) Intracellular Mono-ADP-Ribosylation in Signaling and Disease. *Cells* 4, 569–595.

Camicia, R., Bachmann, S.B., Winkler, H.C., Beer, M., Tinguely, M., Haralambieva, E. and Hassa, P.O. (2013) BAL1/ARTD9 represses the anti-proliferative and pro-apoptotic IFNgamma-STAT1-IRF1-p53 axis in diffuse large B-cell lymphoma. *J Cell Sci* 126, 1969-80.

Carafa, V., Nebbioso, A. and Altucci, L. (2012) Sirtuins and Disease: The Road Ahead. *Frontiers in Pharmacology* 3-4.

Carlile, G.W., Robert, R., Matthes, E., Yang, Q., Solari, R., Hatley, R., Edge, C.M., Hanrahan, J.W., Andersen, R., Thomas, D.Y. and Birault, V. (2016) Latonduine Analogs Restore F508del-Cystic Fibrosis Transmembrane Conductance Regulator Trafficking through the Modulation of Poly-ADP Ribose Polymerase 3 and Poly-ADP Ribose Polymerase 16 Activity. *Mol Pharmacol* 90, 65-79.

Carroll, S.F. and Collier, R.J. (1984) NAD binding site of diphtheria toxin: identification of a residue within the nicotinamide subsite by photochemical modification with NAD. *Proc Natl Acad Sci U S A* 81, 3307-3311.

Carter-O'Connell, I., Jin, H., Morgan, R.K., Zaja, R., David, L.L., Ahel, I. and Cohen, M.S. (2016) Identifying Family-Member-Specific Targets of Mono-ARTDs by Using a Chemical Genetics Approach. *Cell Rep* 14, 621-631.

Cervantes-Laurean, D., Jacobson, E.L. and Jacobson, M.K. (1996) Glycation and glycoxidation of histones by ADP-ribose. *J Biol Chem* 271, 10461-10469.

Chambers, J.E., Dalton, L.E., Clarke, H.J., Malzer, E., Dominicus, C.S., Patel, V., Moorhead, G., Ron, D. and Marciniak, S.J. (2015) Actin dynamics tune the integrated stress response by regulating eukaryotic initiation factor 2α dephosphorylation. *eLife*, e04872.

Chambers, J.E., Petrova, K., Tomba, G., Vendruscolo, M. and Ron, D. (2012) ADP ribosylation adapts an ER chaperone response to short-term fluctuations in unfolded protein load. *J Cell Biol* 198, 371–385.

Chambon, P., Weill, J.D. and Mandel, P. (1963) Nicotinamide mononucleotide activation of new DNA-dependent polyadenylic acid synthesizing nuclear enzyme. *Biochem Biophys Res Commun* 11, 39-43.

Changolkar, L.N. and Pehrson, J.R. (2006) macroH2A1 histone variants are depleted on active genes but concentrated on the inactive X chromosome. *Mol Cell Biol* 26, 4410-4420.

Changolkar, L.N., Costanzi, C., Leu, N.A., Chen, D., McLaughlin, K.J. and Pehrson, J.R. (2007) Developmental changes in histone macroH2A1-mediated gene regulation. *Mol Cell Biol* 27, 2758-2764.

Chatterjee, S., Cheng, M.F., Berger, S.J. and Berger, N.A. (1994) Induction of M(r) 78,000 glucose-regulated stress protein in poly(adenosine diphosphate-ribose) polymerase- and nicotinamide adenine dinucleotide-deficient V79 cell lines and its relation to resistance to the topoisomerase II inhibitor etoposide. *Cancer Res* 54, 4405-4411.

Chen, B., Zang, W., Wang, J., Huang, Y., He, Y., Yan, L., Liu, J. and Zheng, W. (2015) The chemical biology of sirtuins. *Chem Soc Rev* 44, 5246-5264.

Chen, D., Vollmar, M., Rossi, M.N., Phillips, C., Kraehenbuehl, R., Slade, D., Mehrotra, P. V., von Delft, F., Crosthwaite, S.K., Gileadi, O., Denu, J.M. and Ahel, I. (2011) Identification of macrodomain proteins as novel O-acetyl-ADP-ribose deacetylases. *J Biol Chem* 286, 13261-13271.

Chen, W.T. and Lee, A.S. (2011) Measurement and modification of the expression level of the chaperone protein and signaling regulator GRP78/BiP in mammalian cells. *Methods Enzymol* 490, 217-233,

Chen, X., Shen, J. and Prywes, R. (2002) The luminal domain of ATF6 senses endoplasmic reticulum (ER) stress and causes translocation of ATF6 from the ER to the Golgi. *J Biol Chem* 277, 13045-13052.

Chen, Y. and Brandizzi, F. (2013) IRE1: ER stress sensor and cell fate executor. Trends Cell Biol 23, 547-555.

Chen, Y., Weng, G., Li, J., Harry, A., Pieroni, J., Dingus, J., Hildebrandt, J.D., Guarnieri, F., Weinstein, H., and Iyengar, R. (1997) A surface on the G protein beta-subunit involved in interactions with adenylyl cyclases. *Proc Natl Acad Sci U S A* 94, 2711-2714.

Chevalier, M., Rhee, H., Elguindi, E.C. and Blond, S.Y. (2000) Interaction of murine BiP/GRP78 with the DnaJ homologue MTJ1. *J Biol Chem* 275, 19620-19627.

Chiu, C.C., Lin, C.Y., Lee, L.Y., Chen, Y.J., Kuo, T.F., Chang, J.T., Liao, C.T., Wang, H.M., Yen, T.C., Shen, C.R., Liao, S.K. and Cheng, A.J. (2008) Glucose-regulated protein 78 regulates multiple malignant phenotypes in head and neck cancer and may serve as a molecular target of therapeutic intervention. *Mol Cancer Ther* 7, 2788-2797.

Cho, S.H., Ahn, A.K., Bhargava, P., Lee, C.H., Eischen, C.M., McGuinness, O. and Boothby, M. (2011) Glycolytic rate and lymphomagenesis depend on PARP14, an ADP ribosyltransferase of the B aggressive lymphoma (BAL) family. *Proc Natl Acad Sci U S A* 108, 15972-15977.

Cho, S.H., Goenka, S., Henttinen, T., Gudapati, P., Reinikainen, A., Eischen, C.M., Lahesmaa, R. and Boothby, M. (2009) PARP-14, a member of the B aggressive lymphoma family, transduces survival signals in primary B cells. *Blood* 113, 2416-2425.

Choe, S., Bennett, M.J., Fujii, G., Curmi, P.M., Kantardjieff, K.A., Collier, R.J. and Eisenberg, D. (1992) The crystal structure of diphtheria toxin. *Nature* 357, 216-222.

Ciccarone, F., Zampieri, M. and Caiafa, P. (2017) PARP1 orchestrates epigenetic events setting up chromatin domains. *Semin Cell Dev Biol* 63, 123-134.

Citarelli, M., Teotia, S. and Lamb, R.S. (2010) Evolutionary history of the poly(ADP-ribose) polymerase gene family in eukaryotes. *BMC Evol Biol* 10, 308.

Cohen, M. and Petignat, P. (2011) Purified autoantibodies against glucose-regulated protein 78 (GRP78) promote apoptosis and decrease invasiveness of ovarian cancer cells. *Cancer Lett* 309, 104–109.

Colell, A., Green, D.R. and Ricci, J.E. (2009) Novel roles for GAPDH in cell death and carcinogenesis. *Cell Death Differ* 16, 1573-1581.

Cook, B.D., Dynek, J.N., Chang, W., Shostak, G. and Smith, S. (2002) Role for the related poly(ADP-Ribose) polymerases tankyrase 1 and 2 at human telomeres. *Mol Cell Biol* 22, 332–342.

Corda, D. and Di Girolamo, M. (2003) Functional aspects of protein mono-ADPribosylation. *EMBO J* 22, 1953-1958.

Costantini, S., Sharma, A., Raucci, R., Costantini, M., Autiero, I. and Colonna, G. (2013) Genealogy of an ancient protein family: the Sirtuins, a family of disordered members. *BMC Evol Biol* 13, 60.

Cui, W., Li, J., Ron, D. and Sha, B. (2011) The structure of the PERK kinase domain suggests the mechanism for its activation. *Acta Crystallogr D Biol Crystallogr* 67, 423–428.

Curtin, N.J. (2012) Poly(ADP-ribose) polymerase (PARP) and PARP inhibitors. *Drug Discovery Today: Disease Models* 9, e51–e58.

D'Amours, D., Desnoyers, S., D'Silva, I. and Poirier, G.G. (1999) Poly(ADP-ribosyl)ation reactions in the regulation of nuclear functions. *Biochem J* 342, 249-268.

Daneshmand, S., Quek, M.L., Lin, E., Lee, C., Cote, R.J., Hawes, D., Cai. J., Groshen, S., Lieskovsky, G., Skinner, D.G., Lee, A.S. and Pinski, J. (2007) Glucose-regulated protein GRP78 is up-regulated in prostate cancer and correlates with recurrence and survival. *Hum Pathol* 38, 1547-1552.

Dani, N., Barbosa, A.J., Del Rio, A. and Di Girolamo, M. (2013) ADP-Ribosylated Proteins as Old and New Drug Targets for Anticancer Therapy: the Example of ARF6. *Curr Pharm Des* 19, 624-633.

Dani, N., Mayo, E., Stilla, A., Marchegiani, A., Di Paola, S., Corda, D. and Di Girolamo, M. (2011) Mono-ADP-ribosylation of the G protein betagamma dimer is modulated by hormones and inhibited by Arf6. *J Biol Chem* 286, 5995-6005.

Dani, N., Stilla, A., Marchegiani, A., Tamburro, A., Till, S., Ladurner, A.G., Corda, D. and Di Girolamo, M. (2009) Combining affinity purification by ADP-ribose-binding macro domains with mass spectrometry to define the mammalian ADP-ribosyl proteome. *Proc Natl Acad Sci U S A* 106, 4243-4248.

Dantzer, F., Mark, M., Quenet, D., Scherthan, H., Huber, A., Liebe, B., Monaco, L., Chicheportiche, A., Sassone-Corsi, P., de Murcia, G. and Menissier-de Murcia, J. (2006) Poly(ADP-ribose) polymerase-2 contributes to the fidelity of male meiosis I and spermiogenesis. *Proc Natl Acad Sci U S A* 103, 14854-14859.

Daugaard, M., Rohde, M. and Jaattela, M. (2007) The heat shock protein 70 family: Highly homologous proteins with overlapping and distinct functions. *FEBS Lett* 581, 3702-3710.

De Matteis, M.A., Di Girolamo, M., Colanzi, A., Pallas, M., Di Tullio, G., McDonald, L.J., Moss, J., Santini, G., Bannykh, S., Corda, D. and et al. (1994) Stimulation of endogenous ADP-ribosylation by brefeldin A. *Proc Natl Acad Sci U S A* 91, 1114-1118.

de Murcia, G. and Menissier de Murcia, J. (1994) Poly(ADP-ribose) polymerase: a molecular nick-sensor. *Trends Biochem Sci* 19, 172-176.

de Ridder, G.G., Ray, R. and Pizzo, S.V. (2012) A murine monoclonal antibody directed against the carboxylterminal domain of GRP78 suppresses melanoma growth in mice. *Melanoma Res* 22, 225–235.

De Rycker, M., Venkatesan, R.N., Wei, C. and Price, C.M. (2003) Vertebrate tankyrase domain structure and sterile alpha motif (SAM)-mediated multimerization. *Biochem J* 372, 87-96.

De Veer, M.J., Holko, M., Frevel, M., Walker, E., Der, S., Paranjape, J.M., Silverman, R.H. and Williams, B.R. (2001) Functional classification of interferon-stimulated genes identified using microarrays. *J Leukoc Biol* 69, 912–920.

Delpino, A., Piselli, P., Vismara, D., Vendetti, S. and Colizzi, V. (1998) Cell surface localization of the 78 kD glucose regulated protein (GRP 78) induced by thapsigargin. *Mol Membr Biol* 15, 21-26.

Deng, W.G., Ruan, K.H., Du, M., Saunders, M.A., Wu, K.K. (2001) Aspirin and salicylate bind to immunoglobulin heavy chain binding protein (BiP) and inhibit its ATPase activity in human fibroblasts. *FASEB J* 15, 2463–2470.

Denu, J.M. (2005) The Sir 2 family of protein deacetylases. *Curr Opin Chem Biol* 9, 431-440.

Di Girolamo, M., Dani, N., Stilla, A. and Corda, D. (2005) Physiological relevance of the endogenous mono(ADP-ribosyl)ation of cellular proteins. *FEBS J* 272, 4565-4575.

Di Girolamo, M., Silletta, M.G., De Matteis, M.A., Braca, A., Colanzi, A., Pawlak, D., Rasenick, M.M., Luini, A. and Corda, D. (1995) Evidence that the 50-kDa substrate of brefeldin A-dependent ADP-ribosylation binds GTP and is modulated by the G-protein beta gamma subunit complex. *Proc Natl Acad Sci U S A* 92, 7065-7069.

Di Paola, S., Micaroni, M., Di Tullio, G., Buccione, R. and Di Girolamo, M. (2012) PARP16/ARTD15 is a novel endoplasmic-reticulum-associated mono-ADP-ribosyltransferase that interacts with, and modifies karyopherin-β1. *PLoS ONE* 7, e37352.

Di Virgilio, F., Borea, P.A. and Illes, P. (2001) P2 receptors meet the immune system. *Trends Pharmacol Sci* 22, 5-7.

Diani-Moore, S., Ram, P., Li, X., Mondal, P., Youn, D.Y., Sauve, A.A. and Rifkind, A.B. (2010) Identification of the aryl hydrocarbon receptor target gene TiPARP as a mediator of suppression of hepatic gluconeogenesis by 2,3,7,8-tetrachlorodibenzo-p-dioxin and of nicotinamide as a corrective agent for this effect. *J Biol Chem* 285, 38801-38810.

Diani-Moore, S., Zhang, S., Ram, P. and Rifkind, A.B. (2013) Aryl hydrocarbon receptor activation by dioxin targets phosphoenolpyruvate carboxykinase (PEPCK) for ADP-ribosylation via 2,3,7,8-tetrachlorodibenzo-p-dioxin (TCDD)-inducible poly(ADP-ribose) polymerase (TiPARP). *J Biol Chem* 288, 21514-21525.

DiDonato, J.A., Mercurio, F. and Karin, M. (2012) NF-kappaB and the link between inflammation and cancer. *Immunol Rev* 246, 379-400.

Diefenbach, J. and Burkle, A. (2005) Introduction to poly(ADP-ribose) metabolism. *Cell Mol Life Sci* 62, 721-730.

Domenighini, M. and Rappuoli, R. (1996) Three conserved consensus sequences identify the NAD-binding site of ADP-ribosylating enzymes, expressed by eukaryotes, bacteria and T-even bacteriophages. *Mol Microbiol* 21, 667-674.

Domenighini, M., Magagnoli, C., Pizza, M. and Rappuoli, R. (1994) Common features of the NAD-binding and catalytic site of ADP-ribosylating toxins. *Mol Microbiol* 14, 41-50.

Donadini, A., Rosano, C., Felli, L. and Ponassi, M. (2013) Human sirtuins: an overview of an emerging drug target in age-related diseases and cancer. *Curr Drug Targets* 14, 653-661.

Donaldson, J.G. (2003) Multiple roles for Arf6: sorting, structuring, and signaling at the plasma membrane. *J Biol Chem* 278, 41573-41576.

Dong, D., Dubeau, L., Bading, J., Nguyen, K., Luna, M., Yu, H., Gazit-Bornstein, G., Gordon, E.M., Gomer, C., Hall, F.L., Gambhir, S.S. and Lee, A.S. (2004) Spontaneous and controllable activation of suicide gene expression driven by the stress-inducible grp78 promoter resulting in eradication of sizable human tumors. *Hum Gene Ther* 15, 553-561.

Dong, D., Stapleton, C., Luo, B., Xiong, S., Ye, W., Zhang, Y., Jhaveri, N., Zhu, G., Ye, R., Liu, Z., Bruhn, K.W., Craft, N., Groshen, S., Hofman, F.M. and Lee, A.S. (2011) A

critical role for GRP78/BiP in the tumor microenvironment for neovascularization during tumor growth and metastasis. *Cancer Res* 71, 2848-2857.

Druzhyna, N., Smulson, M.E., LeDoux, S.P. and Wilson, G.L. (2000) Poly(ADP-ribose) polymerase facilitates the repair of N-methylpurines in mitochondrial DNA. *Diabetes* 49, 1849–1855.

D'Souza-Schorey, C. and Chavrier, P. (2006) ARF proteins: roles in membrane traffic and beyond. *Nat Rev Mol Cell Biol* 7, 347-358.

Du, X., Matsumura, T., Edelstein, D., Rossetti, L., Zsengellér, Z., Szabó, C. and Brownlee, M. (2003) Inhibition of GAPDH activity by poly(ADP-ribose) polymerase activates three major pathways of hyperglycemic damage in endothelial cells. *J Clin Invest* 112, 1049-1057.

Dulaney, C., Marcrom, S., Stanley, J. and Yang, E.S. (2017) Poly(ADP-ribose) polymerase activity and inhibition in cancer. *Semin Cell Dev Biol* 63, 144-153.

Eckei, L., Krieg, S., Butepage, M., Lehmann, A., Gross, A., Lippok, B., Grimm, A.R., Kummerer, B.M., Rossetti, G., Luscher, B. and Verheugd, P. (2017) The conserved macrodomains of the non-structural proteins of Chikungunya virus and other pathogenic positive strand RNA viruses function as mono-ADP-ribosylhydrolases. *Sci Rep* 7, 41746.

Eckei, L., S.W., Kim, J.E., Park, K.S., Choi, W.J., Hong, Y.H., Kim, S.M., Kim, S.H., Lee, K.W. and Sung, J.J. (2012) The neuroprotective effect of the GSK-3beta inhibitor and influence on the extrinsic apoptosis in the ALS transgenic mice. *J Neurol Sci* 320, 1-5.

Eisemann, T., McCauley, M., Langelier, M.F., Gupta, K., Roy, S., Van Duyne, G.D., Pascal, J.M. (2016) Tankyrase-1 Ankyrin Repeats Form an Adaptable Binding Platform for Targets of ADP-Ribose Modification. *Structure* 24, 1679-1692.

Ellgaard, L. and Helenius, A. (2003) Quality control in the endoplasmic reticulum. *Nat Rev Mol Cell Biol* 4, 181–191.

Ermakova, S.P., Kang, B.S., Choi, B.Y., Choi, H.S., Schuster, T.F., Ma, W.Y., Bode, A.M. and Dong, Z. (2006) (-)-Epigallocatechin gallate overcomes resistance to etoposide-induced cell death by targeting the molecular chaperone glucose-regulated protein 78. *Cancer Res* 66, 9260-9269.

Eustermann, S., Brockmann, C., Mehrotra, P.V., Yang, J.C., Loakes, D., West, S.C., Ahel, I. and Neuhaus, D. (2010) Solution structures of the two PBZ domains from human APLF and their interaction with poly(ADP-ribose). *Nat Struct Mol Biol* 17, 241-243.

Fabrizio, G., Di Paola, S., Stilla, A., Giannotta, M., Ruggiero, C., Menzel, S., Koch-Nolte, F., Sallese, M. and Di Girolamo, M. (2015b) ARTC1-mediated ADP-ribosylation of GRP78/BiP: a new player in endoplasmic-reticulum stress responses. *Cell Mol Life Sci* 72,1209-1225.

Fabrizio, G., Scarpa, E.S. and Di Girolamo, M. (2015a) State of the art of protein mono-ADP-ribosylation: biological role and therapeutic potential. *Front Biosci* 20, 405-430.

Feijs, K.L., Forst, A.H., Verheugd, P. and Luscher, B. (2013c) Macrodomain-containing proteins: regulating new intracellular functions of mono(ADP-ribosyl)ation. *Nat Rev Mol Cell Biol* 14, 443-451.

Feijs, K.L., Kleine, H., Braczynski, A., Forst, A.H., Herzog, N., Verheugd, P., Linzen, U., Kremmer, E. and Luscher, B. (2013b) ARTD10 substrate identification on protein microarrays: regulation of GSK3beta by mono-ADP-ribosylation. *Cell Commun Signal* 11, 5.

Feijs, K.L., Verheugd, P. and Luscher, B. (2013a) Expanding functions of intracellular resident mono-ADP-ribosylation in cell physiology. *FEBS J* 280, 3519-29.

Fendrick, J.L., Iglewski, W.J., Moehring, J.M. and Moehring, T.J. (1992) Characterization of the endogenous ADP-ribosylation of wild-type and mutant elongation factor 2 in eukaryotic cells. *Eur J Biochem* 205, 25-31.

Feng, Y., Yu, S., Lasell, T.K., Jadhav, A.P., Macia, E., Chardin, P., Melancon, P., Roth, M., Mitchison, T. and Kirchhausen, T. (2003) Exo1: a new chemical inhibitor of the exocytic pathway. *Proc Natl Acad Sci U S A* 100, 6469-6474.

Fernandez, P.M., Tabbara, S.O., Jacobs, L.K., Manning, F.C., Tsangaris, T.N., Schwartz, A.M., Kennedy, K.A. and Patierno, S.R. (2000) Overexpression of the glucose-regulated stress gene GRP78 in malignant but not benign human breast lesions. *Breast Cancer Res Treat* 59, 15-26.

Ferreyra, G.A., Elinoff, J.M., Demirkale, C.Y., Starost, M.F., Buckley, M., Munson, P.J., Krakauer, T. and Danner, R.L. (2014) Late multiple organ surge in interferon-regulated target genes characterizes staphylococcal enterotoxin B lethality. *PLoS One* 9, e88756.

Flick, F. and Luscher, B. (2012) Regulation of sirtuin function by posttranslational modifications. *Front Pharmacol* 3, 29.

Flynn, G.C., Pohl, J., Flocco, M.T. and Rothman, J.E. (1991) Peptidebinding specificity of the molecular chaperone BiP. *Nature* 353, 726–730.

Forst, A.H., Karlberg, T., Herzog, N., Thorsell, A.G., Gross, A., Feijs, K.L., Verheugd, P., Kursula, P., Nijmeijer, B., Kremmer, E., Kleine, H., Ladurner, A. G., Schuler, H. and Luscher, B. (2013) Recognition of mono-ADP-ribosylated ARTD10 substrates by ARTD8 macrodomains. *Structure* 21, 462-475.

Friedrich, M., Grahnert, A., Paasch, U., Tannapfel, A., Koch-Nolte, F. and Hauschildt, S. (2006) Expression of toxin-related human mono-ADP-ribosyltransferase 3 in human testes. *Asian J Androl* 8, 281-287.

Frye, R.A. (1999) Characterization of five human cDNAs with homology to the yeast SIR2 gene: Sir2-like proteins (sirtuins) metabolize NAD and may have protein ADPribosyltransferase activity. *Biochem Biophys Res Commun* 260, 273-279.

Frye, R.A. (2000) Phylogenetic classification of prokaryotic and eukaryotic Sir2-like proteins. *Biochem Biophys Res Commun* 273, 793-798.

Fu, Y. and Lee, A.S. (2006) Glucose regulated proteins in cancer progression, drug resistance and immunotherapy. *Cancer Biol Ther* 5, 741-744.

Gabelli, S.B., Bianchet, M.A., Bessman, M.J. and Amzel, L.M. (2001) The structure of ADP-ribose pyrophosphatase reveals the structural basis for the versatility of the Nudix family. *Nat Struct Biol* 8, 467-472.

Gagne, J.P., Isabelle, M., Lo, K.S., Bourassa, S., Hendzel, M.J., Dawson, V.L., Dawson, T.M. and Poirier, G.G. (2008) Proteome-wide identification of poly(ADP-ribose) binding proteins and poly(ADP-ribose)-associated protein complexes. *Nucleic Acids Res* 36, 6959-6976.

Gao, G., Guo, X. and Goff, S. P. (2002) Inhibition of retroviral RNA production by ZAP, a CCCH-type zinc finger protein. *Science* 297, 1703-6.

Gardner, B.M., Pincus, D., Gotthardt, K., Gallagher, C.M. and Walter, P. (2013) Endoplasmic Reticulum Stress Sensing in the Unfolded Protein Response. *Cold Spring Harb Perspect Biol* 5, a013169.

Gertz, M. and Steegborn, C. (2010) Function and regulation of the mitochondrial sirtuin isoform Sirt5 in Mammalia. *Biochim Biophys Acta* 1804, 1658-1665.

Ghosh, R., Roy, S., Kamyab, J., Danzter, F. and Franco, S. (2016) Common and Unique Genetic Interactions of the Poly(ADP-ribose) Polymerases PARP1 and PARP2 with DNA Double-Strand Break Repair Pathways. *DNA Repair* (Amst) 45, 56–62.

Gibson, B.A. and Kraus, W.L. (2012) New insights into the molecular and cellular functions of poly(ADP-ribose) and PARPs. *Nat Rev Mol Cell Biol* 13, 411-424.

Ginsburg, O., Bray, F., Coleman, M.P., Vanderpuye, V., Eniu, A., Kotha, S.R., Sarker, M., Huong, T.T., Allemani, C., Dvaladze, A., Gralow, J., Yeates, K., Taylor, C., Oomman, N., Krishnan, S., Sullivan, R., Kombe, D., Blas, M.M., Parham, G., Kassami, N. and Conteh, L. (2017) The global burden of women's cancers: a grand challenge in global health. *Lancet* 389, 847-860.

Glowacki, G., Braren, R., Cetkovic-Cvrlje, M., Leiter, E.H., Haag, F. and Koch-Nolte, F. (2001) Structure, chromosomal localization, and expression of the gene for mouse ecto-mono(ADP-ribosyl)transferase ART5. *Gene* 275, 267-277.

Glowacki, G., Braren, R., Firner, K., Nissen, M., Kuhl, M., Reche, P., Bazan, F., Cetkovic-Cvrlje, M., Leiter, E., Haag, F. and Koch-Nolte, F. (2002) The family of toxin-related ecto-ADP-ribosyltransferases in humans and the mouse. *Protein Sci* 11, 1657-1670.

Goenka, S. and Boothby, M. (2006) Selective potentiation of Stat-dependent gene expression by collaborator of Stat6 (CoaSt6), a transcriptional cofactor. *Proc Natl Acad Sci U S A* 103, 4210-5.

Goenka, S., Cho, S.H. and Boothby, M. (2007) Collaborator of Stat6 (CoaSt6)-associated poly(ADP-ribose) polymerase activity modulates Stat6-dependent gene transcription. *J Biol Chem* 282, 18732-9.

Goff, C.G. (1974) Chemical structure of a modification of the Escherichia coli ribonucleic acid polymerase alpha polypeptides induced by bacteriophage T4 infection. *J Biol Chem* 249, 6181-6190.

Gorlach, A., Klappa, P. and Kietzmann, T. (2006) The endoplasmic reticulum: folding, calcium homeostasis, signaling, and redox control. *Antioxid Redox Signal* 8, 1391-1418.

Gottschalk, A.J., Timinszky, G., Kong, S.E., Jin, J., Cai, Y., Swanson, S.K., Washburn, M.P., Florens, L., Ladurner, A.G., Conaway, J.W. and Conaway, R.C. (2009) Poly(ADP-ribosyl)ation directs recruitment and activation of an ATP-dependent chromatin remodeler. *Proc Natl Acad Sci U S A* 106, 13770-13774.

Grahnert, A., Friedrich, M., Pfister, M., Haag, F., Koch-Nolte, F. and Hauschildt, S. (2002) Mono-ADP-ribosyltransferases in human monocytes: regulation by lipopolysaccharide. *Biochem J* 362, 717-723.

Greiner, D.L., Mordes, J.P., Handler, E.S., Angelillo, M., Nakamura, N. and Rossini, A.A. (1987) Depletion of RT6.1+ T lymphocytes induces diabetes in resistant biobreeding/Worcester (BB/W) rats. *J Exp Med* 166, 461-475.

Grootjans, J., Kaser, A., Kaufman, R.J. and Blumberg, R.S. (2016) The unfolded protein response in immunity and inflammation. *Nat Rev Immunol* 16, 469–484.

Grubisha, O., Smith, B.C. and Denu, J.M. (2005) Small molecule regulation of Sir2 protein deacetylases. *FEBS J* 272, 4607-4616.

Guo, C., Liu, S. and Sun, M.Z. (2013) Novel insight into the role of GAPDH playing in tumor. *Clin Transl Oncol* 15, 167-172.

Guo, X., Carroll, J.W., Macdonald, M.R., Goff, S.P. and Gao, G. (2004) The zinc finger antiviral protein directly binds to specific viral mRNAs through the CCCH zinc finger motifs. *Journal of virology* 78, 12781-12787.

Guo, X., Ma, J., Sun, J. and Gao, G. (2007) The zinc-finger antiviral protein recruits the RNA processing exosome to degrade the target mRNA. *Proc Natl Acad Sci U S A* 104, 151-156.

Gupte, R., Liu, Z. and Kraus, W.L. (2017) PARPs and ADP-ribosylation: recent advances linking molecular functions to biological outcomes. Genes Dev 31, 101–126.

Gutierrez, T. and Simmen, T. (2014) Endoplasmic Reticulum Chaperones and Oxidoreductases: Critical Regulators of Tumor Cell Survival and Immunorecognition. *Front Oncol* 4, 291.

Haag, F., Koch, F. and Thiele, H.G. (1990) Nucleotide and deduced amino acid sequence of the rat T-cell alloantigen RT6.1. *Nucleic Acids Res* 18, 1047.

Haag, F., Koch-Nolte, F., Kuhl, M., Lorenzen, S. and Thiele, H.G. (1994) Premature stop codons inactivate the RT6 genes of the human and chimpanzee species. *J Mol Biol* 243, 537-546.

Haag, F.A., Kuhlenbaumer, G., Koch-Nolte, F., Wingender, E. and Thiele, H.G. (1996) Structure of the gene encoding the rat T cell ecto-ADP-ribosyltransferase RT6. *J Immunol* 157, 2022-2030.

Haigis, M.C. and Guarente, L.P. (2006) Mammalian sirtuins--emerging roles in physiology, aging, and calorie restriction. *Genes Dev* 20, 2913-2921.

Haigis, M.C., Mostoslavsky, R., Haigis, K.M., Fahie, K., Christodoulou, D.C., Murphy, A.J., Valenzuela, D.M., Yancopoulos, G.D., Karow, M., Blander, G., Wolberger, C., Prolla, T.A., Weindruch, R., Alt, F.W. and Guarente, L. (2006) SIRT4 inhibits glutamate dehydrogenase and opposes the effects of calorie restriction in pancreatic beta cells. *Cell* 126, 941-954.

Haikarainen, T., Krauss, S. and Lehtio, L. (2014) Tankyrases: structure, function and therapeutic implications in cancer. *Curr Pharm Des* 20, 6472-6488.

Hall, T.M. (2005) Multiple modes of RNA recognition by zinc finger proteins. *Curr Opin Struct Biol* 15, 367-373.

Han, S. and Tainer, J.A. (2002) The ARTT motif and a unified structural understanding of substrate recognition in ADP-ribosylating bacterial toxins and eukaryotic ADP-ribosyltransferases. *Int J Med Microbiol* 291, 523-529.

Han, S., Arvai, A.S., Clancy, S.B. and Tainer, J.A. (2001) Crystal structure and novel recognition motif of rho ADP-ribosylating C3 exoenzyme from Clostridium botulinum: structural insights for recognition specificity and catalysis. *J Mol Biol* 305, 95-107.

Han, S., Craig, J.A., Putnam, C.D., Carozzi, N.B. and Tainer, J.A. (1999) Evolution and mechanism from structures of an ADP-ribosylating toxin and NAD complex. *Nat Struct Biol* 6, 932-936.

Han, W., Li, X. and Fu, X. (2011) The macro domain protein family: structure, functions, and their potential therapeutic implications. *Mutat Res* 727, 86-103.

Hara, N., Tsuchiya, M. and Shimoyama, M. (1996) Glutamic acid 207 in rodent T-cell RT6 antigens is essential for arginine-specific ADP-ribosylation. *J Biol Chem* 271, 29552-29555.

Harding, H.P., Novoa, I., Zhang, Y., Zeng, H., Wek, R., Schapira, M. and Ron, D. (2000) Regulated translation initiation controls stress-induced gene expression in mammalian cells. *Mol Cell* 6, 1099-1108.

Harding, H.P., Zhang, Y. and Ron, D. (1999) Protein translation and folding are coupled by an endoplasmic-reticulum-resident kinase. *Nature*, 379, 271-274.

Harding, H.P., Zhang, Y., Zeng, H., Novoa, I., Lu, P.D., Calfon, M., Sadri, N., Yun, C., Popko, B., Paules, R., Stojdl, D.F., Bell, J.C., Hettmann, T., Leiden, J.M. and Ron, D. (2003) An integrated stress response regulates amino acid metabolism and resistance to oxidative stress. *Mol Cell* 11, 619-633.

Hassa, P.O. and Hottiger, M.O. (2008) The diverse biological roles of mammalian PARPS, a small but powerful family of poly-ADP-ribose polymerases. *Front Biosci* 13, 3046-3082.

Hassa, P.O., Haenni, S.S., Elser, M. and Hottiger, M.O. (2006) Nuclear ADP-ribosylation reactions in mammalian cells: where are we today and where are we going? *Microbiol Mol Biol Rev* 70, 789-829.

Hawse, W.F. and Wolberger, C. (2009) Structure-based mechanism of ADP-ribosylation by sirtuins. *J Biol Chem* 284, 33654-33661.

Hayakawa, S., Shiratori, S., Yamato, H., Kameyama, T., Kitatsuji, C., Kashigi, F., Goto, S., Kameoka, S., Fujikura, D., Yamada, T., Mizutani, T., Kazumata, M., Sato, M., Tanaka, J., Asaka, M., Ohba, Y., Miyazaki, T., Imamura, M. and Takaoka, A. (2011) ZAPS is a potent stimulator of signaling mediated by the RNA helicase RIG-I during antiviral responses. *Nat Immunol* 12, 37-44.

Haze, K., Yoshida, H., Yanagi, H., Yura, T. and Mori, K. (1999) Mammalian transcription factor ATF6 is synthesized as a transmembrane protein and activated by proteolysis in response to endoplasmic reticulum stress. *Mol Biol Cell* 10, 3787-3799.

He, F., Tsuda, K., Takahashi, M., Kuwasako, K., Terada, T., Shirouzu, M., Watanabe, S., Kigawa, T., Kobayashi, N., Guntert, P., Yokoyama, S. and Muto, Y. (2012) Structural insight into the interaction of ADP-ribose with the PARP WWE domains. *FEBS Lett* 586, 3858-3864.

Hensel, F., Eckstein, M., Rosenwald, A., Brandlein, S. (2013) Early development of PAT-SM6 for the treatment of melanoma. *Melanoma Res* 23, 264–275.

Herrero-Yraola, A., Bakhit, S.M., Franke, P., Weise, C., Schweiger, M., Jorcke, D. and Ziegler, M. (2001) Regulation of glutamate dehydrogenase by reversible ADPribosylation in mitochondria. *EMBO J* 20, 2404-2412.

Herzog, N., Hartkamp, J.D., Verheugd, P., Treude, F., Forst, A.H., Feijs, K.L., Lippok, B. E., Kremmer, E., Kleine, H. and Luscher, B. (2013) Caspase-dependent cleavage

of the mono-ADP-ribosyltransferase ARTD10 interferes with its pro-apoptotic function. *FEBS J* 280, 1330-1343.

Hetz, C. (2012) The unfolded protein response: controlling cell fate decisions under ER stress and beyond. *Nat Rev Mol Cell Biol* 13, 89-102.

Hinnebusch, A.G. (1994) The eIF-2 alpha kinases: regulators of protein synthesis in starvation and stress. *Semin Cell Biol* 5, 417-426.

Hitomi, J., Katayama, T., Eguchi, Y., Kudo, T., Taniguchi, M., Koyama, Y., Manabe, T., Yamagishi, S., Bando, Y., Imaizumi, K., Tsujimoto, Y. and Tohyama, M. (2004) Involvement of caspase-4 in endoplasmic reticulum stress-induced apoptosis and Abeta-induced cell death. *J Cell Biol* 165, 347-356.

Holbourn, K.P., Shone, C.C. and Acharya, K.R. (2006) A family of killer toxins. Exploring the mechanism of ADP-ribosylating toxins. *FEBS J* 273, 4579-4593.

Honda, A., Nogami, M., Yokozeki, T., Yamazaki, M., Nakamura, H., Watanabe, H., Kawamoto, K., Nakayama, K., Morris, A.J., Frohman, M.A. and Kanaho, Y. (1999) Phosphatidylinositol 4-phosphate 5-kinase alpha is a downstream effector of the small G protein ARF6 in membrane ruffle formation. *Cell* 99, 521-532.

Hong, S., Brass, A., Seman, M., Haag, F., Koch-Nolte, F. and Dubyak, G. R. (2009) Basal and inducible expression of the thiol-sensitive ART2.1 ecto-ADP-ribosyltransferase in myeloid and lymphoid leukocytes. *Purinergic Signal* 5, 369-383.

Honjo, T., Nishizuka, Y. and Hayaishi, O. (1968) Diphtheria toxin-dependent adenosine diphosphate ribosylation of aminoacyl transferase II and inhibition of protein synthesis. *J Biol Chem* 243, 3553-3555.

Hottiger, M.O. (2011) ADP-ribosylation of histones by ARTD1: an additional module of the histone code? *FEBS Lett* 585, 1595-1599.

Hottiger, M.O. (2015) SnapShot: ADP-Ribosylation Signaling. *Mol Cell* 58, 1134-1134.

Hottiger, M.O., Hassa, P.O., Luscher, B., Schuler, H. and Koch-Nolte, F. (2010) Toward a unified nomenclature for mammalian ADP-ribosyltransferases. *Trends Biochem Sci* 35, 208-219.

Hsiao, S.J. and Smith, S. (2008) Tankyrase function at telomeres, spindle poles, and beyond. *Biochimie* 90, 83-92.

Hsu, W.M., Hsieh, F.J., Jeng, Y.M., Kuo, M.L., Tsao, P.N., Lee, H., Lin, M.T., Lai, H.S., Chen, C.N., Lai, D.M. and Chen, W.J. (2005) GRP78 expression correlates with histologic differentiation and favorable prognosis in neuroblastic tumors. *Int J Cancer* 113, 920-927.

Huang, H.Y., Graves, D.J., Robson, R.M. and Huiatt, T.W. (1993) ADP-ribosylation of the intermediate filament protein desmin and inhibition of desmin assembly in vitro by muscle ADP-ribosyltransferase. *Biochem Biophys Res Commun* 197, 570-577.

Hwang, T.C. and Sheppard, D.N. (2009) Gating of the CFTR Cl- channel by ATP-driven nucleotide-binding domain dimerisation. *J Physiol* 587, 2151–2161.

Iurlaro, R. and Munoz-Pinedo, C. (2016) Cell death induced by endoplasmic reticulum stress. *FEBS J* 283, 2640-2652.

Jacobson, M.K. and Jacobson, E.L. (1999) Discovering new ADP-ribose polymer cycles: protecting the genome and more. *Trends Biochem Sci* 24, 415-417.

Jamora, C., Dennert, G. and Lee, A.S. (1996) Inhibition of tumor progression by suppression of stress protein GRP78/BiP induction in fibrosarcoma B/C10ME. *Proc Natl Acad Sci U S A* 93, 7690-7694.

Jankevicius, G., Hassler, M., Golia, B., Rybin, V., Zacharias, M., Timinszky, G. and Ladurner, A.G. (2013) A family of macrodomain proteins reverses cellular mono-ADP-ribosylation. *Nat Struct Mol Biol* 20, 508-514.

Jiang, D., Niwa, M. and Koong, A.C. (2015) Targeting the IRE1α-XBP1 Branch of the Unfolded Protein Response in Human Diseases. *Semin Cancer Biol* 33, 48–56.

Jones, E.M. and Baird, A. (1997) Cell-surface ADP-ribosylation of fibroblast growth factor-2 by an arginine-specific ADP-ribosyltransferase. *Biochem J* 323, 173-177.

Jorcke, D., Ziegler, M., Herrero-Yraola, A. and Schweiger, M. (1998) Enzymic, cysteine-specific ADP-ribosylation in bovine liver mitochondria. *Biochem J* 332, 189-193.

Jungmichel, S., Rosenthal, F., Altmeyer, M., Lukas, J., Hottiger, M.O. and Nielsen, M.L. (2013) Proteome-wide identification of poly(ADP-Ribosyl)ation targets in different genotoxic stress responses. *Mol Cell* 52, 272-285.

Justus, C.R., Sanderlin, E.J. and Yang, L.V. (2015) Molecular Connections between Cancer Cell Metabolism and the Tumor Microenvironment. *Int J Mol Sci* 16, 11055–11086.

Juszczynski, P., Kutok, J.L., Li, C., Mitra, J., Aguiar, R.C. and Shipp, M.A. (2006) BAL1 and BBAP are regulated by a gamma interferon-responsive bidirectional promoter and are overexpressed in diffuse large B-cell lymphomas with a prominent inflammatory infiltrate. *Mol Cell Biol* 26, 5348-5359.

Jwa, M. and Chang, P. (2012) PARP16 is a tail-anchored endoplasmic reticulum protein required for the PERK- and IRE1alpha-mediated unfolded protein response. *Nat Cell Biol* 14, 1223-1230.

Kahali, S., Sarcar, B., Fang, B., Williams, E.S., Koomen, J.M., Tofilon, P.J. and Chinnaiyan, P. (2010) Activation of the unfolded protein response contributes toward the antitumor activity of vorinostat. *Neoplasia* 12, 80-86.

Kaminker, P.G., Kim, S.H., Taylor, R.D., Zebarjadian, Y., Funk, W.D., Morin, G.B., Yaswen, P. and Campisi, J. (2001) TANK2, a new TRF1-associated poly(ADP-ribose) polymerase, causes rapid induction of cell death upon overexpression. *J Biol Chem* 276, 35891-35899.

Kanno, S., Kuzuoka, H., Sasao, S., Hong, Z., Lan, L., Nakajima, S., Yasui, A. (2007) A novel human AP endonuclease with conserved zinc-finger-like motifs involved in DNA strand break responses. *EMBO J* 26, 2094-2103.

Karagiannis, T.C. and Ververis, K. (2012) Potential of chromatin modifying compounds for the treatment of Alzheimer's disease. *Pathobiol Aging Age Relat Dis*, 2.

Karlberg, T., Langelier, M.F., Pascal, J.M. and Schuler, H. (2013) Structural biology of the writers, readers, and erasers in mono- and poly(ADP-ribose) mediated signaling. *Mol Aspects Med* 34, 1088-1108.

Karlberg, T., Thorsell, A.G., Kallas, A. and Schuler, H. (2012) Crystal structure of human ADP-ribose transferase ARTD15/PARP16 reveals a novel putative regulatory domain. *J Biol Chem* 287, 24077-81.

Karras, G.I., Kustatscher, G., Buhecha, H.R., Allen, M.D., Pugieux, C., Sait, F., Bycroft, M. and Ladurner, A.G. (2005) The macro domain is an ADP-ribose binding module. *EMBO J* 24, 1911-1920.

Kato, J., Zhu, J., Liu, C., Stylianou, M., Hoffmann, V., Lizak, M. J., Glasgow, C.G. and Moss, J. (2011) ADP-ribosylarginine hydrolase regulates cell proliferation and tumorigenesis. *Cancer Res* 71, 5327-5335.

Kaufman, R.J., (1999) Stress signaling from the lumen of the endoplasmic reticulum: coordination of gene transcriptional and translational controls. *Genes Dev* 13, 1211–1233.

Kaufmann, M., Feijs, K.L. and Luscher, B. (2016) Function and regulation of the mono-ADP-ribosyltransferase ARTD10. *Curr Top Microbiol Immunol* 384, 178-188.

Kelber, J.A., Panopoulos, A.D., Shani, G., Booker, E.C., Belmonte, J.C., Vale, W.W. and Gray, P.C. (2009) Blockade of Cripto binding to cell surface GRP78 inhibits oncogenic Cripto signaling via MAPK/PI3K and Smad2/3 pathways. *Oncogene* 28, 2324-2336.

Khoury, G.A., Baliban, R.C. and Floudas, C.A. (2011) Proteome-wide post-translational modification statistics: frequency analysis and curation of the swiss-prot database. *Sci Rep* 1, 90.

Kickhoefer, V.A., Siva, A.C., Kedersha, N.L., Inman, E.M., Ruland, C., Streuli, M. and Rome, L.H. (1999) The 193-kD vault protein, VPARP, is a novel poly(ADP-ribose) polymerase. *J Cell Biol* 146, 917-928.

Kim, G., Ison, G., McKee, A.E., Zhang, H., Tang, S., Gwise, T., Sridhara, R., Lee, E., Tzou, A., Philip, R., Chiu, H.J., Ricks, T.K., Palmby, T., Russell, A.M., Ladouceur, G., Pfuma, E., Li, H., Zhao, L., Liu, Q., Venugopal, R., Ibrahim, A. and Pazdur, R. (2015) FDA Approval Summary: Olaparib Monotherapy in Patients with Deleterious Germline BRCA-Mutated Advanced Ovarian Cancer Treated with Three or More Lines of Chemotherapy. *Clin Cancer Res* 21, 4257-4261.

Kim, M.Y., Zhang, T. and Kraus, W.L. (2005) Poly(ADP-ribosyl)ation by PARP-1: 'PAR-laying' NAD+ into a nuclear signal. *Genes Dev* 19, 1951-1967.

Kleine, H. and Luscher, B. (2009) Learning how to read ADP-ribosylation. *Cell* 139, 17-19.

Kleine, H., Herrmann, A., Lamark, T., Forst, A.H., Verheugd, P., Luscher-Firzlaff, J., Lippok, B., Feijs, K.L., Herzog, N., Kremmer, E., Johansen, T., Muller-Newen, G. and Luscher, B. (2012) Dynamic subcellular localization of the mono-ADP-

ribosyltransferase ARTD10 and interaction with the ubiquitin receptor p62. *Cell Commun Signal* 10, 28.

Kleine, H., Poreba, E., Lesniewicz, K., Hassa, P.O., Hottiger, M.O., Litchfield, D.W., Shilton, B.H. and Luscher, B. (2008) Substrate-assisted catalysis by PARP10 limits its activity to mono-ADP-ribosylation. *Mol Cell* 32, 57-69.

Ko, H.L. and Ren, E.C. (2012) Functional Aspects of PARP1 in DNA Repair and Transcription. *Biomolecules*, 2, 524–548.

Koch-Nolte, F., Duffy, T., Nissen, M., Kahl, S., Killeen, N., Ablamunits, V., Haag, F. and Leiter, E.H. (1999) A new monoclonal antibody detects a developmentally regulated mouse ecto-ADP-ribosyltransferase on T cells: subset distribution, inbred strain variation, and modulation upon T cell activation. *J Immunol* 163, 6014-6022.

Koch-Nolte, F., Haag, F., Braren, R., Kuhl, M., Hoovers, J., Balasubramanian, S., Bazan, F. and Thiele, H.G. (1997) Two novel human members of an emerging mammalian gene family related to mono-ADP-ribosylating bacterial toxins. *Genomics* 39, 370-376.

Koch-Nolte, F., Kernstock, S., Mueller-Dieckmann, C., Weiss, M.S. and Haag, F. (2008) Mammalian ADP-ribosyltransferases and ADP-ribosylhydrolases. *Front Biosci* 13, 6716-6729.

Koch-Nolte, F., Petersen, D., Balasubramanian, S., Haag, F., Kahlke, D., Willer, T., Kastelein, R., Bazan, F. and Thiele, H.G. (1996) Mouse T cell membrane proteins Rt6-1 and Rt6-2 are arginine/protein mono(ADPribosyl)transferases and share secondary structure motifs with ADP-ribosylating bacterial toxins. *J Biol Chem* 271, 7686-7693.

Koh, D.W., Dawson, T.M. and Dawson, V.L. (2005) Mediation of cell death by poly(ADP-ribose)polymerase-1. *Pharmacol Res* 52, 5-14.

Kokame, K., Kato, H. and Miyata, T. (2001) Identification of ERSE-II, a new cis-acting element responsible for the ATF6-dependent mammalian unfolded protein response. *J Biol Chem* 276, 9199-9205.

Konczalik, P. and Moss, J. (1999) Identification of critical, conserved vicinal aspartate residues in mammalian and bacterial ADP-ribosylarginine hydrolases. *J Biol Chem* 274, 16736-16740.

Koomagi, R., Mattern, J. and Volm, M. (1999) Glucose-related protein (GRP78) and its relationship to the drug-resistance proteins P170, GST-pi, LRP56 and angiogenesis in non-small cell lung carcinomas. *Anticancer Res* 19, 4333-4336.

Kraus, W.L. and Hottiger, M.O. (2013) PARP-1 and gene regulation: progress and puzzles. *Mol Aspects Med* 34, 1109-1123.

Krishna, S.S., Majumdar, I. and Grishin, N.V. (2003) Structural classification of zinc fingers: survey and summary. *Nucleic Acids Res* 31, 532-550.

Kuimov, A.N., Kuprash, D.V., Petrov, V.N., Vdovichenko, K.K., Scanlan, M.J., Jongeneel, C.V., Lagarkova, M.A. and Nedospasov, S.A. (2001) Cloning and characterization of TNKL, a member of tankyrase gene family. *Genes Immun* 2, 52-55.

Kumar, C., Rani, N., Velan Lakshmi, P.T. and Arunachalam, A. (2017) A comprehensive look of poly(ADP-ribose) polymerase inhibition strategies and future directions for cancer therapy. *Future Med Chem* 9, 37-60.

Kupis, W., Pałyga, J., Tomal, E. and Niewiadomska, E. (2016) The role of sirtuins in cellular homeostasis. *J Physiol Biochem* 72, 371–380.

Kutuzov, M.M., Khodyreva, S.N., Ame, J.C., Ilina, E.S., Sukhanova, M.V., Schreiber, V. and Lavrik, O.I. (2013) Interaction of PARP-2 with DNA structures mimicking DNA repair intermediates and consequences on activity of base excision repair proteins. *Biochimie* 95, 1208–1215.

Laing, S., Unger, M., Koch-Nolte, F. and Haag, F. (2011) ADP-ribosylation of arginine. Amino Acids 41, 257-269.

Laitusis, A.L., Brostrom, M.A. and Brostrom, C.O. (1999) The dynamic role of GRP78/BiP in the coordination of mRNA translation with protein processing. *J Biol Chem* 274, 486–493.

Langelier, M.F. and Pascal, J.M. (2013) PARP-1 mechanism for coupling DNA damage detection to poly(ADP-ribose) synthesis. *Curr Opin Struct Biol* 23, 134-143.

Langelier, M.F., Planck, J.L., Roy, S. and Pascal, J.M. (2011) Crystal structures of poly(ADP-ribose) polymerase-1 (PARP-1) zinc fingers bound to DNA: structural and functional insights into DNA-dependent PARP-1 activity. *J Biol Chem* 286, 10690–10701.

Langelier, M.F., Planck, J.L., Roy, S. and Pascal, J.M. (2012) Structural basis for DNA damage-dependent poly(ADP-ribosyl)ation by human PARP-1. *Science* 336, 728-32.

Langelier, M.F., Riccio, A.A. and Pascal, J.M. (2014) PARP-2 and PARP-3 are selectively activated by 5′ phosphorylated DNA breaks through an allosteric regulatory mechanism shared with PARP-1. *Nucleic Acids Res* 42, 7762–7775.

Langelier, M.F., Ruhl, D.D., Planck, J.L., Kraus, W.L. and Pascal, J.M. (2010) The Zn3 Domain of Human Poly(ADP-ribose) Polymerase-1 (PARP-1) Functions in Both DNA-dependent Poly(ADP-ribose) Synthesis Activity and Chromatin Compaction. *J Biol Chem* 285, 18877–18887.

Langelier, M.F., Servent, K.M., Rogers, E.E. and Pascal, J.M. (2008) A Third Zinc-binding Domain of Human Poly(ADP-ribose) Polymerase-1 Coordinates DNA-dependent Enzyme Activation. *J Biol Chem* 283, 4105–4114.

Langer, R., Feith, M., Siewert, J.R., Wester, H.J. and Hoefler, H. (2008) Expression and clinical significance of glucose regulated proteins GRP78 (BiP) and GRP94 (GP96) in human adenocarcinomas of the esophagus. *BMC Cancer* 8, 70.

Laurencot, C.M., Scheffer, G.L., Scheper, R.J. and Shoemaker, R.H. (1997) Increased LRP mRNA expression is associated with the MDR phenotype in intrinsically resistant human cancer cell lines. *Int J Cancer* 72, 1021–1026.

Ledford, B.E. and Leno, G.H. (1994) ADP-ribosylation of the molecular chaperone GRP78/BiP. *Mol Cell Biochem* 138, 141-148.

Lee, A.H., Iwakoshi, N.N. and Glimcher, L.H. (2003) XBP-1 regulates a subset of endoplasmic reticulum resident chaperone genes in the unfolded protein response. *Mol Cell Biol* 23, 7448–7459.

Lee, A.S. (2001) The glucose-regulated proteins: stress induction and clinical applications. *Trends Biochem Sci* 26, 504–510.

Lee, A.S. (2014) Glucose regulated proteins in cancer: molecular mechanisms and therapeutic potential. *Nat Rev Cancer* 14, 263–276.

Lee, K., Tirasophon, W., Shen, X., Michalak, M., Prywes, R., Okada, T., Yoshida, H., Mori, K. and Kaufman, R.J. (2002) IRE1-mediated unconventional mRNA splicing and S2P-mediated ATF6 cleavage merge to regulate XBP1 in signaling the unfolded protein response. *Genes Dev* 16, 452-466.

Leung, A.K., Vyas, S., Rood, J.E., Bhutkar, A., Sharp, P.A. and Chang, P. (2011) Poly(ADP-ribose) regulates stress responses and microRNA activity in the cytoplasm. *Mol Cell* 42, 489-499.

Li, J. and Lee, A.S. (2006) Stress induction of GRP78/BiP and its role in cancer. *Curr Mol Med* 6, 45-54.

Li, M. and Yu, X. (2013) Function of BRCA1 in the DNA damage response is mediated by ADP-ribosylation. *Cancer Cell* 23, 693–704.

Li, X.D., Huergo, L.F., Gasperina, A., Pedrosa, F.O., Merrick, M. and Winkler, F.K. (2009) Crystal structure of dinitrogenase reductase-activating glycohydrolase (DraG) reveals conservation in the ADP-ribosylhydrolase fold and specific features in the ADP-ribose-binding pocket. *J Mol Biol* 390, 737.746.

Li, W.W., Alexandre, S., Cao, X. and Lee A.S. (1993) Transactivation of the grp78 promoter by Ca2+ depletion. A comparative analysis with A23187 and the endoplasmic reticulum Ca(2+)-ATPase inhibitor thapsigargin. *J Biol Chem* 268, 12003-12009.

Li, Z., Yan, X., Sun, Y. and Yang, X. (2016) Expression of ADP-ribosyltransferase 1 Is Associated with Poor Prognosis of Glioma Patients. *Tohoku J Exp Med* 239, 269-278.

Liang, J., Song, W., Tromp, G., Kolattukudy, P.E. and Fu, M. (2008) Genome-wide survey and expression profiling of CCCH-zinc finger family reveals a functional module in macrophage activation. *PLoS One* 3, e2880.

Lin, W., Ame, J.C., Aboul-Ela, N., Jacobson, E.L. and Jacobson, M.K. (1997) Isolation and characterization of the cDNA encoding bovine poly(ADP- ribose) glycohydrolase. *J Biol Chem* 272, 11895-11901.

Linstedt, A.D. and Hauri, H.P. (1993) Giantin, a novel conserved Golgi membrane protein containing a cytoplasmic domain of at least 350 kDa. *Mol Biol Cell* 4, 679–693.

Liszt, G., Ford, E., Kurtev, M. and Guarente, L. (2005) Mouse Sir2 homolog SIRT6 is a nuclear ADP-ribosyltransferase. *J Biol Chem* 280, 21313-21320.

Liu, C. and Yu, X. (2015) ADP-ribosyltransferases and poly ADP-ribosylation. *Curr Protein Pept Sci* 16, 491-501.

Liu, C.Y., Schroder, M. and Kaufman, R.J. (2000) Ligand-independent dimerization activates the stress response kinases IRE1 and PERK in the lumen of the endoplasmic reticulum. *J Biol Chem* 275, 24881-24885.

Liu, R., Li, X., Gao, W., Zhou, Y., Wey, S., Mitra, S.K., Krasnoperov, V., Dong, D., Liu, S., Li, D., Zhu, G., Louie, S., Conti, P.S., Li, Z., Lee, A.S. and Gill, P.S. (2013) Monoclonal antibody against cell surface GRP78 as a novel agent in suppressing PI3K/AKT signaling, tumor growth and metastasis. *Clin Cancer Res* 19, 6802–6811.

Liu, S.Y., Sanchez, D.J., Aliyari, R., Lu, S. and Cheng, G. (2012) Systematic identification of type I and type II interferon-induced antiviral factors. *Proc Natl Acad Sci U S A* 109, 4239–4244.

Liu, Z., Lv, Y., Zhao, N., Guan, G., and Wang, J. (2015) Protein kinase R-like ER kinase and its role in endoplasmic reticulum stress-decided cell fate. *Cell Death & Disease* 6, e1822.

Liu, Z.X., Yu, Y. and Dennert, G. (1999) A cell surface ADP-ribosyltransferase modulates T cell receptor association and signaling. *J Biol Chem* 274, 17399-17401.

Lodhi, I.J., Clift, R.E., Omann, G.M., Sweeney, J.F., McMahon, K.K. and Hinshaw, D.B. (2001) Inhibition of mono-ADP-ribosyltransferase activity during the execution phase of apoptosis prevents apoptotic body formation. *Arch Biochem Biophys* 387, 66-77.

Loeffler, P.A., Cuneo, M.J., Mueller, G.A., DeRose, E.F., Gabel, S.A. and London, R.E. (2011) Structural studies of the PARP-1 BRCT domain. *BMC Struct Biol* 11:37.

Logue, S.E., Cleary, P., Saveljeva, S. and Samali, A. (2013) New directions in ER stress-induced cell death. *Apoptosis* 18, 537-546.

Loseva, O., Jemth, A.S., Bryant, H.E., Schuler, H., Lehtio, L., Karlberg, T. and Helleday, T. (2010) PARP-3 is a mono-ADP-ribosylase that activates PARP-1 in the absence of DNA. *J Biol Chem* 285, 8054-8060.

Lowery, R.G. and Ludden, P.W. (1988) Purification and properties of dinitrogenase reductase ADP- ribosyltransferase from the photosynthetic bacterium Rhodospirillum rubrum. *J Biol Chem* 263, 16714-16719.

Ludden, P.W. (1994) Reversible ADP-ribosylation as a mechanism of enzyme regulation in procaryotes. *Mol Cell Biochem* 138, 123-129.

Ludden, P.W. and Burris, R.H. (1976) Activating factor for the iron protein of nitrogenase from Rhodospirillum rubrum. *Science* 194, 424-426.

Lukacs, G.L., Chang, X.B., Bear, C., Kartner, N., Mohamed, A., Riordan, J.R. and Grinstein, S. (1993) The delta F508 mutation decreases the stability of cystic fibrosis transmembrane conductance regulator in the plasma membrane. Determination of functional half-lives on transfected cells. *J Biol Chem* 268, 21592–21598.

Luo, B. and Lee, A.S. (2013) The critical roles of endoplasmic reticulum chaperones and unfolded protein response in tumorigenesis and anticancer therapies. *Oncogene* 32, 805-818.

Luo, X. and Kraus, W.L. (2012) On PAR with PARP: cellular stress signaling through poly(ADP-ribose) and PARP-1. *Genes Dev* 26, 417–432.

Lupi, R., Corda, D. and Di Girolamo, M. (2000) Endogenous ADP-ribosylation of the G protein beta subunit prevents the inhibition of type 1 adenylyl cyclase. *J Biol Chem* 275, 9418-9424.

Lupi, R., Dani, N., Dietrich, A., Marchegiani, A., Turacchio, S., Berrie, C.P., Moss, J., Gierschik, P., Corda, D., and Di Girolamo, M. (2002) Endogenous mono-ADPribosylation of the free Gbetagamma prevents stimulation of phosphoinositide 3-kinasegamma and phospholipase C-beta2 and is activated by G-protein-coupled receptors. *Biochem J* 367, 825-832.

Ma, Q., Baldwin, K.T., Renzelli, A.J., McDaniel, A. and Dong, L. (2001) TCDD-inducible poly(ADP-ribose) polymerase: a novel response to 2,3,7,8-tetrachlorodibenzo-p-dioxin. *Biochem Biophys Res Commun* 289, 499-506.

Macpherson, L., Ahmed, S., Tamblyn, L., Krutmann, J., Forster, I., Weighardt, H. and Matthews, J. (2014) Aryl Hydrocarbon Receptor Repressor and TiPARP (ARTD14) Use Similar, but also Distinct Mechanisms to Repress Aryl Hydrocarbon Receptor Signaling. *Int J Mol Sci* 15, 7939-7957.

MacPherson, L., Tamblyn, L., Rajendra, S., Bralha, F., McPherson, J.P. and Matthews, J. (2013) 2,3,7,8-Tetrachlorodibenzo-p-dioxin poly(ADP-ribose) polymerase (TiPARP, ARTD14) is a mono-ADP-ribosyltransferase and repressor of aryl hydrocarbon receptor transactivation. *Nucleic Acids Res* 41, 1604-1621.

Maddalo, D., Neeb, A., Jehle, K., Schmitz, K., Muhle-Goll, C., Shatkina, L., Walther, T.V., Bruchmann, A., Gopal, S.M., Wenzel, W., Ulrich, A.S. and Cato, A.C. (2012) A peptidic unconjugated GRP78/BiP ligand modulates the unfolded protein response and induces prostate cancer cell death. *PLoS One* 7, e45690.

Malanga, M. and Althaus, F.R. (2005) The role of poly(ADP-ribose) in the DNA damage signaling network. *Biochem Cell Biol* 83, 354-364.

Manal, M., Chandrasekar, M.J., Gomathi Priya, J. and Nanjan, M.J. (2016) Inhibitors of histone deacetylase as antitumor agents: A critical review. *Bioorg Chem* 67, 18-42.

Manke, I.A., Lowery, D.M., Nguyen, A. and Yaffe, M.B. (2003) BRCT repeats as phosphopeptidebinding modules involved in protein targeting. *Science* 302, 636–639.

Mao, R., Nie, H., Cai, D., Zhang, J., Liu, H., Yan, R., Cuconati, A., Block, T.M., Guo, J.T. and Guo, H. (2013) Inhibition of hepatitis B virus replication by the host zinc finger antiviral protein. *PLoS Pathog* 9, e1003494.

Mao, Z., Hine, C., Tian, X., Van Meter, M., Au, M., Vaidya, A., Seluanov, A. and Gorbunova, V. (2011) SIRT6 promotes DNA repair under stress by activating PARP1. *Science* 332, 1443-1446.

Mao, Z., Tian, X., Van Meter, M., Ke, Z., Gorbunova, V. and Seluanov, A. (2012) Sirtuin 6 (SIRT6) rescues the decline of homologous recombination repair during replicative senescence. *Proc Natl Acad Sci U S A* 109, 11800-11805.

Marciniak, S.J., Yun, C.Y., Oyadomari, S., Novoa, I., Zhang, Y., Jungreis, R., Nagata, K., Harding, H.P. and Ron, D. (2004) CHOP induces death by promoting protein synthesis and oxidation in the stressed endoplasmic reticulum. *Genes Dev* 18, 3066-3077.

Mariotti, L., Templeton, C.M., Ranes, M., Paracuellos, P., Cronin, N., Beuron, F., Morris, E. and Guettler, S. (2016) Tankyrase Requires SAM Domain-Dependent Polymerization to Support Wnt-β-Catenin Signaling. *Mol Cell* 63, 498–513.

Marsischky, G.T., Wilson, B.A. and Collier, R.J. (1995) Role of glutamic acid 988 of human poly-ADP-ribose polymerase in polymer formation. Evidence for active site similarities to the ADP-ribosylating toxins. *J Biol Chem* 270, 3247-3254.

Martin, S., Lamb, H.K., Brady, C., Lefkove, B., Bonner, M.Y., Thompson, P., Lovat, P.E., Arbiser, J.L., Hawkins, A.R. and Redfern, C.P. (2013) Inducing apoptosis of cancer cells using small-molecule plant compounds that bind to GRP78. *Br J Cancer* 109, 433-443.

Martin-Hernandez, K., Rodriguez-Vargas, J.M., Schreiber, V. and Dantzer, F. (2017) Expanding functions of ADP-ribosylation in the maintenance of genome integrity. *Semin Cell Dev Biol* 63, 92-101.

Mashimo, M., Kato, J. and Moss, J. (2014) Structure and function of the ARH family of ADP-ribose-acceptor hydrolases. *DNA Repair (Amst)* 0, 88–94.

Matsuura, G., Morinaga, N., Yahiro, K., Komine, R., Moss, J., Yoshida, H. and Noda, M. (2009) Novel subtilase cytotoxin produced by Shiga-toxigenic Escherichia coli induces apoptosis in vero cells via mitochondrial membrane damage. *Infect Immun* 77, 2919-2924.

McDonald, L.J. and Moss, J. (1993) Nitric oxide-independent, thiol-associated ADP-ribosylation inactivates aldehyde dehydrogenase. *J Biol Chem* 268, 17878-17882.

McDonald, L.J., Wainschel, L.A., Oppenheimer, N.J. and Moss, J. (1992) Amino acid-specific ADP-ribosylation: structural characterization and chemical differentiation of ADP-ribose-cysteine adducts formed nonenzymatically and in a pertussis toxin-catalyzed reaction. *Biochemistry* 31, 11881-11887.

Mehrotra, P., Hollenbeck, A., Riley, J.P., Li, F., Patel, R.J., Akhtar, N. and Goenka, S. (2013) Poly (ADP-ribose) polymerase 14 and its enzyme activity regulates T(H)2 differentiation and allergic airway disease. *J Allergy Clin Immunol* 131, 521-531.

Merksamer, P.I. and Papa, F.R. (2010) The UPR and cell fate at a glance. *J Cell Sci* 123, 1003–1006.

Messner, S., Altmeyer, M., Zhao, H., Pozivil, A., Roschitzki, B., Gehrig, P., Rutishauser, D., Huang, D., Caflisch, A. and Hottiger, M.O. (2010) PARP1 ADP-ribosylates lysine residues of the core histone tails. *Nucleic Acids Res* 38, 6350–6362.

Miao, Y.R., Eckhardt, B.L., Cao, Y., Pasqualini, R., Argani, P., Arap, W., Ramsay, R.G. and Anderson, R.L. (2013) Inhibition of established micrometastases by targeted drug delivery via cell surface-associated GRP78. *Clin Cancer Res* 19, 2107-2116.

Michan, S. and Sinclair, D. (2007) Sirtuins in mammals: insights into their biological function. *Biochem J* 404, 1-13.

Michishita, E., Park, J.Y., Burneskis, J.M., Barrett, J.C. and Horikawa, I. (2005) Evolutionarily conserved and nonconserved cellular localizations and functions of human SIRT proteins. *Mol Biol Cell* 16, 4623-4635.

Misra, U.K. and Pizzo, S.V. (2010) Modulation of the unfolded protein response in prostate cancer cells by antibody-directed against the carboxyl-terminal domain of GRP78. *Apoptosis* 15, 173-182.

Misra, U.K., Gonzalez-Gronow, M., Gawdi, G. and Pizzo, S.V. (2005) The role of MTJ-1 in cell surface translocation of GRP78, a receptor for alpha 2-macroglobulin-dependent signaling. *J Immunol* 174, 2092-2097.

Misra, U.K., Gonzalez-Gronow, M., Gawdi, G., Hart, J.P., Johnson, C.E. and Pizzo, S.V. (2002) The role of Grp 78 in alpha 2-macroglobulin-induced signal transduction. Evidence from RNA interference that the low density lipoprotein receptor-related protein is associated with, but not necessary for, GRP 78-mediated signal transduction. *J Biol Chem* 277, 42082-42087.

Miwa, M. and Masutani, M. (2007) PolyADP-ribosylation and cancer. *Cancer Sci* 98, 1528–1535.

Montecucco, C. and Molinari, M. (2006) Microbiology: death of a chaperone. *Nature* 443, 511-512.

Mori, K. (2000) Tripartite management of unfolded proteins in the endoplasmic reticulum. *Cell* 101, 451-454.

Moss, J. and Vaughan, M. (1978) Isolation of an avian erythrocyte protein possessing ADP-ribosyltransferase activity and capable of activating adenylate cyclase. *Proc Natl Acad Sci U S A* 75, 3621-3624.

Moss, J., Jacobson, M.K. and Stanley, S.J. (1985) Reversibility of arginine-specific mono(ADP-ribosyl)ation: identification in erythrocytes of an ADP-ribose-L-arginine cleavage enzyme. *Proc Natl Acad Sci U S A* 82, 5603-5607.

Moss, J., Oppenheimer, N.J., West, R.E.Jr and Stanley, S.J. (1986) Amino acid specific ADP-ribosylation: substrate specificity of an ADP-ribosylarginine hydrolase from turkey erythrocytes. *Biochemistry* 25, 5408-5414.

Moss, J., Stanley, S.J., Nightingale, M.S., Murtagh, J.J.Jr., Monaco, L., Mishima, K., Chen, H.C., Williamson, K.C. and Tsai, S.C. (1992) Molecular and immunological characterization of ADP-ribosylarginine hydrolases. *J Biol Chem* 267, 10481-10488.

Mozos, A., Roue, G., Lopez-Guillermo, A., Jares, P., Campo, E., Colomer, D. and Martinez, A. (2011) The expression of the endoplasmic reticulum stress sensor BiP/GRP78 predicts response to chemotherapy and determines the efficacy of proteasome inhibitors in diffuse large b-cell lymphoma. *Am J Pathol* 179, 2601-2610.

Mueller-Dieckmann, C., Kernstock, S., Lisurek, M., von Kries, J.P., Haag, F., Weiss, M.S. and Koch-Nolte, F. (2006) The structure of human ADP-ribosylhydrolase 3 (ARH3) provides insights into the reversibility of protein ADP-ribosylation. *Proc Natl Acad Sci U S A* 103, 15026-15031.

Mueller-Dieckmann, C., Ritter, H., Haag, F., Koch-Nolte, F. and Schulz, G.E. (2002) Structure of the ecto-ADP-ribosyl transferase ART2.2 from rat. *J Mol Biol* 322, 687-96.

Muller, S., Moller, P., Bick, M.J., Wurr, S., Becker, S., Gunther, S. and Kummerer, B.M. (2007) Inhibition of filovirus replication by the zinc finger antiviral protein. *Journal of virology* 81, 2391-400.

Murphy, M.E. (2013) The HSP70 family and cancer. *Carcinogenesis* 34, 1181–1188.

Nakagawa, T., Zhu, H., Morishima, N., Li, E., Xu, J., Yankner, B.A. and Yuan, J. (2000) Caspase-12 mediates endoplasmic-reticulum-specific apoptosis and cytotoxicity by amyloid-beta. *Nature* 403, 98–103.

Negroiu, G., Dwek, R.A. and Petrescu, S.M. (2000) Folding and maturation of tyrosinase-related protein-1 are regulated by the post-translational formation of disulfide bonds and by N-glycan processing. *J Biol Chem* 275, 32200-32207.

Nemoto, E., Yu, Y. and Dennert, G. (1996) Cell surface ADP-ribosyltransferase regulates lymphocyte function-associated molecule-1 (LFA-1) function in T cells. *J Immunol* 157, 3341-3349.

Neuvonen, M. and Ahola, T. (2009) Differential activities of cellular and viral macro domain proteins in binding of ADP-ribose metabolites. *J Mol Biol* 385, 212-225.

Ni, M. and Lee, A.S. (2007) ER chaperones in mammalian development and human diseases. *Febs Lett* 581, 3641–3651.

Ni, M., Zhang, Y. and Lee, A.S. (2011) Beyond the endoplasmic reticulum: atypical GRP78 in cell viability, signaling and therapeutic targeting. *Biochemical Journal* 434, 181-188.

Ni, M., Zhou, H., Wey, S., Baumeister, P. and Lee, A.S. (2009) Regulation of PERK Signaling and Leukemic Cell Survival by a Novel Cytosolic Isoform of the UPR Regulator GRP78/BiP. *PLoS One* 4, e6868.

Nicolae, C.M., Aho, E.R., Vlahos, A.H., Choe, K.N., De, S., Karras, G.I. and Moldovan, G.L. (2014) The ADP-ribosyltransferase PARP10/ARTD10 interacts with proliferating cell nuclear antigen (PCNA) and is required for DNA damage tolerance. *J Biol Chem* 289, 13627-13637.

Nordlund, S. and Hogbom, M. (2013) ADP-ribosylation, a mechanism regulating nitrogenase activity. *FEBS J* 280, 3484-3490.

Nordlund, S. and Ludden, P.W. (2004) in Genetics and regulation of nitrogen fixation in free-living bacteria, eds Klipp, W., Masepohl, B., Gallon, J. R. and Newton, W.E. (Vol. 2) Springer Science & Business Media, pp 175–196.

North, B.J., Marshall, B.L., Borra, M.T., Denu, J.M. and Verdin, E. (2003) The human Sir2 ortholog, SIRT2, is an NAD+-dependent tubulin deacetylase. *Mol Cell* 11, 437-444.

Novoa, I., Zeng, H., Harding, H.P. and Ron, D. (2001) Feedback inhibition of the unfolded protein response by GADD34-mediated dephosphorylation of eIF2alpha. *J Cell Biol* 153, 1011-1022.

Novoa, I., Zhang, Y., Zeng, H., Jungreis, R., Harding, H.P. and Ron, D. (2003) Stress-induced gene expression requires programmed recovery from translational repression. *EMBO J* 22, 1180-1187.

Oka, J., Ueda, K., Hayaishi, O., Komura, H. and Nakanishi, K. (1984) ADP-ribosyl protein lyase. Purification, properties, and identification of the product. *J Biol Chem* 259, 986-995.

Oka, S., Kato, J. and Moss, J. (2006) Identification and characterization of a mammalian 39-kDa poly(ADP-ribose) glycohydrolase. *J Biol Chem* 281, 705-713.

Okayama, H., Honda, M. and Hayaishi, O. (1978) Novel enzyme from rat liver that cleaves an ADP-ribosyl histone linkage. *Proc Natl Acad Sci U S A* 75, 2254-2257.

Okazaki, I.J. and Moss, J. (1999) Characterization of glycosylphosphatidylinositiolanchored, secreted, and intracellular vertebrate mono-ADP-ribosyltransferases. *Annu Rev Nutr* 19, 485-509.

Okazaki, I.J., Kim, H.J. and Moss, J. (1996b) Cloning and characterization of a novel membrane-associated lymphocyte NAD:arginine ADP-ribosyltransferase. *J Biol Chem* 271, 22052-22057.

Okazaki, I.J., Kim, H.J., McElvaney, N.G., Lesma, E. and Moss, J. (1996a) Molecular characterization of a glycosylphosphatidylinositol-linked ADP-ribosyltransferase from lymphocytes. *Blood* 88, 915-921.

Oliver, A.W., Ame, J.C., Roe, S.M., Good, V., de Murcia, G. and Pearl, L.H. (2004) Crystal structure of the catalytic fragment of murine poly(ADPribose) polymerase-2. *Nucleic Acids Res* 32, 456–464.

Olzmann, J.A., Kopito, R.R. and Christianson, J.C. (2013) The Mammalian Endoplasmic Reticulum-Associated Degradation System. *Cold Spring Harb Perspect Biol* 5, a013185.

Oslowski, C.M. and Urano, F. (2011) Measuring ER stress and the unfolded protein response using mammalian tissue culture system. *Methods Enzymol* 490, 71–92.

Otto, H., Reche, P.A., Bazan, F., Dittmar, K., Haag, F. and Koch-Nolte, F. (2005) In silico characterization of the family of PARP-like poly(ADP-ribosyl)transferases (pARTs). *BMC Genomics* 6, 139.

Paone, G., Stevens, L.A., Levine, R.L., Bourgeois, C., Steagall, W.K., Gochuico, B.R. and Moss, J. (2006) ADP-ribosyltransferase-specific modification of human neutrophil peptide-1. *J Biol Chem* 281, 17054-17060.

Paone, G., Wada, A., Stevens, L.A., Matin, A., Hirayama, T., Levine, R.L. and Moss, J. (2002) ADP ribosylation of human neutrophil peptide-1 regulates its biological properties. *Proc Natl Acad Sci U S A* 99, 8231-8235.

Parusel, I., Kahl, S., Braasch, F., Glowacki, G., Halverson, G.R., Reid, M.E., Schawalder, A., Ortolan, E., Funaro, A., Malavasi, F., Hardie, D., Halder, S., Buckley, C.D., Haag, F. and Koch-Nolte, F. (2005) A panel of monoclonal antibodies recognizing GPI-anchored ADP-ribosyltransferase ART4, the carrier of the Dombrock blood group antigens. *Cell Immunol* 236, 59-65.

Paton, A.W., Beddoe, T., Thorpe, C.M., Whisstock, J.C., Wilce, M.C., Rossjohn, J., Talbot, U.M. and Paton, J.C. (2006) AB5 subtilase cytotoxin inactivates the endoplasmic reticulum chaperone BiP. *Nature* 443, 548-552.

Peralta-Leal, A., Rodriguez-Vargas, J.M., Aguilar-Quesada, R., Rodriguez, M.I., Linares, J.L., de Almodovar, M.R. and Oliver, F.J. (2009) PARP inhibitors: new partners in the therapy of cancer and inflammatory diseases. *Free Radic Biol Med* 47, 13–26.

Perina, D., Mikoc, A., Ahel, J., Cetkovic, H., Zaja, R. and Ahel. I. (2014) Distribution of protein poly(ADP-ribosyl)ation systems across all domains of life. *DNA Repair (Amst)* 23, 4-16.

Peterson, J.E., Larew, J.S. and Graves, D.J. (1990) Purification and partial characterization of arginine-specific ADP-ribosyltransferase from skeletal muscle microsomal membranes. *J Biol Chem* 265, 17062-17069.

Pleschke, J.M., Kleczkowska, H.E., Strohm, M. and Althaus, F.R. (2000) Poly(ADP-ribose) binds to specific domains in DNA damage checkpoint proteins. *J Biol Chem* 275, 40974-40980.

Plummer, R., Jones, C., Middleton, M., Wilson, R., Evans, J., Olsen, A., Curtin, N., Boddy, A., McHugh, P., Newell, D., Harris, A., Johnson, P., Steinfeldt, H., Dewji, R., Wang, D., Robson, L. and Calvert, H. (2008) Phase I study of the poly(ADP-ribose) polymerase inhibitor, AG014699, in combination with temozolomide in patients with advanced solid tumors. *Clin Cancer Res* 14, 7917–7923.

Poothong, J.1., Sopha, P., Kaufman, R.J. and Tirasophon, W. (2017) IRE1α nucleotide sequence cleavage specificity in the unfolded protein response. *FEBS Lett* 591, 406-414.

Pope, M.R., Murrell, S.A. and Ludden, P.W. (1985) Covalent modification of the iron protein of nitrogenase from Rhodospirillum rubrum by adenosine diphosphoribosylation of a specific arginine residue. *Proc Natl Acad Sci U S A* 82, 3173-3177.

Prochazka, M., Gaskins, H. R., Leiter, E. H., Koch-Nolte, F., Haag, F. and Thiele, H. G. (1991) Chromosomal localization, DNA polymorphism, and expression of Rt-6, the mouse homologue of rat T-lymphocyte differentiation marker RT6. *Immunogenetics* 33, 152-156.

Qi, L., Tsai, B. and Arvan, P. (2017) New Insights into the Physiological Role of Endoplasmic Reticulum-Associated Degradation. *Trends Cell Biol* 27, 430-440.

Qian, Y., Harris, E.D., Zheng, Y. and Tiffany-Castiglioni, E. (2000) Lead targets GRP78, a molecular chaperone, in C6 rat glioma cells. *Toxicol Appl Pharmacol* 163, 260–266.

Qian, Y., Zheng, Y., Ramos, K.S. and Tiffany-Castiglioni, E. (2005) The involvement of copper transporter in lead-induced oxidative stress in astroglia. *Neurochem Res* 30, 429–438.

Raffaelli, N., Scaife, R.M. and Purich, D.L. (1992) ADPRibosylation of chicken red cell tubulin and inhibition of microtubule self-assembly in vitro by the NAD^+-dependent avian ADPRibosyl transferase. *Biochem Biophys Res Commun* 184, 414–418.

Rasche, L., Duell, J., Morgner, C., Chatterjee, M., Hensel, F., Rosenwald, A., Einsele, H., Topp, M.S. and Brandlein, S. (2013) The natural human IgM antibody PAT-SM6 induces apoptosis in primary human multiple myeloma cells by targeting heat shock protein GRP78. *PLoS One* 8, e63414.

Rauschert, N., Brandlein, S., Holzinger, E., Hensel, F., Muller-Hermelink, H.K. and Vollmers, H.P. (2008) A new tumor-specific variant of GRP78 as target for antibody-based therapy. *Lab Invest* 88, 375-386.

Reddy, R.K., Mao, C., Baumeister, P., Austin, R.C., Kaufman, R.J. and Lee, A.S. (2003) Endoplasmic reticulum chaperone protein GRP78 protects cells from apoptosis

induced by topoisomerase inhibitors: role of ATP binding site in suppression of caspase-7 activation. *J Biol Chem* 278, 20915-20924.

Ribet, D. and Cossart, P. (2010) Post-translational modifications in host cells during bacterial infection. *Febs Lett* 584, 2748-2758.

Riccio, A.A., Cingolani, G. and Pascal, J.M. (2016a) PARP-2 domain requirements for DNA damage-dependent activation and localization to sites of DNA damage. *Nucleic Acids Res* 44, 1691–1702.

Riccio, A.A., McCauley, M., Langelier, M.F. and Pascal, J.M. (2016b) Tankyrase SAM domain polymerization is required for its role in Wnt signaling. *Structure* 24, 1573–1581.

Rippmann, J.F., Damm, K. and Schnapp, A. (2002) Functional characterization of the poly(ADP-ribose) polymerase activity of tankyrase 1, a potential regulator of telomere length. *J Mol Biol* 323, 217-224.

Robert, I., Dantzer, F. and Reina-San-Martin, B. (2009) Parp1 facilitates alternative NHEJ, whereas Parp2 suppresses IgH/c-myc translocations during immunoglobulin class switch recombination. *J Exp Med* 206, 1047-1056.

Rolli, V., O'Farrell, M., Ménissier-de Murcia, J. and de Murcia, G. (1997) Random mutagenesis of the poly(ADP-ribose) polymerase catalytic domain reveals amino acids involved in polymer branching. *Biochemistry* 36, 12147-12154.

Romisch, K. (2005) Endoplasmic reticulum-associated degradation. *Annu Rev Cell Dev Biol* 21, 435–456.

Ron, D. and Walter, P. (2007) Signal integration in the endoplasmic reticulum unfolded protein response. *Nat Rev Mol Cell Biol* 8, 519–529.

Rosenthal, F., Feijs, K.L., Frugier, E., Bonalli, M., Forst, A.H., Imhof, R., Winkler, H.C., Fischer, D., Caflisch, A., Hassa, P.O., Luscher, B. and Hottiger, M.O. (2013)

Macrodomain-containing proteins are new mono-ADP-ribosylhydrolases. *Nat Struct Mol Biol* 20, 502-507.

Rouf Mir, A. and Bashir, Y. (2015) Histone Protein Glycation and Diabetes. *J Dia Res Ther* 1.

Rouleau, M., McDonald, D., Gagne, P., Ouellet, M.E., Droit, A., Hunter, J.M., Dutertre, S., Prigent, C., Hendzel, M.J. and Poirier, G.G. (2007) PARP-3 associates with polycomb group bodies and with components of the DNA damage repair machinery. *J Cell Biochem* 100, 385-401.

Rutkowski, D.T. and Kaufman, R.J. (2004) A trip to the ER: coping with stress. *Trends Cell Biol* 14, 20-28.

Sanders, B.D., Jackson, B. and Marmorstein, R. (2010) Structural Basis for Sirtuin Function: What We Know and What We Don't. *Biochim Biophys Acta* 1804, 1604–1616.

Sano, R. and Reed, J.C. (2013) ER stress-induced cell death mechanisms. *Biochim Biophys Acta* 1833, 3460-3470.

Sauve, A.A. and Schramm, V.L. (2004) SIR2: the biochemical mechanism of NAD(+)-dependent protein deacetylation and ADP-ribosyl enzyme intermediates. *Curr Med Chem* 11, 807-826.

Saxty, B.A. and van Heyningen, S. (1995) The purification of a cysteine-dependent NAD+ glycohydrolase activity from bovine erythrocytes and evidence that it exhibits a novel ADP-ribosyltransferase activity. *Biochem J* 310, 931-937.

Saxty, B.A., Yadollahi-Farsani, M., Upton, P.D., Johnstone, S.R. and MacDermot, J. (2001) Inactivation of platelet-derived growth factor-BB following modification by ADP-ribosyltransferase. *Br J Pharmacol* 133, 1219-1226.

Sbodio, J.I. and Chi, N.W. (2002) Identification of a tankyrase-binding motif shared by IRAP, TAB182, and human TRF1 but not mouse TRF1. NuMA contains this RXXPDG motif and is a novel tankyrase partner. *J Biol Chem* 277, 31887-31892.

Sbodio, J.I., Lodish, H.F. and Chi, N.W. (2002) Tankyrase-2 oligomerizes with tankyrase-1 and binds to both TRF1 (telomere-repeat-binding factor 1) and IRAP (insulin-responsive aminopeptidase). *Biochem J* 361, 451-459.

Scarpa, E.S., Fabrizio, G. and Di Girolamo, M. (2013) A role of intracellular mono-ADP-ribosylation in cancer biology. *FEBS J* 280, 3551-3562.

Scheuplein, F., Adriouch, S., Glowacki, G., Haag, F., Seman, M. and Koch-Nolte, F. (2003) Triggering of T-cell apoptosis by toxin-related ecto-ADP-ribosyltransferase ART2. *Ann N Y Acad Sci* 1010, 296-299.

Schoggins, J.W., Wilson, S.J., Panis, M., Murphy, M.Y., Jones, C.T., Bieniasz, P. and Rice, C.M. (2011) A diverse range of gene products are effectors of the type I interferon antiviral response. *Nature* 472, 481-485.

Schreiber, V., Ame, J.C., Dolle, P., Schultz, I., Rinaldi, B., Fraulob, V., Menissier-de Murcia, J. and de Murcia, G. (2002) Poly(ADP-ribose) polymerase-2 (PARP-2) is required for efficient base excision DNA repair in association with PARP-1 and XRCC1. *J Biol Chem* 277, 23028-23036.

Schreiber, V., Dantzer, F., Ame, J.C. and de Murcia, G. (2006) Poly(ADP-ribose): novel functions for an old molecule. *Nat Rev Mol Cell Biol* 7, 517–528.

Schreiber, V., Hunting, D., Trucco, C., Gowans, B., Grunwald, D., De Murcia, G. and De Murcia, J.M. (1995) A dominant-negative mutant of human poly(ADP-ribose) polymerase affects cell recovery, apoptosis, and sister chromatid exchange following DNA damage. *Proc Natl Acad Sci U S A* 92, 4753-5757.

Schroder, M. and Kaufman, R.J. (2005) ER stress and the unfolded protein response. *Mutat Res* 569, 29-63.

Scott, L.J. (2017) Niraparib: First Global Approval. *Drugs* 77, 1029-1034.

Scovassi, A.I. (2004) Mitochondrial poly(ADPribosylation): from old data to new perspectives. *FASEB J* 18, 1487–1488.

Seidler, N.W. (2013) Basic biology of GAPDH. *Adv Exp Med Biol* 985, 1-36.

Seimiya, H. and Smith, S. (2002) The telomeric poly(ADP-ribose) polymerase, tankyrase 1, contains multiple binding sites for telomeric repeat binding factor 1 (TRF1) and a novel acceptor, 182-kDa tankyrase-binding protein (TAB182). *J Biol Chem* 277, 14116-14126.

Seimiya, H., Muramatsu, Y., Smith, S. and Tsuruo, T. (2004) Functional subdomain in the ankyrin domain of tankyrase 1 required for poly(ADPribosyl)ation of TRF1 and telomere elongation. *Mol Cell Biol* 24, 1944–1955.

Seira, O. and Del Rio, J.A. (2014) Glycogen synthase kinase 3 beta (GSK3beta) at the tip of neuronal development and regeneration. *Mol Neurobiol* 49, 931-944.

Seman, M., Adriouch, S., Scheuplein, F., Krebs, C., Freese, D., Glowacki, G., Deterre, P., Haag, F. and Koch-Nolte, F. (2003) NAD-induced T cell death: ADP-ribosylation of cell surface proteins by ART2 activates the cytolytic P2X7 purinoceptor. *Immunity* 19, 571-582.

Shaffer, A.L. 3rd, Young, R.M. and Staudt, L.M. (2012) Pathogenesis of human B cell lymphomas. *Annu Rev Immunol* 30, 565-610.

Shall, S. (1995) ADP-ribosylation reactions. *Biochimie* 77, 313-318.

Shamu, C.E. and Walter, P. (1996) Oligomerization and phosphorylation of the Ire1p kinase during intracellular singnaling from the endoplasmic reticulum to the nucleus. *EMBO J* 15, 3028-3039.

Shani, G., Fischer, W.H., Justice, N.J., Kelber, J.A., Vale, W. and Gray, P.C. (2008) GRP78 and Cripto form a complex at the cell surface and collaborate to inhibit

transforming growth factor beta signaling and enhance cell growth. *Mol Cell Biol* 28, 666-677.

Sharifi, R., Morra, R., Appel, C.D., Tallis, M., Chioza, B., Jankevicius, G., Simpson, M.A., Matic, I., Ozkan, E., Golia, B., Schellenberg, M.J., Weston, R., Williams, J.G., Rossi, M.N., Galehdari, H., Krahn, J., Wan, A., Trembath, R.C., Crosby, A.H., Ahel, D., Hay, R., Ladurner, A.G., Timinszky, G., Williams, R.S. and Ahel, I. (2013) Deficiency of terminal ADP-ribose protein glycohydrolase TARG1/C6orf130 in neurodegenerative disease. *EMBO J* 32, 1225-1237.

Shen, J. and Prywes, R. (2004) Dependence of site-2 protease cleavage of ATF6 on prior site-1 protease digestion is determined by the size of the luminal domain of ATF6. *J Biol Chem* 279, 43046-43051.

Shen, J., Chen, X., Hendershot, L. and Prywes, R. (2002) ER stress regulation of ATF6 localization by dissociation of BiP/GRP78 binding and unmasking of Golgi localization signals. *Dev Cell* 3, 99–111.

Shi, Y., Vattem, K.M., Sood, R., An, J., Liang, J., Stramm L. and Wek, R.C. (1998) Identification and characterization of pancreatic eukaryotic initiation factor 2 alpha-subunit kinase, PEK, involved in translational control. *Mol Cell Biol* 18, 7499-7509.

Shin, B.K., Wang, H., Yim, A.M., Le Naour, F., Brichory, F., Jang, J.H., Zhao, R., Puravs, E., Tra, J., Michael, C.W., Misek, D.E. and Hanash, S.M. (2003) Global profiling of the cell surface proteome of cancer cells uncovers an abundance of proteins with chaperone function. *J Biol Chem* 278, 7607-7616.

Shiu, R.P., Pouyssegur, J. and Pastan. I. (1977) Glucose depletion accounts for the induction of two transformationsensitive membrane proteins in Rous sarcoma virustransformed chick embryo fibroblasts. *Proc Natl Acad Sci U S A* 74, 3840–3844.

Shu, C.W. and Huang, C.M. (2008) HSP70s: From Tumor Transformation to Cancer Therapy. *Clin Med Oncol* 2, 335-345.

Shuda, M., Kondoh, N., Imazeki, N., Tanaka, K., Okada, T., Mori, K., Hada, A., Arai, M., Wakatsuki, T., Matsubara, O., Yamamoto, N. and Yamamoto, M. (2003) Activation of the ATF6, XBP1 and grp78 genes in human hepatocellular carcinoma: a possible involvement of the ER stress pathway in hepatocarcinogenesis. *J Hepatol* 38, 605-614.

Siva, A.C., Raval-Fernandes, S., Stephen, A.G., LaFemina M.J., Scheper, R.J., Kickhoefer, V.A. and Rome, L.H. (2001) Up-regulation of vaults may be necessary but not sufficient for multidrug resistance. *J Int Cancer* 92, 195–202.

Smith, J.S., Brachmann, C.B., Celic, I., Kenna, M.A., Muhammad, S., Starai, V.J., Avalos, J.L., Escalante-Semerena, J.C., Grubmeyer, C., Wolberger, C. and Boeke, J.D. (2000) A phylogenetically conserved NAD+-dependent protein deacetylase activity in the Sir2 protein family. *Proc Natl Acad Sci U S A* 97, 6658-6663.

Smith, S. (2001) The world according to PARP. *Trends Biochem Sci* 26, 174-179.

Smith, S. and de Lange, T. (1999) Cell cycle dependent localization of the telomeric PARP, tankyrase, to nuclear pore complexes and centrosomes. *J Cell Sci* 112, 3649-3656.

Smith, S., Giriat, I., Schmitt, A. and de Lange, T. (1998) Tankyrase, a poly(ADP-ribose) polymerase at human telomeres. *Science* 282, 1484-1487.

Soman, G., Mickelson, J.R., Louis, C.F. and Graves, D.J. (1984) NAD: guanidino group specific mono ADP-ribosyltransferase activity in skeletal muscle. *Biochem Biophys Res Commun* 120, 973-980.

Steiner, E., Holzmann, K., Elbling, L., Micksche, M. and Berger, W. (2006) Cellular functions of vaults and their involvement in multidrug resistance. *Curr Drug Targets* 7, 923-934.

Stevens, L.A., Levine, R.L., Gochuico, B.R. and Moss, J. (2009) ADP-ribosylation of human defensin HNP-1 results in the replacement of the modified arginine with the noncoded amino acid ornithine. *Proc Natl Acad Sci U S A* 106, 19796-19800.

Stilla, A., Di Paola, S., Dani, N., Krebs, C., Arrizza, A., Corda, D., Haag, F., Koch-Nolte, F. and Di Girolamo, M. (2011) Characterisation of a novel glycosylphosphatidylinositol-anchored mono-ADP-ribosyltransferase isoform in ovary cells. *Eur J Cell Biol* 90, 665-677.

Sun, F.C., Wei, S., Li, C.W., Chang, Y.S., Chao, C.C. and Lai, Y.K. (2006) Localization of GRP78 to mitochondria under the unfolded protein response. *Biochem J* 396, 31-39.

Sung, V.M. (2015) Mechanistic overview of ADP-ribosylation reactions. *Biochimie* 113, 35-46.

Swindall, A.F., Stanley, J.A. and Yang, E.S. (2013) PARP-1: Friend or Foe of DNA Damage and Repair in Tumorigenesis? *Cancers (Basel)* 5, 943–958.

Takada, T., Iida, K. and Moss, J. (1993) Cloning and site-directed mutagenesis of human ADP-ribosylarginine hydrolase. *J Biol Chem* 268, 17837-17843.

Takada, T., Iida, K. and Moss, J. (1995) Conservation of a common motif in enzymes catalyzing ADP-ribose transfer. Identification of domains in mammalian transferases. *J Biol Chem* 270, 541-544.

Tan, J.S., Ong Kc, K.C. and Rhodes, A. (2016) The role of heat shock proteins and glucose regulated proteins in cancer. *Malays J Pathol* 38, 75-82.

Tang, Y., Li, M., Wang, Y.L., Threadgill, M.D., Xiao, M., Mou, C.F., Song, G.L., Kuang, J., Yang, X., Yang, L., Gao, X.J., Wang, Y.P. and Meng, Y.P. (2015) ART1 promotes starvation-induced autophagy: a possible protective role in the development of colon carcinoma. *Am J Cancer Res* 5, 498–513.

Tanuma, S. and Endo, H. (1990) Identification in human erythrocytes of mono(ADP-ribosyl) protein hydrolase that cleaves a mono(ADP-ribosyl) Gi linkage. *FEBS Lett* 261, 381-384.

Tao, Z., Gao, P. and Liu, H.W. (2009) Identification of the ADP-ribosylation sites in the PARP-1 automodification domain: analysis and implications. *J Am Chem Soc* 131, 14258-14260.

Tao, Z., Gao, P., Hoffman, D.W. and Liu, H.W. (2008) Domain C of Human Poly(ADP-ribose) Polymerase-1 Is Important for Enzyme Activity and Contains a Novel Zinc-Ribbon Motif. *Biochemistry* 47, 5804-5813.

Terashima, M., Badruzzaman, M., Tsuchiya, M. and Shimoyama, M. (1996) Exocytosis of arginine-specific ADP-ribosyltransferase and p33 induced by A23187 and calcium or serum-opsonized zymosan in chicken polymorphonuclear leukocytes. *J Biochem* 120, 1209-1215.

Terashima, M., Shimoyama, M. and Tsuchiya, M. (1999) Introduction of NAD decreases fMLP-induced actin polymerization in chicken polymorphonuclear leukocytes--the role of intracellular ADP- ribosylation of actin for cytoskeletal organization. *Biochem Mol Biol Int* 47, 615-620.

Thiele, H.G. and Haag, F. (2001) The RT6 system of the rat: developmental, molecular and functional aspects. *Immunol Rev* 184, 96-108.

Thorsell, A.G., Ekblad, T., Karlberg, T., Low, M., Pinto, A.F., Tresaugues, L., Moche, M., Cohen, M.S. and Schuler, H. (2017) Structural Basis for Potency and Promiscuity in Poly(ADP-ribose) Polymerase (PARP) and Tankyrase Inhibitors. *J Med Chem* 60, 1262-1271.

Till, S. and Ladurner, A.G. (2009) Sensing NAD metabolites through macro domains. *Front Biosci (Landmark Ed)* 14, 3246-3258.

Timinszky, G., Till, S., Hassa, P.O., Hothorn, M., Kustatscher, G., Nijmeijer, B., Colombelli, J., Altmeyer, M., Stelzer, E.H., Scheffzek, K., Hottiger, M.O. and Ladurner, A.G. (2009) A macrodomain-containing histone rearranges chromatin upon sensing PARP1 activation. *Nat Struct Mol Biol* 16, 923-929.

Tirasophon, W., Lee, K., Callaghan, B., Welihinda, A. and Kaufman, R.J. (2000) The endoribonuclease activity of mammalian IRE1 autoregulates its mRNA and is required for the unfolded protein response. *Genes Dev* 14, 2725-2736.

Tirasophon, W., Welihinda, A.A. and Kaufman, R.J. (1998) A stress response pathway from the endoplasmic reticulum to the nucleus requires a novel bifunctional protein kinase/endoribonuclease (Ire1p) in mammalian cells. *Genes Dev* 12, 1812-1824.

Todorova, T., Bock, F.J. and Chang, P. (2015) Poly(ADP-ribose) polymerase-13 and RNA regulation in immunity and cancer. *Trends Mol Med* 21, 373-384.

Tong, L. and Denu, J.M. (2010) Function and metabolism of sirtuin metabolite O-acetyl-ADP-ribose. *Biochim Biophys Acta* 1804, 1617-1625.

Torre, L.A., Islami, F., Siegel, R.L., Ward, E.M. and Jemal, A. (2017) Global Cancer in Women: Burden and Trends. *Cancer Epidemiol Biomarkers* 26, 444-457.

Tsuchiya, M., Hara, N., Yamada, K., Osago, H. and Shimoyama, M. (1994) Cloning and expression of cDNA for arginine-specific ADP-ribosyltransferase from chicken bone marrow cells. *J Biol Chem* 269, 27451-27457.

Tuncel, H., Tanaka, S., Oka, S., Nakai, S., Fukutomi, R., Okamoto, M., Ota, T., Kaneko, H., Tatsuka, M. and Shimamoto, F. (2012) PARP6, a mono(ADP-ribosyl) transferase and a negative regulator of cell proliferation, is involved in colorectal cancer development. *Int J Oncol* 41, 2079-2086.

Ueda, K. and Hayaishi, O. (1985) ADP-ribosylation. *Annu Rev Biochem* 54, 73-100.

Ullman, E., Fan, Y., Stawowczyk, M., Chen, H.M., Yue, Z. and Zong, W.X. (2008) Autophagy promotes necrosis in apoptosis-deficient cells in response to ER stress. *Cell Death Differ* 15, 422-425.

Uramoto, H., Sugio, K., Oyama, T., Nakata, S., Ono, K., Yoshimastu, T., Morita, M. and Yasumoto, K. (2005) Expression of endoplasmic reticulum molecular chaperone Grp78 in human lung cancer and its clinical significance. *Lung Cancer* 49, 55-62.

Urra, H., Dufey, E., Avril, T., Chevet, E. and Hetz, C. (2016) Endoplasmic Reticulum Stress and the Hallmarks of Cancer. *Trends Cancer* 2, 252-262.

Ushioda, R., Miyamoto, A., Inoue, M., Watanabe, S., Okumura, M., Maegawa, K., Uegaki, K., Fujii, S., Fukuda, Y., Umitsu, M., Takagi, J., Inaba, K., Mikoshiba, K. and Nagata, K. (2016). Redox-assisted regulation of Ca^{2+} homeostasis in the endoplasmic reticulum by disulfide reductase ERdj5. Proc Natl Acad Sci U S A 113, E6055-E6063.

Van Meter, M., Mao, Z., Gorbunova, V. and Seluanov, A. (2011a) SIRT6 overexpression induces massive apoptosis in cancer cells but not in normal cells. *Cell Cycle* 10, 3153-3158.

Van Meter, M., Mao, Z., Gorbunova, V. and Seluanov, A. (2011b) Repairing split ends: SIRT6, mono-ADP ribosylation and DNA repair. *Aging (Albany NY)* 3, 829-835.

Vassilopoulos, A., Fritz, K.S., Petersen, D.R. and Gius, D. (2011) The human sirtuin family: Evolutionary divergences and functions. *Hum Genomics* 5, 485–496.

Venkannagari, H., Verheugd, P., Koivunen, J., Haikarainen, T., Obaji, E., Ashok, Y., Narwal, M., Pihlajaniemi, T., Luscher, B. and Lehtio, L. (2016) Small-Molecule Chemical Probe Rescues Cells from Mono-ADP-Ribosyltransferase

ARTD10/PARP10-Induced Apoptosis and Sensitizes Cancer Cells to DNA Damage. *Cell Chem Biol* 23, 1251-1260.

Verheugd, P., Butepage, M., Eckei, L. and Luscher, B. (2016) Players in ADP-ribosylation: Readers and Erasers. *Curr Protein Pept Sci* 17, 654-667.

Verheugd, P., Forst, A.H., Milke, L., Herzog, N., Feijs, K.L., Kremmer, E., Kleine, H. and Luscher, B. (2013) Regulation of NF-kappaB signalling by the mono-ADP-ribosyltransferase ARTD10. *Nat Commun* 4, 1683.

Vincenz-Donnelly, L. and Hipp, M.S. (2017) The endoplasmic reticulum: A hub of protein quality control in health and disease. Free Radic Biol Med 108, 383-393.

Vivelo, C.A., Wat, R., Agrawal, C., Tee, H.Y. and Leung, A.K. (2016) ADPriboDB: The database of ADP-ribosylated proteins. *Nucleic Acids Res* 45.

Vyas, S., Chesarone-Cataldo, M., Todorova, T., Huang, Y.H. and Chang, P. (2013) A systematic analysis of the PARP protein family identifies new functions critical for cell physiology. *Nat Commun* 4, 2240.

Vyas, S., Matic, I., Uchima, L., Rood, J., Zaja, R., Hay, R.T., Ahel, I. and Chang, P. (2014) Family-wide analysis of poly(ADP-ribose) polymerase activity. *Nat. Commun* 5, 4426.

Wahlberg, E., Karlberg, T., Kouznetsova, E., Markova, N., Macchiarulo, A., Thorsell, A.G., Pol, E., Frostell, A., Ekblad, T., Oncu, D., Kull, B., Robertson, G.M., Pellicciari, R., Schuler, H. and Weigelt, J. (2012) Family-wide chemical profiling and structural analysis of PARP and tankyrase inhibitors. Nat Biotechnol 30, 283-288.

Wang, H., Franke, C.C., Nordlund, S. and Noren, A. (2005) Reversible membrane association of dinitrogenase reductase activating glycohydrolase in the regulation of nitrogenase activity in Rhodospirillum rubrum; dependence on GlnJ and AmtB1. *FEMS Microbiol Lett* 253, 273-279.

Wang, M., Wey, S., Zhang, Y., Ye, R. and Lee, A.S. (2009) Role of the Unfolded Protein Response Regulator GRP78/BiP in Development, Cancer, and Neurological Disorders. *Antioxid Redox Signal* 11, 2307–2316.

Wang, Y., Shen, J., Arenzana, N., Tirasophon, W., Kaufman, R.J. and Prywes, R. (2000) Activation of ATF6 and an ATF6 DNA binding site by the endoplasmic reticulum stress response. *J Biol Chem* 275, 27013-27020.

Wang, Z., Michaud, G.A., Cheng, Z., Zhang, Y., Hinds, T.R., Fan, E., Cong, F. and Xu, W. (2012) Recognition of the iso-ADP-ribose moiety in poly(ADP-ribose) by WWE domains suggests a general mechanism for poly(ADP-ribosyl)ation-dependent ubiquitination. *Genes Dev* 26, 235-240.

Wei, H. and Yu, X. (2016) Functions of PARylation in DNA Damage Repair Pathways. *Genomics Proteomics Bioinformatics* 14, 131-139.

Weigert, R., Colanzi, A., Mironov, A., Buccione, R., Cericola, C., Sciulli, M.G., Santini, G., Flati, S., Fusella, A., Donaldson, J.G., Di Girolamo, M., Corda, D., De Matteis, M.A. and Luini, A. (1997) Characterization of chemical inhibitors of brefeldin A-activated mono-ADP-ribosylation. *J Biol Chem* 272, 14200-14207.

Weigert, R., Silletta, M.G., Spanò, S., Turacchio, G., Cericola, C., Colanzi, A., Senatore, S., Mancini, R., Polishchuk, E.V., Salmona, M., Facchiano, F., Burger, K.N., Mironov, A., Luini, A. and Corda, D. (1999) CtBP/BARS induces fission of Golgi membranes by acylating lysophosphatidic acid. *Nature* 402, 429-433.

Wek, R.C., Jiang, H.Y. and Anthony, T.G. (2006) Coping with stress: eIF2 kinases and translational control. *Biochem Soc Trans* 34, 7-11.

Welihinda, A.A. and Kaufman, R.J. (1996) The unfolded protein response pathway in Saccharomyces cerevisiae. Oligomerization and trans-phosphorylation of Ire1p (Ern1p) are required for kinase activation. *J Biol Chem* 271, 18181-18187.

Welihinda, A.A., Tirasophon, W. and Kaufman, R.J. (1999) The cellular response to protein misfolding in the endoplasmic reticulum. *Gene Expr* 7, 293-300.

Welsby, I., Hutin, D., Gueydan, C., Kruys, V., Rongvaux, A. and Leo, O. (2014) PARP12, an interferon-stimulated gene involved in the control of protein translation and inflammation. *J Biol Chem* 289, 26642-26657.

Weng, G., Li, J., Dingus, J., Hildebrandt, J.D., Weinstein, H. and Iyengar, R. (1996) Gbeta subunit interacts with a peptide encoding region 956-982 of adenylyl cyclase 2. Cross-linking of the peptide to free Gbetagamma but not the heterotrimer. *J Biol Chem* 271, 26445-26448.

Williams, D.B. (2006) Beyond lectins: the calnexin/calreticulin chaperone system of the endoplasmic reticulum. *J Cell Sci* 119. 615-623.

Wolfson, J.J., May, K.L., Thorpe, C.M., Jandhyala, D.M., Paton, J.C. and Paton, A.W. (2008) Subtilase cytotoxin activates PERK, IRE1 and ATF6 endoplasmic reticulum stress-signalling pathways. *Cell Microbiol* 10, 1775-1786.

Wooden, S.K. and Lee, A.S. (1992) Comparison of the genomic organizations of the rat grp78 and hsc73 gene and their evolutionary implications. *DNA Seq* 3, 41-48.

Wu, D. and Pan, W. (2010) GSK3: a multifaceted kinase in Wnt signaling. *Trends Biochem Sci* 35, 161-168.

Wu, J. and Kaufman, R.J. (2006) From acute ER stress to physiological roles of the Unfolded Protein Response. *Cell Death Differ* 13, 374-384.

Xiao, M., Tang, Y., Wang, Y.L., Yang, L., Li, X., Kuang, J. and Song, G.L. (2013) ART1 silencing enhances apoptosis of mouse CT26 cells via the PI3K/Akt/NF-κB pathway. *Cell Physiol Biochem* 32, 1587-1599.

Xing, X., Lai, M., Wang, Y., Xu, E. and Huang, Q. (2006) Overexpression of glucose-regulated protein 78 in colon cancer. *Clin Chim Acta* 364, 308-315.

Xu, J.X., Xiong, W., Zeng, Z., Tang, Y., Wang, Y.L., Xiao, M., Li, M., Li, Q.S., Song, G.L. and Kuang, J. (2017) Effect of ART1 on the proliferation and migration of mouse colon carcinoma CT26 cells in vivo. *Mol Med Rep* 15, 1222-1228.

Yan, K. and Gautam, N. (1997) Structural determinants for interaction with three different effectors on the G protein beta subunit. *J Biol Chem* 272, 2056-2059.

Yan, K., Kalyanaraman, V. and Gautam, N. (1996) Differential ability to form the G protein betagamma complex among members of the beta and gamma subunit families. *J Biol Chem* 271, 7141-7146.

Yan, Q., Xu, R., Zhu, L., Cheng, X., Wang, Z., Manis, J. and Shipp, M. A. (2013) BAL1 and its partner E3 ligase, BBAP, link Poly(ADP-ribose) activation, ubiquitylation, and double-strand DNA repair independent of ATM, MDC1, and RNF8. *Mol Cell Biol* 33, 845-57.

Yanagawa, T., Funasaka, T., Tsutsumi, S., Hu, H., Watanabe, H. and Raz, A. (2007) Regulation of phosphoglucose isomerase/autocrine motility factor activities by the poly(ADP-ribose) polymerase family-14. *Cancer Res* 67, 8682-8689.

Yang, J., Aittomaki, S., Pesu, M., Carter, K., Saarinen, J., Kalkkinen, N., Kieff, E. and Silvennoinen, O. (2002) Identification of p100 as a coactivator for STAT6 that bridges STAT6 with RNA polymerase II. *EMBO J* 21, 4950-4958.

Yang, Y.G., Cortes, U., Patnaik, S., Jasin, M. and Wang, Z.Q. (2004) Ablation of PARP-1 does not interfere with the repair of DNA double strand breaks, but compromises the reactivation of stalled replication forks. *Oncogene* 23, 3872–3882.

Yang, L., Xiao, M., Li, X., Tang, Y. and Wang, Y.L. (2016) Arginine ADP-ribosyltransferase 1 promotes angiogenesis in colorectal cancer via the PI3K/Akt pathway. *Int J Mol Med* 37, 734-742.

Ye, J., Rawson, R.B., Komuro, R., Chen, X., Dave, U.P., Prywes, R., Brown, M.S. and Goldstein, J.L. (2000) ER stress induces cleavage of membrane-bound ATF6 by the same proteases that process SREBPs. *Mol Cell* 6, 1355-1364.

Yelamos, J., Monreal, Y., Saenz, L., Aguado, E., Schreiber, V., Mota, R., Fuente, T., Minguela, A., Parrilla, P., de Murcia, G., Almarza, E., Aparicio, P. and Menissier-de Murcia, J. (2006) PARP-2 deficiency affects the survival of CD4+CD8+ double-positive thymocytes. *EMBO J* 25, 4350-4360.

Yoshida, H., Haze, K., Yanagi, H., Yura, T. and Mori, K. (1998) Identification of the cis-acting endoplasmic reticulum stress response element responsible for transcriptional induction of mammalian glucose-regulated proteins. Involvement of basic leucine zipper transcription factors. *J Biol Chem* 273, 33741-33749.

Yoshida, H., Matsui, T., Yamamoto, A., Okada, T. and Mori, K. (2001) XBP1 mRNA is induced by ATF6 and spliced by IRE1 in response to ER stress to produce a highly active transcription factor. *Cell* 107, 881-891.

Yoshida, H., Okada, T., Haze, K., Yanagi, H., Yura, T., Negishi, M., and Mori, K. (2000) ATF6 activated by proteolysis binds in the presence of NF-Y (CBF) directly to the cis-acting element responsible for the mammalian unfolded protein response. *Mol Cell Biol* 20, 6755-6767.

Yu, M., Schreek, S., Cerni, C., Schamberger, C., Lesniewicz, K., Poreba, E., Vervoorts, J., Walsemann, G., Grotzinger, J., Kremmer, E., Mehraein, Y., Mertsching, J., Kraft, R., Austen, M., Luscher-Firzlaff, J. and Luscher, B. (2005) PARP-10, a novel Myc-interacting protein with poly(ADP-ribose) polymerase activity, inhibits transformation. *Oncogene* 24, 1982-1993.

Yu, X., Chini, C.C., He, M., Mer, G. and Chen, J. (2003) The BRCT domain is a phospho-protein binding domain. *Science* 302, 639-642.

Zhang, J., Jiang, Y., Jia, Z., Li, Q., Gong, W., Wang, L., Wei, D., Yao, J., Fang, S. and Xie, K. (2006) Association of elevated GRP78 expression with increased lymph node metastasis and poor prognosis in patients with gastric cancer. *Clin Exp Metastasis* 23, 401-410.

Zhang, J.Y., Zhang, F., Hong, C.Q., Giuliano, A.E., Cui, X.J., Zhou, G.J., Zhang, G.J. and Cui, Y.K. (2015) Critical protein GAPDH and its regulatory mechanisms in cancer cells. *Cancer Biol Med* 12, 10–22.

Zhang, K. and Kaufman RJ. (2008) From endoplasmic-reticulum stress to the inflammatory response. *Nature* 454, 455-62.

Zhang, Y., Liu, R., Ni, M., Gill, P. and Lee, A.S. (2010) Cell surface relocalization of the endoplasmic reticulum chaperone and unfolded protein response regulator GRP78/BiP. *J Biol Chem* 285, 15065–15075.

Zhao, K., Chai, X. and Marmorstein, R. (2003) Structure of the yeast Hst2 protein deacetylase in ternary complex with 2'-O-acetyl ADP ribose and histone peptide. *Structure* 11, 1403-1411.

Zheng, H.C., Takahashi, H., Li, X.H., Hara, T., Masuda, S., Guan, Y.F. and Takano, Y. (2008) Overexpression of GRP78 and GRP94 are markers for aggressive behavior and poor prognosis in gastric carcinomas. *Hum Pathol* 39, 1042-1049.

Zhou, H., Huiatt, T.W., Robson, R.M., Sernett, S.W. and Graves, D.J. (1996) Characterization of ADP-ribosylation sites on desmin and restoration of desmin intermediate filament assembly by de-ADP-ribosylation. *Arch Biochem Biophys* 334, 214-222.

Zhu, G. and Lee, A.S. (2015) Role of the unfolded protein response, GRP78 and GRP94 in organ homeostasis. *J Cell Physiol* 230, 1413-1420.

Zhu, Y. and Gao, G. (2008) ZAP-mediated mRNA degradation. *RNA biology* 5, 65-67.

Zhu, Y., Chen, G., Lv, F., Wang, X., Ji, X., Xu, Y., Sun, J., Wu, L., Zheng, Y. T. and Gao, G. (2011) Zinc-finger antiviral protein inhibits HIV-1 infection by selectively targeting multiply spliced viral mRNAs for degradation. *Proc Natl Acad Sci U S A* 108, 15834-15839.

Zolkiewska, A. and Moss, J. (1993) Integrin alpha 7 as substrate for a glycosylphosphatidylinositol- anchored ADP-ribosyltransferase on the surface of skeletal muscle cells. *J Biol Chem* 268, 25273-25276.

Zolkiewska, A., Nightingale, M.S. and Moss, J. (1992) Molecular characterization of NAD:arginine ADP-ribosyltransferase from rabbit skeletal muscle. *Proc Natl Acad Sci U S A* 89, 11352-11356.

Zweifel, M.E., Leahy, D.J. and Barrick, D. (2005) Structure and Notch receptor binding of the tandem WWE domain of Deltex. *Structure* 13, 1599-1611.